PERFORMANCE CAPABILITIES OF LIGHT-FRAME SHEAR WALLS SHEATHED WITH LONG OSB PANELS

By:
Daniel Howard Bredel, Jr.

Thesis Submitted to the faculty of the
Virginia Polytechnic Institute and State University
In Partial fulfillment of the requirements for the degree of

MASTER OF SCIENCE
IN
CIVIL ENGINEERING

Approved by:

_____
J. Daniel Dolan

_____ _____
Thomas E. Cousins Joseph R. Loferski

April 2003
Blacksburg, Virginia Tech

Keywords: long osb panels, cyclic loading, overturning restraint, tall shear walls

Performance Capabilities of Light-Frame Shear Walls Sheathed With Long OSB Panels

By:
Daniel H. Bredel, Jr.

Committee Chairman: Dr. J. Daniel Dolan

(Abstract)

In this investigation, thirty-six shear walls measuring 8 feet (2.4 m) in width and possessing heights of 8, 9 and 10 feet (2.4, 2.7 and 3.0 m) were subjected to the reversed, cyclic loading schedule of the standard CUREE protocol in order to determine the performance capabilities of shear walls greater than 8 feet (2.4 m) in height sheathed with long panels. Of the thirty-six walls, a total of twelve walls measuring 9 and 10 feet (2.7 and 3.0 m) in height were sheathed with 4 x 8 feet (1.2 x 2.4 m) panels which required additional blocking members between the studs of the frame. Values obtained from the tests performed on these walls provided a direct comparison to those obtained from the walls of equal height, but sheathed with a long panel capable of spanning the entire height of the wall. The capabilities of long panels were investigated when used as the sheathing elements of shear walls with and without a mechanical hold-down device attached to the base of the end stud. An advantage of the long panel was investigated in which it was extended past the bottom plate and down onto the band joist to determine if significant resistance to the uplift present in walls without mechanical hold-down devices could be provided. Also, the effects of orienting the fibers of a 4 x 9 feet (1.2 x 2.7 m) panel in the alternate direction were examined.

Average values of the parameters produced by walls sheathed with long panels either matched or exceeded those of its counterpart sheathed with 4 x 8 feet (1.2 x 2.4 m) panels in all configurations except the 10 feet (3.0 m) tall wall without hold-down devices. In fact, 4 x 9 feet (1.2 x 2.7 m) panels increased the performance of 9 feet (2.7 m) tall walls equipped with hold-down restraint significantly.

Extending the long panels past the bottom plate and down onto the band joist improved the performance of both 8 and 9 feet (2.4 and 2.7 m) tall prescriptive shear walls significantly.

Walls sheathed with panels made of fibers oriented in the alternate direction performed identically to those sheathed with panels of typical fiber orientation until the point of peak load.

Once peak load was reached, walls sheathed with panels of alternate oriented fibers failed in a more sudden and brittle manner.

Acknowledgements

A most sincere thank you is owed to Dr. Dan Dolan, my committee chairman, for his time, effort, guidance and knowledge. I would also like to thank Dr. Joe Loferski and Dr. Thomas Cousins for their participation as committee members and the suggestions and recommendations that they put forth.

I would also like to display my appreciation to Will Jacobs, Adam Toothman and Rick Caudill for their assistance during testing.

A thank you is in line to Norbord Inc. for the materials and funding of the project.

To my parents, thank you for all your love throughout the years.

Table of Contents

Table of Figures

Index of Tables

Chapter 1: Introduction

1.1 Shear Wall Overview

A typical structure of light-frame construction resists lateral loads through the use of horizontal floor or roof diaphragms and vertical shear walls (Faherty and Williamson 1997). The walls standing perpendicular to the lateral load collect the force and transfer it to the horizontal diaphragm. The horizontal diaphragm distributes the force to the shear walls standing in the plane of the lateral load. The shear wall then transfers the load to the foundation. This system is diagramed in Figure 1.1.

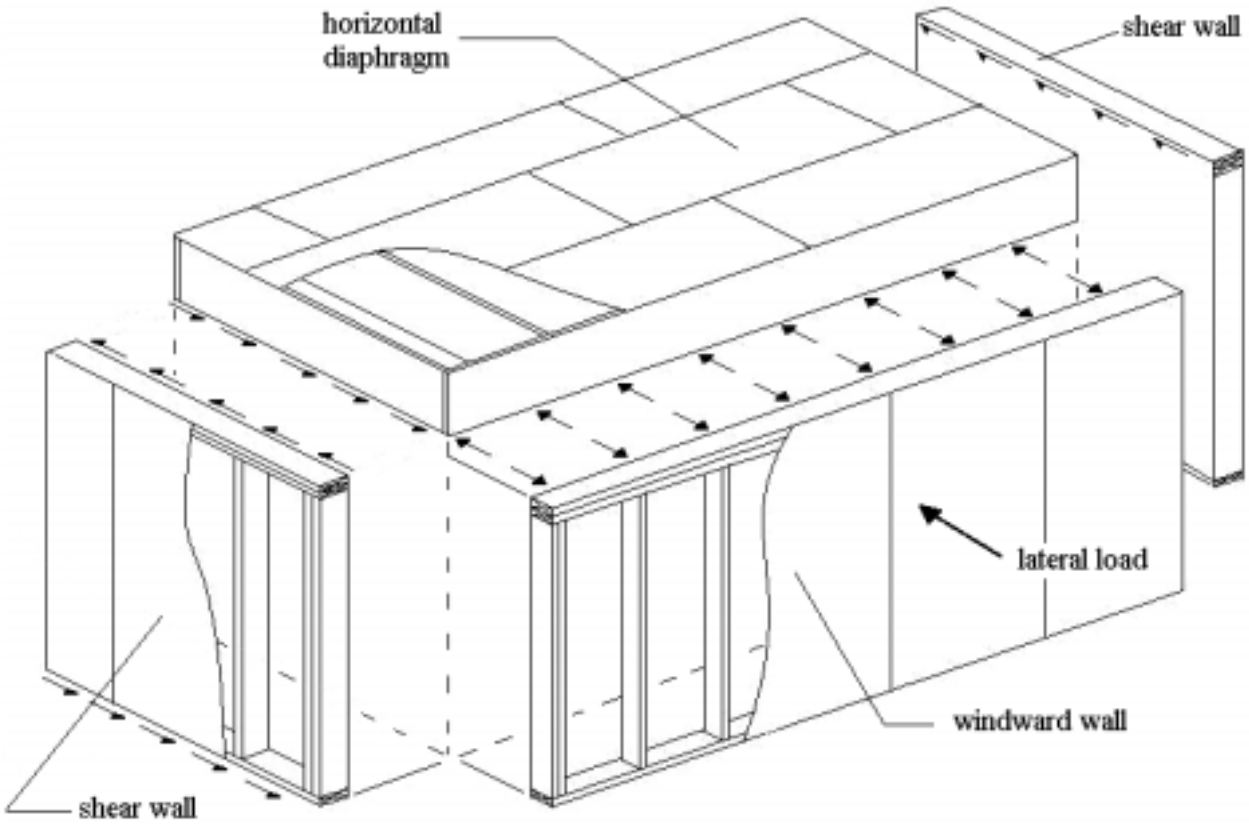

Figure 1.1. Lateral load resisting system of light-frame structure

A diaphragm is designed as a simply supported, deep beam and resists these loads through shear and bending. The shear wall, designed as a deep, cantilever beam, provides the support for the diaphragm. Therefore, the load the shear wall must be designed to resist is that of shear in the diaphragm at its support. Now that a brief discussion of the lateral load path present in a typical light-frame structure has been given, the remainder of the paper will focus solely upon shear walls.

In order to explain how a shear wall resists force, an explanation of its components and the forces developed with in these components will be given. The frame of a wall designed to support gravity loads can be transformed into a shear wall with the addition of two elements. These elements are sheathing panels, either oriented strand board or plywood, attached to one face of the wall and a double end stud at each end of the wall. The importance of these elements will be explained shortly. The components of a shear wall are presented in Figure 1.2.

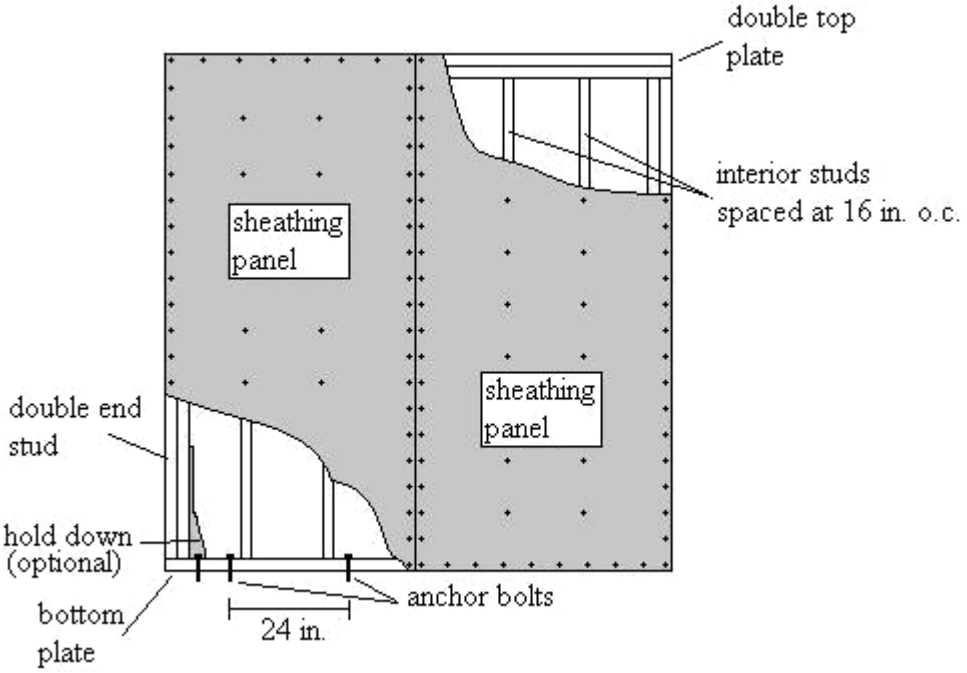

Figure 1.2. Shear wall

The sheathing panels are assumed to resist the entire shear force acting on the wall because the frame alone is virtually incapable of supporting a lateral load. The force applied to the double top plate is transferred into the sheathing panels through nails connecting the panels to the framing. The force is then transferred out of the panel and into the bottom plate through sheathing nails and then into the foundation via shear in the anchor bolts.

The end studs support the bending moment developed within the wall. The moment is resolved into a couple by dividing its magnitude by the wall length, and these equal and opposite forces are those acting on the end studs. Therefore, one end stud supports a compression force and the other supports a tensile force. According to structural theory, the forces discussed above have been diagramed on a simple line element representation of a cantilevered beam and on the actual components of a shear wall in Figures 1.3 and 1.4, respectively.

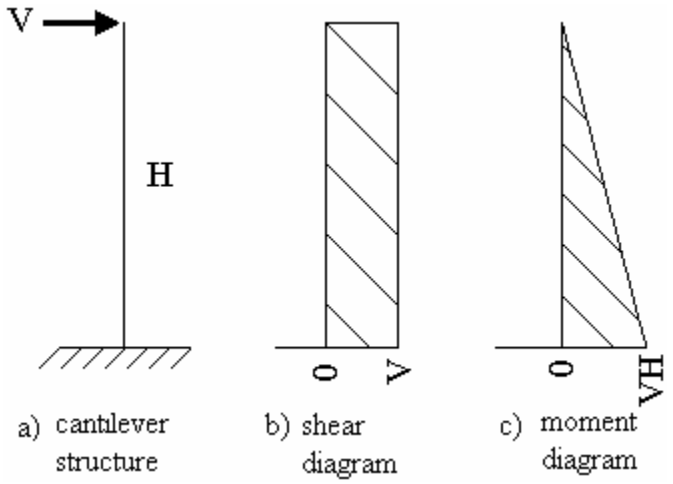

Figure 1.3. Forces present in a cantilever structure

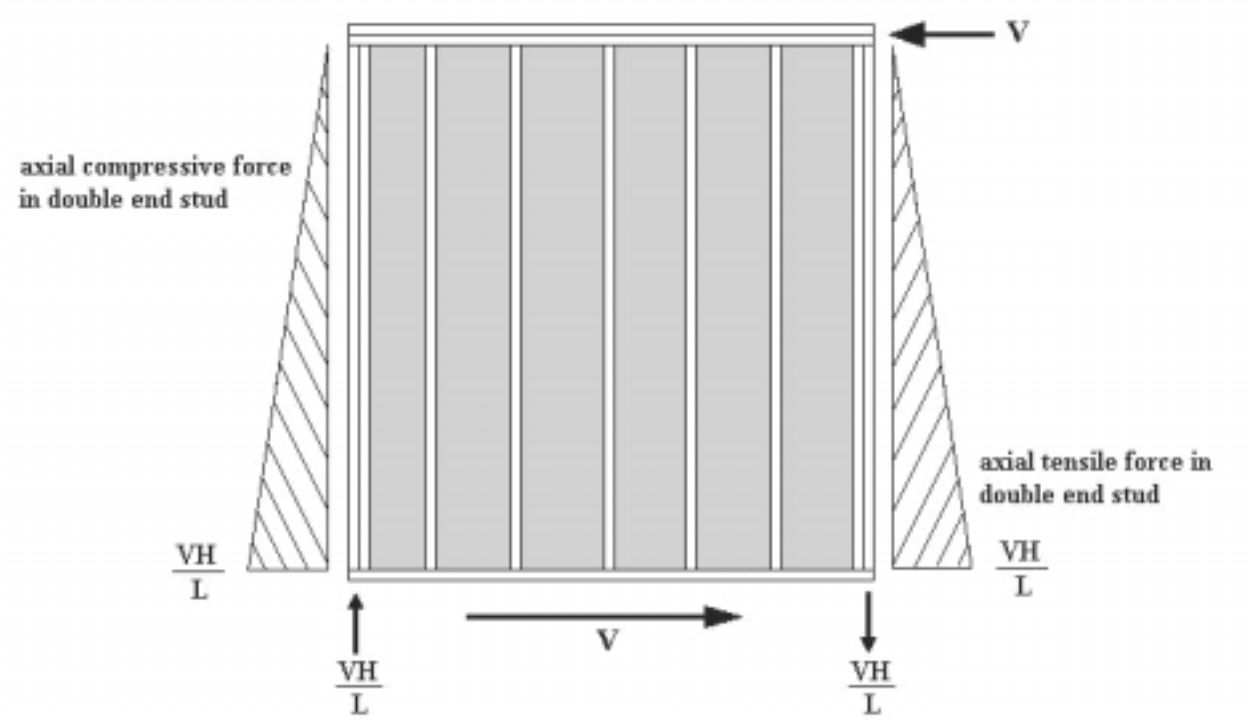

Figure 1.4. Forces present in components of shear wall
(H and L represent height and length of wall, respectively)

Several key attributes of a shear wall can greatly influence its response when subjected to lateral load. These are the schedule and characteristics of the sheathing-to-framing connections, anchorage condition and aspect ratio (ratio of height-to-length).

The sheathing-to-framing connection is the most important parameter of a shear wall. Characteristics and schedule of these connections determine the wall's overall performance. Strength, stiffness and amount of energy dissipated are all functions of the sheathing-to-framing connection (Dolan 1991). Increasing the number of connections along the perimeter of the panel will increase these values (Filiatrault and Folz 2002).

The anchorage provided between the bottom plate of the wall and substructure is the second most important parameter governing the performance characteristics of a shear wall. There are two basic anchorage conditions: prescriptive and engineered. Prescriptive anchorage conditions provide anchor bolts capable of transferring the shear load developed in the wall to the structure below. Engineered anchorage conditions include anchor bolts and a mechanical hold-down device attached to each end stud.

The ideal mode of deflection of a shear wall is termed “racking” and is portrayed in Figure 1.5.

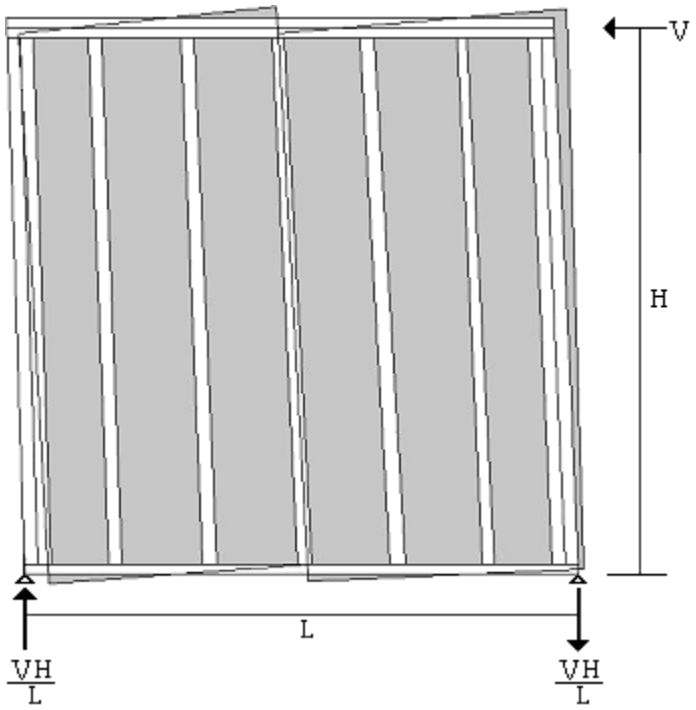

Figure 1.5. Racking deformation due to lateral load

Shear walls not equipped with hold-downs are only capable of developing racking deformations at low levels of load. As the magnitude of the shear force acting on the wall increases, the tensile force in the end stud increases and eventually exceeds the capacity of the connection between the end stud and bottom plate. The end stud then separates from the bottom plate and the deformed shape of the wall is no longer one of pure racking. The wall is now experiencing rigid body motion. However, the addition of a mechanical hold-down device greatly increases the capacity of the connection in tension and inhibits separation of the end stud and bottom plate. Therefore, the wall is able to develop racking deformation at very high levels of load.

Aspect ratio (height-to-length) is a crucial parameter of prescriptive walls. A wall with a high ratio of height-to-length will develop a large uplift force at the base of the end stud. If a hold-down is not present, rigid body motion will occur in walls of short length at very low levels of load.

1.2 Objectives

The main objective of this investigation is to determine the performance characteristics of shear walls greater than 8 feet (2.4 m) in height sheathed with long oriented strand board (OSB) panels by subjecting them to a reversed cyclic loading protocol. The effects of long OSB sheathing panels will be observed in shear walls with prescriptive and engineered anchorage conditions. If the performance characteristics of walls greater than 8 feet (2.4 m) in height sheathed with long panels can be proven to meet those of corresponding walls sheathed with 4 x 8 feet (1.2 x 2.4 m) panels in which blocking members must be placed, the amount of time and effort required to build shear walls greater than 8 feet (2.4 m) in height can be greatly reduced.

Two additional objectives will be investigated by examining the effects of sheathing two wall configurations with long OSB panels. One configuration will be tested to determine if long sheathing panels could be used to enhance the performance of 8 and 9 feet (2.4 and 2.7 m) tall prescriptive shear walls. The other wall configuration consists of 9 feet (2.7 m) tall prescriptive shear walls sheathed with 4 x 9 feet (1.2 x 2.7 m) panels made from strands oriented 90° to the direction of which they are normally.

Traditionally, sheathing panels have been manufactured in 4 x 8 feet (1.2 x 2.4 m) sheets. Shear walls greater than 8 feet (2.4 m) in height require one full panel and an additional segment of a panel. Also, additional pieces of lumber framing have to be placed between each stud along the horizontal seam of the two pieces of sheathing. These framing members are known as blocking and provide a load path for the shear present in the sheathing panels. Walls constructed in this manner require much more time and effort to build than that required of 8 feet (2.4 m) tall walls: the frame must be blocked, an additional sheathing segment must be cut and the number of sheathing nails is increased.

However, NorBord Inc. has developed sheathing panels with which they hope to alleviate the problems associated with the construction of tall walls. The dimensions of these new, long panels are 4 x 9 feet (1.2 x 2.7 m) and 4 x 10 feet (1.2 x 3.0 m). Thus, the amount of time and effort required to build a 9 or 10 feet (2.7 or 3.0 m) tall wall is nearly the same as an 8 feet (2.4 m) wall. For these tests, the amount of time required to build a blocked wall sheathed with 4 x 8 feet (1.2 x 2.4 m) panels was 1.5 times that of a wall sheathed with oversized panels.

Another application of an oversized panel presents itself in the design of 8 feet (2.4 m) tall prescriptive walls. A long panel can be extended past the bottom plate and down onto the

band joist. Nailing the sheathing panel into both the bottom plate and the band joist could provide increased resistance against uplift under the end stud in tension. This would increase the strength, stiffness and energy dissipation characteristics of the wall.

The third wall configuration was tested in order to determine if the direction of strand orientation in the OSB panel affects shear wall performance.

The following list presents the wall configurations tested in order to determine the capabilities of long OSB sheathing panels. Three specimens of each configuration were constructed and tested.

- Walls measuring 8 feet (2.4 m) in length by 8 feet (2.4 m) in height to be used as a control group
- Walls measuring 8 x 9 feet (2.4 x 2.7 m) sheathed with 4 x 8 feet (1.2 x 2.4 m) panels and blocked
- Walls measuring 8 x 9 feet (2.4 x 2.7 m) sheathed with 4 x 9 feet (1.2 x 2.7 m) panels
- Walls measuring 8 x 10 feet (2.4 x 3.0 m) sheathed with 4 x 8 feet (1.2 x 2.4 m) panels and blocked
- Walls measuring 8 x 10 feet (2.4 x 3.0 m) sheathed with 4 x 10 feet (1.2 x 3.0 m) panels
- Walls measuring 8 x 8 feet (2.4 x 2.4 m) sheathed with 4 x 8.5 feet (1.2 x 2.55 m) panels extended on to a band joist
- Walls measuring 8 x 9 feet (2.4 x 2.7 m) sheathed with 4 x 9.5 feet (1.2 x 2.85 m) panels extended on to a band joist
- Walls measuring 8 x 9 feet (2.4 x 2.7 m) sheathed with 4 x 9 feet (1.2 x 2.7 m) panels of which the strands were oriented 90° to the normal direction

1.3 Outline of Thesis

Chapter 2 is a brief discussion of previous investigations and outlines the testing methods used, configurations of walls tested and characteristics determined from these tests. Chapter 3 is a detailed description of the construction of each wall, instruments used to collect data during tests and the testing procedure. The material presented in Chapter 4 describes the analyses performed to determine the performance characteristics of the wall and the results of each wall configuration. The last chapter addresses the objectives of this investigation and summarizes the capabilities of long OSB sheathing panels.

Chapter 2: Background

2.1 General

The walls of light-frame structures support both vertical and lateral loads. Up until the 1940's, let-in bracing was used to supply lateral stiffness to the walls. This usually consisted of a 1 x 6 inch (25 x 150 mm) member laid diagonally across the exterior face of the framing and nailed to each stud. However, this method was rather time consuming because a notch had to be made in each stud in order for the let-in brace to remain flush with the exterior of the wall.

The introduction of panel products, such as plywood, in the 1940's revolutionized construction of light-frame shear walls. Panels not only provided lateral stiffness to the walls, but also increased load sharing between vertical studs, enclosed large amounts of the structure and required less time to assemble than the let-in brace.

However, new methods must always be tested experimentally in order to verify their capabilities. Over the last 50 years, many investigations have been conducted to determine the performance characteristics of various shear wall components and their relation to the performance of shear walls as a whole. Unfortunately, a standardized set of cyclic testing methods and procedures has not been established. Although this has produced results that are not truly comparable, a great deal of knowledge has been acquired from these investigations.

Testing methods used in past research and the results obtained from these tests are presented in the following sections.

2.2 Test Protocols

This section discusses the various testing protocols used to determine performance characteristics of light-frame shear walls. The original protocols consisted of static, monotonic loading functions in which the load was only applied in one direction. However, these did not adequately represent the true response of the structure. In order to incorporate the effects of reversed loading over time, quasi-static, reversed cyclic protocols were developed. The term quasi-static refers to tests in which the rate of cycling was low enough to inhibit the development of inertial forces (0.5 Hz). Tests conducted by Dinehart and Shenton (1998) proved that the

Sequential Phase Displacement (SPD) protocol produces peak loads similar to those of monotonic tests, but the peak occurs at much smaller displacements. Thus, the ductility of a wall tested according to SPD protocol is much less. Investigators, such as Shenton et al. (1998) and Dinehart et al. (1999), produced pseudo-dynamic protocols by increasing the rate of cycling of reversed cyclic tests above 1.0 Hz. Dolan (1989) and Filiatrault and Foschi (1991) performed shake table testing in order to determine the true response of a shear wall when subjected to seismic loading.

The majority of previous shear wall investigations have been performed according to monotonic and quasi-static, reversed cyclic protocols, with the latter becoming more prevalent over the last fifteen years. Brief summaries of these protocols are presented in the following subsections.

2.2.1 Monotonic Protocols

The defining parameter of a monotonic protocol is a constant rate of loading in one direction. The American Society of Testing Materials (ASTM) has standardized two protocols for testing light-frame shear walls sheathed with structural panels: E 72 and E 564.

A specimen tested according to ASTM E 72-98 is loaded to 788 lbs (3.5 kN), 1575 lbs (7.0 kN) and 2395 lbs (10.5 kN). Once each peak load is attained, the specimen is returned to the position of zero displacement before the next load is applied. After the specimen has been loaded to 2395 lbs (10.5 kN) and returned to zero displacement, it is then loaded until failure. However, this test can only be used to supply information about the sheathing panel and not that of the shear wall as a whole. This is due to placement of a steel rod (next to the double end stud in tension) that connects the top plate to the foundation and completely inhibits the effects of uplift.

ASTM E 564-95 can be used to provide information about a shear wall acting as a unit. According to this protocol, the rod used in E 72 is removed and replaced by mechanical hold-down devices attached to each end stud. The loading function is similar to that of E 72 except an initial load, 10% of ultimate, is applied and removed to seat the connections and the magnitudes are 33%, 67% and 100% of the ultimate load of the wall. Also, a static push over test is not performed after the third cycle. The drawback of this protocol is that the ultimate load of the wall must be determined before the test is performed.

It should be noted that the values provided in the Uniform Building Code used in the design of shear walls were obtained from tests performed according to these protocols (Dolan 1999). However, the extreme damage experienced by light-frame structures in the Northridge Earthquake of 1994 is evidence that these protocols do not provide accurate information about the forces required to resist severe dynamic loads.

2.2.2 Quasi-Static, Reversed Cyclic Protocols

The majority of testing performed today is done according to quasi-static, reversed cyclic protocols. These protocols typically consist of groups of cycles defining displacements of equal amounts in both a positive and negative direction. The amplitude of each set is increased until failure occurs in the specimen. Also, the amplitudes of the protocols are typically a function of a reference deformation that must be determined from a prior monotonic test. The frequency of each cycle remains constant. Thus, the rate at which the load is applied increases as displacement is increased.

2.2.2.1 Sequential Phase Displacement (SPD) Protocol

This protocol was originally developed to test masonry structures by the Technical Coordinating Committee on Masonry Research (Porter 1987) and has been modified for use in the testing of light-frame shear walls. The loading function is illustrated graphically in Figure 2.1.

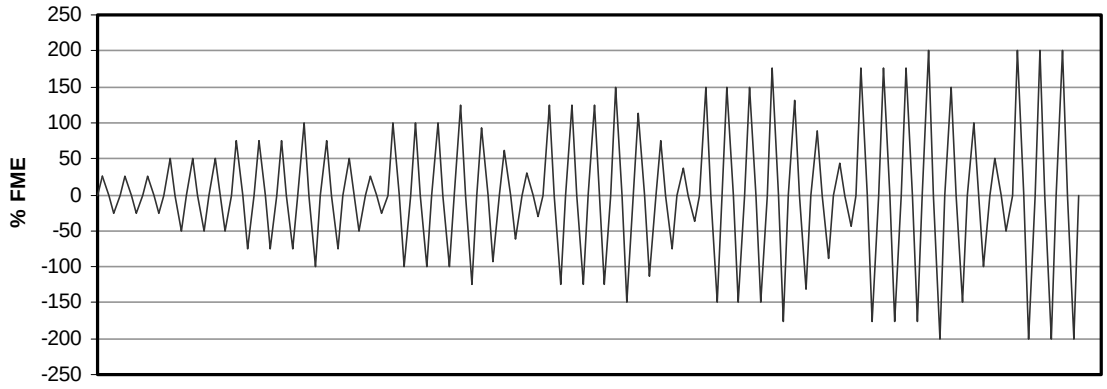

Figure 2.1. SPD protocol

The amplitudes of the waves are a function of the first major event (FME) which is defined as the displacement of the structure at yield. However, this presents a problem in light-frame testing because wood structures do not display a definitive yield point. The FME values used in prior research have ranged from 0.1 inches (2.5 mm) to 0.75 inches (19 mm). Also, the failure modes of walls tested according to SPD are not representative of those found during post earthquake investigations of actual structures (He et al 1997). The excessive number of cycles in the SPD test cause the sheathing-to-framing connections along the bottom plate to fail in bending fatigue. Walls examined after an actual earthquake occurred did not display this type of failure. In order for a protocol to be accurate, it must represent the true failure modes of the structure.

2.2.2.2 International Standards Organization (ISO) Protocol

The ISO Protocol was developed by the Working Group 7 of the ISO Technical Committee on Timber Structures in 1998 (Gatto and Uang 2001) and is displayed in Figure 2.2. The amplitude of each cycle is a percentage of the displacement at ultimate load determined from a monotonic test.

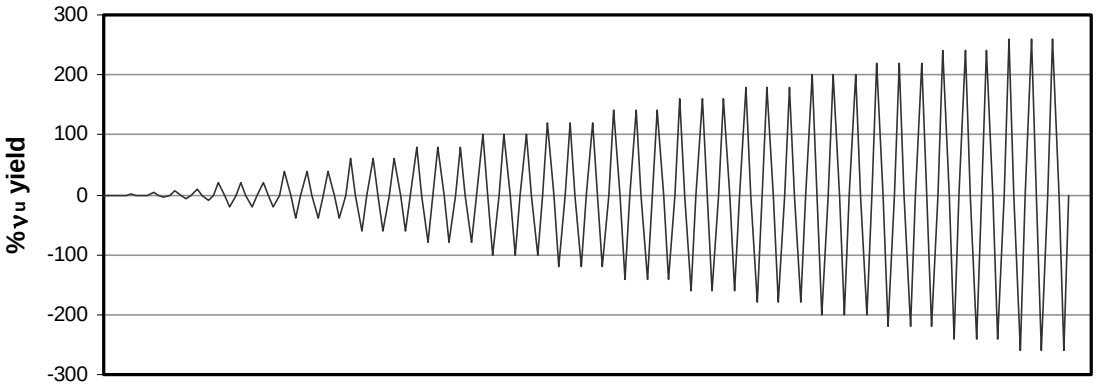

Figure 2.2. ISO protocol

2.2.2.3 Forintek Canada Corporation (FCC) Protocol

This protocol was developed by the Forintek Canada Corporation in 1993 and is similar to the SPD Protocol. The amplitudes of the cycles are determined from the nominal yield slip of a monotonic test. This is defined as 50% of the displacement at ultimate load (Gatto and Uang 2001). The large number of cycles in this test also produce fatigue failures in the sheathing-to-framing connections (He et al. 1997). The load function is displayed in Figure 2.3.

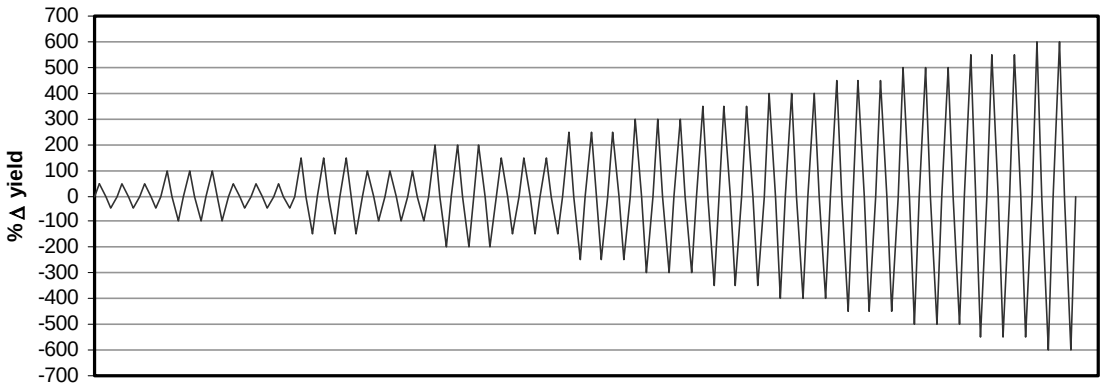

Figure 2.3. FCC protocol

2.2.2.4 Comite European de Normalisation (CEN) Short Protocol

This protocol was developed to determine the performance of a structure at a certain level of ductility. The amplitudes of the cycles are determined by multiplying the yield slip and desired level of ductility (Δ_{yield} x D). A ductility factor of 3 was used by He et al. (1997). The yield slip is determined from a monotonic test and is defined as the intersection of two lines on the load vs. displacement graph. One of the lines passes through the points of $0.1P_{max}$ and $0.4P_{max}$ and the other possesses a 1:6 slope placed tangent to the load vs. displacement curve. The load history of the CEN short protocol is displayed in figure 2.4.

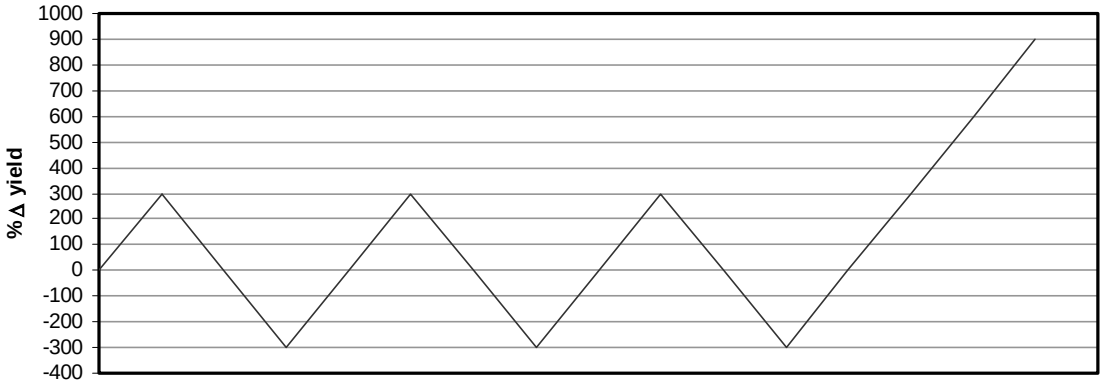

Figure 2.4. CEN short protocol

2.2.2.5 CUREE-Caltech Protocol

The CUREE-Caltech Woodframe Project was developed in1998 to improve the seismic performance of light-frame structures (Filiatrault et al. 2000). The displacement history of the protocol was determined by modeling structures of this type as nonlinear, dynamic, single degree-of-freedom systems (Gatto and Uang 2001) and is displayed in Figure 2.5.

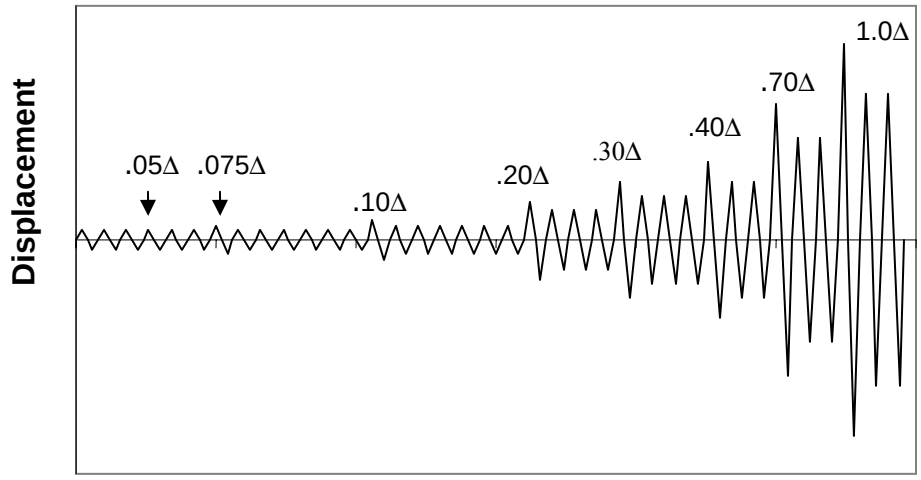

Figure 2.5. CUREE protocol

The amplitudes of the waves are a function of a reference deformation, Δ. This is defined as 60% of the displacement at 80% peak load on the degradation portion of the load vs. displacement curve of a monotonic test (Krawinkler et al. 2000). Defining Δ in this manner allows the researcher to be aware of the number of cycles and amplitude that will cause the wall to fail. Also, the number of reversed cycles is limited in order to induce failure modes representative of those in actual structures having undergone true seismic events.

2.3 Shear Wall Theory

The frame of a shear wall by itself provides no resistance to lateral loads. The sheathing panel, once attached, is the entire source of lateral resistance. Therefore, one would think that the shear strength and rigidity of the sheathing panel governs the performance of a shear wall. However, this is not the case. It is the connection between the sheathing panel and framing that dominates the performance of a shear wall.

Light-frame shear wall theory assumes each member of the framing to be rigid and the connections between them pinned. This produces a system with no lateral stiffness and allows the frame to deform into a parallelogram when acted upon by a lateral load. The sheathing

panel, a very rigid member when loaded in shear, can withstand the load while incurring only minimal shear deformation. Therefore, the members connecting the two, typically nails, will determine the overall performance of the structure. This is evident upon examination of load vs. displacement graphs for both a single sheathing-to-framing connection and an entire shear wall: they are virtually identical.

Idealized deformation of a shear wall when subjected to a lateral load is depicted in Figure 2.6. The frame has distorted in the form of a parallelogram and the panel, a very rigid member, has rotated about a point on the wall. The kinematics of the sheathing panel have been defined by Filiatrault (1990). While the majority of the rotation is a result of yielding in the sheathing-to-framing connection due to bending, some can be attributed to crushing of the wood fibers of the OSB. The point of rotation is located at the center of the panel along the top plate for prescriptive walls and at the overall center of the panel for engineered walls (Salenikovich 2000). Gupta and Kuo (1987) determined that the amount of rotation experienced by each panel of the wall is equal.

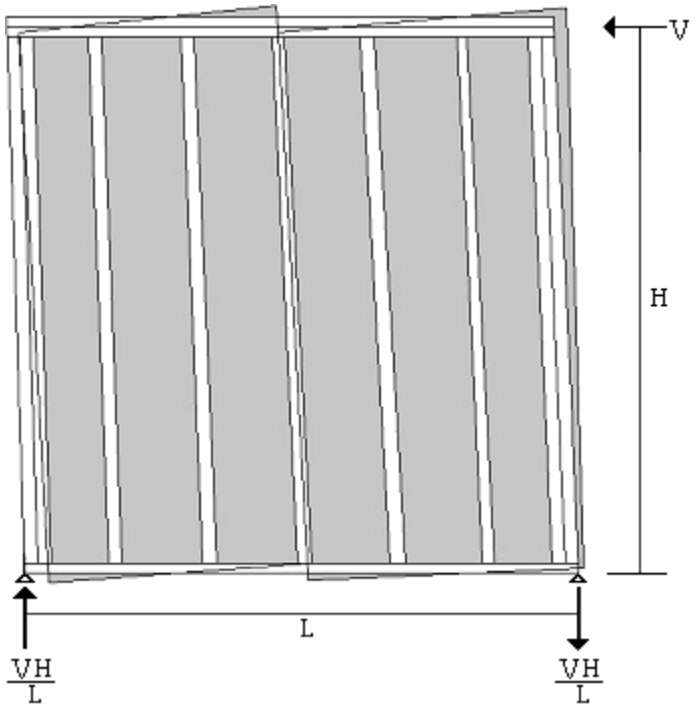

Figure 2.6. Racking deformation of a shear wall

A wall experiencing racking deformation is performing in the most efficient manner possible because the force in the panel is distributed fairly evenly to each sheathing-to-framing connection along the perimeter of the panel. The largest amount of force will occur in the connection farthest from the center of rotation (Dolan and Madsen 1992b). Therefore, the connections in and near the corners of the panel will perform the most work. The connections along the interior studs serve only to inhibit out-of-plane buckling of the panel.

An element that can greatly improve a shear wall's performance is the amount of hold-down restraint provided to resist the uplift force of the overturning moment. While dead load from the structure above will provide some resistance to uplift, a mechanical hold-down device attached to each end stud is the only sure method. In the absence of a hold-down, the connection between the end stud in tension and the bottom plate can be exceeded. This was examined by Gupta and Kuo (1987). Once this occurs, the wall is no longer experiencing pure racking deformation, but is also deforming as a rigid body. The sheathing-to-framing connections attached to the bottom plate under the end stud will then try to help resist uplift, but they soon fail by tearing through the edge of the panel. These connections fail in this manner because they are resisting both the lateral load acting on the wall and the uplift force of the overturning moment. This type of failure begins under the end stud in tension and proceeds along the bottom plate towards the end stud in compression.

A wall is not performing efficiently when deforming as a rigid body because the force in the panel is no longer distributed evenly to each sheathing-to-framing connection along the perimeter, but is concentrated to those along the bottom plate (Salenikovich 2000). Also, the panel is no longer rotating about its geometrical center. This reduces the amount of bending deformation experienced by the sheathing connections along the end studs and top plate. Therefore, work in the form of inelastic bending in the sheathing nails at these locations will no longer occur.

The global displacement of a shear wall when subjected to lateral load consists of four components: shear deformation of the sheathing panel, slip of sheathing connections, rigid body motion and bending of the end studs. Shear deformation of the sheathing panel will always contribute the least and is almost negligible, except in narrow walls due to the high aspect ratio. Rigid body motion is a significant source of displacement in walls that are not restrained against

uplift. Typically, bending of studs does not contribute to the global wall displacement (Gupta and Kuo 1985).

2.4 Importance of Individual Components of a Shear Wall

The following subsections present the importance of each individual component of a shear wall in relation to its performance as a whole. Their importance has been determined through prior investigations.

2.4.1 Framing Members and their Connections

Many investigators have noted that the majority of failures occurring in framing members are associated with the bottom plate of prescriptive walls. In the absence of hold-down restraint, bending frequently occurs in the bottom plate between the end stud in tension and the first anchor bolt. This can lead to the formation of a cross grain crack at high levels of load and is a source of rigid body motion at low load levels. This type of behavior occurs in bottom plate members possessing a low modulus of elasticity or significant slope of grain. Also, splitting along the grain of the bottom plate can occur when the spacing of the sheathing-to-framing connections is less than 6 inches (150 mm). The process of driving a nail produces tensile forces between the grains of the wood. If the nails are spaced closely, any additional force acting on the nail will help the tensile forces open a crack. This was experienced in tests performed by Filiatrault and Foschi (1991) and Dinehart and Shenton (1998).

The importance of the connection between the end stud in tension and the bottom plate has been noted, but some separation also occurs between the end stud and top plate. Dolan and Madsen (1992b) applied a steel angle bracket to connect these members and observed an increase in load capacity of the wall.

Typically, shear walls tested experimentally are sheathed on one side with a structural panel. In actual buildings, the exterior structural panel is often accompanied by nonstructural elements such as gypsum wall board and stucco. Gatto and Uang (2001) found that the addition of nonstructural elements increased the stiffness of the wall. Thus, more force acted on the wall and caused some studs to break near the bottom plate.

Horizontal blocking is necessary in order to provide a direct load path from the panel above the seam to the one below. Durham et al. (2001) conducted tests on walls sheathed with 4

x 8 feet (1.2 x 2.4 m) panels oriented horizontally. These tests displayed the importance of blocking. However, the author is unaware of any previous investigations pertaining to the performance of shear walls taller than 8 feet (2.4 m) requiring blocking.

2.4.2 Sheathing-to-Framing Connections

The importance of these elements is obvious. They must adequately transfer the force from the frame, a system possessing no lateral stiffness, to the panel which provides the entire source of resistance. It is well understood that the nonlinear, inelastic load-slip behavior of the sheathing-to-framing connection governs the performance of the entire shear wall (McCutcheon 1985, Foschi 1977 and Folz and Filiatrault 2001). The elastic region of the connection's load-displacement curve is small. Once the connection is displaced into the inelastic region, it displays a pinched hysteresis effect caused by residual forces present in the element (Foliente 1995). The strength, stiffness and energy dissipation characteristics of the shear wall are directly related to the strength, stiffness and energy dissipation characteristics of the sheathing-to-framing connection.

Foschi (1974), Dolan (1989) and Salenikovich (2000) have subjected individual connections to both monotonic and cyclic loading protocols. The monotonic tests have provided information about the nonlinear load vs. displacement characteristics of the connection including the peak load attained and its corresponding displacement. The cyclic tests display the hysteretic response of the connection, thus providing its energy dissipation characteristics. If the energy dissipated by each connection can be determined, the amount of energy dissipated by the entire wall can then be found by summing each connection's contribution. Also, a comforting observation noted by all researchers performing both monotonic and cyclic connection tests is that the envelope curve of the monotonic tests coincides with the peaks of the hysteresis loops of the cyclic tests. However, strength and stiffness degradation of the connection did occur when subsequently cycled to displacements of equal magnitude (Dolan and Madsen 1992a, Foliente 1995 and Shenton et al. 1998).

Foschi (1977), Dolan (1989), Dolan and Foschi (1991) and Dolan and White (1995) fitted curves through the data points obtained from their respective connection tests and used them to model nonlinear springs of finite element programs. Filiatrault (1990) developed a finite element program using the connection test data of Dolan (1989). Their programs successfully modeled

the response of entire shear walls based on the load vs. displacement characteristics of the connection.

Tuomi and McCutcheon (1978), McCutcheon (1985) and Schmidt and Moody (1989) developed equations capable of determining the displacement components of individual sheathing connections using energy principles. Kasal and Leichti (1992) developed a finite element program capable of modeling a three dimensional system of vertical shear walls and horizontal diaphragms. They also decreased the number of degrees-of-freedom (DOF) by using master DOF's and greatly reduced the computation time. Itani and Cheung (1984) developed a finite element program capable of handling any type of wall configuration (openings, number of panels and spacing of sheathing connections).

Dolan and Madsen (1992a) studied the effects of grain orientation of the panel on the performance of the connection. Plywood and waferboard panels were tested and it was concluded that the effects of grain orientation are negligible. Based on this observation, the walls sheathed with panels of alternate OSB in this investigation should perform identically to those sheathed with panels of conventional strand orientation. These researchers also noted that the performance of the connection is determined from the mechanical properties of the nail and not from those of the sheathing or lumber.

The effect of loading rate on the connections was investigated by Dolan and Madsen (1992a) and Gatto and Uang (2001). They determined that loading rate does not affect the performance of the sheathing-to-framing connection.

The performance of a shear wall can be greatly affected by the amount of care used when driving the sheathing nail. Salenikovich (2000) performed connection tests that displayed the importance of adequate edge distance. Tuomi and McCutcheon (1978) also arrived at this conclusion. Jones and Fonseca (2002) studied the effects of overdriving the sheathing nail past the surface of the panel and found this to be detrimental to the shear wall's performance. The aforementioned investigators observed brittle failures, such as the nail tearing through or pulling out of the panel, in connections assembled in this manner.

2.4.3 Sheathing

The sheathing panel must be a very rigid member when loaded in shear in order to supply lateral resistance to the wall. It must also be able to transfer the force to the sheathing nails without experiencing crushing around the nail shank.

The shear rigidity and out-of-plane bending stiffness of the panel are functions of the panel's thickness. Dolan (1989) monitored the effects of out-of-plane bending and found them to be negligible in panels with thicknesses of 3/8 inch (9 mm) or greater. The thickness of the panel also plays a role in the mode of failure in the connections. Thin panels fail in a brittle mode when the nail tears through or pulls out of the panel. Thicker panels allow the connection to develop a more ductile failure because the clamping force of the sheathing acts to withdraw the nail from the framing (Salenikovich 2000).

Tests conducted by Shenton et al. (1997) determined that plywood and OSB panels behave similarly until their respective ultimate displacement is reached. The loads and displacements attained using either panel are comparable. However, once ultimate displacement is reached, the stiffness and energy dissipation characteristics of OSB panels decrease more rapidly. Investigations conducted by Dinehart and Shenton (1998) produced similar results.

Orientation of the panels, either horizontally or vertically, does affect the wall's performance. Horizontal orientation increases the peak load, but decreases displacement capacity. Of course adequate blocking must be provided for panels oriented horizontally. The addition of a gypsum sheathing panel on the opposite face of the wall increases its strength and stiffness, but decreases its ductility. Gypsum panels also display more strength and stiffness when oriented horizontally. Wolfe (1983) tested walls with gypsum panels oriented horizontally and observed a 40% increase in strength.

Typically, all sheathing panels measure 4 feet (1.2 m) in length by 8 feet (2.4 m) in height. However, mills are capable of producing larger panels and their use has been the focus of several investigations. Durham et al. (2001) subjected 8 x 8 feet (2.4 x 2.4 m) walls sheathed with 8 x 8 feet (2.4 x 2.4 m) OSB panels to monotonic, cyclic and dynamic protocols. They determined that a significant increase in stiffness and lateral load carrying capacity can be achieved by using large panels. Lam et al. (1997) tested walls 24 feet (7.3 m) in length by 8 feet (2.4 m) in height sheathed with 24 x 8 feet (7.3 x 2.4 m) panels and discovered similar results. However, Lam et al. (1997) noted that walls sheathed with one large panel did not dissipate as

much energy as walls sheathed with 4 x 8 feet (1.2 x 2.4 m) panels when subjected to cyclic protocols. Also, walls sheathed with one large panel exhibited a decrease in displacement at peak load and a more brittle failure when compared to walls sheathed with 4 x 8 feet (1.2 x 2.4 m) panels. The researchers determined that the increased performance associated with large panels is attributed to the elimination of internal seams and increased efficiency of connections along the perimeter of the panel (Durham et al. 2001).

2.4.4 Overturning Restraint and Aspect Ratio

Overturning restraint, in the form of a mechanical hold-down device attached to each end stud, and the aspect ratio (height-to-length) directly influence the shear wall's ability to deform in a racking manner. The investigations conducted by Salenikovich (2000), in which he tested walls of 8 feet (2.4 m) in height and lengths ranging from 2 to 12 feet (0.6 to 3.6 m), quantified the effects of these two parameters. He determined that walls with an aspect ratio of 2:3 without overturning restraint are capable of developing significant racking behavior in the third panel. Also, walls with an aspect ratio of 4:1 restrained against overturning are incapable of developing racking deformation due to significant bending deformation. This observation was also made by Commins and Gregg (1996).

2.5 Influence of Cyclic Protocols

Currently, a standardized cyclic loading protocol used to test light-frame shear walls does not exist. As discussed previously, each protocol contains its own set of parameters and this makes data comparison difficult. The main source of discrepancy is the method used to define the amplitudes of the cycles. Most protocols define the amplitudes of the cycles as a percentage of the yield displacement which is not a definitive property of wood structures. Therefore, two different researchers could be using the same protocol and still subject their specimens to different displacements. Due to the fact that behavior of a sheathing connection is only elastic at very small displacements, load-history can greatly affect the structural performance of a shear wall.

Also, different protocols produce different types of failure modes. Protocols containing many cycles, such as SPD and FCC, cause fatigue failures in the sheathing-to-framing connections. This is inconsistent with the failure modes of walls subjected to shake table tests or

actual seismic events. The CEN short protocol has attempted to alleviate the problem of fatigue failure in the connections by decreasing the number of cycles. However, the increased amplitudes of the CEN short protocol may produce large inelastic deformations of the connection on the first excursion and this is certainly not representative of a seismic event. The CUREE protocol displays great promise because the number of cycles is not excessive and the amplitudes are determined from the largest displacement the wall can withstand. He et al. (1997), Karacabeyli and Ceccotti (1996) and Gatto and Uang (2001) have investigated the influence of various cyclic protocols on shear wall performance.

He et al. (1997) conducted tests on identical shear walls using the FCC and CEN short protocols. The dimensions of the walls tested were 24 feet (7.2 m) in length by 8 feet (2.4 m) in height. A wall tested according to the FCC protocol obtained a peak load of 23 kips (102 kN) before the sheathing connections along the bottom plate began to experience fatigue failure. The peak load of an identical wall tested according to the CEN short protocol was 25.5 kips (113 kN) and was reached in the first cycle. The displacements at failure of the walls tested according to FCC and CEN short were 21.46 and 23.38 mm, respectively. It is difficult to formulate a comparison between the amounts of energy dissipated according to the two protocols. The many cycles of the FCC protocol dissipated almost four times as much energy compared to that of the three cycled CEN short protocol.

Gatto and Uang (2001) compared the effects of the CUREE, ISO and SPD protocols on 8 x 8 feet (2.4 x 2.4 m) shear walls of identical construction. A monotonic test was also performed according to ASTM E 564. The peak strength of the walls tested according to the ISO and CUREE protocols were similar to that of the wall tested monotonically. The SPD protocol produced a peak strength equal to 75% of that produced by the monotonic test. The decreased peak load of the SPD protocol was attributed to the fatigue failure of sheathing connections along the bottom plate.

Ultimate load and displacement of the wall tested according to the CUREE protocol was 9 kips (40 kN) and 4.5 inches (114 mm), respectively. These values are similar to those produced from the monotonic test. Therefore, the envelope curve (curve through the peaks of cyclic test) produced from the CUREE protocol was similar to the load vs. displacement curve of the monotonic test. The ISO and SPD protocols produced ultimate displacements of 3.25 and 2.5

inches (89 and 70 mm), respectively. Thus, the envelope curve of the ISO and SPD protocols did not resemble the load vs. displacement curve produced by the monotonic test.

Comparisons made in the previous paragraph used the values of load and displacement produced from the positive excursion of the hydraulic ram. Ultimate load and displacement produced from the negative excursion of the hydraulic ram decreased for all three protocols. This is evidence of the effects of reversed, cyclic loading and the importance of such testing protocols.

Skaggs and Rose (1996) subjected identical walls to the SPD protocol and to a modified SPD protocol in which the degradation cycles were removed. Results of the tests were identical. They concluded that the degradation cycles do not influence the performance of the wall.

2.6 Summary

Although there have not been any investigations conducted on the performance of shear walls taller than 8 feet (2.4 m), the observations of previous research will provide valuable insight to this investigation. Key elements of a shear wall and their relation to its performance are listed below:

- Strength, stiffness, displacement and energy dissipation of a shear wall are determined by the nonlinear, inelastic load-displacement characteristics of the sheathing-to-framing connection.
- A shear wall is capable of experiencing racking deformation until the end stud in tension begins to lift and separate from the bottom plate.
- A mechanical hold-down device inhibits uplift and greatly improves strength, stiffness and energy dissipation.
- Aspect ratio directly affects the wall's ability to experience racking deformation.
- A standardized protocol for cyclic testing of light-frame shear walls must be established so that the results of different investigations can be compared directly and seismic design of wood structures can be advanced.

Chapter 3: Wall Configurations and Testing Procedure

3.1 General

Twelve different wall configurations were built and tested in order to observe the effects of long sheathing panels on the performance of tall light-frame shear walls. Three specimens of each configuration were constructed. Table 3.1 provides the dimensions, size of sheathing panel and anchorage conditions of each specimen. The length of each wall was held constant at 8 feet (2.4 m).

Table 3.1. Wall configurations

Wall Specimen	L x H (ft)	Blocked	Sheathing Size (ft)	Anchorage Condition	Reason for Test	
8-8-P	8 x 8	No	4 x 8	Prescriptive	Control specimens for basis of current building code	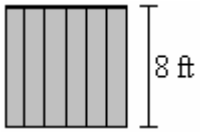
9-8-P	8 x 9	Yes	4 x 8	Prescriptive	Current code requirements for configuration	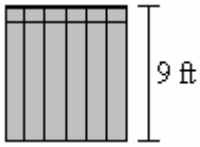
9-9-P	8 x 9	No	4 x 9	Prescriptive	Display equivalent or increased design values compared to blocked wall	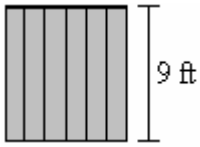
10-8-P	8 x 10	Yes	4 x 8	Prescriptive	Current code requirements for configuration	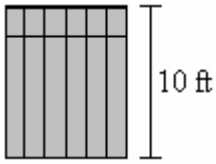

Table 3.1 Continued: Wall Configurations

Wall Specimen	L x H (ft)	Blocked	Sheathing Size (ft)	Anchorage Condition	Reason for Test	
10-10-P	8 x 10	No	4 x 10	Prescriptive	Display equivalent or increased design values compared to blocked wall	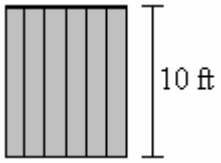
9-ALT9-P	8 x 9	No	4 x 9	Prescriptive	Investigate ability of OSB made from alternate oriented fibers	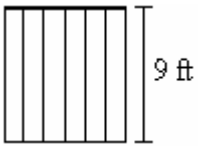
8-8.5-P	8 x 8	No	4 x 8.5	Prescriptive	Possible increase in design values by extending sheathing 6 inches on to band joist	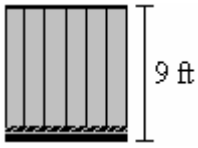
9-8-E	8 x 9	Yes	4 x 8	Engineered	Control specimens for basis of current engineered design values in building code	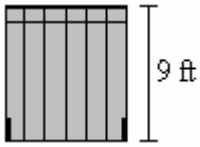
9-9-E	8 x 9	No	4 x 9	Engineered	Display equivalent or increased design values compared to blocked wall	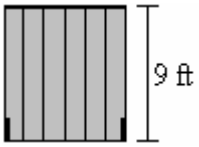
10-8-E	8 x 10	Yes	4 x 8	Engineered	Control specimens for basis of current engineered design values in building code	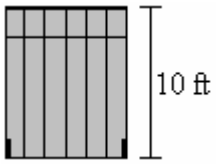
10-10-E	8 x 10	No	4 x 10	Engineered	Display equivalent or increased design values compared to blocked wall	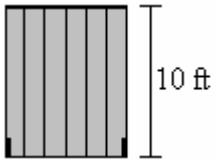
9-9.5-P	8 x 9	No	4 x 9.5	Prescriptive	Possible increase in design values by extending sheathing 6 inches on to band joist	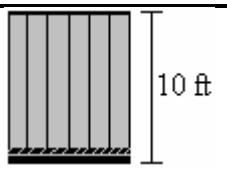

The base of the wall was attached to the rigid foundation of the testing apparatus according to either prescriptive or engineered design specifications. Prescriptive anchorage conditions were used to represent construction of a typical wall in a common light-frame structure with a slab on grade foundation. This consisted of a 5/8 inch (15.9 mm) diameter A307 anchor bolt placed 12 inches (305 mm) from the edge of the wall and every 24 inches (610 mm) on center. This form of anchorage was able to transfer the shear load from the base of the wall to the foundation, but did not resist uplift of the end studs. In the walls of configurations **8-8.5-P** and **9-9.5-P**, anchor bolts were replaced by 5/8 inch (15.9 mm) diameter, 24 inch (610 mm) long all-thread rod. Engineered anchorage conditions consisted of the four anchor bolts of prescriptive design and a mechanical hold-down device attached to the inside face of each end stud. This anchorage condition was able to transfer the shear load from the base of the wall to the foundation and resist the uplift force due to the overturning moment. The hold-down device was a Simpson HTT22 and was connected to the foundation using a 5/8 inch (15.9 mm) diameter A307 bolt. The HTT22 was attached to the end stud by thirty-two 16 penny sinker nails. The uplift restraint provided by the hold-down greatly improved the overall strength and stiffness of the wall. The two anchorage conditions are displayed in Figure 3.1.

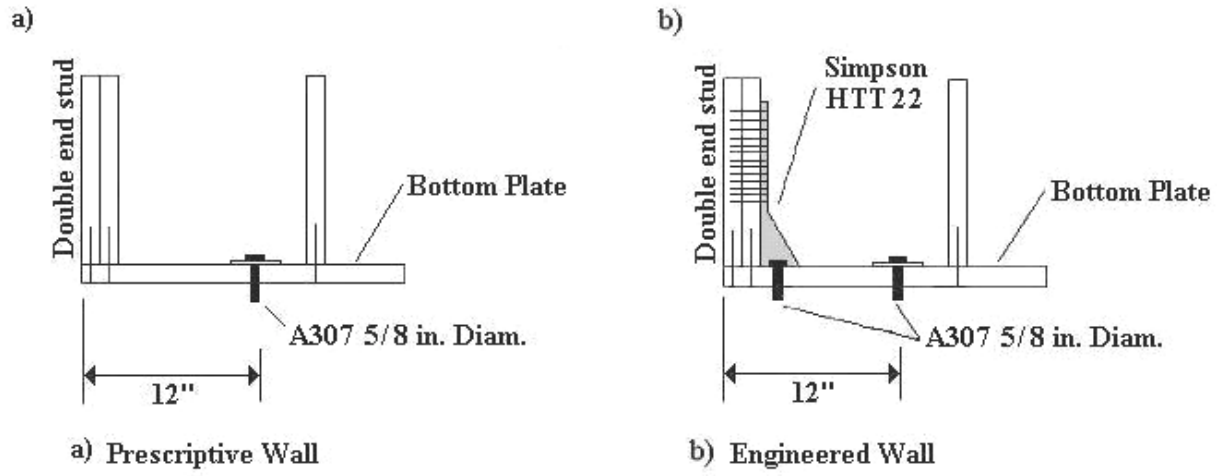

Figure 3.1. Anchorage Conditions:
a) Engineered, b) Prescriptive

Each wall was subjected to a cyclic loading pattern. The force and displacement of the hydraulic actuator used to test the walls was governed by the CUREE Standard Protocol (Krawinkler et al. 2000). Specifications of the CUREE protocol will be presented in a later

section. All walls were tested in a horizontal position. This produced conservative data because the self-weight of the wall was not providing any additional resistance to uplift.

3.2 Materials and Wall Assembly

Framing and sheathing materials were provided by NorBord Inc. Upon arrival, they were stored in an indoor laboratory. All framing members were made of Spruce-Pine-Fir. The quality of the framing members was stud grade. The sheathing material was 7/16 inch (11.1 mm) thick oriented strand board (OSB). All framing connections were made using 16 d common nails (0.165 inch diameter and 3.5 inch smooth shank) bought at a local hardware store. The sheathing-to-framing connection consisted of a SENCO 8 d nail with a full round head (0.131 inch diameter and 2.5 inch smooth shank). These were driven with a pneumatic gun.

The frame of each wall consisted of a single bottom plate, double end studs, interior studs spaced at 16 inches (406mm) on center and a double top plate. The connection between each stud and plate was two 16 d nails end nailed. Members making up double end studs and double top plates were connected to each other using two 16 d common nails spaced at 12 inches (305 mm) on center. If the wall required blocking, it was connected to the studs by two 16 d common nails at each end which were end nailed at one end and toe nailed at the other. The frame was built entirely of 2 x 4 dimension lumber. A typical frame is pictured in Figure 3.2.

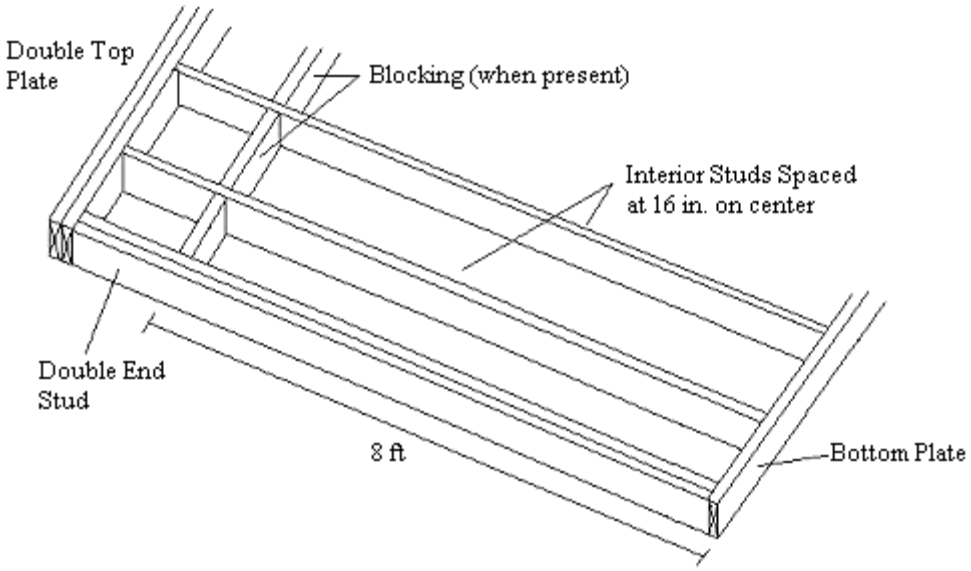

Figure 3.2. Wall frame

The nail schedule used to attach the sheathing panel to the framing was a spacing of 6 inches (152 mm) along the perimeter and 12 inches (305 mm) along interior studs. The nails were driven into the exterior members of the double end studs and double top plate.

In the walls of configurations **8-8.5-P** and **9-9.5-P**, where the sheathing was extended 6 inches (152 mm) past the wall onto the 2 x 12 representing a band joist, sheathing nails spaced at 6 inches (152 mm) on center were driven into both the bottom plate and the 2 x 12 at the edge of the panel. The 2 x 12 used to replicate a band joist was actually two 2 x 12 members with 7/16 inch (11.1 mm) OSB placed in between. This was done to provide an adequate connection width for both the bottom plate and rigid foundation. Care was taken in order to ensure the 2.5 inch (63.5 mm) shank of the sheathing nail only penetrated the top 2 x 12 and not the OSB filler. This resembled the true field connection into a one-ply band joist. The bottom plate was secured to the two-ply member by one 16 d common nail into each 2 x 12 every 6 inches (152 mm). Figure 3.3 displays these nailing schedules.

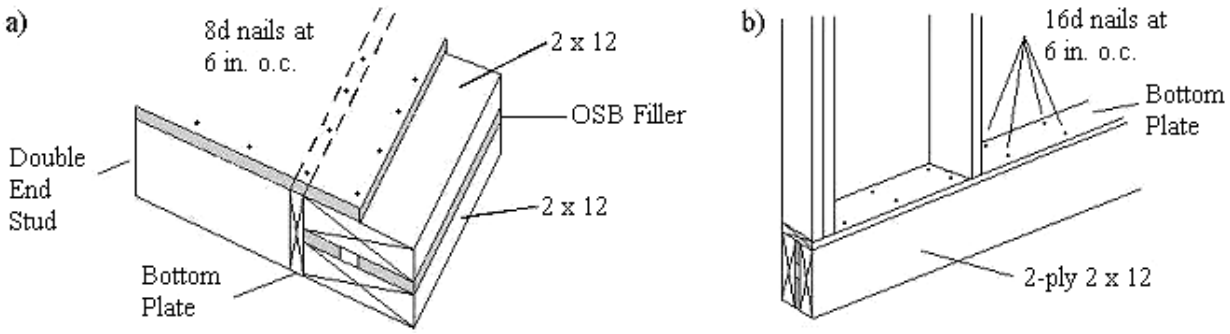

Figure 3.3. Connections of walls attached to 2 x 12:
a) Sheathing connection, b) Bottom plate connection

The distance between the edge of the sheathing panel and nail was 3/4 inch (19.1 mm) along the perimeter except at the common middle stud. Due to both panels sharing this stud, the edge distance was limited to 3/8 inch (9.5 mm). Similarly, the edge distance along blocking members was limited to 3/8 inch (9.5 mm) as well. Sheathing was oriented vertically with the long edge parallel to the studs. A 1/8 inch (3.2 mm) gap was placed between the two adjacent

panels of each wall. This accounted for any possible swelling the OSB might experience and is typical of field construction.

3.3 Test Frame and Instrumentation

The walls were tested in a horizontal position. The bottom plate was attached to a rigid foundation using the anchor bolts representing either prescriptive or engineered anchorage conditions. The foundation was a 3 x 5 inch (76 x 127 mm) steel tube bolted to a concrete base. The double top plate was bolted to a 3 x 5 inch (76 x 127 mm) load distribution beam. It was connected to the load distribution beam using 5/8 inch (19.9 mm) diameter A307 bolts placed 12 inches (305 mm) from the edge of the wall and every 24 inches (610 mm) on center. A 3 x 3 x 1/4 inch (76 x 76 x 6 mm) square steel washer accompanied each bolt (except hold down) attaching the wall to the testing apparatus in order to inhibit the effects of bending on the plates.

The load distribution beam was attached to a hydraulic actuator on one end and supported vertically by a rolling wheel on the other. The steel tubes were oriented such that top and bottom plates were bolted to the 3 inch (76 mm) face. This allowed the sheathing to deform freely past the steel tube at high displacements. If this was not permitted to occur, an erroneous source of resistance to the lateral load would be present and values of strength and stiffness would be exaggerated. The hydraulic actuator was capable of displacing the wall 6 inches (152 mm) in both directions and applying a force of 55,000 lbs (245 kN). Figure 3.4 is a diagram of the testing apparatus and the location of instruments used to record data.

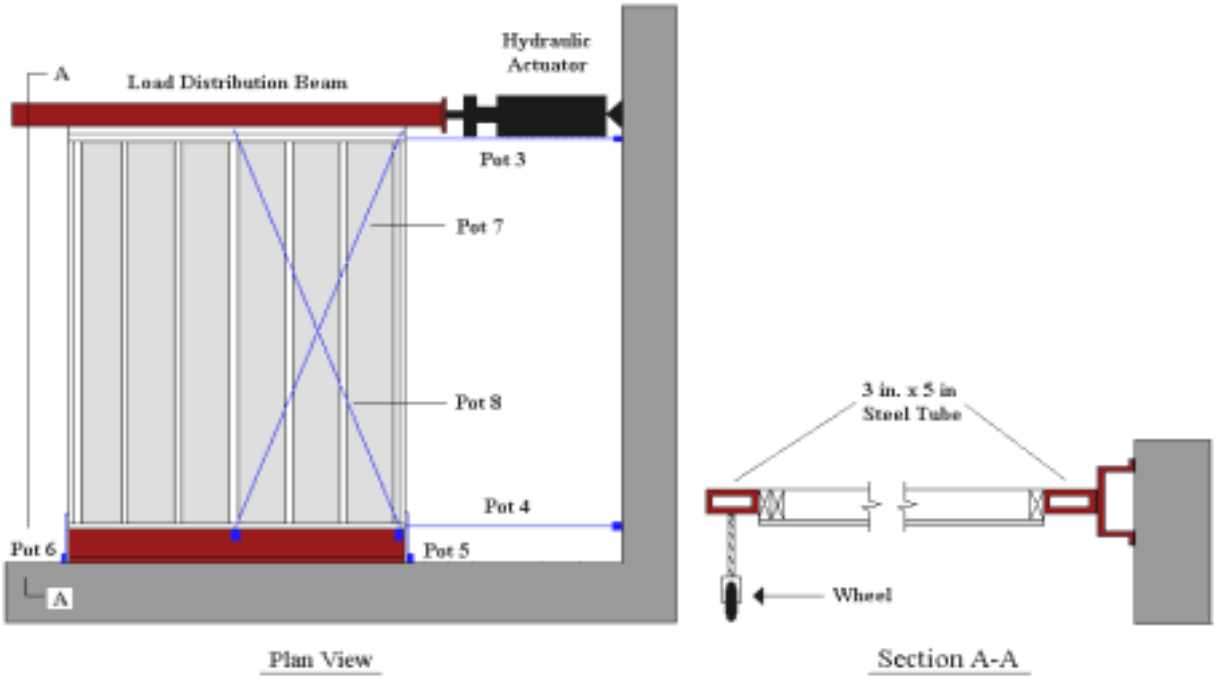

Figure 3.4. Test frame and instrumentation set up

A total of eight data channels were used to measure the response of the wall when acted upon by cyclic loading. Channels 1 and 2 are built into the hydraulic actuator and recorded the force and displacement applied to the wall, respectively. These two channels provided the data used to plot the hysteresis loops on the load-displacement graph of each wall.

Six channels were attached to the wall in order to monitor the different components of displacement experienced by the wall. The instruments used to record data on Channels 3 through 8 were resistance potentiometers (Pot). A Pot is basically a string on a coil capable of lengthening and shortening corresponding to the displacements of the wall to which it is attached. The base of the Pot is attached to the foundation and the string is then uncoiled and attached to the location of the wall where displacement data is desired. Proper placement of the Pot is important in order to ensure the displacement data retrieved is along the correct axis. A misaligned Pot could be reading displacements in all three axes and separating these into the proper x, y and z components would be very time consuming. In this investigation, only Pots 5 and 6 had to be placed with a great deal of care. Pots 3, 4, 7 and 8 were uncoiled to lengths large enough that the data recorded along the line of action would dominate any minor displacement along an incorrect axis.

Pot 3 measured the horizontal displacement of the double top plate. This data was used to determine if any slip was occurring with respect to the load distribution beam and to ensure Channel 2 was providing accurate data. The slip between top plate and load distribution beam proved to be negligible. However, 0.1 inch (2.5 mm) of slip was experienced by nine of the walls tested.

In order to ensure the bottom plate was not displacing relative to the foundation, Pot 4 was included in the data acquisition set up. This displacement also proved to be negligible ($\leq$ 0.03 inches). If lateral displacement of the bottom plate did occur, this would be subtracted from the displacement measured by Channel 2 in order to determine interstory drift.

Pots 5 and 6 measured the uplift and compressive displacements of the end studs with respect to the rigid foundation. Uplift displacement of the end stud was a result of the four end nails' minimal resistance to withdrawal. Once the capacity of the four nails was exceeded, the sheathing-to-framing connection under the double end stud was forced to resist the uplift. This caused the sheathing connection to fail. Failure of sheathing connections then progressed towards the center of the panel along the bottom plate. However, the failure previously described was only present in prescriptive walls. The hold-down connection in engineered walls provided a direct load path from the end stud to the foundation. Uplift displacements did occur in engineered walls, but these were less than 0.3 inches (7.5 mm). These were attributed to deformation of the hold-down and the eccentricity between the hold-down connection bolt and the outside edge of the end stud where the Pot was attached (approximately 4.5 inches). Compressive displacements occurred when the stress perpendicular to the grain of the bottom plate was exceeded by the force supplied from the end stud in compression. Also, small gaps between the end stud and bottom plate, less than 0.1 inches (2.5 mm), were closing. The Pots were aligned and attached to the exterior face of the end stud. This was probably the largest source of error in the entire data acquisition set up. Ideally, the Pots would have been attached in alignment with the center of the double end stud for prescriptive design and in line with the anchor bolt of the hold-down for engineered design because these were the respective points of rotation. However, this was simply not feasible and an amplification of the data recorded by Pots 5 and 6 occurred.

The data obtained from these Pots provided the information necessary to determine the rigid body displacement experienced by the wall. In this state, the wall is simply rotating and very little racking deformation is occurring. Rigid body motion is diagramed in Figure 3.5.

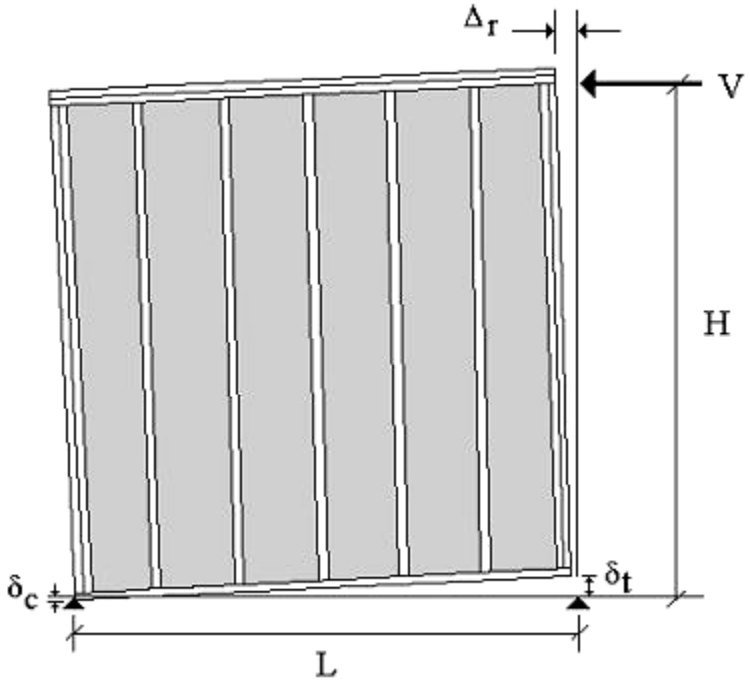

Figure 3.5. Rigid body rotation

Although a wall never deforms purely in shear, a component of the overall displacement can be attributed to this type of deformation. Figure 3.6 displays a wall experiencing idealized shear deformation.

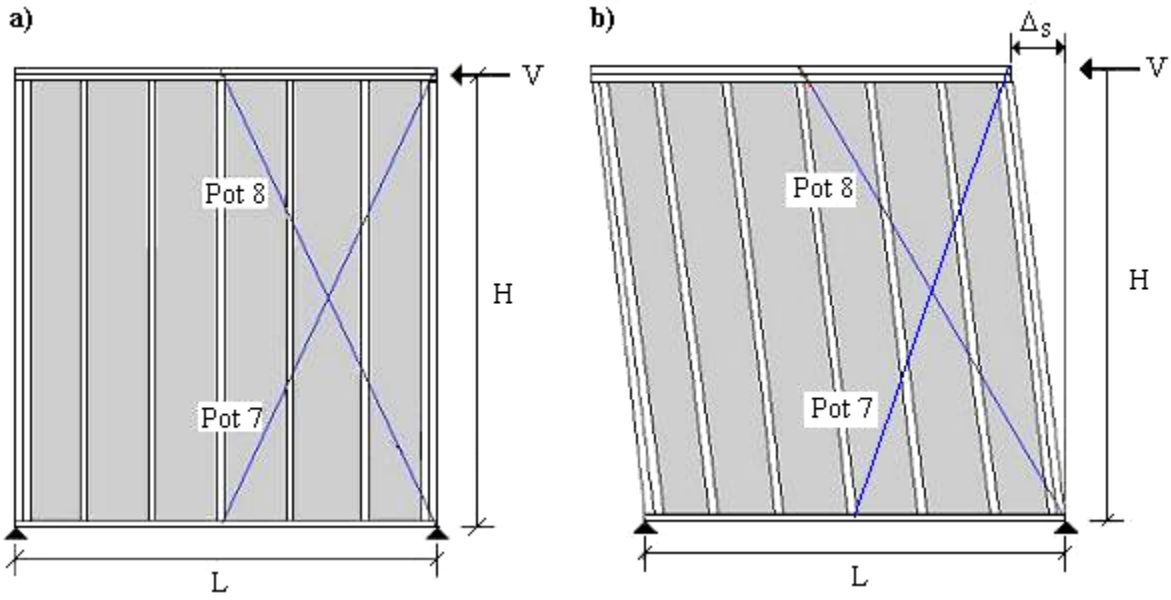

Figure 3.6: Shear deformation

a) Undeformed, b) Deformed

The lateral displacement of the top right corner of Figure 3.6b is the shear displacement component. This displacement was determined by placing Pots 7 and 8 as shown in Figure 3.4. Based on the original geometry of the wall and the data recorded by Pots 7 and 8, the shear displacement component can be determined.

3.4 Test Protocol

The cyclic loading pattern applied to the wall was a deformation controlled, quasi-static protocol developed by the Consortium of Universities for Research in Earthquake Engineering (CUREE). This protocol was chosen because it has been specifically designed to model the effects of seismic events on light-frame structures. The amplitudes of the triangular waves are a function of a reference deformation (Δ) based on the configuration of the wall and must be determined before the test can be performed. It is scaled from a monotonic test of the same wall configuration and is defined as 60% of the displacement corresponding to 0.8Fpeak on the degradation portion of the load vs. displacement curve of the monotonic test. A graphical depiction of the protocol is displayed in Figure 3.7.

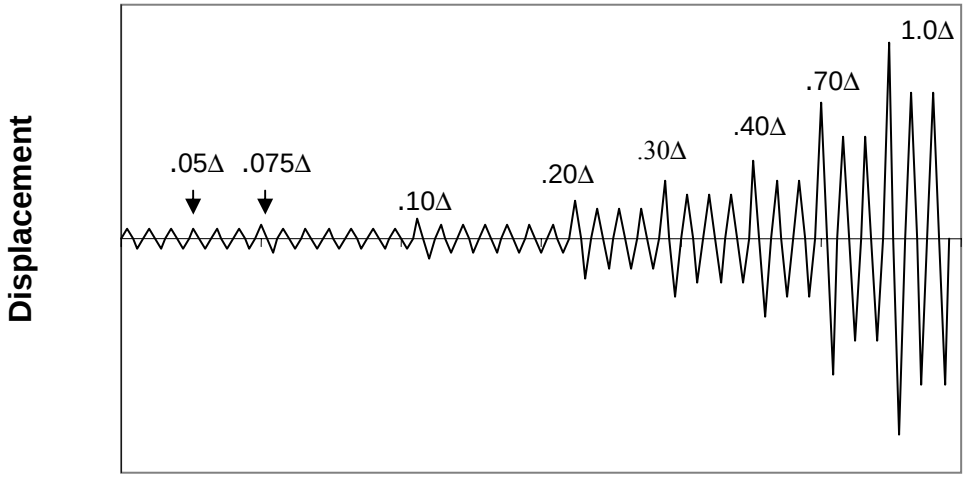

Figure 3.7. CUREE Protocol

The loading pattern consisted of six initiation cycles with an amplitude of 0.05Δ followed by a series of cycle groups consisting of one primary cycle and a series of trailing cycles. A primary cycle is defined as a cycle possessing an amplitude larger than any previous cycle. The amplitude of a trailing cycle is 75% of the primary cycle by which it was preceded. Table 3.2 displays the amplitude and number of initiation, primary and trailing cycles of the test protocol.

The tests were performed until the wall experienced complete failure or a displacement of $\pm$ 6 inches (152 mm) was reached. The cycling frequency of the tests was 0.5 Hz.

Table 3.2. CUREE Protocol displacement profile

Phase	Cycle	Displacement
Initiation	1	0.05Δ
	2	0.05Δ
	3	0.05Δ
	4	0.05Δ
	5	0.05Δ
	6	0.05Δ
1	7	0.075Δ
	8	0.05625Δ
	9	0.05625Δ
	10	0.05625Δ
	11	0.05625Δ
	12	0.05625Δ
	13	0.05625Δ
2	14	0.1Δ
	15	0.075Δ
	16	0.075Δ
	17	0.075Δ
	18	0.075Δ
	19	0.075Δ
	20	0.075Δ
3	21	0.2Δ
	22	0.15Δ
	23	0.15Δ
	24	0.15Δ
4	25	0.3Δ
	26	0.225Δ
	27	0.225Δ
	28	0.225Δ
5	29	0.4Δ
	30	0.3Δ
	31	0.3Δ
6	32	0.7Δ
	33	0.525Δ
	34	0.525Δ
7	35	1.0Δ
	36	0.75Δ
	37	0.75Δ
8	38	1.5Δ
	39	1.125Δ
	40	1.125Δ
9	41	2.0Δ
	42	1.5Δ
	43	1.5Δ
10	44	2.5Δ
	45	1.875Δ
	46	1.875Δ
11	47	3.0Δ
	48	2.25Δ
	49	2.25Δ
12	50	3.5Δ
	51	2.625Δ
	52	2.625Δ
13	53	4.0Δ
	54	3.0Δ
	55	3.0Δ

Although the symmetric cyclic loading function described above will never truly depict the loading history produced by a seismic event, several key parameters can be obtained from its use. Primary cycles adequately represent the amount of energy dissipated by the system during that one cycle when subjected to the corresponding displacement of an actual seismic event. The cumulative energy dissipated by the system up until that point may not reflect that of an actual seismic event, but the energy dissipated during the primary cycle is representative of that which would occur during an equivalent seismic event. Trailing cycles are used to monitor strength and stiffness degradation of the system. Strength degradation is defined as a decrease in load from that attained by a previous cycle of equal amplitude. A smaller load at an equal displacement signifies a decrease in stiffness and inelastic behavior in the system.

The protocol used to test mechanically connected wood systems can have a significant effect on the results of the test. Two important elements of a cyclic loading protocol are the method by which the increase in displacement is determined and the number of cycles performed. The CUREE protocol has been developed, based on these elements, to adequately model the behavior of wood structures under cyclic loading. The reference deformation was scaled off the degradation portion of a monotonic test. Therefore, it is representative of the largest cycle the wall will experience (Krawinkler et al. 2000).

Previous cyclic test protocols, such as the Sequential Phase Displacement (Porter 1987) and the Forintek Canada Corporation (Karacabeyli 1995), derived the reference displacement from the yield point of a monotonic test. The amplitudes of the waves are computed as percentages of this yield displacement. This may not adequately represent the behavior in a wood structure because the yield point of a wood structure is not definitive. Also, the displacement of the largest cycle is decided from the "yield" displacement and this may not produce the proper number and amplitude of displacements (Krawinkler et al. 2000).

An excessive number of cycles in a cyclic test protocol will produce fatigue failure in the sheathing-to-framing connections. Examinations of actual structures after an earthquake occurred revealed that nail fatigue is not a true failure mode (He et al. 1997). This type of failure was not experienced by the sheathing-to-framing connections in the tests performed during this investigation. Gatto and Uang (2001) and He et al. (1997) investigated the effects of different cyclic loading protocols. They determined that protocols with an excessive number of cycles produce a decrease in peak load and a large increase in the amount of energy dissipated.

Finally, the CUREE protocol was chosen for this investigation because it is the only cyclic protocol with a statistical basis for the number and magnitude of cycles used, and it replicates the typical failure observed after earthquakes have occurred.

3.5 Summary

A total of 36 walls were subjected to a cyclic loading pattern governed by the CUREE protocol in order to investigate the effects of long sheathing panels on the performance of light-frame shear walls greater than 8 feet (2.4 m) in height. Instrumentation attached to the walls recorded the load resisted and displacements experienced by the wall when displaced by the hydraulic actuator. In the next chapter, the analyses performed using the data recorded by these instruments will be explained. These analyses produce the performance characteristics of the wall and determine the effectiveness and capabilities of long sheathing panels.

Chapter 4: Analysis and Results

4.1.1 General

Twelve different shear wall configurations were subjected to the CUREE standard cyclic protocol in order to determine the effects of long oriented strand board (OSB) panels. Three specimens of each configuration were built and tested. The configurations are named according to their height, the length of panel with which it was sheathed and its anchorage conditions. For example, the 8 feet (2.4 m) tall prescriptive wall configuration, which was sheathed with 4 x 8 feet (1.2 x 2.4 m) panels, is named **8-8-P**. Thus, the first character of the name represents the wall **H**eight, the second the panel **L**ength and the third either **P**rescriptive or **E**ngineered anchorage conditions. Table 3.1 displays the naming schedule of the wall configurations. The characteristics used to define a wall's performance are strength, stiffness, ductility and energy dissipation. Individual components of displacement were also determined in order to observe the effects of long OSB panels.

The test results of each individual wall are included in the Appendix. It includes values of the parameters discussed in the following subsections and values of force, displacement, hysteretic energy, cyclic stiffness and equivalent viscous damping ratio for each primary cycle. Also, the data of each Pot used to determine displacement components is plotted.

4.1.2 Equivalent Energy Elastic Plastic (EEEP) Parameters

Unlike a material such as structural steel, wood does not display well defined yield limits. Also, the force versus displacement behavior of wood is nonlinear. Therefore, identification of such parameters as the yield limit and elastic stiffness becomes difficult. In order to make accurate comparisons of different walls, a consistent method must be used to identify the parameters that determine a wall's performance. In this investigation, the Equivalent Energy Elastic Plastic (EEEP) method, which was first discussed by Porter (1987), is used. This method transforms a nonlinear, inelastic system into an idealized, bilinear elastic-plastic system. This is done by positioning two linear line segments on the load vs. displacement graph of the nonlinear, inelastic system such that the area under them is equal to the area under the nonlinear curve

produced by the actual system. The area of the actual system is defined as that enclosed by the nonlinear load vs. displacement curve, the displacement axis and an imaginary vertical line projected down (or up) from $0.8F_{peak}$ on the degradation portion of the curve. Thus, the amount of energy dissipated by the elastic-plastic system has been set equal to that of the actual nonlinear, inelastic system. The actual load vs. displacement, envelope and EEEP curves used to analyze a cyclic test are displayed in Figure 4.1.

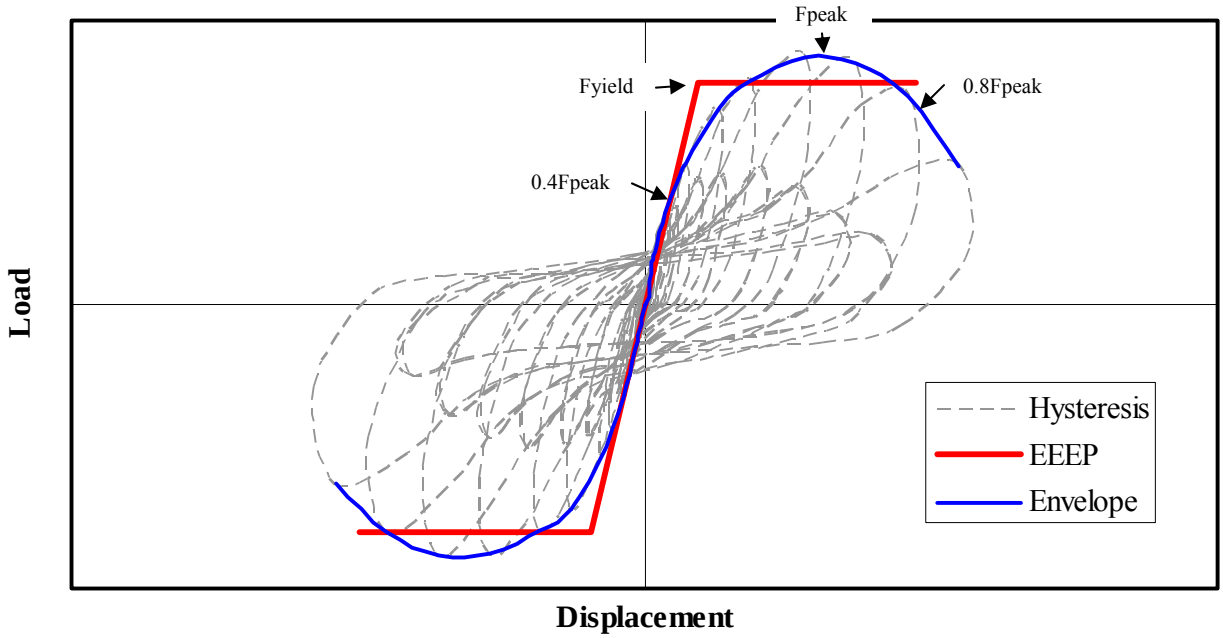

Figure 4.1. EEEP parameters

The line segment that represents the elastic properties of the system is placed such that it passes through the origin and the point of $0.4F_{peak}$ on the nonlinear curve of the actual system. The horizontal line segment, representing the plastic properties of the system, is positioned such that the energy dissipated by both the actual and EEEP systems is equal. The load intercept of this line must always be greater than or equal to $0.8F_{peak}$. The intersection of the two lines determines the yield load and displacement of the nonlinear, inelastic system.

The EEEP method was originally developed to transform nonlinear, inelastic systems tested monotonically. However, this method can also be used to transform test data of cyclic tests once an envelope curve is fitted through the peaks of the cyclic test. The envelope curve

resembles the load vs. displacement curve of a monotonic test and the procedure is identical. It should be noted that the area under the envelope curve is not the total energy dissipated by the system. The actual amount of energy dissipated by the system is much greater because the many hysteresis loops of a cyclic test overlap one another. However, the EEEP method is still an effective measure to determine and compare the performance characteristics of nonlinear, inelastic systems. Also, a cyclic test produces results in both a negative and positive direction. Each performance characteristic reported is the average of the absolute value of both the negative and positive result.

4.1.3 Strength and Displacement

Strength is defined as the load capacity of the wall. The peak load (F_{peak}) is the maximum load resisted by the wall during testing. Walls of light-frame construction rarely exhibit a sudden decrease in load capacity. Therefore, the wall is considered to have failed once the load capacity of the wall decreases to $0.8F_{peak}$ on the degradation portion of the envelope curve. The yield strength determined from the bilinear EEEP curve is not the load at which the actual system begins to display inelastic behavior. The actual yield strength of the system is much lower and usually occurs around $0.4F_{peak}$. The yield strength reported is simply a comparative parameter.

The displacements at which these loads occur provide almost as much insight to the response of the wall as the load itself. Parameters defined in the following subsections, such as stiffness and ductility, are functions of displacement. In fact, the displacement at failure provides much more information about the behavior of the system than the corresponding load. In this investigation, and many other light-frame shear wall investigations, the failure load is found by multiplying peak load by 0.8. This parameter does not provide any additional information when comparing two wall configurations. The configuration with the higher peak load will possess a higher failure load. However, the displacement at which this load occurs can be a valuable parameter because it is a function of the wall properties and not the load. Thus, a wall that is able to resist load at a greater level of displacement is indicative of a ductile configuration and would perform well when subjected to earthquake loadings.

4.1.4 Elastic Stiffness

The elastic stiffness, k_e, is defined as the slope of the elastic line segment of the EEEP curve. It is actually a secant stiffness that passes through the origin and $0.4F_{peak}$ on the envelope curve. The load at $0.4F_{peak}$ is a good approximation of the elastic limit of a light-frame shear wall. Once the displacement corresponding to $0.4F_{peak}$ is exceeded, the wall begins to behave inelastically and permanent deformations are present. Elastic stiffness is determined by the following equation:

$$k_e = 0.4F_{peak} / \Delta_{0.4Fpeak} \quad (4.1)$$

4.1.5 Cyclic Stiffness

The stiffness of each cycle, k_c, is the slope of the line passing through the origin and the point of peak load on the load vs. displacement graph. A cyclic test produces peak loads in the negative and positive directions; therefore, the two slopes of each cycle are averaged. This parameter provides excellent information about the ability of the structure to resist load at various levels of displacement. A graph of the cyclic stiffness of each primary cycle vs. the peak displacement reached in that cycle is included in the Appendix. This plot clearly displays the stiffness degradation of the structure. Stiffness degradation of a shear wall is the result of two phenomena's: displacement of the sheathing nail past the elastic limit and crushing of the fibers in the sheathing panel and framing around the shank of the sheathing nail.

4.1.6 Ductility

Ductility is an important aspect of a structure designed to resist seismic forces. It can be defined as the structure's ability to deform and resist load without suffering sudden failure. In this investigation, it is defined as the ratio of the displacement at failure ($\Delta_{failure}$) to the displacement at yield (Δ_{yield}).

$$\mu = \Delta_{failure} / \Delta_{yield} \quad (4.2)$$

A large ductility factor represents a structure that will not fail in a sudden, brittle manner. However, the ductility factor defined in this manner is not a direct indication of a wall that will

perform well when subjected to seismic forces. Walls that have large aspect ratios and no hold-down restraint can experience large deformations without incurring failure due to the presence of significant rigid body rotation. Therefore, $\Delta_{failure}$ increases while Δ_{yield} remains low and the ductility factor is exaggerated. These types of walls do not actually perform well when subjected to seismic forces because they dissipate only minimal amounts of energy.

4.1.7 Energy Dissipation

Another important aspect of a structure designed to resist seismic forces is its ability to dissipate energy. Shear walls dissipate energy through the hysteretic behavior of the sheathing-to-framing connections. Some energy is dissipated through the occurrence of friction forces between adjacent panels and panels and framing members, but this is minimal.

Hysteretic behavior of a member is defined as permanent deformation upon load removal. On a microscopic level, loads acting on the sheathing nail that are greater than its yield strength cause the atomic bonds connecting the crystalline structure of the elements comprising the sheathing nail to break and realign (Boresi 1993). The realignment of the crystalline structure is permanent. Therefore, permanent deformation has occurred.

Theoretically, shear walls cycled to displacements within the elastic limit will not dissipate any hysteretic energy. At displacements greater than the elastic limit (0.2 to 0.35 in.), the nails in the panel experience inelastic bending and a permanent deformation. The hysteretic behavior of the sheathing nails can be represented by plotting the load vs. displacement response of the wall when subjected to a reversed, cyclic loading. When the wall is cycled to displacements within the elastic limit, any deformations that occur in the nail will be recovered upon unloading and the load vs. displacement graph will plot a straight line. Once the wall is cycled to displacements greater than the elastic limit, permanent deformations will occur that will not be recovered upon unloading and the load vs. displacement graph will plot a loop. The area enclosed within the "hysteresis" loop represents the energy dissipated in that cycle and is determined by integration. In this investigation, the energy dissipated by each primary cycle and the cumulative energy dissipated until failure were determined and are tabulated in the Appendix.

The ability of a vibrating system to bring itself to rest is defined as damping. This occurs once the energy imparted upon the system has been radiated away, usually in the form of heat.

Depending on the structure, damping can originate from many sources; thus, it is a complex, nonlinear parameter which is difficult to model. In an attempt to ease analysis, the damping ability of a structure is typically modeled as a viscous damping coefficient which behaves linearly at low levels of velocity (Humar 2002). In this investigation, the amount of damping present in the system has been determined experimentally. A parameter known as the equivalent viscous damping ratio, $\zeta_{eq,}$ has been developed in order to relate the actual damping present in the structure (hysteretic damping, W_D) per cycle to the damping that would be present in the structure if viscous damping was assumed. It is determined according to Equation 4.3.

$$\zeta_{eq} = W_D / 2\pi U_o \tag{4.3}$$

The term U_o in Equation 4.3 represents the strain energy of the system that would be recovered once the load acting on the system is removed. U_o is determined by computing the area of the triangles ABC and ADE in Figure 4.2. The ξ_{eq} changes throughout the test and has been tabulated in the Appendix for each primary cycle.

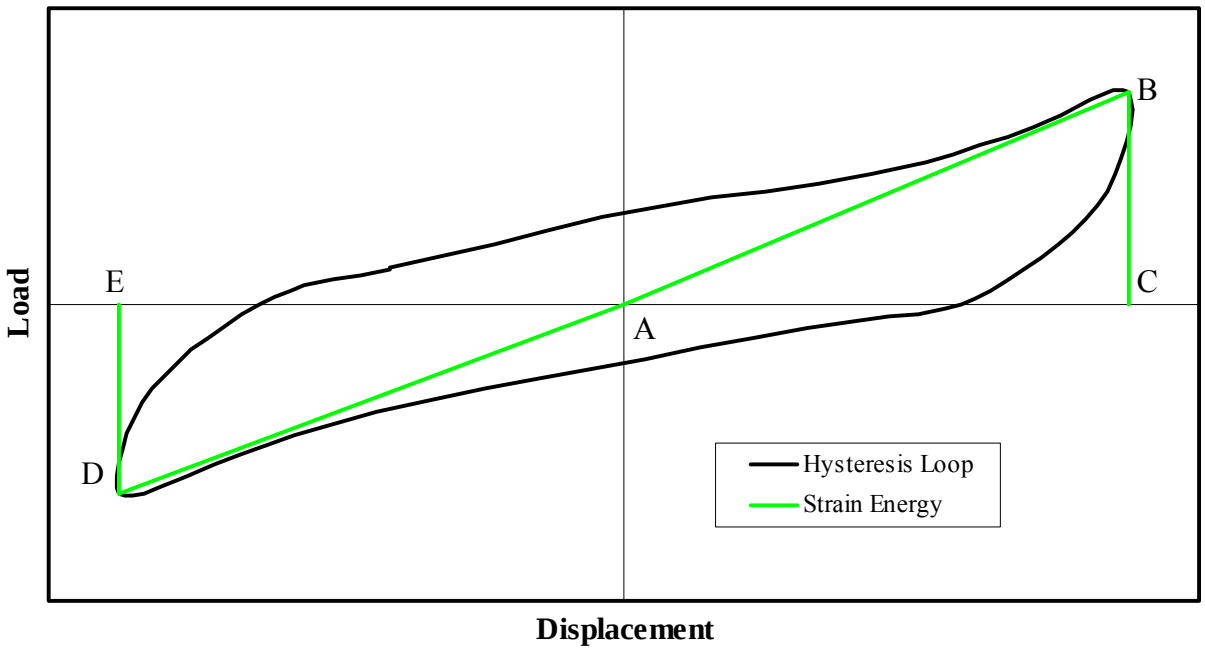

Figure 4.2. Hysteretic damping and strain energy of one cycle

4.1.8 Displacement Components

In this investigation, the global lateral displacement of the top of the wall has been separated into three individual components of displacement: rigid body rotation of the entire wall (Δ_r), shear deformation of the entire wall (Δ_s) and a component that is the combination of bending in the double end studs and slip of the sheathing connections ($\Delta_{b\ \&\ slip}$).

The global displacement of walls without hold-down restraint has been separated into two components: Δ_r and Δ_s. In the absence of a mechanical hold-down device, the double end stud lacks the sufficient stiffness necessary to develop bending deformations. Therefore, this component of displacement is not present in prescriptive walls. The global displacement of walls equipped with mechanical hold-down devices has been separated into the three components discussed above: Δ_r, Δ_s and Δ_b.

The components of displacement have been determined according to the global lateral displacement at peak load. Also, only the displacements produced from contraction of the ram have been analyzed. The line of action of the ram when contracted was much more representative of an actual loading than when it was extended. Due to the hinge between the piston of the ram and the load distribution beam, the line of action of the force buckled away from the base of the wall when extended; thus, additional uplift force was acting on the wall.

4.1.8.1 Rigid Body Rotation

Rigid body rotation is present when the double end stud in tension lifts from the bottom plate. Once this occurs, the wall is simply rotating about the toe of the wall. This is the most undesirable form of displacement. A wall displacing in this manner is not performing efficiently because the majority of the force in the sheathing panel is acting on the sheathing-to-framing connections along the bottom plate. Therefore, the rest of the sheathing connections along the perimeter of the panel are not performing work. Rigid body rotation has been diagramed in Figure 4.3. The component of lateral displacement attributed to rigid body motion is determined according to Equation 4.4.

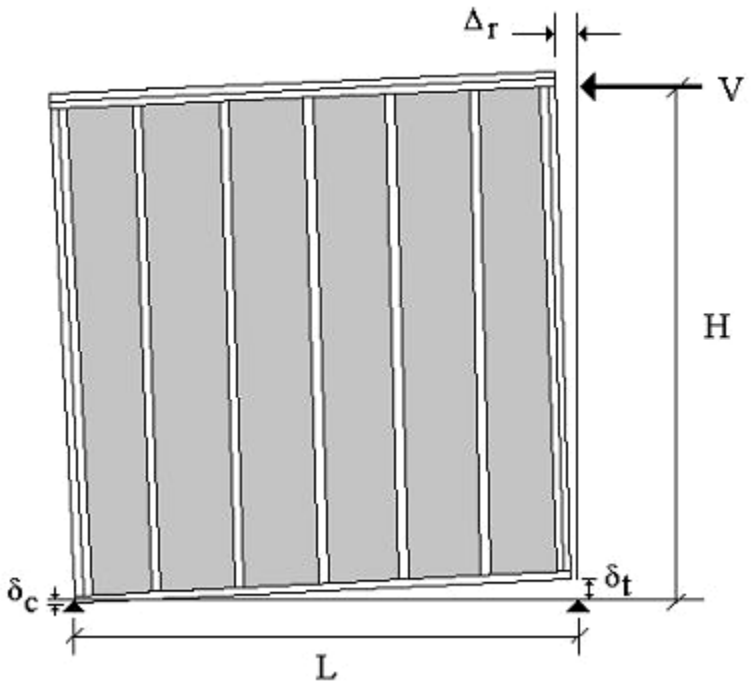

Figure 4.3. Rigid body rotation

$$\Delta_r = (\delta_c + \delta_t)\, H / L \tag{4.4}$$

4.8.1.2 Shear Deformation of Entire Wall Assembly

If the component of shear deformation of the entire wall is large, the wall is performing very efficiently. When this occurs, the frame of the wall is displacing in the shape of a parallelogram and the sheathing panels are rotating about their centroids. Rotation of the sheathing panels is a result of bending deformations in the sheathing connections. This type of displacement is also known as racking behavior and has been displayed in Figure 4.4. In prescriptive walls, Δ_s was determined by subtracting Δ_r from the total lateral displacement (Δ_T). The data obtained from Pots 7 and 8 can not be used to determine Δ_s because they also contain a component of uplift displacement. The component of shear deformation in prescriptive walls was calculated according to Equation 4.5.

$$\Delta_s = \Delta_T - \Delta_r \tag{4.5}$$

The hold-downs of engineered walls eliminate uplift displacement of the double end stud in tension; therefore, Δ_s can be computed using the data obtained from Pots 7 and 8. The component of Δ_s in engineered walls was determined according to Equation 4.7 (or 4.9). In these equations, the angle theta (θ) between the original vertical edge of the double end stud (or common center stud) and the deformed diagonal was determined first using equation 4.6 (or 4.8). In order to calculate theta, it was assumed that the height of the wall remained constant during testing and that no axial shortening occurred. Then, Δ_s was determined by substituting the value of theta in Equation 4.7 (or 4.9). Both Equations 4.7 and 4.9 determine the same parameter, Δ_s. Equation 4.7 uses the data obtained by Pot 7 and Equation 4.9 uses that of Pot 8. The values of Δ_s determined by Equations 4.7 and 4.9 were then averaged to arrive at the value of Δ_s presented in the Appendix.

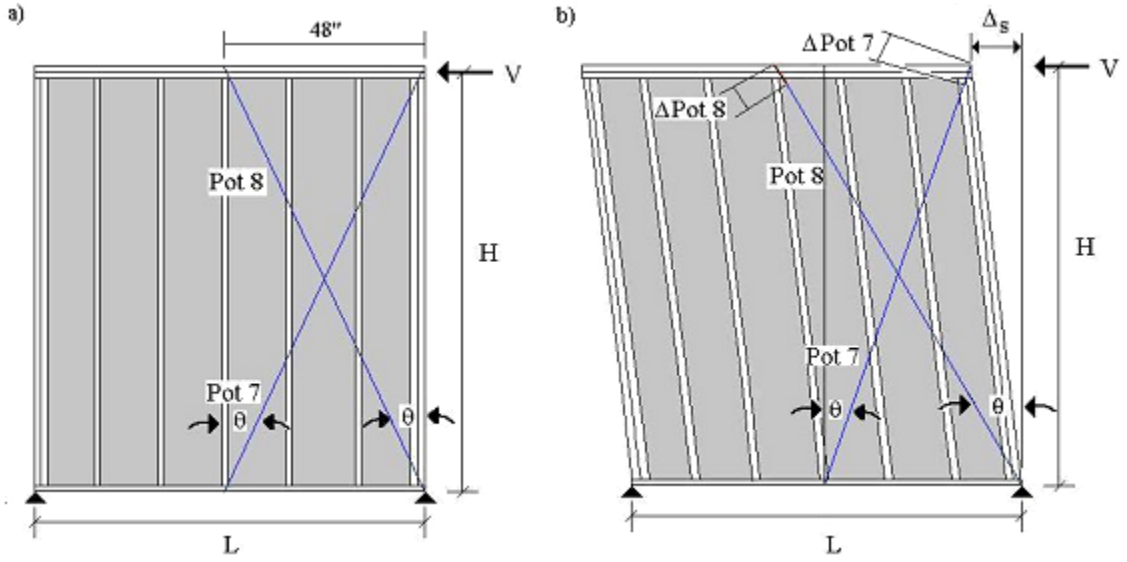

Figure 4.4. Shear deformation of entire wall assembly

a) Undeformed, b) Deformed

Shear deformation of engineered walls:

Using the data of Pot 7:

$$\text{Cos}(\theta) = H / [(H^2 + (0.5L)^2)^{1/2} + \Delta_{Pot\,7}] \quad (4.6)$$

$$\text{Sin}(\theta) = (48 - \Delta_s) / [(H^2 + (0.5L)^2)^{1/2} + \Delta_{Pot\,7}] \quad (4.7)$$

Using the data of Pot 8:

$$\text{Cos}(\theta) = H / [(H^2 + (0.5L)^2)^{1/2} + \Delta_{\text{Pot 8}}] \quad (4.8)$$

$$\text{Sin}(\theta) = (48 + \Delta_s) / [(H^2 + (0.5L)^2)^{1/2} + \Delta_{\text{Pot 8}}] \quad (4.9)$$

$$\Delta_s = (\Delta_{s\,4.7} + \Delta_{s\,4.9}) / 2 \quad (4.10)$$

4.8.1.3 Bending Deformation of Double End Studs and Nail slip

The combination of the mechanical hold-down device and sheathing connections at the base of an engineered wall produced some what of a fixed connection to the rigid foundation. This allowed the double end studs to behave like cantilever beams. Also, the hold-down device caused the force in the panel to be distributed evenly to all sheathing connections along the perimeter of the sheathing panels. Therefore, more force was present at the top of the double end stud in an engineered wall than was in a prescriptive wall. The some what fixed connection at the base and greater force at the top caused slight bending deformations to occur in the double end stud. However, the amount of deformation due to bending of the double end stud is very small, usually less than 0.2 inches (Salenikovich 2000). Also, this component accounts for any slip that occurred between the sheathing nail and wood. In this investigation, Δ_b was determined by subtracting Δ_r and Δ_s from the global lateral displacement (Δ_T). The equation of Δ_b is:

$$\Delta_b = \Delta_T - \Delta_s - \Delta_r \quad (4.11)$$

Usually, this equation produced a small negative value of bending. If this occurred, Δ_b was assumed to be zero. There was obviously a source of error in the data acquisition set up because a negative value of bending is not possible. The source of error was in the placement of the Pots that determined the uplift and compressive displacements of the double end studs. This placement caused a slight magnification of the values recorded by these Pots because they were not placed directly in line with the point of rotation of the wall (the hold-down bolt of an engineered wall). However, as was explained in Chapter 3, this was simply not possible. Thus, Δ_r computed according to Equation 4.4 was slightly larger than what actually occurred and small negative values of Δ_b were usually determined according to Equation 4.11.

4.2 8 Feet Tall Prescriptive Shear Walls

Two 8 feet (2.4 m) tall prescriptive shear wall configurations were tested in order to determine the performance capabilities of long sheathing panels. The walls of **8-8-P** were sheathed with 4 x 8 feet (1.2 x 2.4 m) panels. Configuration **8-8.5-P** was designed to determine if long sheathing panels could be used to produce increased values of strength and stiffness. The configuration of these walls consisted of an 8 feet (2.4 m) tall wall attached to a 2 x 12 and sheathed with an 8.5 feet (2.55 m) long panel extended past the bottom plate onto the 2 x 12.

The response of configurations **8-8-P** and **8-8.5-P**, when subjected to lateral load, is displayed in Figure 4.5. In this figure, the envelope curve of each configuration is presented. These envelope curves were produced from the average load vs. displacement values of the three walls that comprised each configuration. The arrows in Figure 4.5 display the range of values between the three walls of each configuration at peak load.

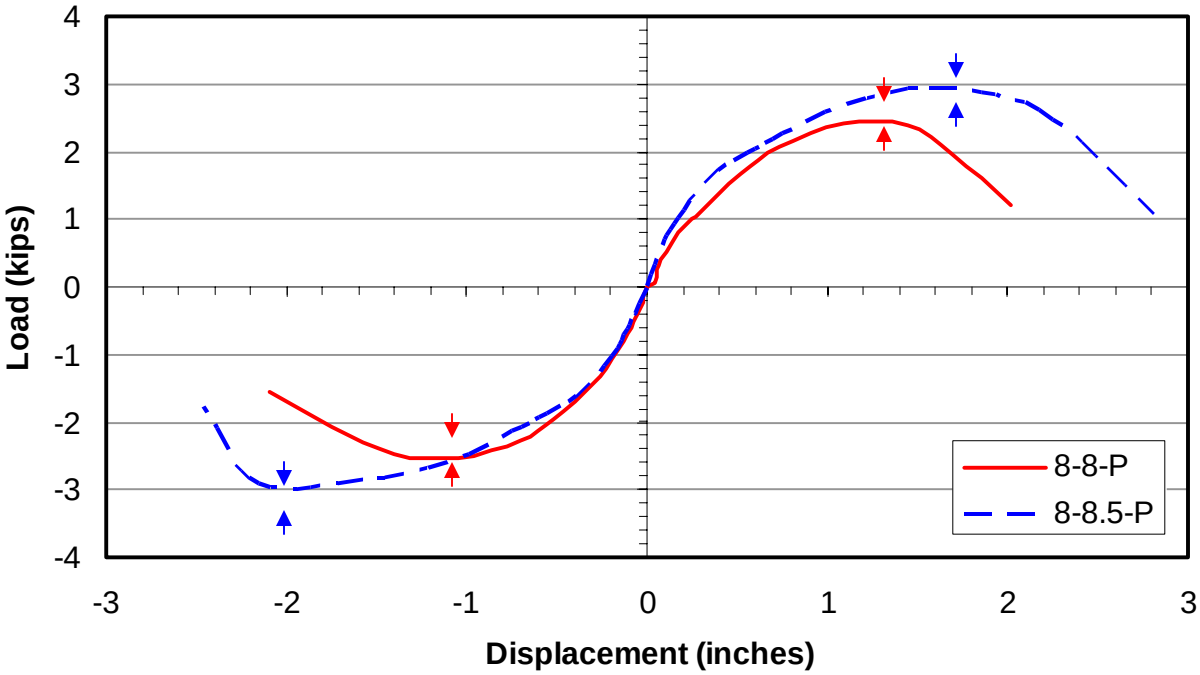

Figure 4.5. Average load vs. displacement of configuration **8-8-P** and **8-8.5-P**

The values of F_{yield}, F_{peak}, $0.8F_{peak}$ and the corresponding displacements of **8-8-P** and **8-8.5-P** are presented in Table 4.1. These are the average values of load and displacement produced from both the positive and negative excursions of the ram for each wall of the configuration. One wall of **8-8-P** and two walls of **8-8.5-P** attained peak load due to contraction

of the ram at a greater lateral displacement than due to extension of the ram. This occurred because contraction of the ram produced a truer line of action of force which allowed the wall to display more racking behavior.

Table 4.1. Average strength and displacement values of **8-8-P** and **8-8.5-P**

Configuration	$\mathbf{F_{yield}}$ (kips)	$\mathbf{\Delta_{yield}}$ (inches)	$\mathbf{F_{peak}}$ (kips)	$\mathbf{\Delta_{peak}}$ (inches)	$\mathbf{F_{failure}}$ (kips)	$\mathbf{\Delta_{failure}}$ (inches)
8-8-P	2.26	0.5	2.50	1.2	2.00	1.7
8-8.5-P	2.58	0.5	2.97	1.5	2.37	2.3

The long panels used in **8-8.5-P** produced average values of F_{peak} and $0.8F_{peak}$ that were 18% greater than those produced by **8-8-P**. Values of force and displacement at yield were determined according to the EEEP Curve. These curves have been included in the Appendix. The F_{yield} of **8-8.5-P** was approximately 15% larger than F_{yield} of **8-8-P**. It should be noted that yield values can only be used to compare the configurations and are not the actual values at which the structure begins to behave inelastically. Typically, the proportional limit of a shear wall is about $0.4F_{peak}$.

The long panels used in **8-8.5-P** also increased the amount of additional displacement necessary to fail the configuration. The amount of additional displacement that was required to induce failure of **8-8-P** and **8-8.5-P** was 0.5 and 0.8 inches (12.7 and 20.3 mm), respectively. Thus, a 60% increase in displacement capacity was achieved by extending long panels onto the 2 x 12 in **8-8.5-P**.

The average values of elastic stiffness at $0.4F_{peak}$ of **8-8-P** and **8-8.5-P** are displayed in Table 4.2. These values were determined by averaging the values of each wall of the configuration. The long sheathing panels extended down onto the 2 x 12 in **8-8.5-P** increased k_e slightly.

Table 4.2. k_e of **8-8-P** and **8-8.5-P**

	8-8-P	**8-8.5-P**
k_e (kips/inch)	4.8	5.0

The k_c values of **8-8-P** and **8-8.5-P** are displayed in Figure 4.6. These values were determined by averaging the values of each wall of the configuration. The arrows in Figure 4.6 display the range of values at peak k_c for all three walls of each configuration. The stiffness degradation of the two configurations is readily apparent. Also, the stiffness degradation at lateral displacements greater than 1.0 inch (25.4 mm) was greater in **8-8-P** than **8-8.5-P**.

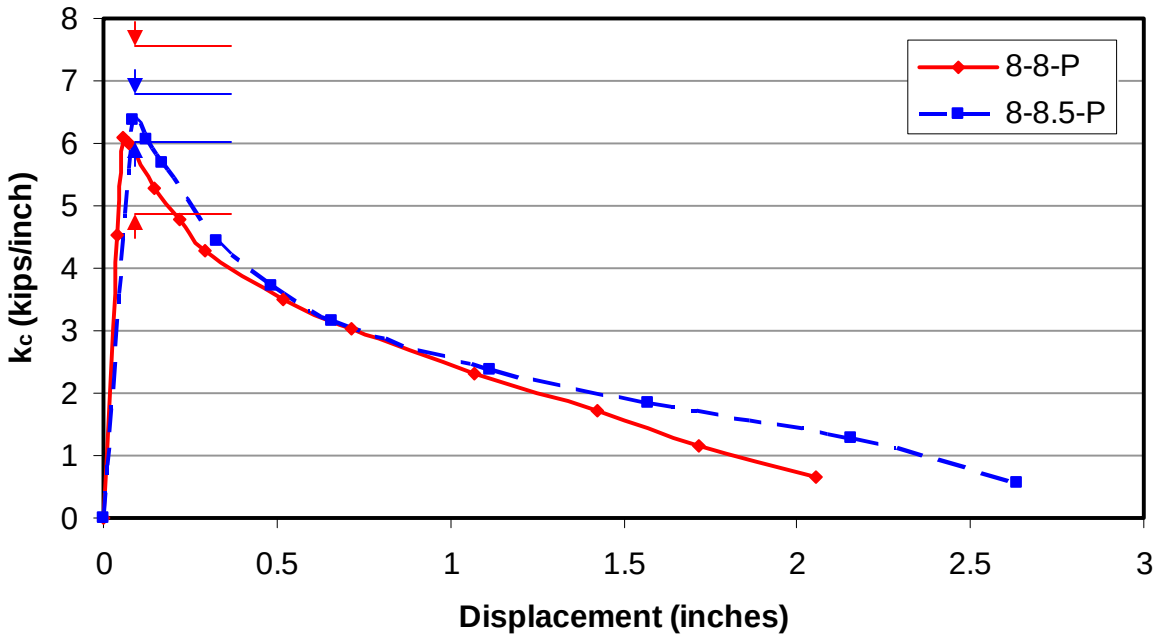

Figure 4.6. Average cyclic stiffness vs. displacement of **8-8-P** and **8-8.5-P**

The amount of energy dissipated until failure by **8-8-P** and **8-8.5-P** is displayed in Table 4.3. The amount of energy dissipated until failure by **8-8.5-P**, 3.9 kip-ft (5.3 kN-m), was 40% greater than the amount of energy dissipated by **8-8-P**. This occurred because the extended sheathing panel inhibited rigid body motion until larger lateral displacements of the ram had taken place. Thus, the sheathing connections along the perimeter of the panel at the top and sides of the wall were able to perform more work. Also, once rigid body motion begins to take place, the majority of force in the panel of a typical prescriptive shear wall acts on the sheathing connections along the bottom plate. Thus, increasing the number of connections along the bottom edge of a panel increases the amount of energy that the wall is capable of dissipating.

Table 4.3 Hysteretic energy dissipated until failure by **8-8-P** and **8-8.5-P**

	8-8-P	**8-8.5-P**
Energy Dissipated Until Failure (kip-ft)	2.8	3.9

Simply comparing the amount of energy dissipated until failure by the two configurations does not provide information related to the ability of the structure to dissipate energy at specific levels of displacement. An efficient means of doing this is to plot the energy dissipated per cycle vs. the displacement of that cycle. The amount of energy dissipated by **8-8-P** and **8-8.5-P,** when displaced to various amplitudes, is displayed in Figure 4.7. The arrows in Figure 4.7 display the range of values of all three walls of each configuration at the point of maximum energy dissipation. At displacements greater than 0.7 inches (17.8 mm), **8-8.5-P** dissipated more energy. This is due to the fact that significant rigid body motion began to occur in **8-8-P** at 1.0 inch (25.4 mm) of lateral displacement. Once this began to occur, the amount of energy dissipation decreased because the point of rotation of the panel shifted to the bottom plate; thus, only the sheathing nails connecting the panel to the bottom plate were performing significant amounts of work. The long sheathing panels of **8-8.5-P** inhibited rigid body motion until the wall was displaced to 2.0 inches (50.8 mm) of lateral displacement. This allowed the rotation point of the panel to remain at its center until larger lateral displacements had taken place; therefore, all the sheathing nails along the perimeter were performing work.

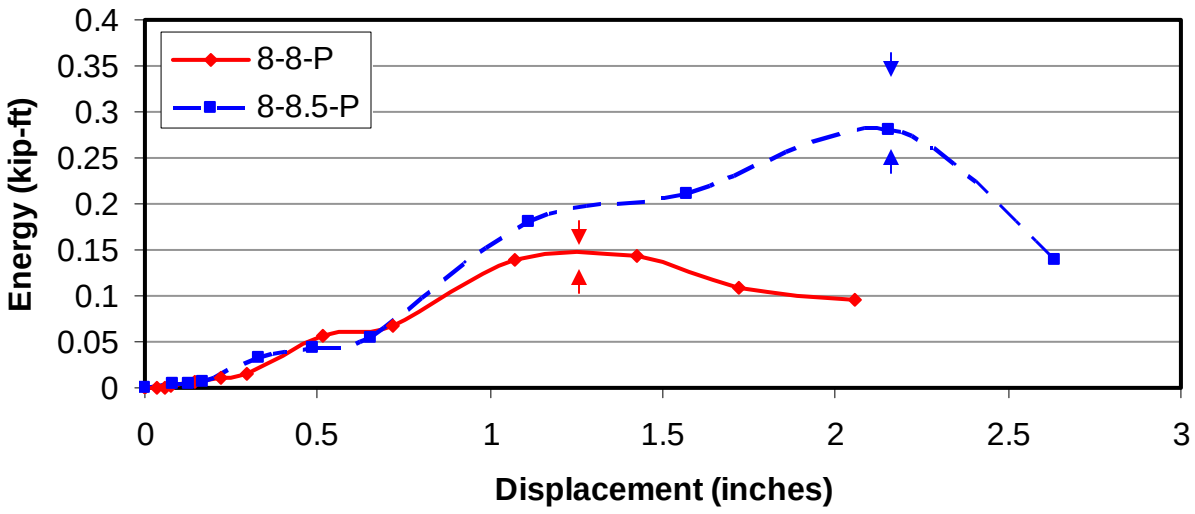

Figure 4.7. Hysteretic energy dissipated per cycle vs. displacement for **8-8-P** and **8-8.5-P**

Rigid body motion dominated the displacement motion of **8-8-P** and **8-8.5-P**. Therefore, neither configuration was able to develop significant racking deformation. Although, the percentage of rigid body motion did decrease from 80% in **8-8-P** to 60% in **8-8.5-P**. Also, significant compressive displacements of almost 0.4 inches (10.2 mm) were recorded under the double end stud in compression in **8-8.5-P** due to the presence of initial curvature in the 2 x 12. This source of rigid body motion would not be present in an actual structure. Therefore, extending a long panel onto the band joist improves racking behavior.

The failure modes of **8-8-P** and **8-8.5-P** were similar. Uplift between the end stud in tension and the bottom plate caused the sheathing connections to tear through the edge of the panel along the bottom plate of **8-8-P**. This is displayed in Figure 4.8. The sheathing connections in the 2 x 12 at the bottom edge of the panel also tore through the edge in **8-8.5-P**. The sheathing nails in the bottom plate of **8-8.5-P** pulled heads through the panel. This is displayed in Figure 4.9. Significant bending deformations occurred in the sheathing connections along the bottom plate of **8-8-P** and **8-8.5-P** and in the sheathing connections in the 2 x 12 of **8-8.5-P** before tear through occurred. Also, the studs separated from the bottom plate in both configurations. At peak load, the largest value of separation occurred under the end stud in tension and varied linearly to zero under the compressive double end stud. The average amount of separation under the double end stud at F_{peak} was 0.9 inches (22.9 mm) for both configurations. This is an interesting point because the global lateral displacement of **8-8.5-P** was on average 0.8 inches (20.3 mm) greater than **8-8-P**. This proves that extending the sheathing panel down onto the 2 x 12 limited uplift of the end stud.

Figure 4.8. Uplift displacement of **8-8-P**

Figure 4.9. Sheathing nail tear through along bottom plate and edge of panel in **8-8.5-P**

4.3 9 Feet Tall Prescriptive Shear Walls

Four 9 feet (2.7 m) tall prescriptive shear wall configurations were tested in order to determine the capabilities of long sheathing panels. The three walls of **9-8-P** were sheathed with 4 x 8 feet (1.2 x 2.4 m) panels. The three walls of **9-9-P** were sheathed with 4 x 9 feet (1.2 x 2.7

m) panels. The three walls of **9-ALT9-P** were sheathed with 4 x 9 feet (1.2 x 2.7 m) panels made from fibers oriented in the alternate direction. The three walls of **9-9.5-P** were sheathed with 4 x 9.5 feet (1.2 x 2.85 m) panels extended past the bottom plate and down onto a 2 x 12.

The response of configurations **9-8-P**, **9-9-P**, **9-ALT9-P and 9-9.5-P**, when subjected to lateral load, is displayed in Figures 4.10, 4.11 and 4.12, respectively. Plotting **9-8-P** and **9-9-P** together, as was done in Figure 4.10, displays the effects of sheathing a 9 feet (2.7 m) tall prescriptive wall with 4 x 9 feet (1.2 x 2.7 m) panels. Plotting **9-9-P** and **9-ALT9-P** together, as was done in Figure 4.11, displays the effects of sheathing a 9 feet (2.7 m) tall prescriptive shear wall with 4 x 9 feet (1.2 x 2.7 m) panels made of fibers oriented in the alternate direction. Plotting **9-9-P** and **9-9.5-P** together, as was done in Figure 4.12, displays the effects of extending a long panel past the bottom plate and onto the band joist of a 9 feet (2.7 m) tall prescriptive wall.

In these figures, the envelope curve of each configuration is presented. These envelope curves were produced from the average load vs. displacement values of the three walls that comprised each configuration. The arrows in Figures 4.10, 4.11 and 4.12 display the range of values between the three walls of each configuration at peak load.

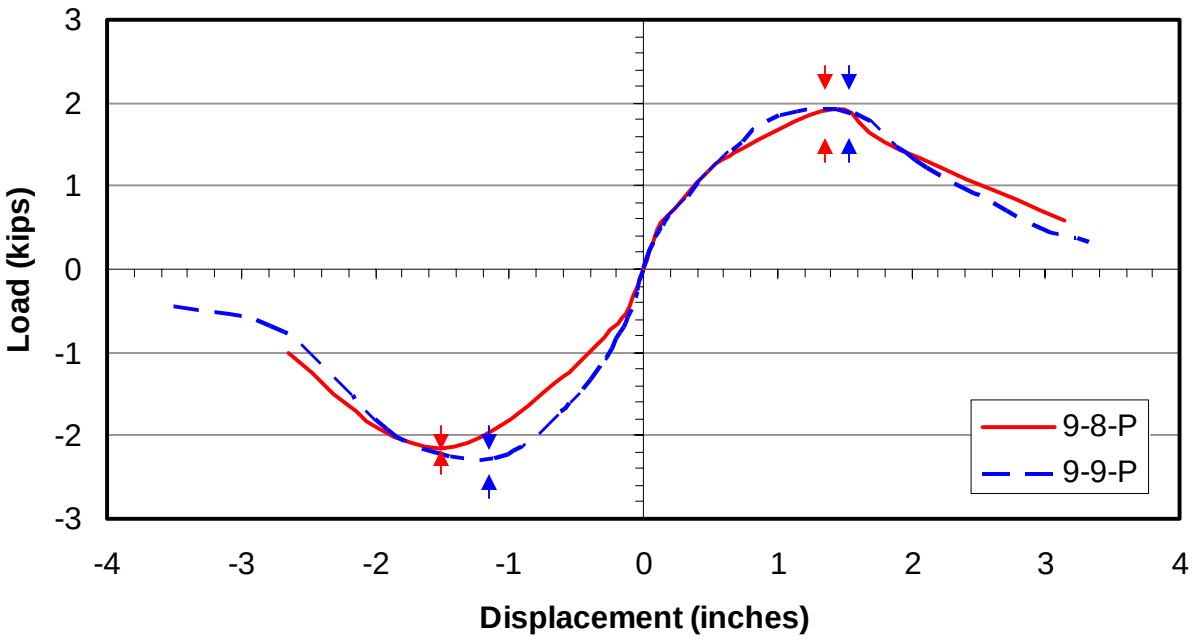

Figure 4.10. Average load vs. displacement of **9-8-P** and **9-9-P**

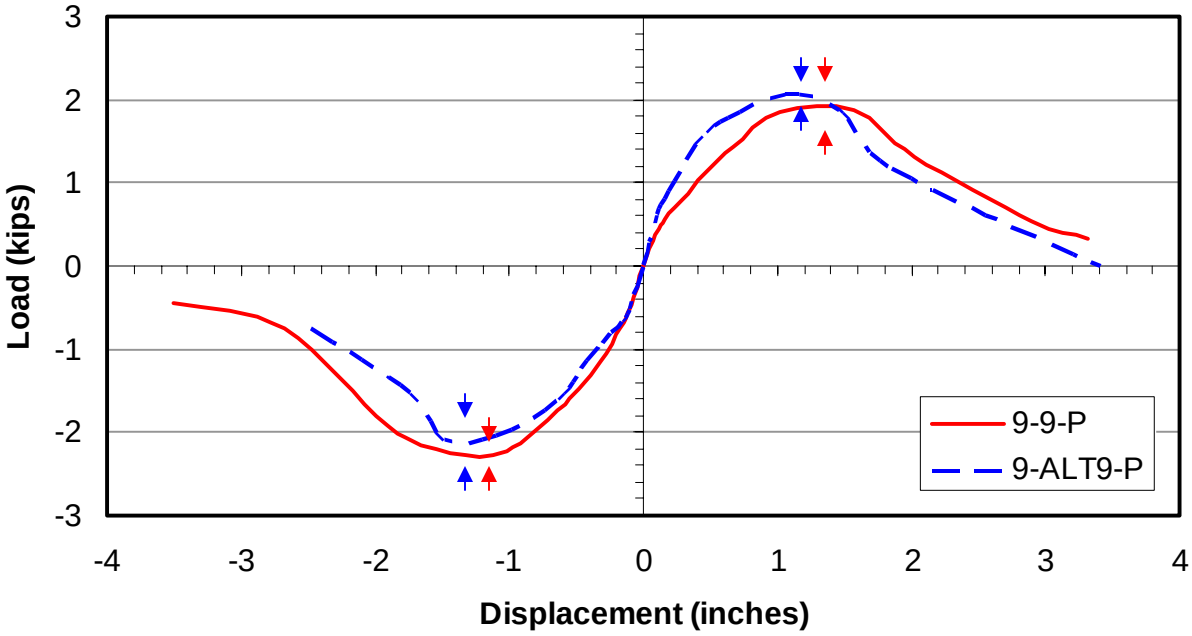

Figure 4.11. Average load vs. displacement of **9-9-P** and **9-ALT9-P**

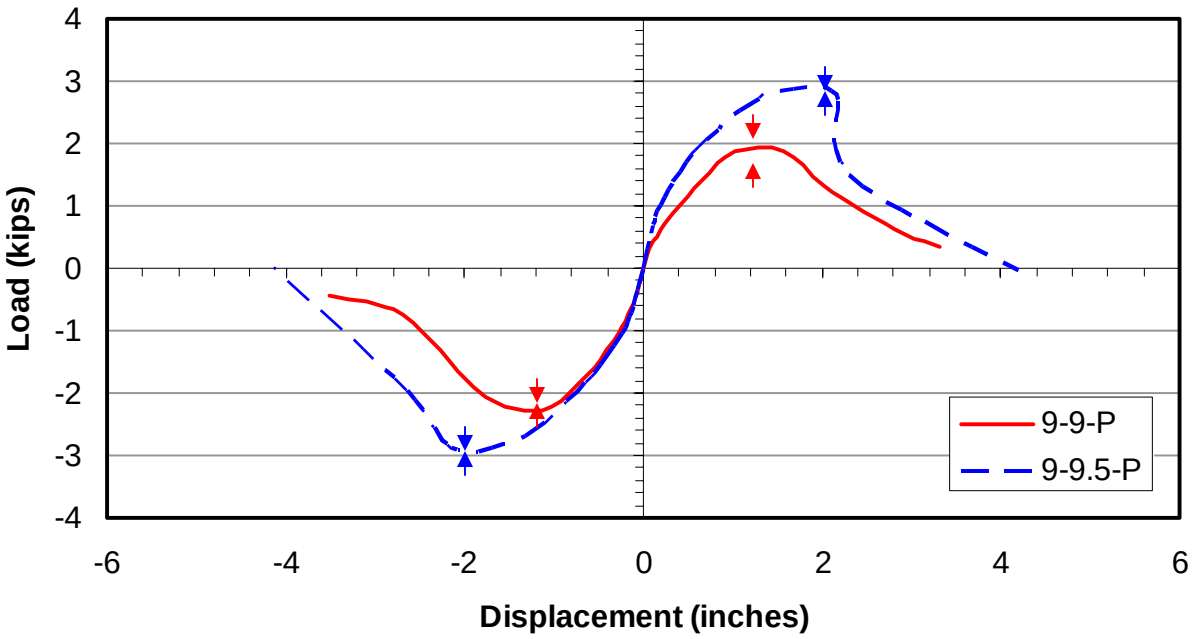

Figure 4.12. Average load vs. displacement of **9-9-P** and **9-9.5-P**

The values of F_{yield}, F_{peak}, $0.8F_{peak}$ and the corresponding displacements of **9-8-P**, **9-9-P**, **9-ALT9-P** and **9-9.5-P** are presented in Table 4.4. These are the average values of load and displacement produced from both the positive and negative excursions of the ram for each wall of the configuration.

Table 4.4. Average strength and displacement values of **9-8-P, 9-9-P, 9-ALT9-P** and **9-9.5-P**

Configuration	$\mathbf{F_{yield}}$ (kips)	$\mathbf{\Delta_{yield}}$ (inches)	$\mathbf{F_{peak}}$ (kips)	$\mathbf{\Delta_{peak}}$ (inches)	$\mathbf{F_{failure}}$ (kips)	$\mathbf{\Delta_{failure}}$ (inches)
9-8-P	1.80	0.7	2.07	1.6	1.63	2.0
9-9-P	1.88	0.6	2.10	1.3	1.69	1.9
9-ALT9-P	1.87	0.5	2.09	1.3	1.66	1.6
9-9.5-P	2.52	0.6	2.90	1.8	2.32	2.3

The average values of F_{yield}, F_{peak} and $0.8F_{peak}$ produced by **9-8-P**, **9-9-P** and **9-ALT9-P** were virtually identical. The alternate orientation of the fibers in the panels used to sheath **9-ALT9-P** did not affect the load capacity. This is consistent with the findings of previous investigators. The long panels extended down onto the 2 x 12 of **9-9.5-P** increased the F_{yield}, F_{peak} and $0.8F_{peak}$ values of a 9 feet (2.7 m) tall prescriptive shear wall 40%. The values of F_{yield} were determined according to the EEEP Curve. These curves have been included in the Appendix. It should be noted that yield values can only be used to compare the configurations and are not the actual values at which the structure begins to behave inelastically. Typically, the proportional limit of a shear wall is about $0.4F_{peak}$.

Use of long panels in **9-9-P** and **9-ALT9-P** did not increase the load capacity of a 9 feet (2.7 m) tall prescriptive shear wall by any significant amount. Although, the long panels did reduce the displacements at which F_{peak} of **9-9-P** and **9-ALT9-P** occurred. The decrease in Δ_{peak} is attributed to the elimination of the internal seam of sheathing connections along the blocking.

The amount of additional displacement (past Δ_{peak}) necessary to induce failure was greatest in **9-9-P**. Typically, structural failures are the result of weak connections. The long panel used in **9-9-P** eliminated the internal seam of sheathing connections along the blocking. The least amount of additional displacement (past Δ_{peak}) required to induce failure occurred in **9-ALT9-P**. One possible explanation of this behavior is that the alternate oriented fibers of the

panels used in **9-ALT9-P** provided less resistance to the source of failure in prescriptive shear walls, sheathing nail tear through along the bottom plate. The largest amount of displacement required to induce failure was recorded in **9-9.5-P**. The extension of the long panel down on to the 2 x 12 provided more resistance to uplift; thus, failure of **9-9.5-P** occurred at a greater level of displacement.

The average values of elastic stiffness, k_e, at $0.4F_{peak}$ of **9-8-P**, **9-9-P**, **9-ALT9-P** and **9-9.5-P** are displayed in Table 4.5. These values were determined by averaging the values of each wall of the configuration. The long sheathing panels of **9-9-P** increased k_e slightly. However, a rather significant increase of k_e occurred in **9-ALT9-P**. Apparently, the alternate oriented fibers increased the stiffness of the system. Extending the long panel down onto the 2 x 12 in **9-9.5-P** produced the largest value of k_e.

Table 4.5. k_e of **9-8-P**, **9-9-P**, **9-ALT9-P** and **9-9.5-P**

	9-8-P	**9-9-P**	**9-ALT9-P**	**9-9.5-P**
k_e (kips/inch)	3.3	3.6	4.3	4.4

Cyclic stiffness (k_c) values of **9-8-P**, **9-9-P**, **9-ALT9-P** and **9-9.5-P** are displayed in Figures 4.13, 4.14 and 4.15. These values were determined by averaging the values of each wall of the configuration. The arrows in Figures 4.13, 4.14 and 4.15 display the range of values at peak k_c for all three walls of each configuration. The stiffness degradation of the configurations is readily apparent. Also, the rate of stiffness degradation at displacements greater than Δ_{peak} was least in **9-9.5-P**. This type of behavior is one of the factors that helped **9-9.5-P** dissipate the most energy.

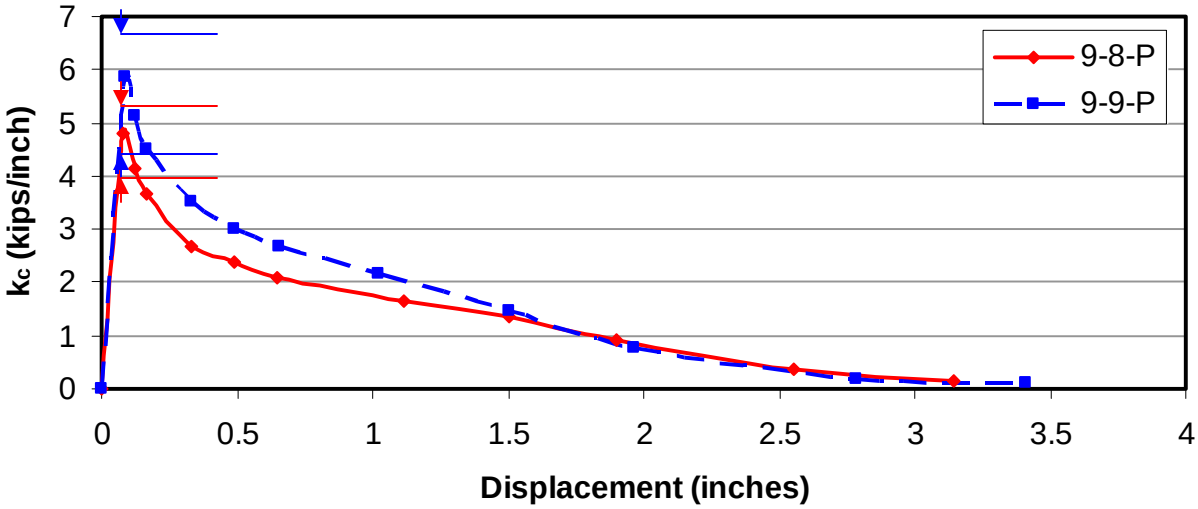

Figure 4.13. Average cyclic stiffness vs. displacement of **9-8-P** and **9-9-P**

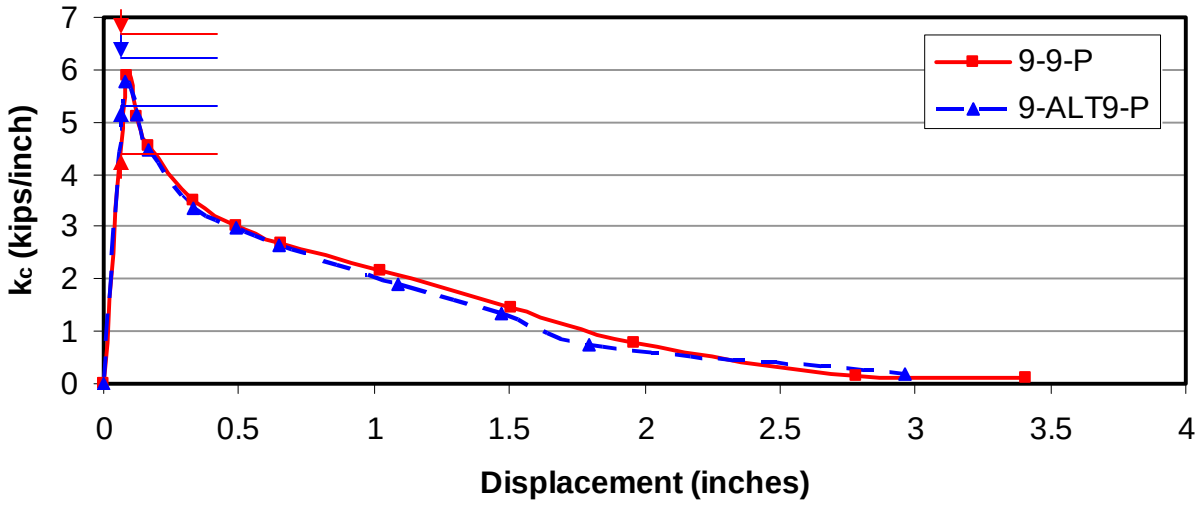

Figure 4.14. Average cyclic stiffness vs. displacement of **9-9-P** and **9-ALT9-P**

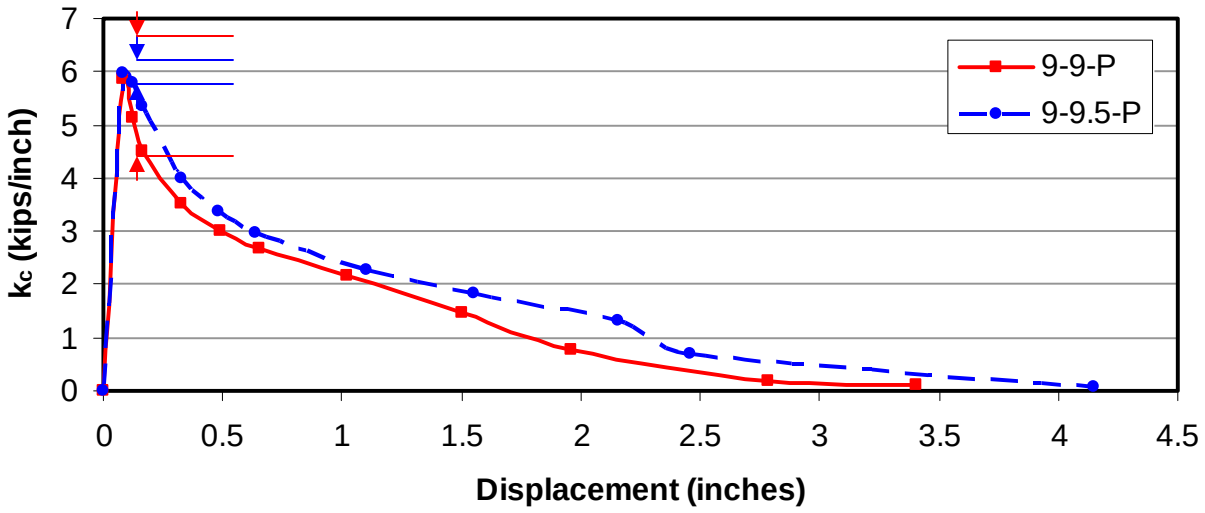

Figure 4.15. Average cyclic stiffness vs. displacement of **9-9-P** and **9-9.5-P**

The amount of energy dissipated until failure by **9-8-P**, **9-9-P**, **9-ALT9-P** and **9-9.5-P** is displayed in Table 4.6. The long panels of **9-9-P** and **9-ALT9-P** did not dissipate as much energy as the 4 x 8 feet (1.2 x 2.4 m) panels of **9-8-P**. This was due to the fact that **9-8-P** was able to resist the same amount of load as **9-9-P** and **9-ALT9-P**, but at a greater level of displacement; thus, it was subjected to more cycles during testing. Extending long panels down onto the 2 x 12 in **9-9.5-P** increased the amount of energy dissipated by a 9 feet (2.7 m) tall prescriptive shear wall 65%. This occurred because the extended sheathing panel inhibited rigid body motion until larger lateral displacements of the ram had taken place. The sheathing connections along the perimeter of the panel at the top and sides of the wall were able to perform more work. Also, once rigid body motion began to take place, the majority of force in the panel of **9-9.5-P** was acting on the sheathing connections along the bottom plate. Thus, increasing the number of connections along the bottom edge of the panel increased the amount of energy that the wall was capable of dissipating.

Table 4.6. Hysteretic energy dissipated until failure by **9-8-P**, **9-9-P**, **9-ALT9-P** and **9-9.5-P**

	9-8-P	**9-9-P**	**9-ALT9-P**	**9-9.5-P**
Energy Dissipated Until Failure (kip-ft)	2.6	2.3	2.4	4.3

Simply comparing the amount of energy dissipated until failure by the configurations does not provide information related to the ability of the structure to dissipate energy at specific levels of displacement. An efficient means of illustrating this variable is to plot the energy dissipated per cycle vs. the displacement of that cycle. The amount of energy dissipated by **9-8-P**, **9-9-P**, **9-ALT9-P** and **9-9.5-P,** when displaced to various amplitudes, is displayed in Figures 4.16, 4.17 and 4.18. The arrows in Figures 4.16, 4.17 and 4.18 display the range of values of all three walls of each configuration at the point of maximum energy dissipation.

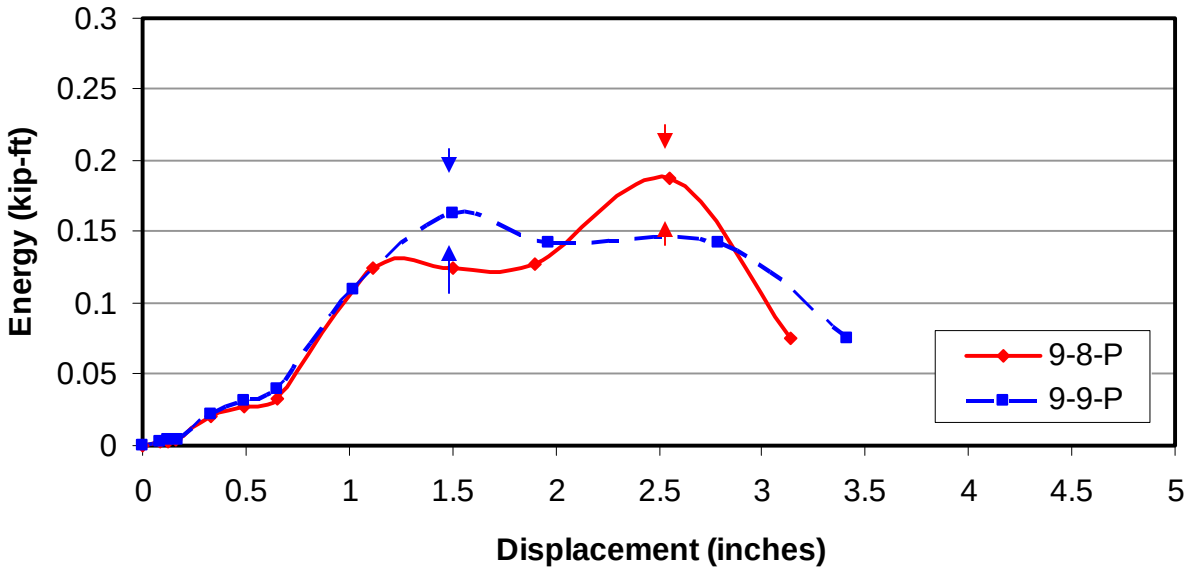

Figure 4.16. Hysteretic energy dissipated per cycle of **9-8-P** and **9-9-P**

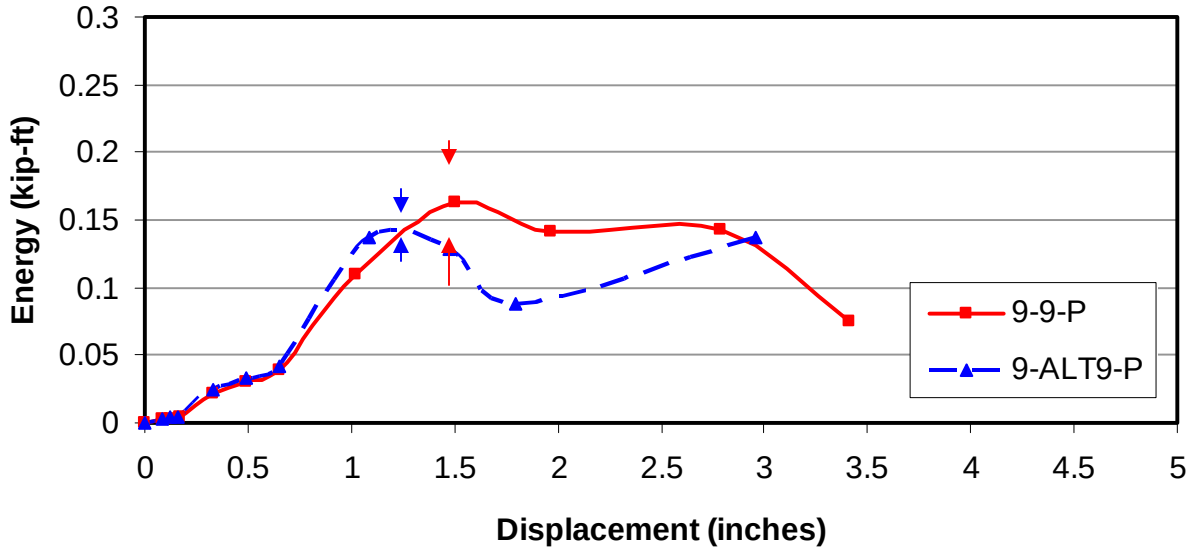

Figure 4.17. Hysteretic energy dissipated per cycle of **9-9-P** and **9-ALT9-P**

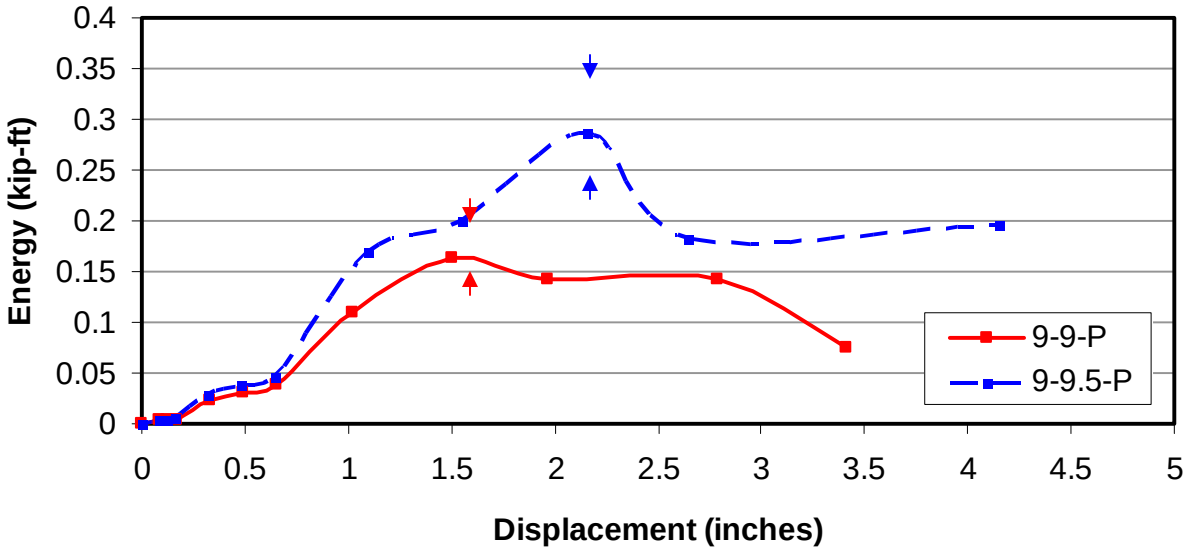

Figure 4.18. Hysteretic energy dissipated per cycle of **9-9-P** and **9-9.5-P**

At lateral displacements of 1.0 inch (25.4 mm), **9-8-P** and **9-ALT9-P** began to experience rigid body motion and the amount of energy dissipated by these two configurations did not increase as lateral displacement was increased. However, between lateral displacements of 2.0 and 2.5 inches (50.8 and 63.5 mm), the panels of **9-8-P** acquired a significant increase in rigidity and the increased movement of the frame relative to the panels caused a large amount of energy to be dissipated. This could have been the result of the four panels of this wall binding upon one another at large displacements. Rigid body motion began to occur in **9-9-P** at 1.5 inches (38.1 mm) of lateral displacement. The amount of energy dissipated by this configuration remained fairly constant as lateral displacement was increased. The long sheathing panels of **9-9.5-P** inhibited rigid body motion until the wall was displaced to 2.5 inches (63.5 mm) of lateral displacement. This allowed **9-9.5-P** to dissipate much more energy than any other 9 feet (2.7 m) tall prescriptive shear wall.

Once rigid body motion began to occur, the amount of energy dissipation decreased because the point of rotation of the panel shifted to the bottom plate; thus, only the sheathing nails connecting the panel to the bottom plate were performing significant amounts of work. The long sheathing panels of **9-9.5-P** inhibited rigid body motion until the wall was displaced to greater amplitudes. This allowed the rotation point of the panel to remain at its center until

larger lateral displacements had taken place; therefore, all the sheathing nails along the perimeter were performing work.

Figures 4.16, 4.17 and 4.18 also provide information pertaining to the behavior of the system after $\Delta_{failure}$. Figure 4.17 shows that the ability to dissipate energy of walls with sheathing panels made from alternate oriented fibers (**9-ALT9-P**) decreased severely after $\Delta_{failure}$.

None of the configurations were able to develop significant racking deformation. At peak load, an average of 0.75 inches (19.1 mm) of uplift occurred between the bottom plate and end stud in tension in **9-8-P**, **9-9-P** and **9-ALT9-P**. Average displacement at peak load of these configurations was 1.5 inches (38.1 mm). Thus, rigid body motion accounted for at least two-thirds of the global lateral displacement. A slight increase in racking behavior was present in **9-9.5-P**. The average amount of uplift under the end stud in tension at Δ_{peak} was 0.8 inches (20.3 mm). The average Δ_{peak} of **9-9.5-P** was 2.0 inches (50.8 mm). Therefore, extending the long panels down on to the 2 x 12 reduced uplift significantly. However, rigid body motion was still present and accounted for 60% of the total lateral displacement of **9-9.5-P**. As discussed for **8-8.5-P**, compressive displacements of almost 0.4 inches (10.2 mm) occurred in two walls of **9-9.5-P** due to initial curvature of the 2 x 12 members. Thus, rigid body motion would be less significant in an actual structure.

The typical failure mode of **9-8-P**, **9-9-P** and **9-ALT9-P** consisted of sheathing nails tearing through the edge of the panel under the end stud in tension. This type of failure progressed inwards along the bottom plate as the lateral displacement was increased. Figure 4.19 displays sheathing nail tear through along the bottom plate after the wall had been tested to complete failure. The sheathing connections along the bottom plate experienced significant bending deformations. Also, separation between the bottom plate and studs occurred. At peak load, the amount of separation varied linearly from 0.75 inches (19.1 mm) under the end stud in tension to zero at the compressive stud. There was no significant separation between studs and double top plate nor were there any significant failures around the small panel segments of **9-8-P**. A cross grain crack formed in the bottom plate at the first anchor bolt in 22 walls of configuration **9-ALT9-P**, but it did not result in complete failure of the bottom plate.

The failure mode of **9-9.5-P** was similar to that described for **8-8.5-P,** except the sheathing nails in the 2 x 12 experienced withdrawal instead of tear through. Withdrawal occurred because there was not as much force acting on the sheathing nails of **9-9.5-P** as there

was in **8-8.5-P** because the length of the panel was increased. This allowed some of the nails to work themselves out in withdrawal instead of tearing through the edge of the panel. Figure 4.20 displays this type of behavior. Two walls of **9-9.5-P** also experienced sheathing nail tear through in both panels along the bottom half of the center stud. However, the amount of force and displacement attained by **9-9.5-P** was much greater than any other 9 feet (2.7 m) tall prescriptive wall. Also, only a 3/8 inch (9.5 mm) edge distance was possible at these locations.

Figure 4.19. Sheathing nail tear through along bottom plate of **9-ALT9-P**

Figure 4.20. Withdrawal of connections along bottom plate and edge of panel in **9-9.5-P**

4.4 10 Feet Tall Prescriptive Shear Walls

Two 10 feet (3.0 m) tall prescriptive shear wall configurations were tested in order to determine the performance capabilities of long sheathing panels. The two walls of **10-8-P** were sheathed with 4 x 8 feet (1.2 x 2.4 m) panels. A third wall was tested in this configuration, but the data of this wall had to be censored due to the presence of an error during testing. The three walls of **10-10-P** were sheathed with panels measuring 4 x 10 feet (1.2 x 3.0 m).

The response of configurations **10-8-P** and **10-10-P**, when subjected to lateral load, is displayed in Figure 4.21. In this figure, the envelope curve of each configuration is presented. The envelope curve of **10-8-P** was produced from the average load vs. displacement values of the two walls that comprised the configuration. The envelope curve of **10-10-P** was produced from the average load vs. displacement values of the three walls that comprised the configuration. The arrows in Figure 4.21 display the range of values between the three walls of each configuration at peak load.

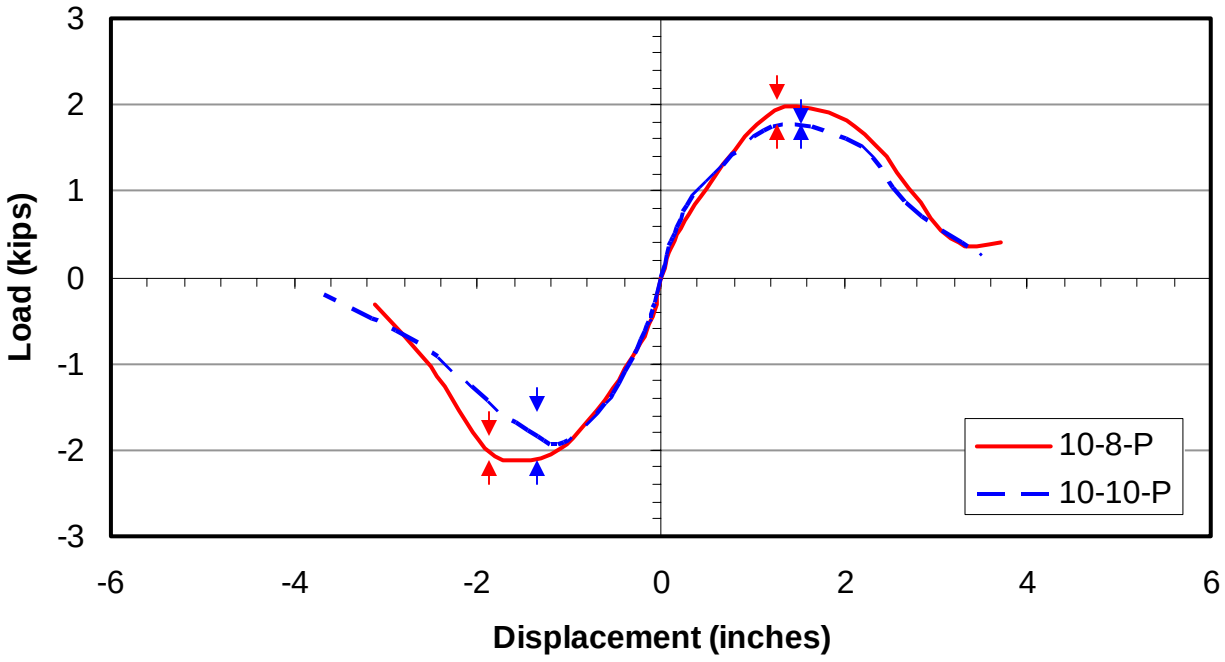

Figure 4.21. Average load vs. displacement of **10-8-P** and **10-10-P**

The values of F_{yield}, F_{peak}, $0.8F_{peak}$ and the corresponding displacements of **10-8-P** and **10-10-P** are presented in Table 4.7. These are average values of load and displacement produced from both positive and negative excursions of the ram for each wall of the configuration.

Table 4.7. Average strength and displacement values of **10-8-P** and **10-10-P**

Configuration	$\mathbf{F_{yield}}$ (kips)	$\mathbf{\Delta_{yield}}$ (inches)	$\mathbf{F_{peak}}$ (kips)	$\mathbf{\Delta_{peak}}$ (inches)	$\mathbf{F_{failure}}$ (kips)	$\mathbf{\Delta_{failure}}$ (inches)
10-8-P	1.83	0.7	2.05	1.6	1.60	2.2
10-10-P	1.65	0.6	1.87	1.3	1.50	2.0

The average values of F_{yield} and F_{peak} produced by **10-8-P** were 180 pounds greater than those produced by **10-10-P**. The average $F_{failure}$ value of **10-8-P** was 100 pounds greater than the $F_{failure}$ value of **10-10-P**. Values of F_{yield} were determined according to the EEEP Curve. These curves have been included in the Appendix. It should be noted that yield values can only be used to compare the configurations and are not the actual values at which the structure begins to behave inelastically. Typically, the proportional limit of a shear wall is about $0.4F_{peak}$.

Use of long panels in **10-10-P** reduced the displacements at which F_{yield}, F_{peak} and $F_{failure}$ occurred. The decrease in Δ is attributed to the elimination of the internal seam of sheathing connections along the blocking.

The amount of additional displacement (past Δ_{peak}) necessary to induce failure was slightly greater in **10-10-P**. Typically, structural failures are the result of weak connections. The long panel used in **10-10-P** eliminated the internal seam of sheathing connections along the blocking.

Average values of elastic stiffness, k_e, at $0.4F_{peak}$ of **10-8-P** and **10-10-P** are displayed in Table 4.8. The long sheathing panels of **10-10-P** increased k_e slightly. This is attributed to the elimination of the internal seam of sheathing connections along the blocking.

Table 4.8. k_e of **10-8-P** and **10-10-P**

	10-8-P	**10-10-P**
$\mathbf{k_e}$ **(kips/inch)**	2.9	3.0

The cyclic stiffness, k_c, values of **10-8-P** and **10-10-P** are displayed in Figure 4.22. The arrows in Figure 4.22 display the range of values at peak k_c for all three walls of each configuration. The stiffness degradation of the configurations is readily apparent. This figure shows that the long panels used to sheath **10-10-P** provided a slightly greater stiffness at lateral displacements less than 0.5 inches (12.7 mm). As the lateral displacement was increased past 1.0 inch (25.4 mm), **10-8-P** became the stiffer system. This could have been caused by the four panels of **10-8-P** binding upon one another.

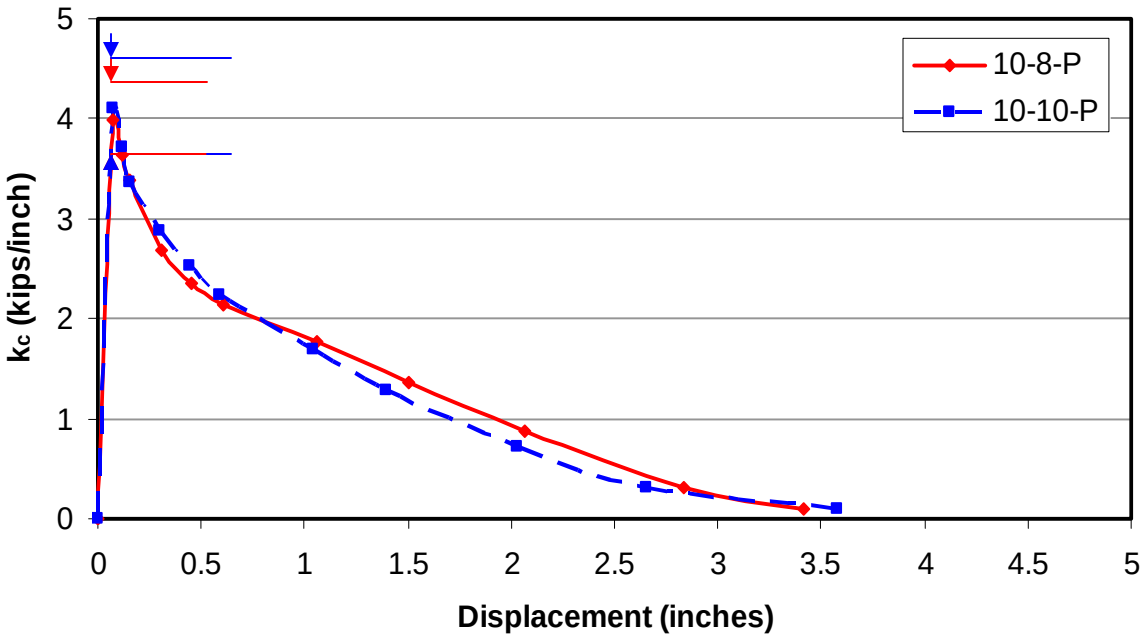

Figure 4.22. Average cyclic stiffness vs. displacement of **10-8-P** and **10-10-P**

The amount of energy dissipated until failure by **10-8-P** and **10-10-P** is displayed in Table 4.9. The long panels of **10-10-P** did not dissipate as much energy as the 4 x 8 feet (1.2 x 2.4 m) panels of **10-8-P**. This was due to the fact that **10-8-P** was able to resist more load and do so at a greater level of displacement. Also, the ability to attain greater levels of displacement allowed it to experience more cycles during testing.

Table 4.9. Hysteretic energy dissipated until failure by **10-8-P** and **10-10-P**

	10-8-P	**10-10-P**
Energy Dissipated Until Failure (kip-ft)	2.4	2.3

Simply comparing the amount of energy dissipated until failure by the configurations does not provide information related to the ability of the structure to dissipate energy at specific levels of displacement. An efficient means of doing this is to plot the hysteretic energy dissipated per cycle vs. the displacement of that cycle. The amount of energy dissipated by **10-8-P** and **10-10-P,** when displaced to various amplitudes, is displayed in Figure 4.23. The arrows in Figure 4.23 display the range of values of all three walls of each configuration at the point of maximum energy dissipation.

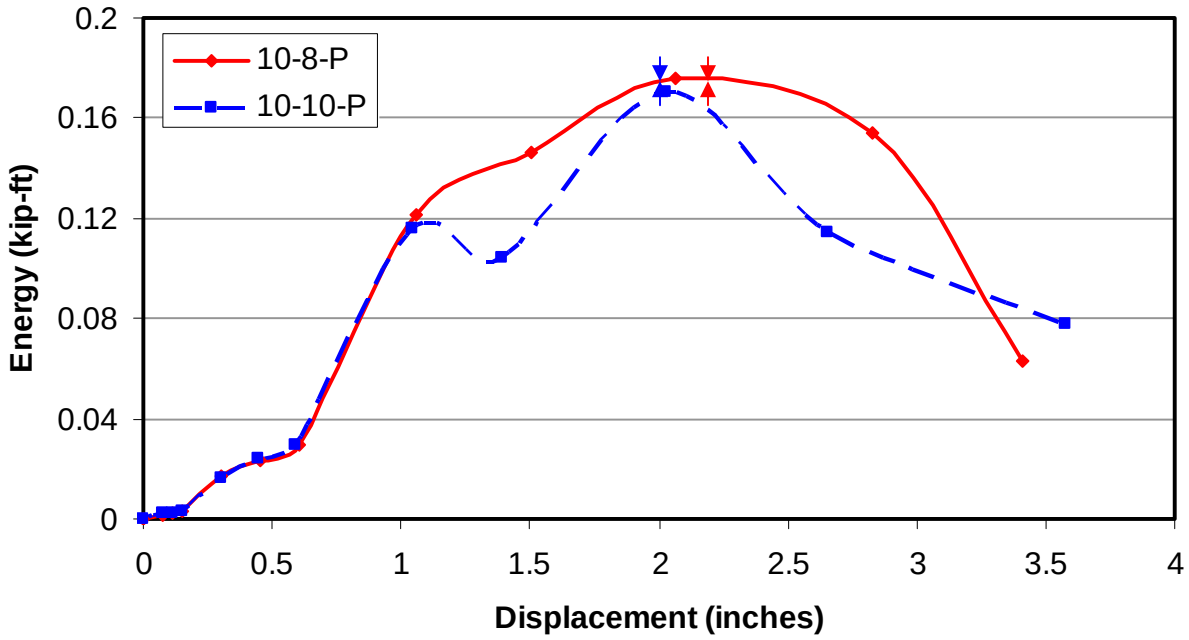

Figure 4.23. Hysteretic energy dissipated per cycle vs. displacement of **10-8-P** and **10-10-P**

At lateral displacements of 1.0 inch (25.4 mm), **10-8-P** and **10-10-P** began to experience rigid body motion and their ability to dissipate energy decreased. This is evident upon examination of Figure 4.23. The slope of each line decreases at 1.0 inch (25.4 mm) of lateral

displacement. As lateral displacement was increased past 1.0 inch (25.4 mm), the contribution of the connections along the top and sides of the wall decreased.

Configuration **10-8-P** was able to dissipate more energy than **10-10-P** between lateral displacements of 1.0 and 2.0 inches (25.4 and 50.8 mm). In **10-8-P**, the sheathing connections along the blocking of the 4 x 8 feet (1.2 x 2.4 m) sheathing panels were a source of energy dissipation that was not present in **10-10-P**. The sheathing connections in the 4 x 2 feet (1.2 x 0.6 m) panels were not performing significant amounts of work at these displacements. Once a lateral displacement of 2.0 inches (50.8 mm) was reached, the sheathing connections along the blocking of the 4 x 8 feet (1.2 x 2.4 m) panels were no longer performing work; thus, the amount of energy dissipated at this displacement by **10-8-P** and **10-10-P** was very similar. At 2.0 inches (50.4 mm) of lateral displacement, the sheathing connections in the bottom plate were the primary source of energy dissipation. Beyond 2.0 inches (50.4 mm) of lateral displacement, sheathing nail tear through began to occur in the sheathing connections along the bottom plate which left them incapable of dissipating energy.

Significant racking behavior was not present in either configuration. In **10-8-P**, 0.9 inches (22.9 mm) of uplift was produced by an average lateral displacement at peak load of 1.7 inches (43.2 mm); thus, rigid body motion accounted for 75% of the global lateral displacement. In **10-10-P**, 0.6 inches (15.2 mm) of uplift was produced by an average lateral displacement at peak load of 1.3 inches (33.0 mm); thus, rigid body motion accounted for 72% of the global lateral displacement.

The failure modes of both configurations were similar. This consisted of sheathing nail tear through of the connections under the double end stud in tension along the bottom plate and separation of the studs and bottom plate. However, the connections along the middle half of the bottom plate of **10-8-P** also experienced tear through where as the corresponding connections of **10-10-P** experienced withdrawal. This is displayed in Figure 4.24 and 4.25. This type of behavior is attributed to a larger value of force acting on the sheathing nails at this location of **10-8-P**. More force was acting on the connections of **10-8-P** because it possessed a shorter lever arm of rotation within the panel. For example, if equivalent values of uplift force are to be resisted by the corner nail of **10-8-P** and **10-10-P**, more force from within the panel will be placed on the nail of **10-8-P** because it possesses a shorter lever arm. Thus, the connections of **10-10-P** were able to work themselves out in withdrawal instead of experiencing tear through.

Therefore, the sheathing connections along the bottom plate of **10-8-P** experienced more bending deformations. In **10-8-P**, there was no visible damage around the 4 x 2 feet (1.2 x 0.6 m) pieces of sheathing panel. Also, there was no separation between stud and double top plate in either configuration.

Figure 4.24. Tear through of connections along middle half of bottom plate in **10-8-P**

Figure 4.25. Withdrawal of connections along middle half of bottom plate in **10-10-P**

4.5 9 Feet Tall Engineered Shear Walls

Two 9 feet (2.7 m) tall engineered shear wall configurations were tested in order to determine the performance capabilities of long sheathing panels. The three walls of **9-8-E** were sheathed with 4 x 8 feet (1.2 x 2.4 m) panels and the three walls of **9-9-E** were sheathed with 4 x 9 feet (1.2 x 2.7 m) panels. The average responses of configurations **9-8-E** and **9-9-E**, when subjected to lateral load, are displayed in Figure 4.26. In this figure, the envelope curve of each configuration is presented. The arrows in Figure 4.26 display the range of values between the three walls of each configuration at peak load.

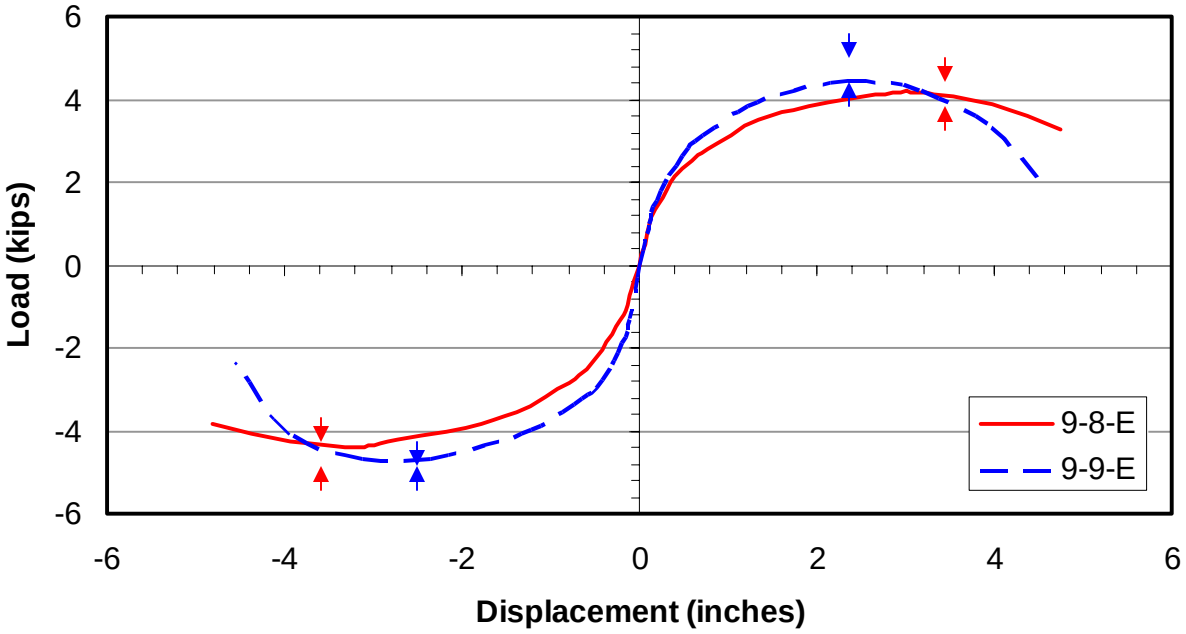

Figure 4.26. Average load vs. displacement of **9-8-E** and **9-9-E**

Average values of F_{yield}, F_{peak}, $0.8F_{peak}$ and corresponding displacements of walls **9-8-E** and **9-9-E** are presented in Table 4.10. The peak loads of all three walls of **9-8-E** due to contraction of the ram occurred at much greater displacements than those due to extension. This occurred because the peak load attained at contraction caused some of the connections to fail; thus the wall could not sustain an equivalent value of load when extended in the same primarily cycle because the number of connections had been decreased. Therefore, the value of peak load attained upon extension would have occurred on the previous primary cycle which possessed a smaller displacement. Configuration **9-9-E** recorded peak loads due to contraction and extension in the same primary cycle.

Table 4.10. Average strength and displacement values of **9-8-E** and **9-9-E**

Configuration	**F_{yield}** (kips)	**Δ_{yield}** (inches)	**F_{peak}** (kips)	**Δ_{peak}** (inches)	**$F_{failure}$** (kips)	**$\Delta_{failure}$** (inches)
9-8-E	3.86	0.7	4.33	3.1	3.81	4.5
9-9-E	4.09	0.5	4.60	2.5	3.68	3.9

The 9 feet (2.7 m) long panels used in conjunction with hold-down devices in **9-9-E** improved the strength characteristics of a 9 feet (2.7 m) tall engineered shear wall. The average values of F_{yield} and F_{peak} increased 230 and 270 pounds (1022 and 1200 N), respectively. Configuration **9-8-E** sheathed with 4 x 8 feet (1.2 x 2.4 m) panels produced a larger value of $F_{failure}$. However, the value of $F_{failure}$ displayed in Table 4.10 is not equal to $0.8F_{peak}$. This is because the walls of **9-8-E** did not reach $0.8F_{peak}$ during the course of the test. Therefore, the values used to determine $F_{failure}$ of **9-8-E** were the peak loads of the last primary cycle. The values of F_{yield} were determined according to the EEEP Curve. These curves have been included in the Appendix. It should be noted that yield values can only be used to compare the configurations and are not the actual values at which the structure begins to behave inelastically. Typically, the proportional limit of a shear wall is about $0.4F_{peak}$.

The use of long panels in **9-9-E** reduced the displacements at which F_{yield}, F_{peak} and $F_{failure}$ occurred. The decrease in Δ is attributed to the elimination of the internal seam of sheathing connections along the blocking.

It is difficult to compare the amount of additional displacement (past Δ_{peak}) necessary to induce failure because **9-8-E** did not reach the definition of failure used throughout this investigation. However, the values of Table 4.10 display that an equivalent amount of displacement was necessary to induce failure of the two configurations. Also, **9-8-E** did not reach the definition of $F_{failure}$. Therefore, it is safe to say that more additional displacement is required to induce failure in **9-8-E**. It is apparent that the additional rows of sheathing connections along the blocking of **9-8-E** provide ductility to the system which allow it to attain larger values of lateral displacement.

Average values of elastic stiffness, k_e, at $0.4F_{peak}$ of **9-8-E** and **9-9-E** are displayed in Table 4.11. The long sheathing panels of **9-9-E** increased k_e significantly. This is attributed to the elimination of the internal seam of sheathing connections along the blocking.

Table 4.11. k_e values of **9-8-E** and **9-9-E**

	9-8-E	**9-9-E**
k_e (kips/inch)	6.0	8.7

The cyclic stiffness (k_c) values for **9-8-E** and **9-9-E** are displayed in Figure 4.27. The arrows in Figure 4.27 display the range of values at peak k_c for all three walls of each configuration. The stiffness degradation of the configurations is readily apparent. This figure shows that the long panels used to sheath **9-9-E** provided greater stiffness until lateral displacements of 2.5 inches (63.5 mm). Again, this was a result of the elimination of the internal seam of sheathing connections along the blocking.

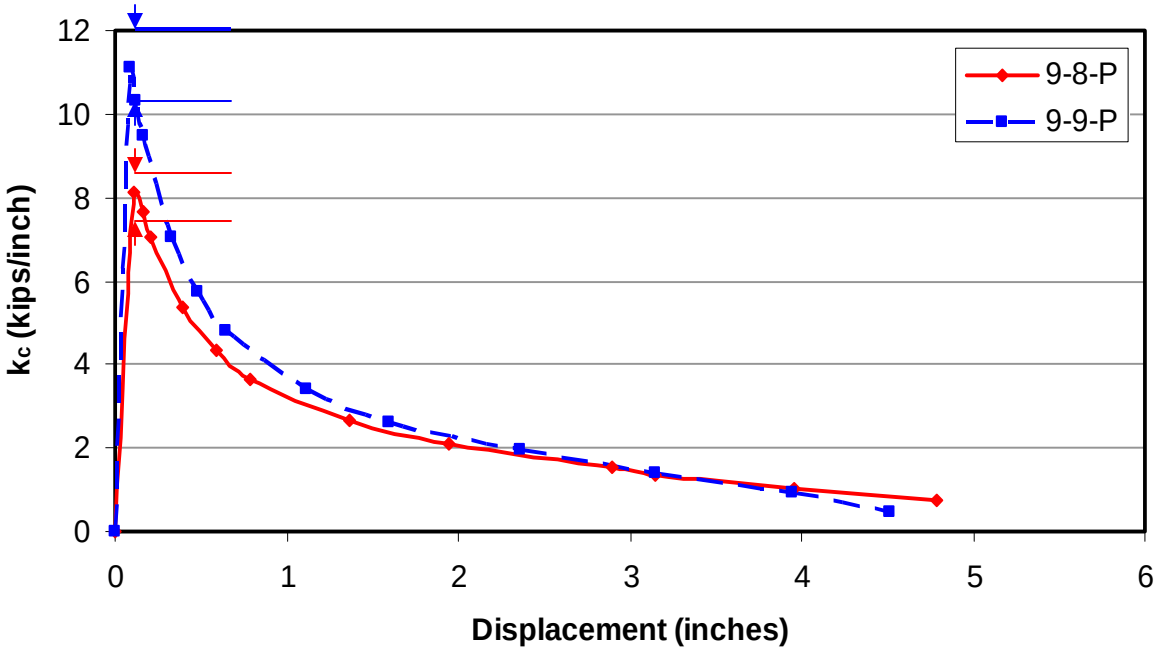

Figure 4.27. Average cyclic stiffness vs. displacement of **9-8-E** and **9-9-E**

The amount of hysteretic energy dissipated until failure by **9-8-E** and **9-9-E** is displayed in Table 4.12. The long panels of **9-9-E** did not dissipate as much energy as the 4 x 8 feet (1.2 x 2.4 m) panels of **9-8-E**. The additional line of sheathing connections along the blocking of the 4 x 8 feet (1.2 x 2.4 m) and 4 x 1 feet (1.2 x 0.3 m) panels provided a source of energy dissipation that was not present in **9-9-E**. Also, the ability of **9-8-E** to attain greater levels of displacement allowed it to experience more cycles during testing. However, the ability of **9-9-E** to resist larger values of load allowed it to dissipate almost as much energy as **9-8-E** until just prior to failure.

Table 4.12 Hysteretic energy dissipated until failure by **9-8-E** and **9-9-E**

	9-8-E	**9-9-E**
Energy Dissipated Until Failure (kip-ft)	9.3	8.9

Simply comparing the amount of hysteretic energy dissipated until failure by the configurations does not provide information related to the ability of the structure to dissipate energy at specific levels of displacement. An efficient means of doing this is to plot the energy dissipated per cycle vs. the displacement of that cycle. The amount of hysteretic energy dissipated by **9-8-E** and **9-9-E**, when displaced to various amplitudes, is displayed in Figure 4.28. The arrows in Figure 4.28 display the range of values of all three walls of each configuration at the point of maximum energy dissipation.

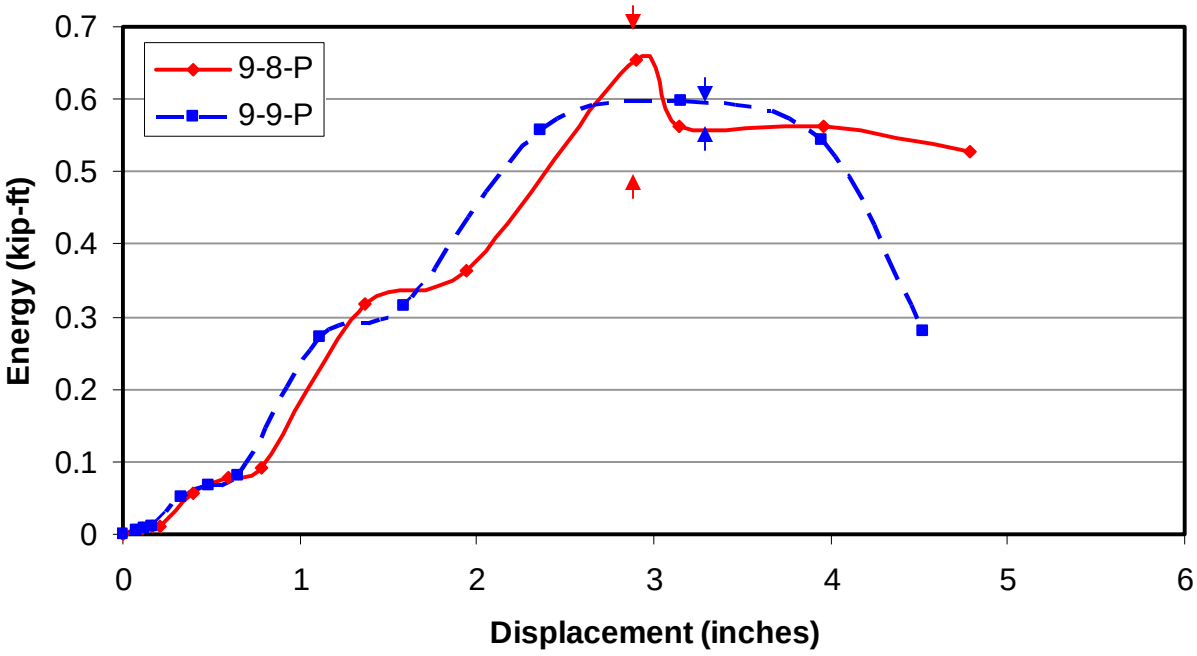

Figure 4.28. Hysteretic energy dissipated per cycle vs. displacement of **9-8-E** and **9-9-E**

At lateral displacements less than 2.5 inches (63.5 mm), **9-9-E** dissipated more energy per cycle. This was a result of the larger stiffness of **9-9-E** which allowed it to resist more load. Therefore, larger deformations were occurring in the sheathing connections of **9-9-E**. Configuration **9-8-E** dissipated more energy per cycle between 1.2 and 1.6 inches (30.5 and 40.6

mm) of lateral displacement. However, this occurred because the displacement values of the primary cycles were slightly larger during the testing of **9-8-E**. If the data points of Figure 4.28 had the same values of displacement, the amount of energy dissipated per cycle would have been greater in **9-9-E**. The data points of Figure 4.28 are not the same because slightly different values of the reference deformation were entered into the program that determined the displacements of the hydraulic actuator. However, this slight error should not compromise the data. Configuration **9-8-E**, which was sheathed with 4 x 8 feet (1.2 x 2.4 m) panels, dissipated more energy per cycle at a lateral displacement of 2.9 inches (73.7 mm). At this point of displacement, values of cyclic stiffness and load of both configurations were equal. At lateral displacements greater than 3.0 inches (76.2 mm), **9-8-E** displayed a slightly larger k_c because the sheathing connections of **9-8-E** had not experienced as much bending stress due to less load resisted by the wall up until this point. Thus, more force was acting on the sheathing connections of **9-8-E** at displacements greater than 3.0 inches (76.2 mm) and more energy was dissipated. Also, the 4 panels of **9-8-E** could have been binding upon one another which would have increased the stiffness of the system. The decrease in energy dissipation per cycle experienced by both configurations at lateral displacements greater than 3.0 inches (76.2 m) was caused by sheathing nail tear through of the sheathing connections near the corners of the panels.

Both configurations developed significant racking behavior. The hold-down device limited uplift of the end stud in tension to no more than 0.3 inches (7.6 mm) at peak load. Thus, rigid body motion never accounted for more than 20% of the global lateral displacement at peak load. Also, bending deformations in the end studs were negligible. Therefore, racking deformations accounted for 80% of the lateral displacement. The mechanical hold-down devices increased the Δ_s component of lateral displacement from 25% in 9 feet (2.7 m) prescriptive walls to 80% in 9 feet (2.7 m) engineered walls. Thus, the engineered walls performed more efficiently because the force in the panel was distributed more evenly to each sheathing connection along the perimeter of the panel.

The failure mode of **9-8-E** consisted of major nail tear through and nail heads pulled through the panel at all four corners and along the blocking of the 4 x 8 feet (1.2 x 2.4 m) panels. The 4 x 1 feet (1.2 x 0.3 m) panels suffered minor nail tear through along the line of blocking. No damage was observed in the sheathing connections along the top plate. All connections along the center stud and blocking experienced a degree of tear through at the upper limits of

lateral displacement. This was a result of the limited distance between the nail and edge of the sheathing panel. Also, some rather significant withdrawal was present in the sheathing connections along the end studs of the 4 x 8 feet (1.2 x 2.4 m) panels in one wall of **9-8-E**. This could have been caused by a low modulus of elasticity in these members and is displayed in Figure 4.29. Before tear through occurred, the sheathing nails along the perimeter of the 4 x 8 feet (1.2 x 2.4 m) panels experienced significant bending deformation. Some minor separation between top plate and studs was also present, but this did not lead to failure of the wall. This is displayed in Figure 4.30. The amount of separation between the bottom plate and studs was negligible.

Figure 4.29. Withdrawal of connections in **9-8-E**

Figure 4.30. Separation of double top plate and stud in **9-8-E**

The failure mode of **9-9-E** consisted of nail tear through and pulled heads along the 9 feet (2.7 m) edges and corners of the panel and minor nail tear through along the 4 feet (1.2 m) edges. All sheathing connections along the perimeter experienced some withdrawal. Sheathing nail tear through at the corner of the panel and withdrawal of the connections are displayed in Figures 4.31 and 4.32, respectively. Significant bending deformation was present in all sheathing connections along the perimeter of the panel. Some separation occurred between the double top plate and studs, but not enough to induce failure. The amount of separation between the bottom plate and studs was negligible.

Figure 4.31. Sheathing nail tear through at corner of panel in **9-9-E**

Figure 4.32. Withdrawal of connections along double end stud in **9-9-E**

4.6 10 Feet Tall Engineered Shear Walls

Two 10 feet (3.0 m) tall engineered shear wall configurations were tested in order to determine the performance capabilities of long sheathing panels. The three walls of **10-8-E** were sheathed with 4 x 8 feet (1.2 x 2.4 m) panels and the three walls of **10-10-E** were sheathed with 4 x 10 feet (1.2 x 3.0 m) panels.

Average response of configurations **10-8-E** and **10-10-E,** when subjected to lateral load, is displayed in Figure 4.33. In this figure, the envelope curve of each configuration is presented. The arrows in Figure 4.33 display the range of values between the three walls of each configuration at peak load.

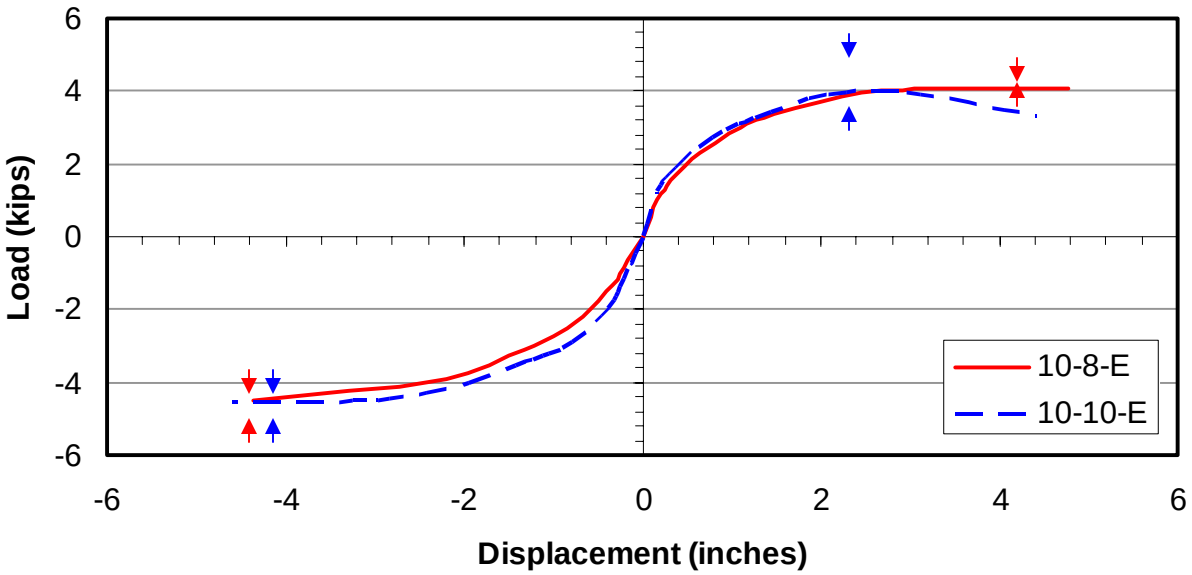

Figure 4.33. Average load vs. displacement of **10-8-E** and **10-10-E**

Average values of F_{yield}, F_{peak}, $0.8F_{peak}$ and corresponding displacements of walls **10-8-E** and **10-10-E** are presented in Table 4.13. Average peak loads of one wall in **10-8-E** and two walls in **10-10-E** due to contraction of the ram occurred at much greater displacements than those due to extension. This occurred because the peak load attained at contraction caused some of the connections to fail; thus the wall could not sustain an equivalent value of load when extended in the same primarily cycle because the number of connections had been decreased. Therefore, the value of peak load attained upon extension would have occurred on the previous primary cycle which possessed a smaller displacement.

Table 4.13. Average strength and displacement values of **10-8-E** and **10-10-E**

Configuration	$\mathbf{F_{yield}}$ (kips)	$\mathbf{\Delta_{yield}}$ (inches)	$\mathbf{F_{peak}}$ (kips)	$\mathbf{\Delta_{peak}}$ (inches)	$\mathbf{F_{failure}}$ (kips)	$\mathbf{\Delta_{failure}}$ (inches)
10-8-E	3.80	1.0	4.29	4.3	4.28	4.6
10-10-E	3.84	0.8	4.28	3.5	3.95	4.5

The F_{yield} and F_{peak} values obtained for **10-8-E** and **10-10-E** were similar. The values of $F_{failure}$ can not be compared because the displacement limitations of the testing apparatus did not allow the wall to be tested to failure. The values used to determine $F_{failure}$ were the peak loads of the last primary cycle. The walls did not reach failure because a longer wall reduces the angle through which the panel rotates for a given racking displacement. Therefore, the sheathing connections do not experience as much bending stress for a given racking displacement and the wall is able to resist load at high values of lateral displacement. It does appear that F_{peak} was reached for **10-10-E**, but not for **10-8-E**. The values of F_{yield} were determined according to the EEEP Curve. These curves have been included in the Appendix. It should be noted that yield values can only be used to compare the configurations and are not the actual values at which the structure begins to behave inelastically. Typically, the proportional limit of a shear wall is about $0.4F_{peak}$.

The use of long panels in **10-10-E** reduced the displacements at which F_{yield}, F_{peak} and $F_{failure}$ occurred. The decrease in Δ is attributed to the elimination of the internal seam of sheathing connections along the blocking.

The amount of additional displacement (past Δ_{peak}) necessary to induce failure can not be compared because neither **10-8-E** nor **10-10-E** reached the definition of failure used throughout this investigation. However, examination of Figure 4.33 reveals that the slope of **10-8-E** is still increasing at the limits of testing and that it is behaving in a more ductile manner. It is apparent that the additional rows of sheathing connections along the blocking of **10-8-E** provide ductility to the system which allow it to attain larger values of lateral displacement.

The average values of elastic stiffness, k_e, at $0.4F_{peak}$ of **10-8-E** and **10-10-E** are displayed in Table 4.14. These values were determined by averaging the values of each wall of the configuration. The long sheathing panels of **10-10-E** increased k_e significantly. This is attributed to the elimination of the internal seam of sheathing connections along the blocking.

Table 4.14. k_e values of **10-8-E** and **10-10-E**

	10-8-E	**10-10-E**
k_e (kips/inch)	4.1	6.1

The cyclic stiffness (k_c) values of **10-8-E** and **10-10-E** are displayed in Figure 4.34. The arrows in Figure 4.34 display the range of values at peak k_c for all three walls of each configuration. These values were determined by averaging the values of each wall of the configuration. The stiffness degradation of the configurations is readily apparent. This figure shows that the long panels used to sheath **10-10-E** provided greater stiffness until lateral displacements of 2.0 inches (50.8 mm). Again, this was a result of the elimination of the internal seam of sheathing connections along the blocking.

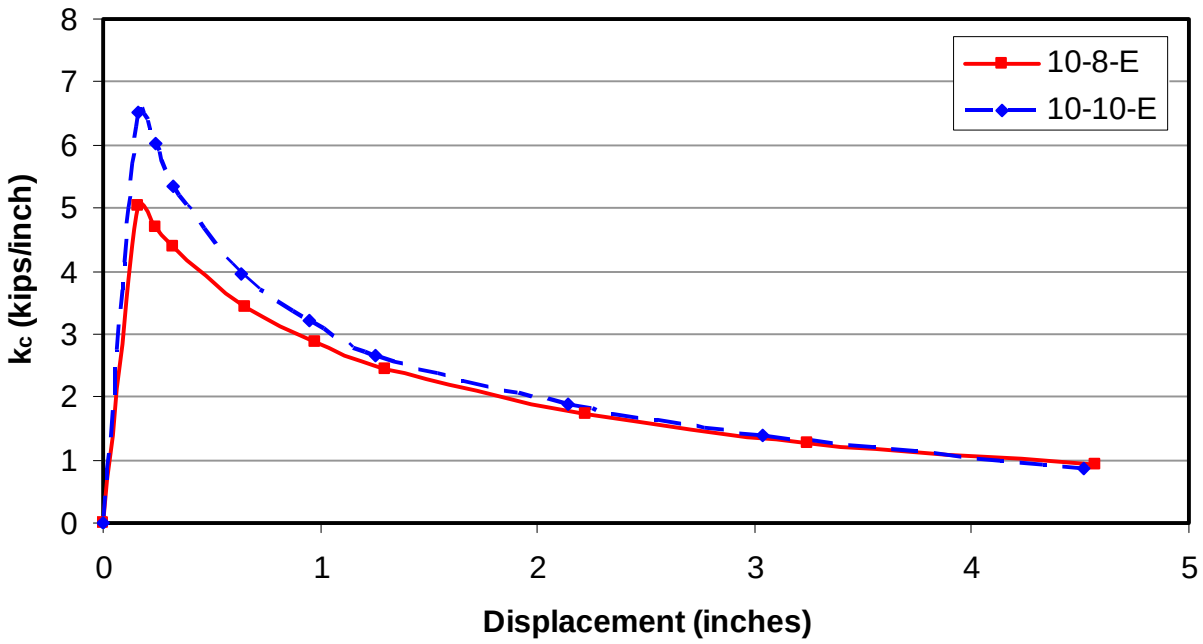

Figure 4.34. Average cyclic stiffness vs. displacement of **10-8-E** and **10-10-E**

The amount of hysteretic energy dissipated until failure by **10-8-E** and **10-10-E** is displayed in Table 4.15. The table displays that the long panels of **10-10-E** were able to dissipate more energy than the 4 x 8 feet (1.2 x 2.4 m) panels of **10-8-E**. However, this is not a good comparison because neither configuration reached failure. Based on inferences made according to the 9 feet (2.7 m) tall engineered shear walls, it is certain that **10-8-E** would have

dissipated more energy than **10-10-E**. The additional line of sheathing connections along the blocking of the 4 x 8 feet (1.2 x 2.4 m) and 4 x 2 feet (1.2 x 0.6 m) panels provided an additional source of energy dissipation that was not present in **10-10-E**. Also, the ability of **10-8-E** to attain greater levels of displacement would have allowed it to experience more cycles during testing.

Table 4.15 Hysteretic energy dissipated until failure by **10-8-E** and **10-10-E**

	10-8-E	**10-10-E**
Energy Dissipated Until Failure (kip-ft)	7.2	7.8

Simply comparing the amount of hysteretic energy dissipated until failure by the configurations does not provide information related to the ability of the structure to dissipate energy at specific levels of displacement. An efficient means of doing this is to plot the hysteretic energy dissipated per cycle vs. the displacement of that cycle. The amount of energy dissipated by **10-8-E** and **10-10-E**, when displaced to various amplitudes, is displayed in Figure 4.35. The arrows in Figure 4.35 display the range of values of all three walls of each configuration at the point of maximum energy dissipation.

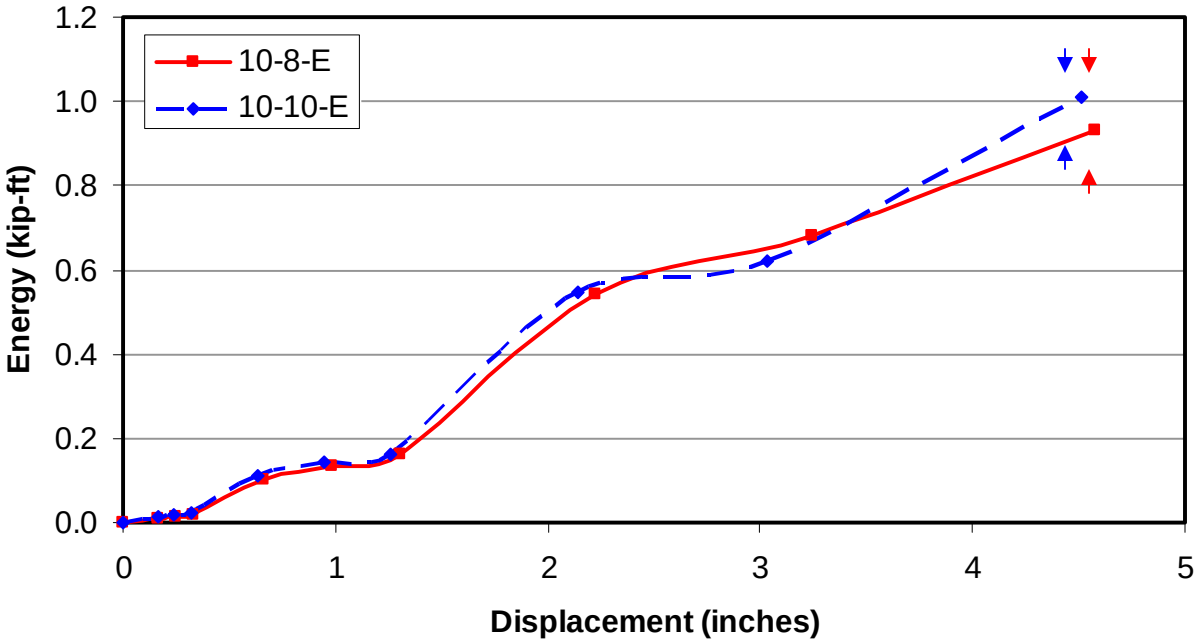

Figure 4.35. Hysteretic energy dissipated per cycle vs. displacement of **10-8-E** and **10-10-E**

The amount of energy dissipated per cycle by **10-8-E** and **10-10-E** was comparable. Configuration **10-10-E** appeared to dissipate slightly more energy per cycle. This is attributed to the greater stiffness of the system. Based on inferences made from the 9 feet (2.7 m) tall engineered shear walls, **10-8-E** would have dissipated more energy per cycle at high levels of lateral displacement.

Both configurations developed significant racking behavior. The hold-down device limited uplift of the end stud in tension to no more than 0.3 inches (7.6 mm) at peak load. Thus, rigid body motion never accounted for more than 15% of the global lateral displacement, except for one wall of **10-10-E** in which it accounted for 20%. Also, bending deformation of the end studs and nail slip were determined to be negligible in all walls except one wall of **10-8-E**. Therefore, racking deformations accounted for 80% of the lateral displacement. Hold-downs increased the percentage of lateral displacement attributed to shear deformation from 25% in 10 feet (3.0 m) tall prescriptive walls to 80% in 10 feet (3.0 m) tall engineered walls.

The failure mode of **10-8-E** consisted of nail tear through at all four corners, the 8 feet (2.4 m) edge along the common center stud and along the blocking of the 4 x 8 feet (1.2 x 2.4 m) panels. Tear through was not as significant in **10-8-E** as it was in **9-8-E** due to displacement limitations of the testing apparatus. Also, some withdrawal, less than 0.5 inches (12.7 mm), was present in the sheathing connections along the end studs and bottom plate of the 4 x 8 feet (1.2 x 2.4 m) panels. Sheathing connections along the blocking of the 2 x 4 feet panels (0.6 x 1.2 m) experienced minor nail tear through and significant withdrawal. This is displayed in Figure 4.36. All of the connections along the center stud and blocking, except those at the midpoint of the panel edges, experienced tear through. This was a result of the limited distance between the nail and edge of the sheathing panel. Before tear through occurred, the sheathing nails along the perimeter of the 4 x 8 feet (1.2 x 2.4 m) panels experienced significant bending deformation. Some separation between double top plate and studs was also present, but not enough to result in failure. The amount of separation between the bottom plate and studs was negligible.

Figure 4.36. Withdrawal of sheathing connections along the blocking in **10-8-E**

The failure mode of **10-10-E** consisted of nail tear through of all connections within 4 feet (1.2 m) of the corner along the 10 feet (3.0 m) edge and minor nail tear through of the connections near the corner of the 4 feet (1.2 m) edge. However, it was not as severe as that which occurred in **9-9-E** due to displacement limitations of the testing apparatus. Sheathing connections in the end studs and plates experienced some minor withdrawal. Significant bending deformation was present in all sheathing connections along the perimeter of the panels. Some minor separation occurred between the top plate and studs, but not enough to induce failure. The amount of separation between the bottom plate and studs was negligible.

4.7 Effects of Hold-Down Restraint

Configurations **9-9-P** and **9-9-E** are compared in order to display the effects of a mechanical hold-down device attached to each end stud. The walls of **9-9-P** are 9 feet (2.7 m) tall prescriptive shear walls and the walls of **9-9-E** are 9 feet (2.7 m) tall engineered shear walls. Both configurations were sheathed with 4 x 9 feet (1.2 x 2.7 m) panels. The responses of configurations **9-9-P** and **9-9-E,** when subjected to lateral load, are displayed in Figure 4.37. In this figure, the average envelope curve of each configuration is presented. The arrows in Figure 4.37 display the range of values between the three walls of each configuration at peak load.

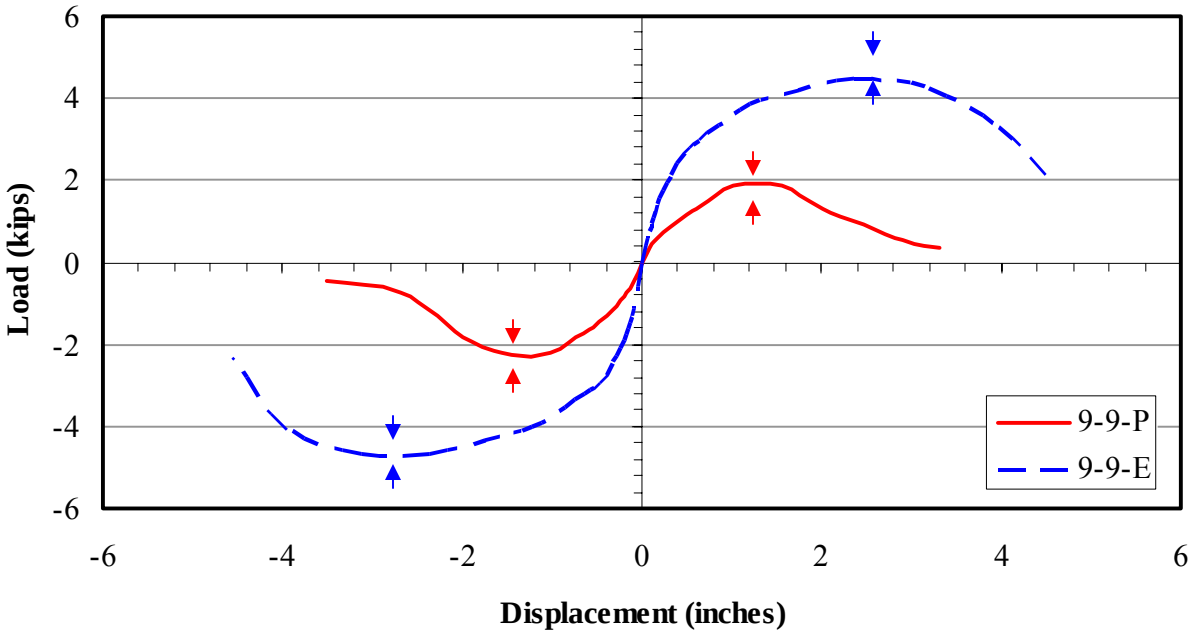

Figure 4.37. Average load vs. displacement of **9-9-P** and **9-9-E**

Average values of F_{yield}, F_{peak}, $0.8F_{peak}$ and corresponding displacements for **9-9-P** and **9-9-E** are presented in Table 4.16.

Table 4.16. Average strength and displacement values of **9-9-P** and **9-9-E**

Configuration	**F_{yield}** (kips)	**Δ_{yield}** (inches)	**F_{peak}** (kips)	**Δ_{peak}** (inches)	**$F_{failure}$** (kips)	**$\Delta_{failure}$** (inches)
9-9-P	1.90	0.6	2.11	1.3	1.68	1.9
9-9-E	4.09	0.5	4.60	2.5	3.68	3.9

Average values of F_{yield}, F_{peak} and $F_{failure}$ produced by the engineered configuration of **9-9-E** were more than twice those produced by the prescriptive configuration of **9-9-P**. This is due to the fact that the mechanical hold-down device provided a direct load path into the foundation for the tensile force developed in the double end stud. Thus, the uplift force of the overturning moment was resisted by the framing and the wall behaved primarily in a racking manner. This produced rotation of the sheathing panel about its geometrical center, which then distributed the force in the panel more evenly to each sheathing connection along the perimeter.

Mechanical hold-down devices allowed **9-9-E** to attain much larger average values of Δ_{peak} and $\Delta_{failure}$. In fact, these values were twice as large as those of **9-9-P**. Average values of Δ_{yield} of the two configurations were very similar. This provides support to the idea that the EEEP parameters are an adequate method of comparison.

The displacement (past Δ_{peak}) necessary to induce failure in **9-9-E** was more than twice the corresponding value of **9-9-P**. The hold-down removed the typical failure mode of a prescriptive wall, sheathing nail tear through under the end stud in tension, and made more efficient use of each connection along the perimeter of the panel.

Average values of elastic stiffness, k_e, at $0.4F_{peak}$ of **9-9-P** and **9-9-E** are displayed in Table 4.17. The mechanical hold-down devices of **9-9-E** increased k_e significantly.

Table 4.17. k_e values of **9-9-P** and **9-9-E**

	9-9-P	**9-9-E**
k_e (kips/inch)	3.6	8.7

The average cyclic stiffness (k_c) values for **9-9-P** and **9-9-E** are displayed in Figure 4.38. The arrows in Figure 4.38 display the range of values at peak k_c for all three walls of each configuration. The stiffness degradation of the configurations is readily apparent. This figure shows that the mechanical hold-down devices used to resist uplift in **9-9-E** provided much greater stiffness per cycle.

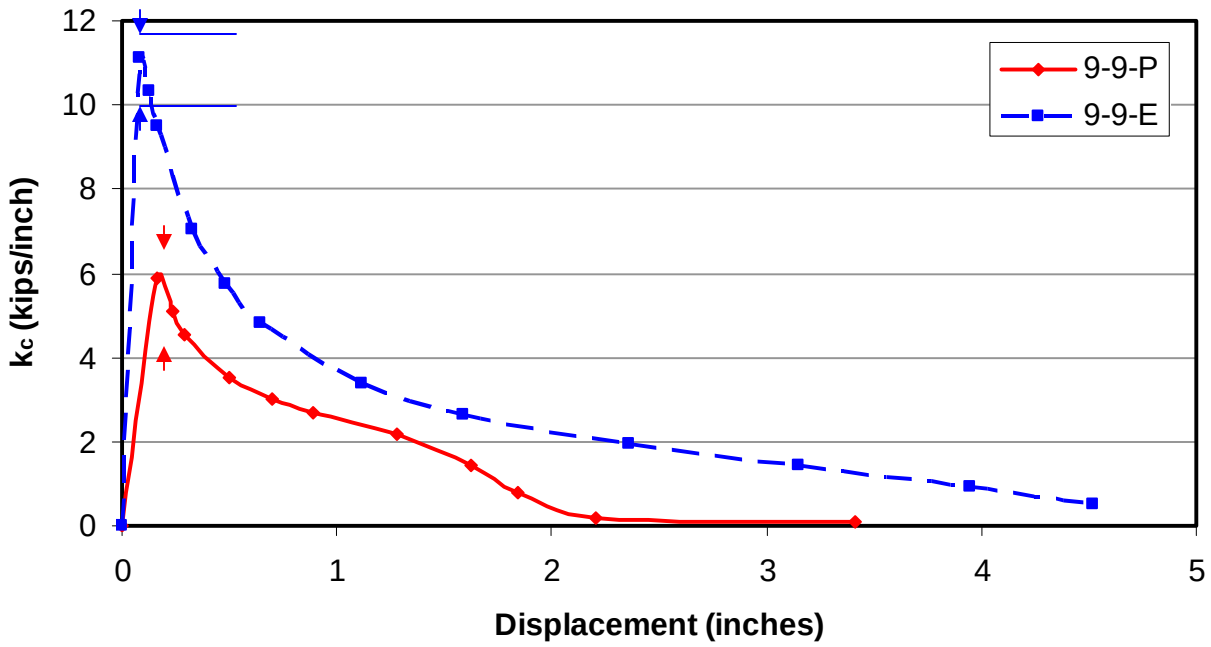

Figure 4.38. Average cyclic stiffness vs. displacement of **9-9-P** and **9-9-E**

The amount of hysteretic energy dissipated until failure by **9-9-P** and **9-9-E** is displayed in Table 4.18. Configuration **9-9-E** was able to dissipate over three times as much energy as **9-9-P** because the mechanical hold-down devices inhibited rigid body motion; thus, all the sheathing connections along the perimeter of the panel were experiencing bending deformations due to rotation of the panel. Also, the ability of **9-9-E** to attain greater levels of displacement allowed it to experience more cycles during testing.

Table 4.18 Hysteretic energy dissipated until failure by **9-9-P** and **9-9-E**

	9-9-P	**9-9-E**
Energy Dissipated Until Failure (kip-ft)	2.3	8.9

Simply comparing the amount of energy dissipated until failure by the configurations does not provide information related to the ability of the structure to dissipate energy at specific levels of displacement. An efficient means of doing this is to plot the energy dissipated per cycle vs. the displacement of that cycle. The amount of energy dissipated by **9-9-P** and **9-9-E**, when displaced to various amplitudes, is displayed in Figure 4.39. The arrows in Figure 4.39 display

the range of values of all three walls of each configuration at the point of maximum energy dissipation.

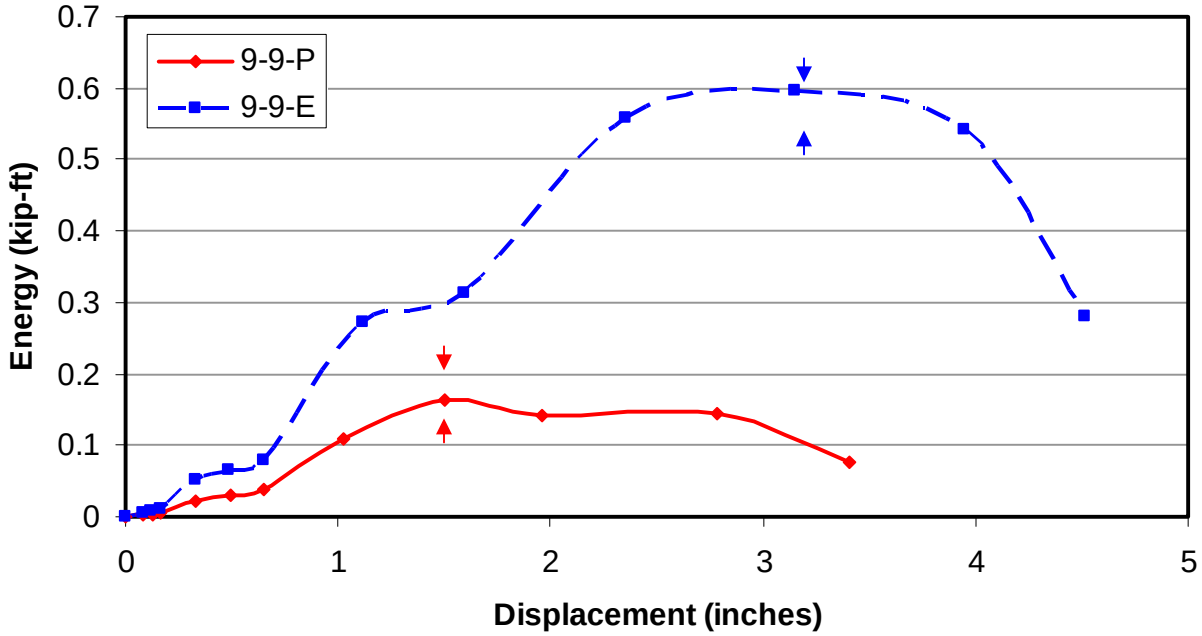

Figure 4.39. Hysteretic energy dissipated per cycle vs. displacement of **9-9-P** and **9-9-E**

Figure 4.39 displays the effects of rigid body motion on the ability of a prescriptive shear wall to dissipate energy. Even at lateral displacements less than 1.0 inch (25.4 mm), rigid body motion caused the hysteretic energy dissipation abilities of **9-9-P** to be half of **9-9-E**. At lateral displacements greater than 1.5 inches (38.1 mm), the mechanical hold-down devices allowed **9-9-E** to dissipate more than three times the amount of energy that **9-9-P** dissipated.

Configuration **9-9-P** did not develop significant racking deformation. At peak load, an average of 0.7 inches (17.8 mm) of uplift occurred between the bottom plate and end stud in tension. The average displacement at peak load of this configuration was 1.3 inches (33.0 mm). Thus, rigid body motion accounted for two-thirds of the global lateral displacement.

The hold-downs used in **9-9-E** allowed significant racking deformation to occur. At peak load, an average of 0.2 inches (5.1 mm) of uplift displacement occurred between the bottom plate and end stud in tension. The average displacement at peak load was 2.4 inches (61.0 mm). Thus, rigid body motion only accounted for 16% of the lateral displacement.

The failure modes of **9-9-P** and **9-9-E** were different. The mode of failure for **9-9-P** was sheathing nail tear through along the connections in the bottom plate under the end stud in tension, which then led to separation of the studs and bottom plate. Also, there was only significant bending deformation in the sheathing nails along the bottom plate. The failure mode for **9-9-E** consisted of major nail tear through along the 9 feet (2.7 m) edges of the panel and minor nail tear through along the 4 feet (1.2 m) edges. All sheathing connections along the perimeter experienced some minor withdrawal. Significant bending deformation was present in all sheathing connections along the perimeter of the panel. Some minor separation occurred between the top plate and studs, but not enough to induce failure of the wall. The amount of separation between the bottom plate and studs was negligible.

4.8 Effects of Aspect Ratio

Configurations **8-8-P** and **10-10-P** are compared in order to display the effects of aspect ratio. The walls of **8-8-P** are 8 feet (2.4 m) tall prescriptive shear walls that possess an aspect ration of 1:1. The walls of **10-10-P** are 10 feet (3.0 m) tall prescriptive shear walls that possess an aspect ratio of 1.25:1. Configuration **10-10-P** was sheathed with 4 x 10 feet (1.2 x 3.0 m) panels. The response of configurations **8-8-P** and **10-10-P,** when subjected to lateral load, is displayed in Figure 4.40. In this figure, the average envelope curve of each configuration is presented. The arrows in Figure 4.40 display the range of values between the three walls of each configuration at peak load.

The abscissa of each plot in this section is the drift ratio and is determined by dividing displacement by wall height. Therefore, the values of displacement of **8-8-P** and **10-10-P** have been divided by 96 and 120, respectively. This allows direct comparisons of the two configurations to be made at a given drift ratio. Also, the maximum drift ratio allowed by the Uniform Building Code is 2.5% of the story height.

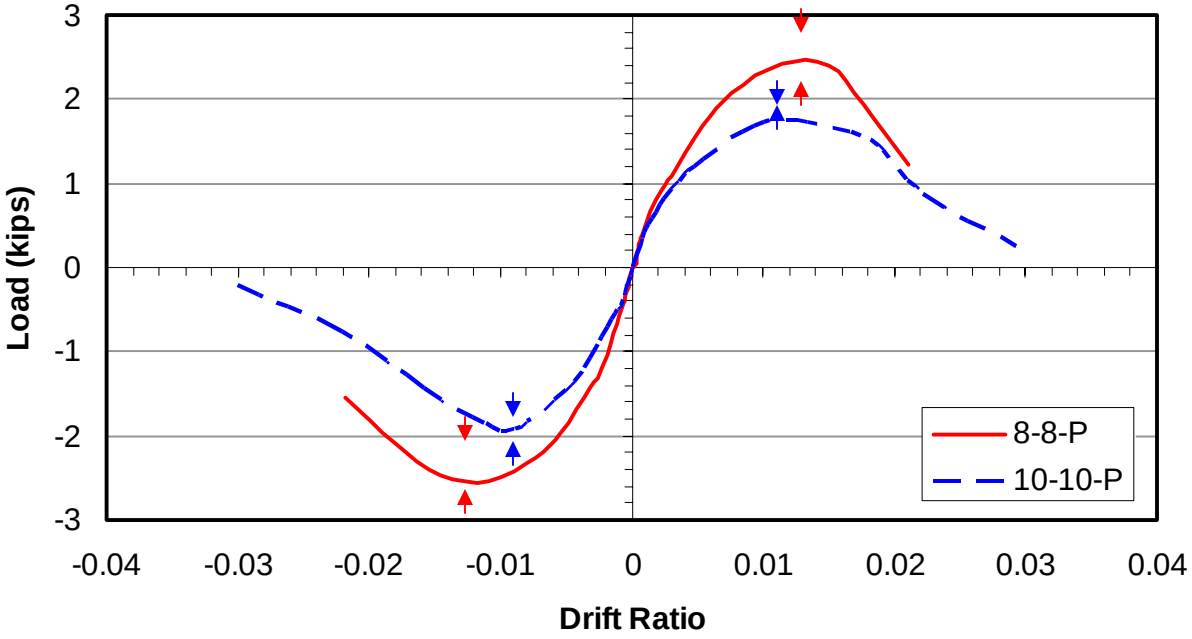

Figure 4.40. Average load vs. drift ratio of **8-8-P** and **10-10-P**

Average values of F_{yield}, F_{peak}, $0.8F_{peak}$ and corresponding displacements of **8-8-P** and **10-10-P** are presented in Table 4.19.

Table 4.19. Average strength and displacement values of **8-8-P** and **10-10-P**

Configuration	**F_{yield}** (kips)	**Δ_{yield}** (inches)	**F_{peak}** (kips)	**Δ_{peak}** (inches)	**$F_{failure}$** (kips)	**$\Delta_{failure}$** (inches)
8-8-P	2.26	0.5	2.50	1.2	2.0	1.7
10-10-P	1.65	0.6	1.87	1.3	1.50	2.0

The average values of F_{yield}, F_{peak} and $F_{failure}$ produced by **8-8-P** were 30% higher than those produced by **10-10-P**. This was a direct result of the aspect ratios of the two configurations. At equivalent values of load applied by the ram, the 1.25:1 aspect ratio of **10-10-P** produced an uplift force at the base of the end stud in tension that was 25% larger than the uplift force of **8-8-P**. Therefore, uplift displacements and sheathing nail tear through under the double end stud in tension occurred at much smaller values of lateral load in **10-10-P**.

The higher aspect ratio allowed **10-10-P** to attain larger values of Δ_{peak} and $\Delta_{failure}$, but this type of behavior should not be viewed as exemplary in relation to earthquake performance because it will not dissipate much energy. Between Δ_{peak} and Δ_{yield}, **10-10-P** was experiencing significant amounts of rotation in which very little movement of the sheathing panel relative to the framing was occurring at the top half of the wall. Therefore, the sheathing connections in the upper half of the wall were not stressed as much as those in the upper half of **8-8-P**. Also, **10-10-P** was not as stiff as **8-8-P**; therefore, it did not resist as much load at a given displacement. This allowed it to attain higher values of lateral displacement before $\Delta_{failure}$ occurred. For the same reasons, the amount of additional displacement (past Δ_{peak}) necessary to induce failure was slightly greater in **10-10-P**.

The average values of elastic stiffness, k_e, at $0.4F_{peak}$ of **8-8-P** and **10-10-P** are displayed in Table 4.20. These values were determined by averaging the values of each wall of the configuration. The smaller aspect ratio of **8-8-P** provided a much larger value of k_e.

Table 4.20. k_e values of **8-8-P** and **10-10-P**

	8-8-P	**10-10-P**
k_e (kips/inch)	4.8	3.0

Average cyclic stiffness (k_c) values of **8-8-P** and **10-10-P** are displayed in Figure 4.41. The arrows in Figure 4.41 display the range of values at peak k_c for all three walls of each configuration. The stiffness degradation of the configurations is readily apparent. This figure shows that a larger aspect ratio decreases the stiffness of the wall significantly.

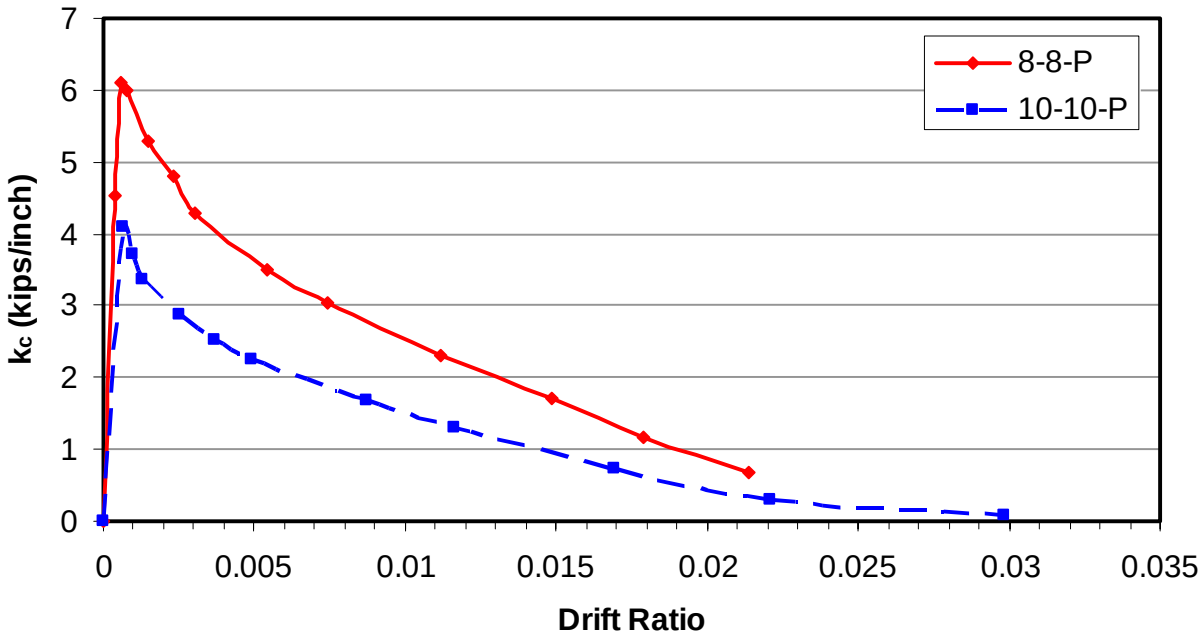

Figure 4.41. Average cyclic stiffness vs. drift ratio of **8-8-P** and **10-10-P**

The amount of hysteretic energy dissipated until failure by **8-8-P** and **10-10-P** is displayed in Table 4.21. Configuration **8-8-P** was able to dissipate more hysteretic energy until failure because it was a stiffer system. At equivalent drift ratios, more force was acting on the sheathing connections of **8-8-P** than on the connections of **10-10-P**. Thus, more deformation due to bending occurred which led to the dissipation of more hysteretic energy.

Table 4.21 Energy dissipated until failure by **8-8-P** and **10-10-P**

	8-8-P	**10-10-P**
Energy Dissipated Until Failure (kip-ft)	2.8	2.3

Simply comparing the amount of hysteretic energy dissipated until failure by the configurations does not provide information related to the ability of the structure to dissipate energy at specific drift ratios. An efficient means of doing this is to plot the energy dissipated per cycle vs. the drift ratio. The amount of hysteretic energy dissipated by **8-8-P** and **10-10-P** is

displayed in Figure 4.42 at various drift ratios. The arrows in Figure 4.42 display the range of values of all three walls of each configuration at the point of maximum energy dissipation.

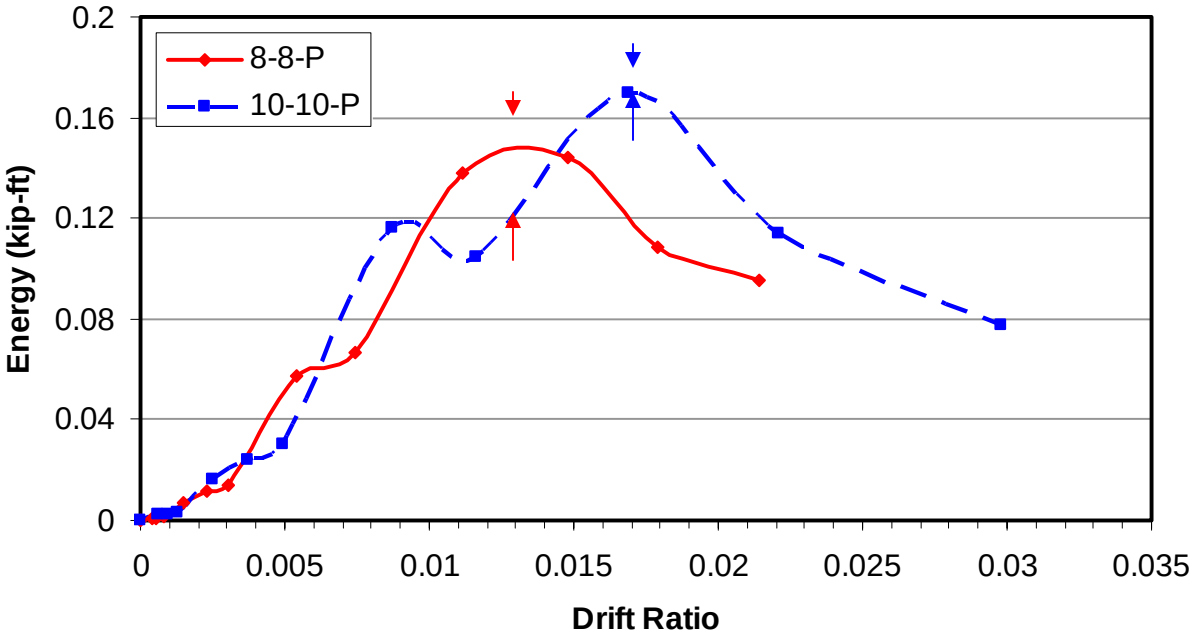

Figure 4.42. Hysteretic energy dissipated per cycle vs. displacement of **8-8-P** and **10-10-P**

Figure 4.42 displays the effects of aspect ratio on the ability of a prescriptive shear wall to dissipate hysteretic energy. Both configurations dissipated similar amounts of hysteretic energy until a drift ratio of 0.014 was reached. At this point, the amount of hysteretic energy dissipated by **8-8-P** decreased because the sheathing connections along the bottom plate under the end stud in tension began to experience tear through. This type of failure was not experienced by **10-10-P** until a drift ratio of 0.017. Thus, **10-10-P** was capable of dissipating more hysteretic energy at drift ratios greater than 0.014.

Neither configuration was able to develop significant racking deformation. At an average Δ_{peak} of 1.2 inches (30.5 mm), 0.9 inches (22.9 mm) of uplift displacement occurred between the end stud and bottom plate in **8-8-P**. Thus, rigid body motion accounted for 80% of the lateral displacement. The average Δ_{peak} of **10-10-P** was 1.3 inches (33.0 mm). This produced 0.6 inches (15.2 mm) of uplift displacement between the end stud and bottom plate; therefore, rigid body motion accounted for 70% of the lateral displacement. Rigid body motion was more prevalent in **8-8-P** at Δ_{peak} because it was closer to failure at this displacement.

The failure modes of **8-8-P** and **10-10-P** were identical. Both exhibited sheathing nail tear through along the connections in the bottom plate under the end stud in tension. Once this occurred, the studs and bottom plate separated. Also, the only location of significant bending deformation in the sheathing nails was along the bottom plate. There were no other sources of failure.

4.9 Summary

A total of 36 shear walls were subjected to the standard CUREE cyclic protocol in order to determine the performance capabilities of long oriented strand board panels. Walls possessing heights of 8, 9 and 10 feet (2.4, 2.7 and 3.0 m) were tested. The width of the walls remained constant at 8 feet (2.4 m). Three 8 feet (2.4 m) tall prescriptive walls were built. Twelve 9 feet (2.7 m) tall walls were built, six of which were blocked and sheathed with conventional 4 x 8 feet (1.2 x 2.4 m) panels. The other six were sheathed with 4 x 9 feet (1.2 x 2.7 m) long panels. The end studs of three walls sheathed with 4 x 8 feet (1.2 x 2.4 m) panels and three walls sheathed with 4 x 9 feet (1.2 x 2.7 m) panels were equipped with a mechanical hold-down device. Twelve 10 feet (3.0 m) tall walls were constructed in the same manner. Three 8 feet (2.4 m) tall prescriptive walls were sheathed with panels that measured 8.5 feet (2.55 m) in length which were extended past the bottom plate onto a 2 x 12. Three 9 feet (2.7 m) tall prescriptive walls were built in the same manner. Also, three 9 feet (2.7 m) tall prescriptive shear walls were sheathed with 4 x 9 feet (1.2 x 2.7 m) panels that possessed fibers oriented in the short direction.

This chapter has presented the information obtained from each test in order to determine whether or not long OSB sheathing panels provide adequate lateral resistance to tall light-frame structures. Also, an innovative use of the long OSB panels, in which they were extended past the bottom plate onto a band joist, was investigated to determine if increased resistance to uplift can be provided. Finally, the effects of orienting the fibers of the panels in the short direction were observed. The following conclusions have been made:

(1) Nine feet long panels provided a slight increase in the strength values of a 9 feet (2.7 m) tall prescriptive shear wall (F_{yield}, F_{peak} and $F_{failure}$).

(2) Ten feet long panels did not increase the strength values of a 10 feet (3.0 m) tall prescriptive shear wall. On a per foot basis, the amount of lateral resistance

provided by 4 x 8 feet (1.2 x 2.4 m) panels exceeded that of long panels by 22 pounds (97.8 N).

(3) When used in conjunction with mechanical hold-down devices, the strength values of 9 feet (2.7 m) tall engineered shear walls constructed with 4 x 9 feet (1.2 x 2.7 m) panels were much greater than those constructed with 4 x 8 feet (1.2 x 2.4 m) panels. On a per foot basis, the amount of lateral resistance provided by 4 x 9 feet (1.2 x 2.7 m) panels exceeded that of 4 x 8 feet (1.2 x 2.4 m) panels by 33 pounds (147 N). To put this increase in perspective, the tables of shear wall design provided by the APA display an increase in capacity of 25 lbs/ft when the panel thickness is increased from 7/16 to 15/32 inch (11.1 to 11.9 mm) and sheathing nail and schedule remain the same as was used in this investigation.

(4) When used in conjunction with mechanical hold-down devices, 10 feet (3.0 m) tall engineered shear walls sheathed with either 4 x 10 feet (1.2 x 3.0 m) panels or 4 x 8 feet (1.2 x 2.4 m) panels produced similar values of F_{peak}.

(5) Long panels decreased the values of Δ_{yield}, Δ_{peak} and $\Delta_{failure}$ of both prescriptive and engineered shear walls. This was a result of the elimination of the internal seam of sheathing connections along the blocking.

(6) Long panels increased the stiffness of a prescriptive wall slightly.

(7) Long panels increased the stiffness of an engineered wall rather significantly.

(8) Long panels did not dissipate as much hysteretic energy until failure as 4 x 8 feet (1.2 x 2.4 m) panels when used to sheath 9 and 10 feet (2.7 and 3.0 m) tall prescriptive shear walls. However, the amount of energy dissipated at equivalent levels of lateral displacement was similar.

(9) Long panels did not dissipate as much energy until failure as 4 x 8 feet (1.2 x 2.4 m) panels when used to sheath 9 feet (2.7 m) tall engineered shear walls. However, the amount of hysteretic energy dissipated at equivalent levels of lateral displacement was similar.

(10) Long panels dissipated more hysteretic energy until failure than 4 x 8 feet (1.2 x 2.4 m) panels when used to sheath 10 feet (3.0 m) tall engineered shear walls.

(11) Extending long panels past the bottom plate and down onto the band joist of a prescriptive shear wall greatly increased the values of strength, stiffness and

energy dissipation. F_{peak} and the amount of hysteretic energy dissipated until failure of an 8 feet (2.4 m) tall wall were increased 20% and 40%, respectively. F_{peak} and the amount of hysteretic energy dissipated until failure of a 9 feet (2.7 m) tall wall were increased 40% and 65%, respectively.

(12) Extending long panels down onto the band joist provided greater resistance to uplift of the end stud in tension.

(13) Panels made of fibers oriented in the short direction provided greater values of stiffness and equivalent values of strength, but failed in a sudden, brittle manner.

(14) When used in conjunction with mechanical hold-down devices, long panels outperformed 4 x 8 feet (1.2 x 2.4 m) panels in every aspect except energy dissipation until failure. However, the discrepancy of this parameter was small in 9 feet (2.7 m) tall walls and 10 feet (3.0 m) tall walls actually dissipated more energy when sheathed with 4 x 10 feet (1.2 x 3.0 m) panels.

Chapter 5: Summary, Conclusions and Recommendations

5.1 Summary

Thirty-six shear walls measuring 8 feet (2.4 m) in width and possessing heights of 8, 9 and 10 feet (2.4, 2.7 and 3.0 m) were subjected to the reversed, cyclic loading schedule of the standard CUREE protocol in order to determine the performance capabilities of shear walls greater than 8 feet (2.4 m) in height sheathed with long panels. Of the thirty-six walls, a total of twelve walls measuring 9 and 10 feet (2.7 and 3.0 m) in height were sheathed with 4 x 8 feet (1.2 x 2.4 m) panels which required additional blocking members between the studs of the frame. Values obtained from the tests performed on these walls provided a direct comparison to those obtained from the walls of equal height, but sheathed with a long panel capable of spanning the entire height of the wall. The capabilities of long panels were investigated when used as the sheathing elements of both prescriptive and engineered shear walls. An advantage of the long panel was investigated in which it was extended past the bottom plate and down onto the band joist to determine if significant resistance to the uplift present in prescriptive walls could be provided. Also, the effects of orienting the fibers of a 4 x 9 feet (1.2 x 2.7 m) panel in the alternate direction were examined. The parameters used to evaluate and compare the walls were strength, displacement, elastic and cyclic stiffness and the amount of hysteretic energy dissipated until failure and at specific levels of displacement.

5.2 Conclusions

5.2.1 Characteristics of 9 and 10 feet tall shear walls sheathed with long panels

Average values of the parameters produced by walls sheathed with long panels either matched or exceeded those of its counterpart sheathed with 4 x 8 feet (1.2 x 2.4 m) panels in all configurations except the 10 feet (3.0 m) tall prescriptive wall. The presence of blocking and more sheathing connections in a 10 feet (3.0 m) tall prescriptive shear wall sheathed with 4 x 8 feet (1.2 x 2.4 m) panels produced a system that was capable of achieving larger values of load and dissipating slightly more energy. However, 4 x 9 feet (1.2 x 2.7 m) panels can be used to provide adequate lateral resistance to 9 feet (2.7 m) tall prescriptive shear walls. When used to

sheath engineered shear walls, the long panels produced parameter values that exceeded those produced by 9 feet (2.7 m) tall walls sheathed with 4 x 8 feet (1.2 x 2.4 m) panels and matched those of 10 feet (3.0 m) tall walls sheathed with 4 x 8 feet (1.2 x 2.4 m) panels. Therefore, long sheathing panels can be used to provide adequate lateral resistance to 9 and 10 feet (2.7 and 3.0 m) tall engineered shear walls. In fact, long panels should be used to sheath 9 feet (2.7 m) tall engineered shear walls if maximum performance is of utmost importance.

Long panels are capable of great performance when used to sheath engineered shear walls because the mechanical hold-down device invokes rotation of the panel about its center of stiffness which causes the force in the panel to be distributed more evenly to each sheathing connection along the perimeter. This behavior produces greater levels of force and displacement at the sheathing connections along the blocking of an engineered shear wall sheathed with 4 x 8 feet (1.2 x 2.4 m) panels than are present at these connections in a prescriptive shear wall; thus, they are susceptible to tear through failures due to the limited edge distance at this location. This is not a source of failure in walls sheathed with panels capable of spanning the entire height of the wall because adequate edge distance is provided for the connections at all locations except along the common center stud.

One consistently noted observation was that the amount of lateral displacement that had occurred in all walls sheathed with long panels was significantly less than that of corresponding walls sheathed with 4 x 8 feet (1.2 x 2.4 m) panels. This was true of both prescriptive and engineered walls. This type of behavior was present in walls sheathed with long panels because a source of displacement and failure, the sheathing connections along the blocking, had been eliminated. Therefore, the stiffness of all walls sheathed with long panels was greater than corresponding walls sheathed with 4 x 8 feet (1.2 x 2.4 m) panels.

Another consistently noted observation was that walls sheathed with 4 x 8 feet (1.2 x 2.4 m) panels dissipated more hysteretic energy until failure than their counterparts sheathed with long panels. This was true for all configurations except 10 feet (3.0 m) tall engineered walls. However, this would have also been true for this configuration if the testing apparatus had not limited the amount of displacement that occurred during testing. Walls sheathed with 4 x 8 feet (1.2 x 2.4 m) panels dissipated more hysteretic energy until failure because they possessed a greater number of sheathing connections and their displacement at failure was greater than that of walls sheathed with long panels.

The following list summarizes the capabilities of long panels when used to sheath shear walls greater than 8 feet (2.4 m) in height:

(1) Long panels can only be used to sheath prescriptive shear walls of heights no greater than 9 feet (2.7 m) when maximum performance is desired. Ten feet tall prescriptive shear walls sheathed with 4 x 8 feet (1.2 x 2.4 m) panels outperformed corresponding walls sheathed with long panels by 22 pounds (98 N) per foot. To put this in perspective, the tables of shear wall design provided by the APA display a difference in capacity of 25 lbs/ft between panel thicknesses of 7/16 inch (11.1 mm) and 15/32 inch (11.9 mm) provided sheathing nail and schedule remain the same as was used in this investigation.

(2) Long panels can be used to sheath engineered shear walls of heights up to 10 feet (3.0 m). At heights less than 10 feet (3.0 m), a significant increase in performance can be achieved by sheathing engineered walls with panels capable of spanning the entire height of the wall. In this investigation, 9 feet (2.7 m) tall engineered shear walls sheathed with long panels produced a value of peak load that was 270 pounds (1200 N) greater than the peak load of the corresponding wall sheathed with 4 x 8 feet (1.2 x 2.4 m) panels.

(3) Use of panels capable of spanning the entire height of the wall decreased the amount of lateral displacement in both prescriptive and engineered walls. This is attributed to elimination of the internal seam of connections along the blocking present in a wall greater than 8 feet (2.4 m) in height sheathed with 4 x 8 feet (1.2 x 2.4 m) panels.

(4) Walls sheathed with 4 x 8 feet (1.2 x 2.4 m) panels dissipated slightly more hysteretic energy until failure than those sheathed with long panels.

5.2.2 Characteristics of walls sheathed with long panels extended onto the band joist

Extending the long panels past the bottom plate and down onto the band joist greatly improved the performance of both 8 and 9 feet (2.4 and 2.7 m) tall prescriptive shear walls. In essence, this provided an extra row of sheathing connections at the base of the wall to help resist the uplift force that is produced by the overturning moment. This allowed these walls to attain much larger values of peak load which in turn increased the amount of hysteretic energy

dissipated until failure. Extending the long panels onto the band joist was more beneficial in 9 feet (2.7 m) tall walls than it was in 8 feet (2.4 m) tall walls. This is because the larger aspect ratio of the 9 feet (2.7 m) tall wall produced greater uplift forces between the end stud in tension and the bottom plate.

The failure modes of these walls were very similar to those of the corresponding walls in which the sheathing panel was not extended past the bottom plate. Only the sheathing nails in the bottom plate and at the edge of the panel in the band joist experienced bending deformations. Sheathing nails removed from the end studs and top plate were in excellent condition.

The following list summarizes the advantages of extending long panels past the bottom plate and onto the band joist in an 8 feet (2.4 m) tall prescriptive shear wall:

(1) Peak load was increased 470 pounds (2089 N).
(2) Elastic stiffness was increased from 4.8 to 5.0 kips/inch (0.84 and 0.87 kN/mm).
(3) The amount of energy dissipated until failure increased from 2.8 to 3.9 kip-ft (3.8 and 5.3 kN-m).
(4) Displacement capacity was increased from 1.7 to 2.3 inches (43.2 to 58.4 mm) which essentially increases the toughness of the wall.

The following list summarizes the advantages of extending long panels past the bottom plate and onto the band joist in a 9 feet (2.7 m) tall prescriptive shear wall:

(1) Peak load was increased 830 pounds (3689 N).
(2) Elastic stiffness was increased from 3.3 to 4.4 kips/inch (0.58 and 0.77 kN/mm).
(3) The amount of energy dissipated until failure increased from 2.6 to 4.3 kip-ft (3.5 and 5.8 kN-m).
(4) Displacement capacity was increased from 1.9 to 2.3 inches (48.3 to 58.4 mm) which essentially increases the toughness of the wall.

5.2.3 Characteristics of walls sheathed with panels made from alternate oriented fibers

Only one configuration was sheathed with panels made from alternate oriented fibers. This was a 9 feet (2.7 m) tall prescriptive wall sheathed with panels measuring 4 x 9 feet (1.2 x 2.7 m). The values of strength and displacement produced by this configuration were consistent with those produced by the 9 feet (2.7 m) tall prescriptive walls sheathed with normal 4 x 9 feet (1.2 x 2.7 m) panels up until the point of failure. The amount of load at which both configurations failed was similar, but only 0.3 inches (7.6 mm) of additional displacement past the point of peak load was required to cause the walls sheathed with alternate oriented fibers to fail. This was half the amount that was required to cause the walls sheathed with normal 4 x 9 feet (1.2 x 2.7 m) panels to fail. Therefore, the failure mode of the walls sheathed with panels made from alternate oriented fibers, which was sheathing nail tear through under the end stud in tension, was much more sudden and brittle than any other 9 feet (2.7 m) tall prescriptive shear wall. These panels should not be used as the sheathing element of light-frame structures that are subjected to any kind of dynamic lateral loading because they do not display the ability to deform while still resisting load.

5.3 Recommendations

The main objective of this investigation was to determine the performance capabilities of long panels such that their use as the sheathing element of 9 and 10 feet (2.7 and 3.0 m) tall shear walls would eliminate the required blocking members when such walls are sheathed with 4 x 8 feet (1.2 x 2.4 m) panels.

In this investigation, a constant nail schedule of 6/12 was used throughout. Therefore, the effects of a smaller nail spacing, such as 4/12 and 3/12, should be investigated when used in conjunction with panels capable of spanning the entire height of a wall greater than 8 feet (2.4 m). In particular, great advantages in performance were obtained by using long panels to sheath 9 feet (2.7 m) tall engineered shear walls. It is the author's opinion that these advantages would be increased even further if a smaller nail spacing was used. Ten feet tall engineered shear walls sheathed with long panels produced values equivalent to those produced by the corresponding configuration sheathed with 4 x 8 feet (1.2 x 2.4 m) panels. A smaller nail spacing could improve the performance parameters of 10 feet (3.0 m) tall engineered shear walls sheathed with long panels such that they outperform their counterparts sheathed with 4 x 8 feet (1.2 x 2.4 m)

panels. The previous arguments are based on the fact that long panels distribute the load present in the engineered wall more evenly to each connection along the perimeter of the panel. Engineered walls sheathed with 4 x 8 feet (1.2 x 2.4 m) panels can only distribute the load within that panel, not the load acting within the entire height of the wall. Therefore, engineered walls sheathed with long panels would utilize a smaller nail spacing much more efficiently and effectively.

The effects of sheathing the opposite side of the framing with gypsum wall board should also be investigated. The fact that long panels decrease the amount of lateral displacement experienced by a shear wall greater than 8 feet (2.4 m) in height has been proven in this investigation. It is the author's opinion that gypsum wall board would perform better if attached to the opposite side of a tall shear wall sheathed with long panels as opposed to 4 x 8 feet (1.2 x 2.4 m) panels. The reasoning behind this statement is that gypsum wall board crushes around the shank of the nail as the wall experiences lateral displacement; thus, the nail shank bores a hole in the gypsum at each connection which significantly reduces the performance capabilities of gypsum wall board.

The testing protocol used in this investigation was the standard CUREE protocol. The failure modes produced by the protocol were representative of what has been reported to occur in actual seismic events. Low cycle fatigue of the sheathing connections, synonymous with the SPD protocol, did not occur in any of the tests conducted in this investigation. However, the values of lateral displacement at which failure occurred in all walls tested fell between the primary cycles of 1.0Δ and 1.5Δ. The sudden increase of displacement from 1.0Δ to 1.5Δ caused every wall to fail. It is the author's opinion that the increment at which the amplitude of primary cycles past 1.0Δ is increased should be decreased. Perhaps increasing the displacement amplitudes of primary cycles past 1.0Δ by 0.33Δ instead of 0.5Δ would provide greater insight to the behavior of light-frame systems subjected to reversed, cyclic loading.

The limits of the testing apparatus did not allow the 10 feet (3.0 m) tall engineered shear walls to be tested to failure. In order to reach the failure load of these configurations, a hydraulic actuator with greater displacement capabilities should be used.

Literature Cited

(1) American Society for Testing and Materials. (2000). "Standard Test Methods of Conducting Strength Tests of Panels for Building Construction," ASTM E72-98, Annual Book of Standards. Vol. 4.11. West Conshohocken, PA.

(2) American Society for Testing and Materials. (2000). "Standard Practice for Static Load Test for Shear Resistance of Framed Walls for Buildings," ASTM E564-95, Annual Book of Standards. Vol. 4.11. West Conshohocken, PA.

(3) Boresi, A.P., Schmidt, R.J. and Sidebottom, O.M. (1993). Advanced Mechanics of Materials. 5th Edition, John Wiley & Sons, New York.

(4) Commins, A.D. and Gregg, R.C. (1996). "Effect of Hold-downs and Stud-frame Systems on the Cyclic Behavior of Wood Shear Walls." Simpson Strong-Tie Co., Pleasanton, CA.

(5) Dinehart, D.W., and Shenton III, H.W. (1998). "Comparison of Static and Dynamic Response of Timber Shear Walls." *Journal of Structural Engineering*, Vol. 124, No. 6, pp 686-695.

(6) Dinehart, D.W., Shenton III, H.W. and Elliott, T.E. (1999). "The Dynamic Response of Wood-Frame Shear Walls with Viscoelastic Dampers." *Earthquake Spectra*, Vol. 15, No. 1, pp 67-85.

(7) Dolan, J.D. (1989). *The Dynamic Response of Timber Shear Walls*, thesis submitted in partial fulfillment of the Doctor of Philosophy Degree at the University of British Columbia, Vancouver, British Columbia.

(8) Dolan, J.D. and Foschi, R.O. (1991). "Structural Analysis Model for Static Loads On Timber Shear Walls." *Journal of Structural Engineering*, Vol. 117, No. 3, pp 851-861.

(9) Dolan, J.D. and Madsen, B. (1992a). "Monotonic and Cyclic Nail Connection Tests." *Canadian Journal of Civil Engineering*, Vol. 19, pp 97-104.

(10) Dolan, J.D. and Madsen, B. (1992b). "Monotonic and Cyclic Tests of Timber Shear Walls." *Canadian Journal of Civil Engineering*, Vol. 19, pp 415-422.

(11) Durham, J., Lam, F., and Prion, H.G.L. (2001). "Seismic Resistance of Wood Shear Walls with Large OSB Panels." *Journal of Structural Engineering*, Vol. 127, No. 12, pp 1460-1466.

(12) Faherty, K.F. and Williamson, T.G. (1997). Wood Engineering and Construction Handbook. 3rd Edition, McGraw-Hill, New York.

(13) Filiatrault, A. (1990). “Static and Dynamic Analysis of Timber Shear Walls.” *Canadian Journal of Civil Engineering*, Vol. 17, pp 643-651.

(14) Filiatrault, A. and Foschi, R.O. (1991). “Static and Dynamic Tests of Timber Shear Walls Fastened with Nails and Wood Adhesive.” *Canadian Journal of Civil Engineering*, Vol. 18, pp 749-755.

(15) Filiatrault, A. and Folz, B. (2002). “Performance-Based Seismic Design of Wood Framed Buildings.” *Journal of Structural Engineering*, Vol. 128, No. 1, pp 39-47.

(16) Foliente, G.C. (1995). “Hysteresis Modeling of Wood Joints and Structural Systems.” *Journal of Structural Engineering*, Vol. 121, No. 6, pp 1013-1022.

(17) Folz, B. and Filiatrault, A. (2001). “Cyclic Analysis of Wood Shear Walls.” *Journal of Structural Engineering*, Vol. 127, No. 4, pp 433-441.

(18) Foschi, R.O. (1974). “Load-Slip Characteristics of Nails.” *Wood Science*, Vol. 7, No. 1, pp 69-76.

(19) Foschi, R.O. (1977). “Analysis of Wood Diaphragms and Trusses, Part One: Diaphragms.” *Canadian Journal of Civil Engineering*, Vol. 4, pp 345-352.

(20) Gatto, Kip and C.M. Uang. (2001). "Cyclic Response of Woodframe Shearwalls: Loading Protocol and Rate of Loading Effects." CUREE-Caltech Project Report No. W-13, Consortium of Universities for Research in Earthquake Engineering, Richmond, CA.

(21) Gupta, A.K. and Kuo, G.P. (1985). “Behavior of Wood-Framed Shear Walls.” *Journal of Structural Engineering*, Vol. 111, No. 8, pp 1722-1733.

(22) Gupta, A.K. and Kuo, G.P. (1987). “Wood Framed Shear Walls with Uplifting.” *Journal of Structural Engineering*, Vol. 113, No. 2, pp 241-259.

(23) He, M., Lam, F. and Prion, H.G.L. (1998). “Influence of Cyclic Test Protocols on Performance of Wood-Based Shear Walls.” *Canadian Journal of Civil Engineering*, Vol. 25, pp 539-550.

(24) Humar, J.L. (2002). Dynamics of Structures. 2nd Edition, A.A. Balkema, Lisse, Netherlands.

(25) International Conference of Building Officials (ICBO). (1997). Uniform building code. Whittier, CA.

(26) Itani, R.Y. and Cheung, C.K. (1984). “Nonlinear Analysis of Sheathed Wood Diaphragms.” *Journal of Structural Engineering*, Vol. 110, No. 9, pp 2137-2147.

(27) Jones, S.N. and Fonseca, F.S. (2002) "Capacity of Oriented Strand Board Shear Walls with Overdriven Sheathing Nails." *Journal of Structural Engineering*, Vol. 128, No. 7, pp 898-907.

(28) Karacabeyli, E. and Ceccotti, A. (1998). Nailed Wood-Frame Shear Walls for Seismic Loads: Test Results and Design Considerations." Paper Reference; T207-6.

(29) Kasal, B. and Leichti, R.J. (1992). "Nonlinear Finite Element Model for Light-Frame Stud Walls." *Journal of Structural Engineering*, Vol. 118, No. 11, pp 3122-3135.

(30) Krawinkler, H., Parisi, F., Ibarra, L., Ayoub, A. and Medina, R. (2000). "Development of a Testing Protocol for Wood Frame Structures." CUREE Publication No. W-02, Richmond, CA.

(31) Lam, F., Prion, H.G.L. and He, M. (1997) "Lateral Resistance of Wood Shear Walls with Large Sheathing Panels." *Journal of Structural Engineering*, Vol. 123, No. 12, pp 1666-1673.

(32) McCutcheon, W.J. (1985). "Racking Deformations in Wood Shear Walls." *Journal of Structural Engineering*, Vol. 111, No. 2, pp 257-269.

(33) Porter, M.L. (1987). "Sequential Phase Displacement (SPD) Procedure for TCCMAR Testing." In: *Proceedings, 3rd Meeting of the Joint Technical Coordination Committee on Masonry Research*. U.S.-Japan Coordinated Earthquake Research Program, Tomamu, Japan.

(34) Salenikovich, A.J. (2000). *Racking Performance of Light-Frame Shear Walls*, thesis submitted in partial fulfillment of the Doctor of Philosophy Degree at Virginian Polytechnic Institute and State University, Blacksburg, Virginia.

(35) Schmidt, R.J. and Moody, R.C. (1989). "Modeling Laterally Loaded Light-Frame Buildings." *Journal of Structural Engineering*, Vol. 115, No. 1, pp 201-215.

(36) Shenton III, H.W., Dinehart, D.W. and Elliott, T.E. (1998). "Stiffness and Energy Degradation of Wood Frame Shear Walls." *Canadian Journal of Civil Engineering*, Vol. 25, pp 412-423.

(37) Skaggs, T.D. and Rose, J.D. (1996) "Cyclic Load Testing of Wood Structural Panel Shear Walls." *Proceedings of the 1996 International Wood Engineering Conference, New Orleans*, Vol. 2, pp 195-200.

(38) Tuomi, R.L., and McCutcheon, W.J. (1978). "Racking Strength of Light-Frame Nailed Walls." *Journal of the Structural Division*, Vol. 104, No. ST7, pp 1131-1141.

(39) White, M. and Dolan, J.D. (1995). "Nonlinear Shear-Wall Analysis." *Journal of Structural Engineering*, Vol. 121, No. 11, pp 1629-1635.

(40) Wolfe, R.W. (1983). “Research Paper FPL 439-Contribution of Gypsum Wallboard to the Racking Resistance of Light-Frame Walls.” United States Department of Agriculture, Forest Products Laboratory, Madison, WI.

Appendix

This table displays the values of each wall recorded by the data acquisition instruments used to determine the performance capabilities.

Specimen	Wall X	
Peak load, F_{peak}	Kips	
	KN	
Drift at peak load, Δ_{peak}	in.	
	Mm	
Yield load, F_{yield}	Kips	
	KN	
Drift at yield load, Δ_{yield}	in.	
	Mm	
Proportional limit, $0.4F_{peak}$	Kips	
	KN	
Drift at prop. limit, $\Delta@0.4F_{peak}$	In.	
	Mm	
Failure load or $0.8F_{peak}$	Kips	
	KN	
Drift at failure, $\Delta_{failure}$	in.	
	Mm	
Elastic stiffness, K_e $@0.4F_{peak}$	Kip/in.	
	KN/mm	
Work until failure	Kip·ft.	
	KN·m	
Ductility factor, μ		

Observations and failure modes:
The comments made in this section provide details about the failure experienced by the wall.

The values of the EEEP curve are displayed in the table below.

EEEP Parameters	units	negative	positive
F_{yield}	Kips		
	KN		
Δ_{yield}	In.		
	mm		
$\Delta_{failure}$	In.		
	mm		

	inches	mm	% of Total
Total Displacement			
Shear Deformation			
Rigid Body Motion			
Bending and Slip			

The table above provides information about the displacement experienced by the wall at peak load.

Primary	average displacement		Average load		work per cycle		cyclic stiffness		damping
cycle #	in.	mm	Kips	KN	Kip·ft.	KN·m	Kip/in.	KN/mm	ratio
1									
2									
3									

The table above displays the data of each primary cycle recorded during testing.

Five graphs of each wall are also included in the Appendix. These are plots of EEEP curves, hysteretic energy dissipated per cycle vs. displacement, load vs. ram displacement, change of Pots 7 and 8 vs. ram displacement and uplift (or compressive) displacements recorded by Pots 5 and 6 vs. ram displacement.

Table A.1. Performance Parameters of 8-8-P-1

Specimen	8-8-P-1	
Peak load, F_{peak}	Kips	2.628
	KN	11.691
Drift at peak load, Δ_{peak}	in.	1.277
	mm	32.44
Yield load, F_{yield}	Kips	2.371
	KN	10.545
Drift at yield load, Δ_{yield}	in.	0.373
	mm	9.48
Proportional limit, $0.4F_{peak}$	Kips	1.051
	KN	4.676
Drift at prop. limit, $\Delta@0.4F_{peak}$	in.	0.166
	mm	4.21
Failure load or $0.8F_{peak}$	Kips	2.103
	KN	9.353
Drift at failure, $\Delta_{failure}$	in.	1.944
	mm	49.37
Elastic stiffness, K_e $@0.4F_{peak}$	Kip/in.	6.351
	KN/mm	1.112
Work until failure	Kip·ft.	3.253
	KN·m	4.410
Ductility factor, μ	5.21	

Observations and failure modes:

- Mode of failure was sheathing nail tear through under the end stud in tension. This led to significant amounts of uplift displacement between end stud in tension and bottom plate.
- Sheathing nails removed from bottom plate displayed significant bending deformation. Sheathing nails removed from any other location experienced virtually no bending deformation.

Table A.2. EEEP Parameters of 8-8-P-1

EEEP Parameters	units	negative	positive
F_{yield}	Kips	-2.405	2.336
	KN	-10.697	10.393
Δ_{yield}	in.	-0.374	0.372
	mm	-9.51	9.46
$\Delta_{failure}$	in.	-1.996	1.891
	mm	-50.71	48.03

Table A.3. Displacement components of 8-8-P-1

	inches	mm	% of Total
Total Displacement	1.1	27.9	
Shear Deformation	0.2	5.1	18.1
Rigid Body Motion	0.9	22.9	81.8
Bending and Slip	0.0	0.0	0.0

Table A.4. Data of each Primary cycle of 8-8-P-1

Primary	average displacement		Average load		work per cycle		cyclic stiffness		damping
cycle #	in.	mm	Kips	KN	Kip·ft.	KN·m	Kip/in.	KN/mm	ratio
1	0.053	1.356	0.403	1.792	0.001	0.001	7.547	1.322	0.097
2	0.073	1.867	0.553	2.460	0.002	0.003	7.529	1.318	0.098
3	0.147	3.744	0.969	4.310	0.010	0.013	6.574	1.151	0.130
4	0.220	5.587	1.298	5.772	0.020	0.027	5.901	1.033	0.132
5	0.293	7.445	1.548	6.886	0.031	0.042	5.282	0.925	0.131
6	0.516	13.110	2.110	9.387	0.092	0.124	4.090	0.716	0.161
7	0.734	18.633	2.376	10.568	0.156	0.212	3.239	0.567	0.171
8	1.098	27.890	2.618	11.647	0.292	0.396	2.385	0.418	0.194
9	1.456	36.986	2.596	11.548	0.391	0.530	1.784	0.312	0.198
10	1.816	46.133	2.307	10.262	0.466	0.632	1.271	0.223	0.212
11	2.175	55.240	1.666	7.412	0.472	0.640	0.767	0.134	0.249

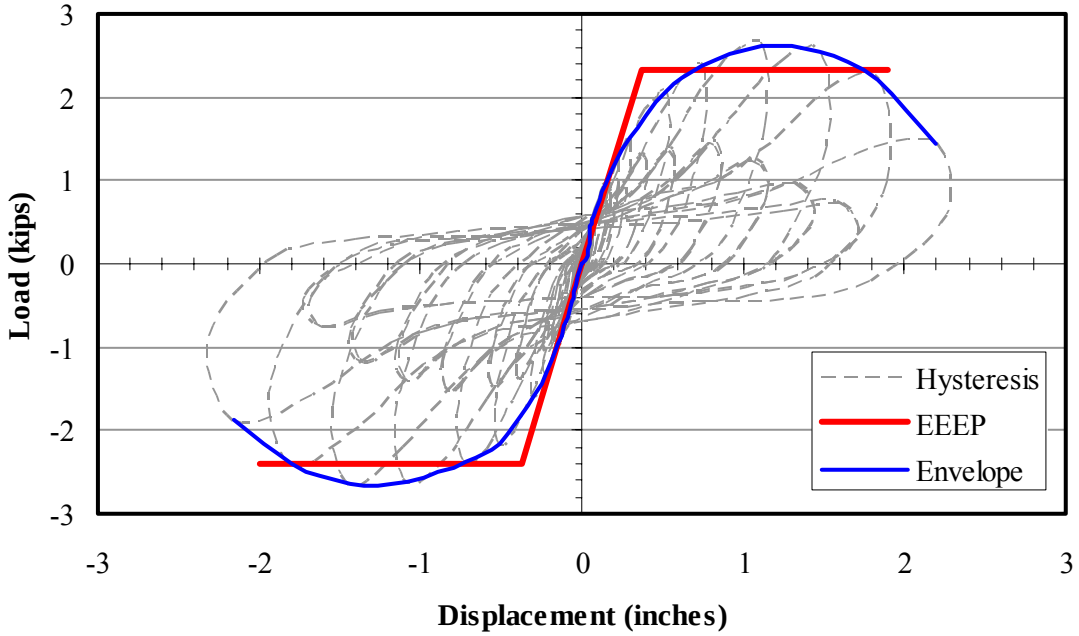

Figure A.1. Load vs. displacement, envelope and EEEP curves of 8-8-P-1

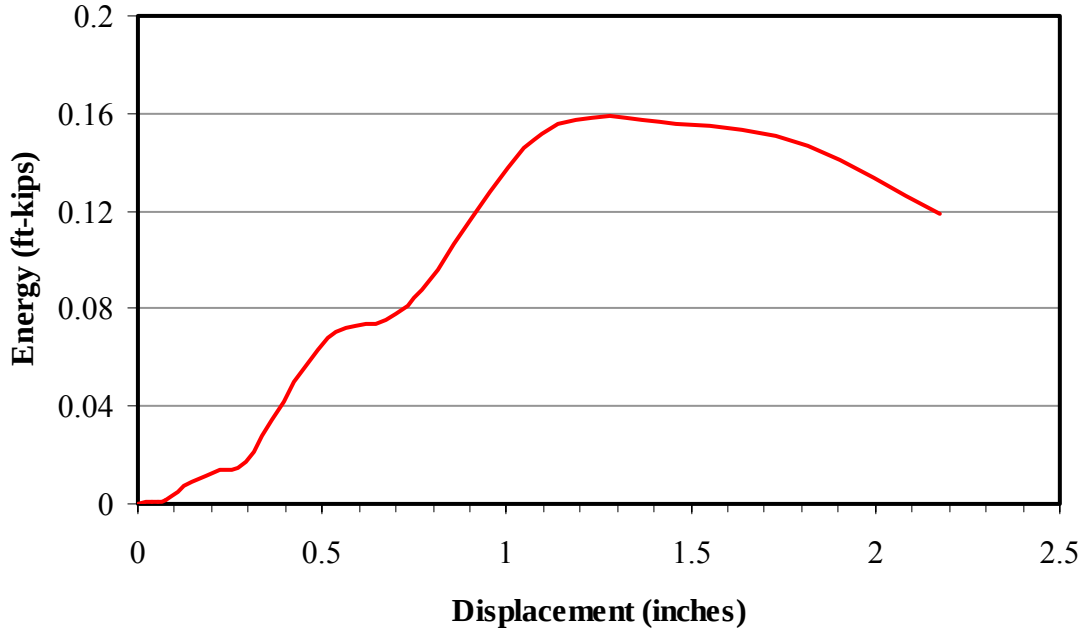

Figure A.2. Hysteretic energy dissipated per cycle vs. displacement of 8-8-P-1

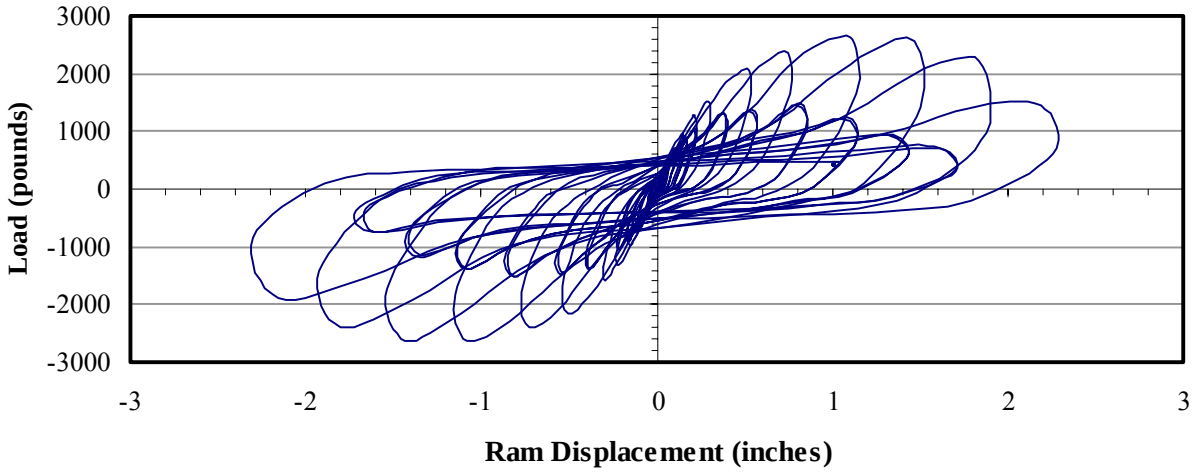

Figure A.3. Load vs. displacement of 8-8-P-1

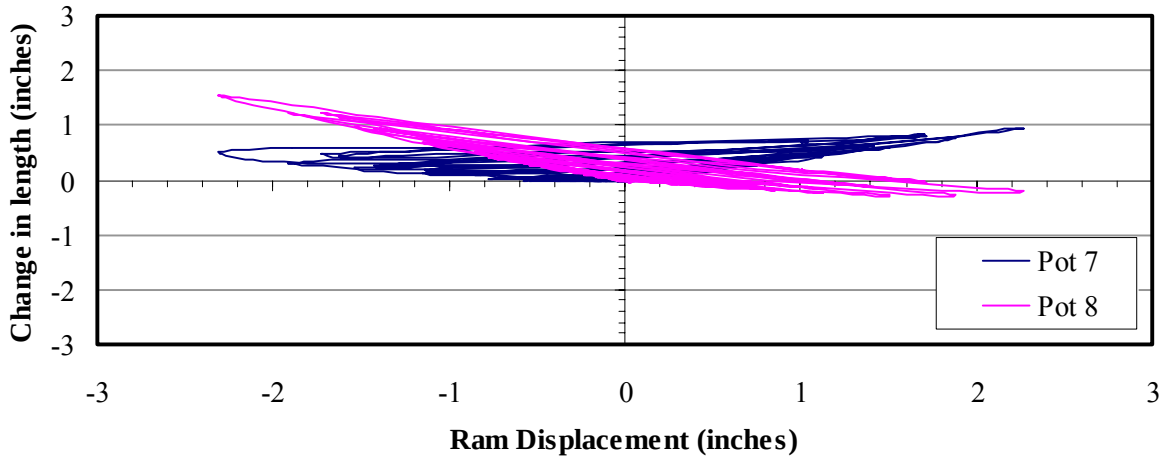

Figure A.4. Change in length of diagonal measuring Pots 7 and 8 vs. ram displacement of 8-8-P-1

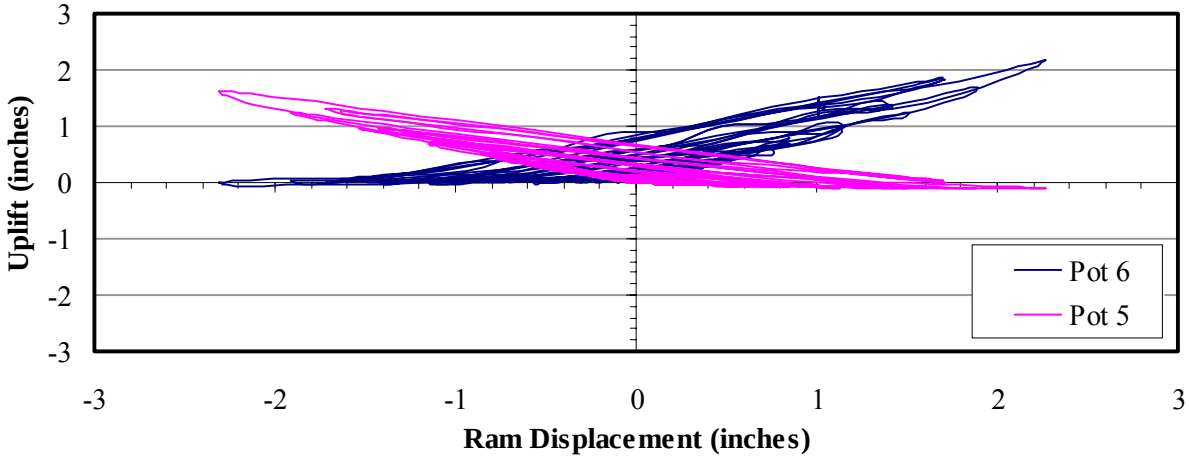

Figure A.5. Uplift displacement vs. ram displacement of 8-8-P-1

Table A.5. Performance Parameters of 8-8-P-2

Specimen	8-8-P-2	
Peak load, F_{peak}	Kips	2.688
	KN	11.955
Drift at peak load, Δ_{peak}	in.	1.289
	mm	32.74
Yield load, F_{yield}	Kips	2.408
	KN	10.712
Drift at yield load, Δ_{yield}	in.	0.583
	mm	14.80
Proportional limit, $0.4F_{peak}$	Kips	1.075
	KN	4.782
Drift at prop. limit, $\Delta@0.4F_{peak}$	in.	0.261
	mm	6.64
Failure load or $0.8F_{peak}$	Kips	2.150
	KN	9.564
Drift at failure, $\Delta_{failure}$	in.	1.677
	mm	42.59
Elastic stiffness, K_e $@0.4F_{peak}$	Kip/in.	4.906
	KN/mm	0.859
Work until failure	Kip·ft.	3.179
	KN·m	4.311
Ductility factor, μ	3.44	

Observations and failure modes:

- Mode of failure was sheathing nail tear through under the end stud in tension. This led to significant amounts of uplift displacement between end stud in tension and bottom plate.
- Sheathing nails removed from bottom plate displayed significant bending deformation. Sheathing nails removed from any other location experienced virtually no bending deformation.

Table A.6. EEEP Parameters of 8-8-P-2

EEEP Parameters	units	negative	positive
F_{yield}	Kips	-2.500	2.317
	KN	-11.119	10.304
Δ_{yield}	in.	-0.361	0.805
	mm	-9.16	20.44
$\Delta_{failure}$	in.	-1.767	1.587
	mm	-44.88	40.30

Table A.7. Displacement components of 8-8-P-2

	inches	mm	% of Total
Total Displacement	1.5	38.1	
Shear Deformation	0.3	7.6	20.0
Rigid Body Motion	1.2	30.5	80.0
Bending and Slip	0.0	0.0	0.0

Table A.8. Data of each Primary cycle of 8-8-P-2

Primary	average displacement		average load		work per cycle		cyclic stiffness		Damping
cycle #	in.	mm	Kips	KN	Kip·ft.	KN·m	Kip/in.	KN/mm	ratio
1	0.036	0.912	0.198	0.879	0.001	0.001	5.872	1.028	0.206
2	0.054	1.384	0.332	1.476	0.001	0.002	6.053	1.060	0.137
3	0.075	1.895	0.436	1.938	0.002	0.003	5.826	1.020	0.123
4	0.148	3.757	0.792	3.523	0.008	0.011	5.374	0.941	0.133
5	0.221	5.612	1.091	4.853	0.017	0.023	4.943	0.866	0.132
6	0.295	7.496	1.313	5.840	0.027	0.037	4.463	0.782	0.134
7	0.519	13.191	1.828	8.131	0.083	0.112	3.534	0.619	0.168
8	0.740	18.809	2.267	10.086	0.146	0.197	3.071	0.538	0.166
9	1.107	28.108	2.612	11.616	0.291	0.394	2.363	0.414	0.192
10	1.475	37.474	2.615	11.630	0.380	0.516	1.772	0.310	0.188
11	1.678	42.619	2.183	9.709	0.479	0.650	1.312	0.230	0.250
12	2.003	50.866	1.441	6.410	0.463	0.628	0.724	0.127	0.306

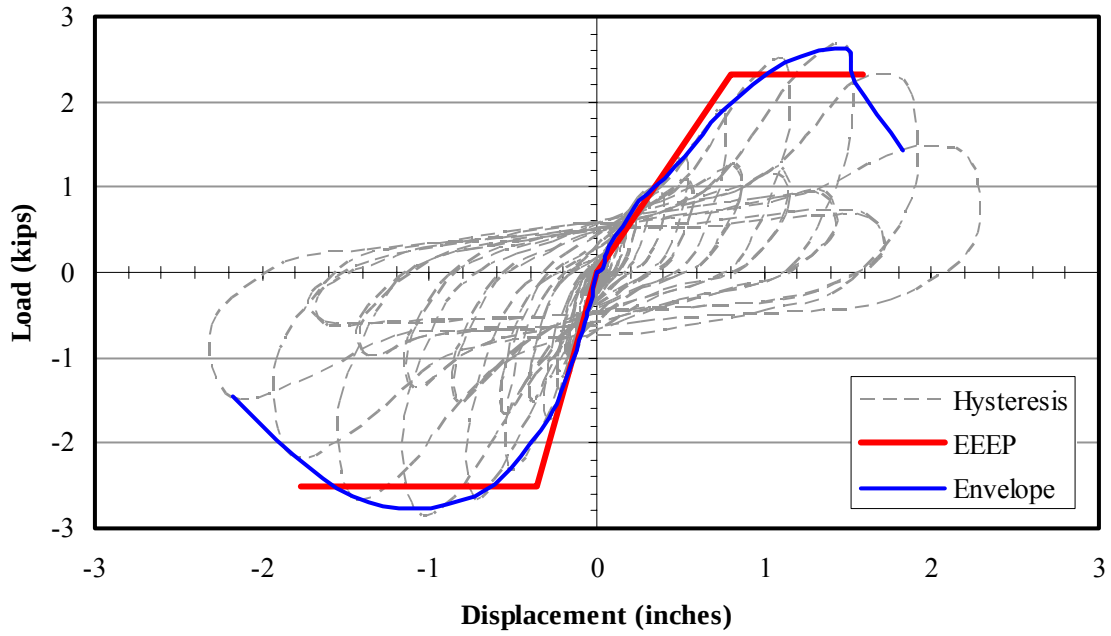

Figure A.6. Load vs. displacement, envelope and EEEP curves of 8-8-P-2

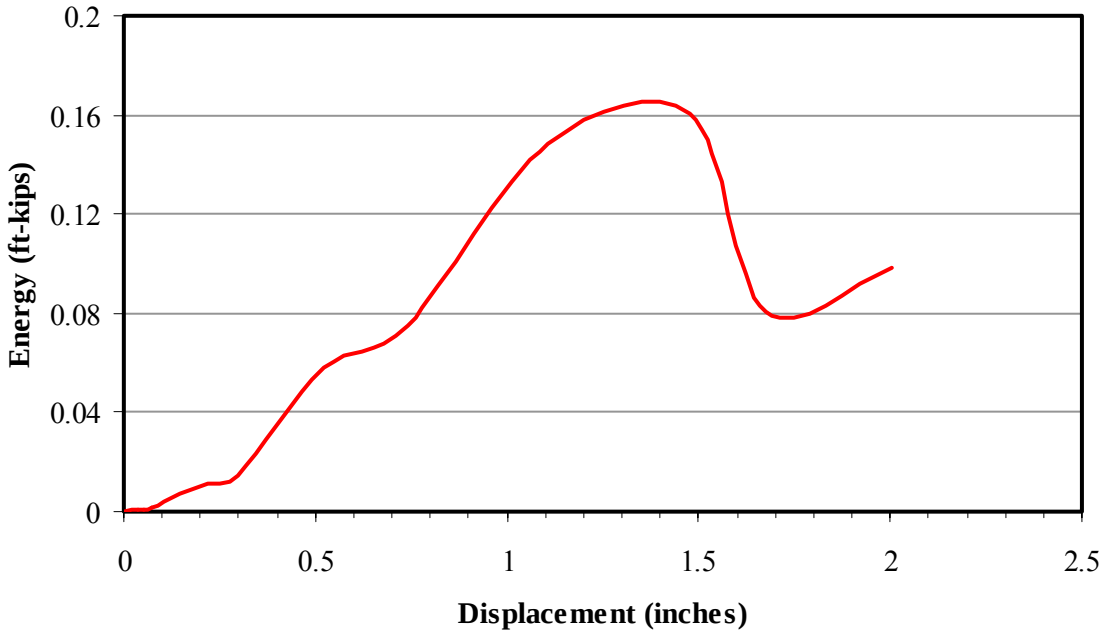

Figure A.7. Hysteretic energy dissipated per cycle vs. displacement of 8-8-P-2

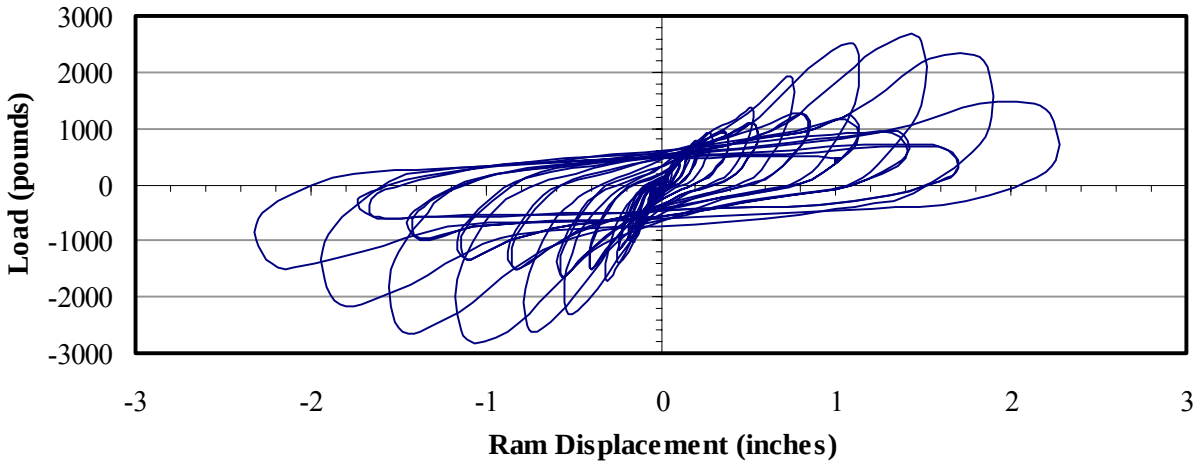

Figure A.8. Load vs. displacement of 8-8-P-2

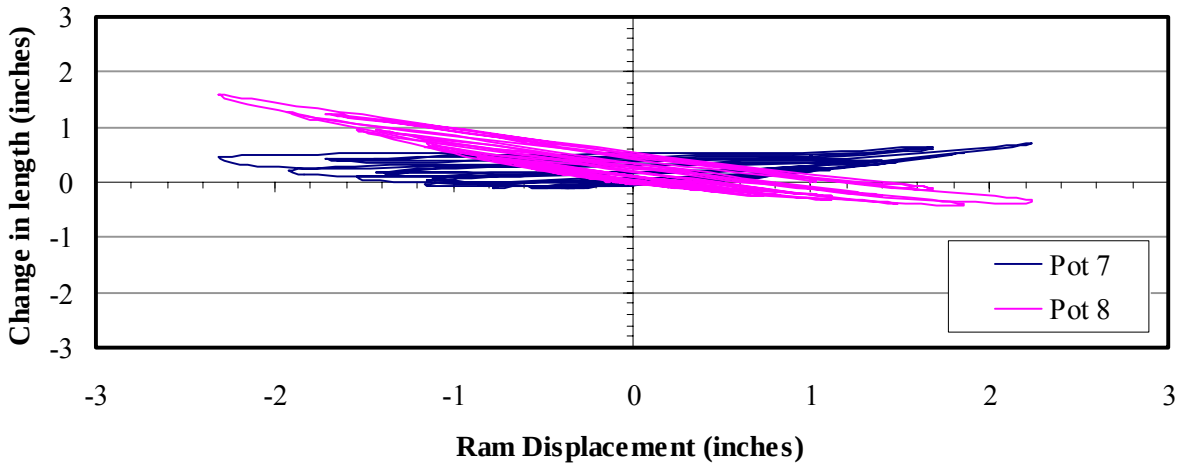

Figure A.9. Change in length of diagonal measuring Pots 7 and 8 vs. ram displacement of 8-8-P-2

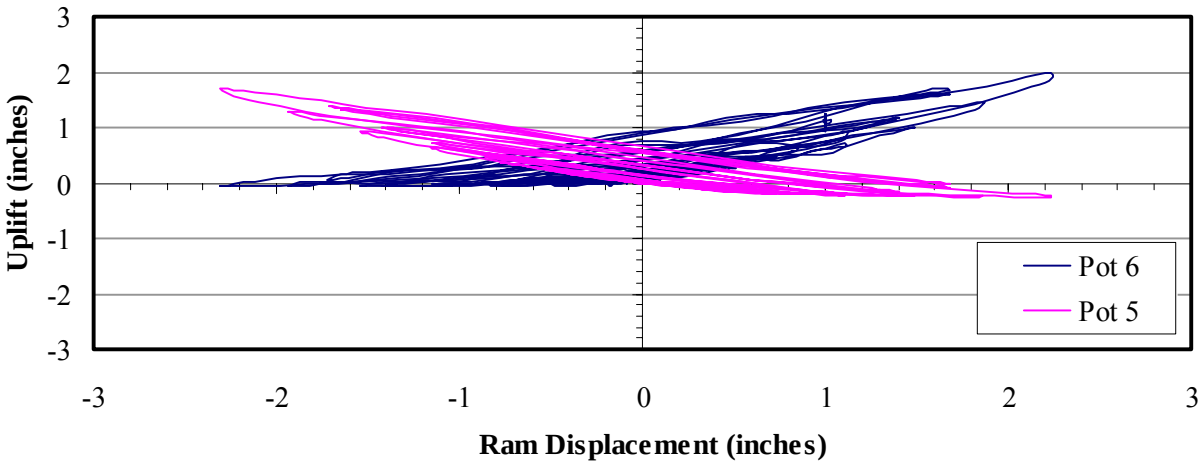

Figure A.10. Uplift displacement vs. ram displacement of 8-8-P-2

Table A.9. Performance Parameters of 8-8-P-3

Specimen	8-8-P-3	
Peak load, F_{peak}	Kips	2.200
	KN	9.784
Drift at peak load, Δ_{peak}	in.	1.009
	mm	25.63
Yield load, F_{yield}	Kips	2.013
	KN	8.954
Drift at yield load, Δ_{yield}	in.	0.614
	mm	15.58
Proportional limit, $0.4F_{peak}$	Kips	0.880
	KN	3.913
Drift at prop. limit, $\Delta@0.4F_{peak}$	in.	0.267
	mm	6.79
Failure load or $0.8F_{peak}$	Kips	1.760
	KN	7.827
Drift at failure, $\Delta_{failure}$	in.	1.540
	mm	39.10
Elastic stiffness, K_e $@0.4F_{peak}$	Kip/in.	3.316
	KN/mm	0.581
Work until failure	Kip·ft.	1.921
	KN·m	2.605
Ductility factor, μ	2.55	

Observations and failure modes:

- Mode of failure was sheathing nail tear through under the end stud in tension. This led to significant amounts of uplift displacement between end stud in tension and bottom plate.
- Sheathing nails removed from bottom plate displayed significant bending deformation. Sheathing nails removed from any other location experienced virtually no bending deformation.

Table A.10. EEEP Parameters of 8-8-P-3

EEEP Parameters	units	negative	positive
F_{yield}	Kips	-1.944	2.081
	KN	-8.649	9.258
Δ_{yield}	in.	-0.539	0.688
	mm	-13.69	17.48
$\Delta_{failure}$	in.	-1.565	1.514
	mm	-39.74	38.46

Table A.11. Displacement components of 8-8-P-3

	inches	mm	% of Total
Total Displacement	1.0	25.4	
Shear Deformation	0.0	0.0	0.0
Rigid Body Motion	1.0	25.4	100.0
Bending and Slip	0.0	0.0	0.0

Table A.12. Data of each Primary cycle of 8-8-P-3

Primary	average displacement		average load		work per cycle		cyclic stiffness		Damping
cycle #	in.	mm	Kips	KN	Kip·ft.	KN·m	Kip/in.	KN/mm	ratio
1	0.040	1.016	0.130	0.580	0.001	0.001	3.364	0.589	0.222
2	0.058	1.461	0.269	1.195	0.001	0.001	4.671	0.818	0.126
3	0.078	1.990	0.362	1.609	0.002	0.003	4.614	0.808	0.129
4	0.139	3.538	0.549	2.440	0.007	0.010	3.927	0.688	0.183
5	0.220	5.596	0.780	3.468	0.015	0.020	3.531	0.618	0.164
6	0.295	7.494	0.931	4.140	0.022	0.030	3.146	0.551	0.155
7	0.519	13.175	1.508	6.709	0.068	0.092	2.924	0.512	0.167
8	0.672	17.070	1.871	8.324	0.125	0.169	2.783	0.487	0.189
9	1.009	25.627	2.200	9.784	0.235	0.318	2.182	0.382	0.202
10	1.337	33.966	2.091	9.302	0.339	0.460	1.566	0.274	0.232
11	1.662	42.226	1.538	6.841	0.356	0.482	0.928	0.162	0.266
12	1.988	50.486	1.047	4.656	0.376	0.510	0.530	0.093	0.347

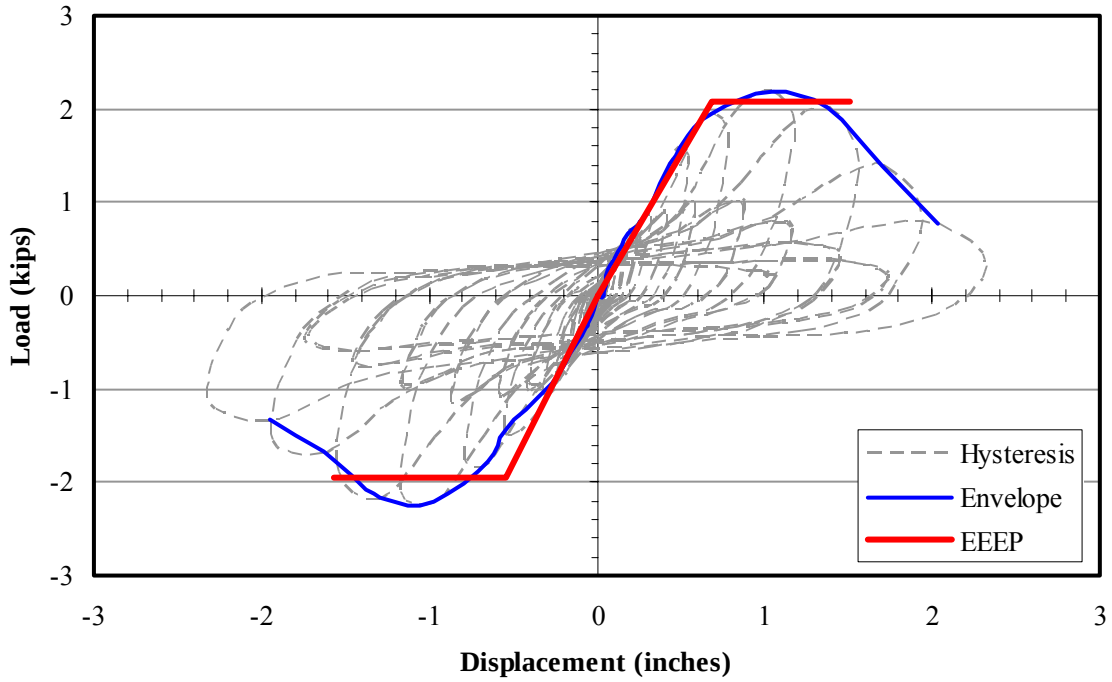

Figure A.11. Load vs. displacement, envelope and EEEP curves of 8-8-P-3

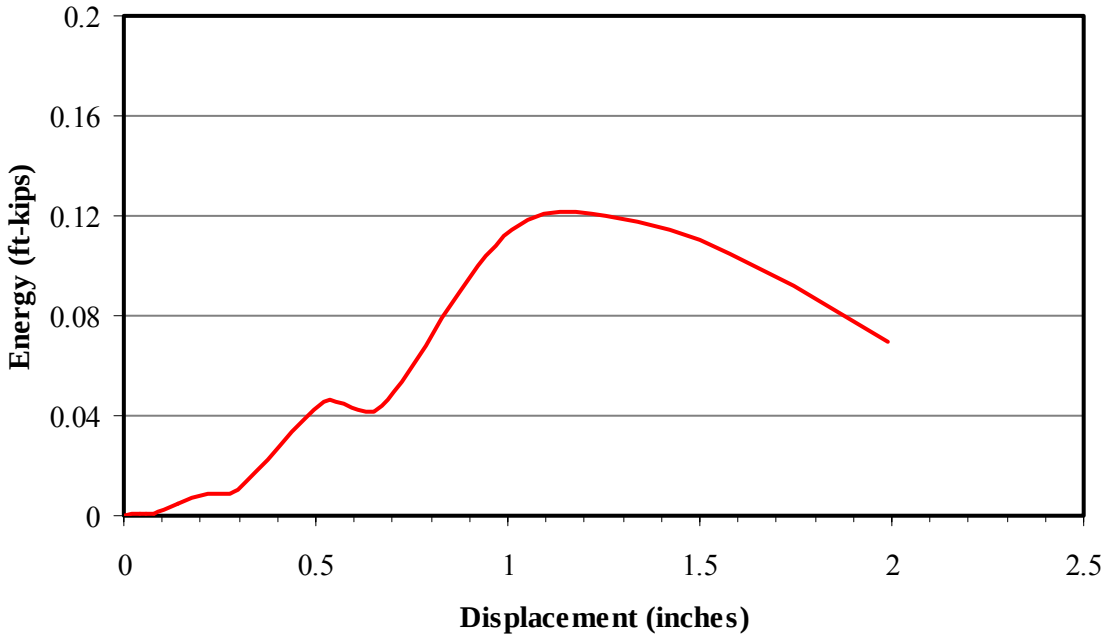

Figure A.12. Hysteretic energy dissipated per cycle vs. displacement of 8-8-P-3

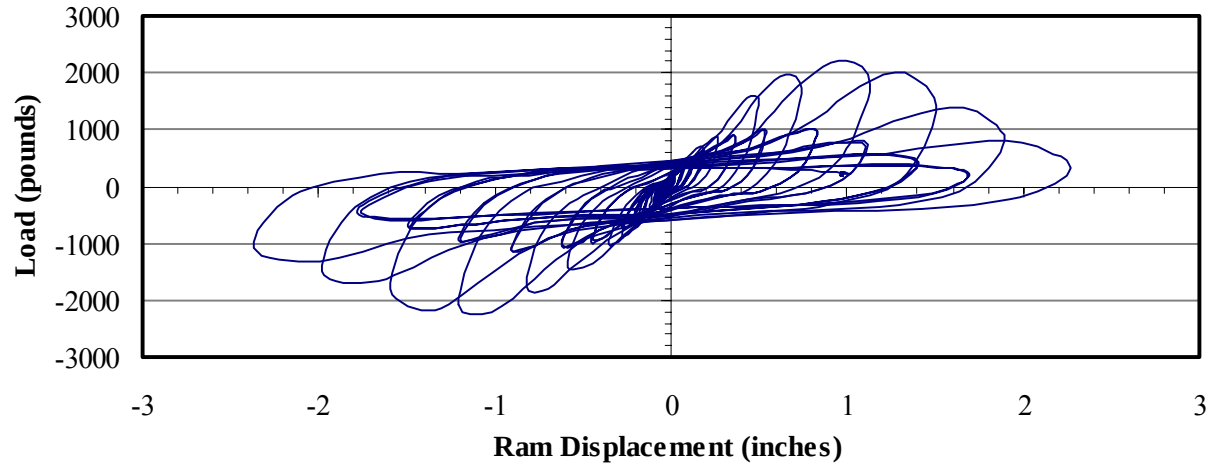

Figure A.13. Load vs. displacement of 8-8-P-3

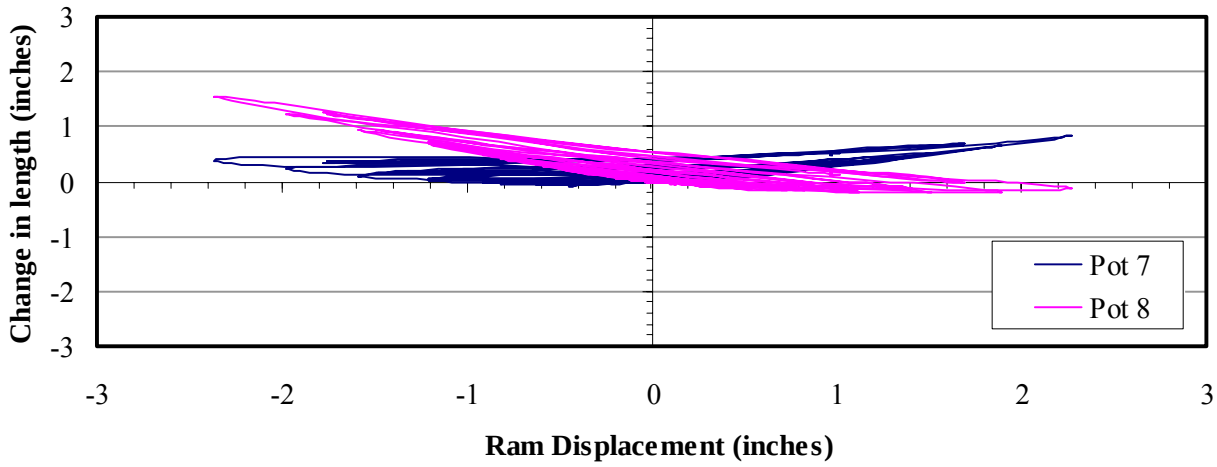

Figure A.14. Change in length of diagonal measuring Pots 7 and 8 vs. ram displacement of 8-8-P-3

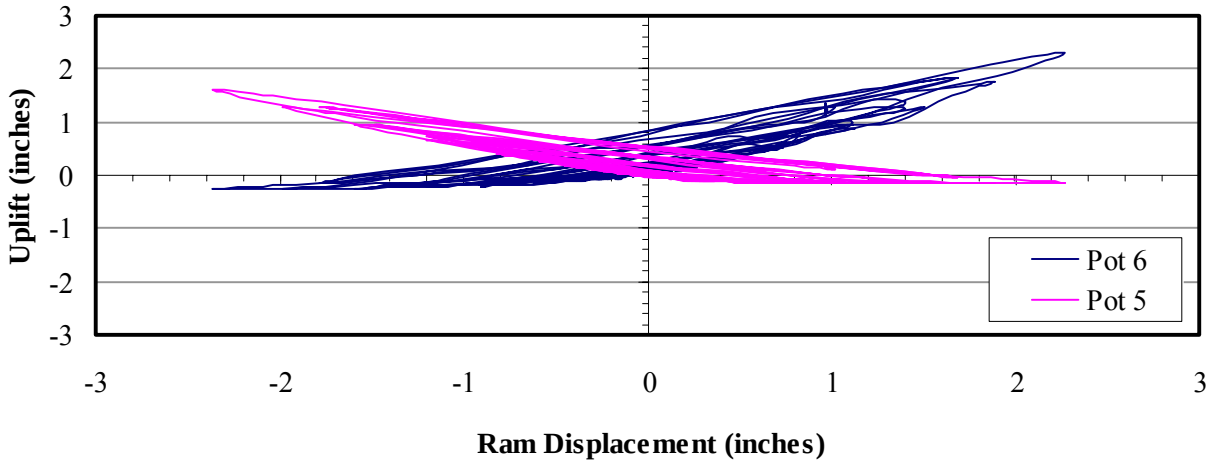

Figure A.15. Uplift displacement vs. ram displacement of 8-8-P-3

Table A.13. Performance Parameters of 9-8-P-1

Specimen	9-8-P-1	
Peak load, F_{peak}	Kips	2.071
	KN	9.210
Drift at peak load, Δ_{peak}	in.	1.406
	mm	35.71
Yield load, F_{yield}	Kips	1.855
	KN	8.252
Drift at yield load, Δ_{yield}	in.	0.804
	mm	20.42
Proportional limit, $0.4F_{peak}$	Kips	0.828
	KN	3.684
Drift at prop. limit, $\Delta@0.4F_{peak}$	in.	0.359
	mm	9.12
Failure load or $0.8F_{peak}$	Kips	1.656
	KN	7.368
Drift at failure, $\Delta_{failure}$	in.	2.027
	mm	51.48
Elastic stiffness, K_e $@0.4F_{peak}$	Kip/in.	2.308
	KN/mm	0.404
Work until failure	Kip·ft.	2.912
	KN·m	3.948
Ductility factor, μ	2.52	

Observations and failure modes:

- Mode of failure was sheathing nail tear through under the end stud in tension. This led to significant amounts of uplift displacement between end stud in tension and bottom plate.
- Sheathing nails removed from bottom plate displayed significant bending deformation. Sheathing nails removed from any other location experienced virtually no bending deformation.
- No failure around 4 x 1 ft panel segments

Table A.14. EEEP Parameters of 9-8-P-1

EEEP Parameters	units	negative	positive
F_{yield}	Kips	-1.853	1.858
	KN	-8.240	8.264
Δ_{yield}	In.	-0.807	0.801
	mm	-20.49	20.34
$\Delta_{failure}$	In.	-1.889	2.165
	mm	-47.97	54.99

Table A.15. Displacement components of 9-8-P-1

	inches	mm	% of Total
Total Displacement	1.4	35.6	
Shear Deformation	0.3	7.6	21.4
Rigid Body Motion	1.1	27.9	78.6
Bending and Slip	0.0	0.0	0.0

Table A.16. Data of each Primary cycle of 9-8-P-1

Primary	average displacement		average load		Work per cycle		cyclic stiffness		Damping
cycle #	in.	mm	Kips	KN	Kip·ft.	KN·m	Kip/in.	KN/mm	ratio
1	0.085	2.154	0.319	1.419	0.003	0.003	3.772	0.660	0.178
2	0.125	3.179	0.448	1.992	0.004	0.006	3.578	0.627	0.150
3	0.169	4.305	0.521	2.318	0.008	0.011	3.074	0.538	0.169
4	0.340	8.623	0.793	3.529	0.025	0.035	2.337	0.409	0.181
5	0.507	12.879	1.144	5.087	0.050	0.067	2.256	0.395	0.163
6	0.674	17.117	1.382	6.146	0.084	0.114	2.051	0.359	0.173
7	1.102	27.979	1.902	8.460	0.227	0.308	1.729	0.303	0.206
8	1.406	35.707	2.071	9.210	0.353	0.479	1.473	0.258	0.231
9	1.905	48.393	1.797	7.992	0.566	0.768	0.947	0.166	0.316
10	2.074	52.690	0.861	3.831	0.461	0.624	0.544	0.095	0.555

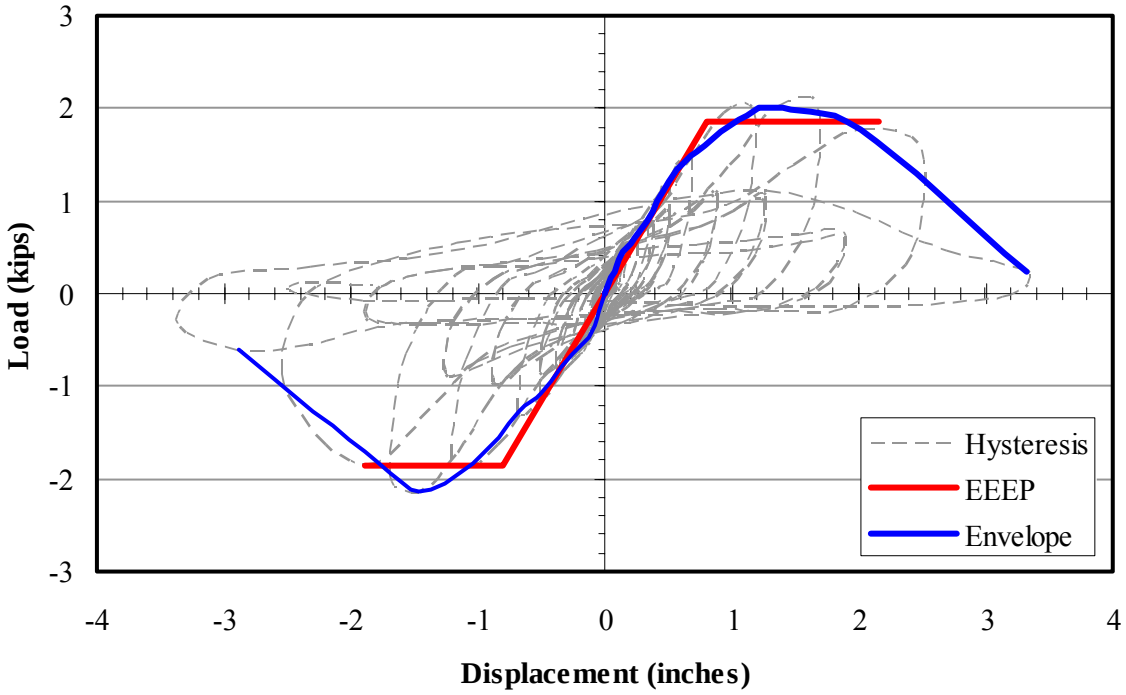

Figure A.16. Load vs. displacement, envelope and EEEP curves of 9-8-P-1

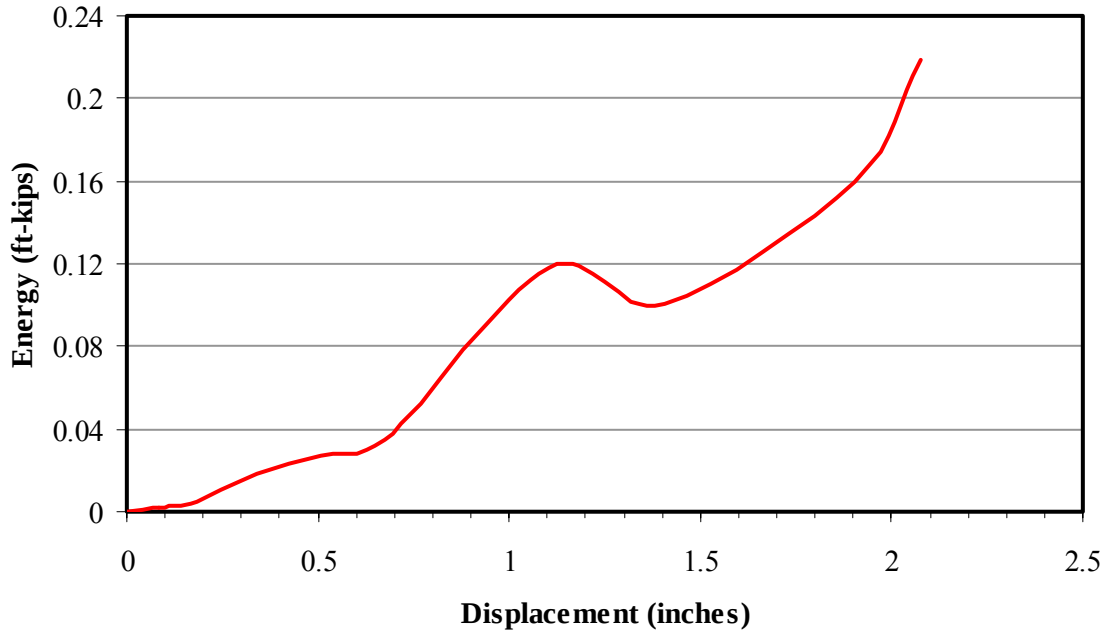

Figure A.17. Hysteretic energy dissipated per cycle vs. displacement of 9-8-P-1

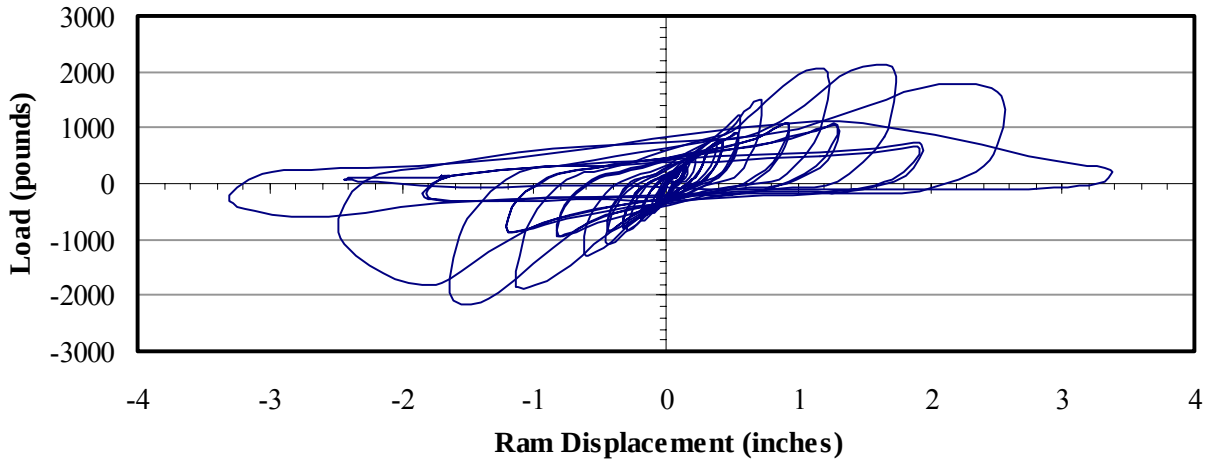

Figure A.18. Load vs. displacement of 9-8-P-1

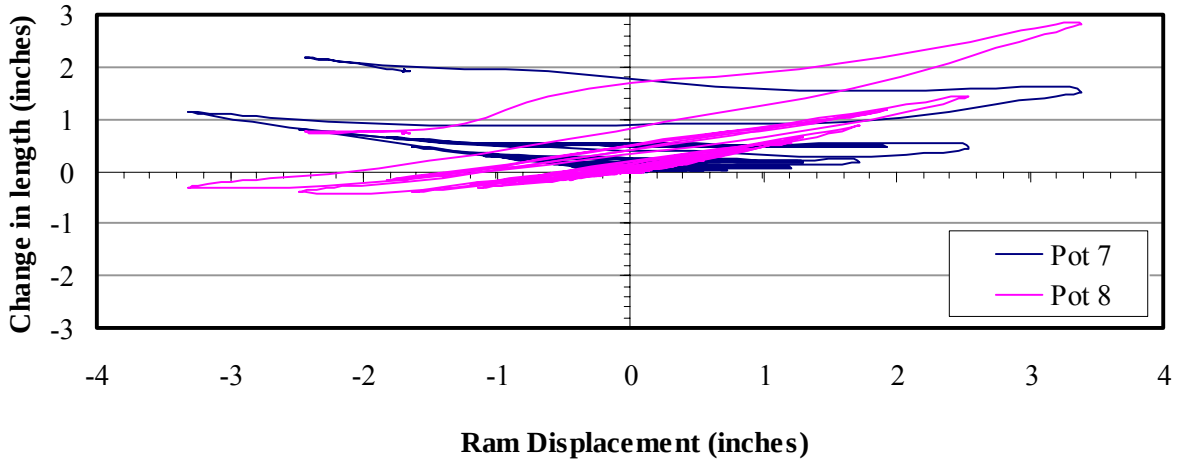

Figure A.19. Change in length of diagonal measuring Pots 7 and 8 vs. ram displacement of 9-8-P-1

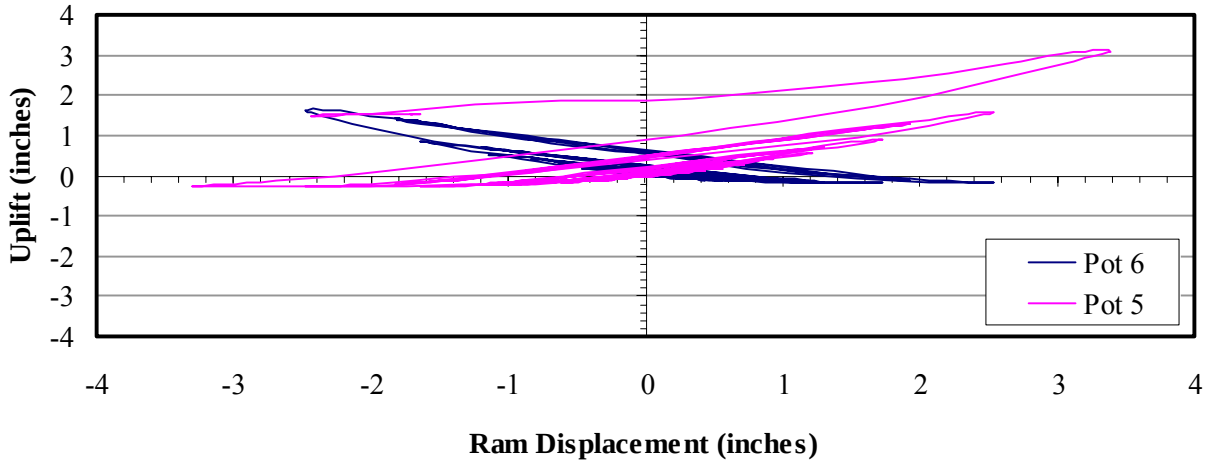

Figure A.20. Uplift displacement vs. ram displacement of 9-8-P-1

Table A.17. Performance Parameters of 9-8-P-2

Specimen	9-8-P-2	
Peak load, F_{peak}	Kips	1.925
	KN	8.562
Drift at peak load, Δ_{peak}	in.	1.987
	mm	50.48
Yield load, F_{yield}	Kips	1.718
	KN	7.642
Drift at yield load, Δ_{yield}	in.	0.711
	mm	18.05
Proportional limit, $0.4F_{peak}$	Kips	0.770
	KN	3.425
Drift at prop. limit, $\Delta@0.4F_{peak}$	in.	0.315
	mm	8.00
Failure load or $0.8F_{peak}$	Kips	1.540
	KN	6.850
Drift at failure, $\Delta_{failure}$	in.	2.232
	mm	56.68
Elastic stiffness, K_e $@0.4F_{peak}$	Kip/in.	4.200
	KN/mm	0.736
Work until failure	Kip·ft.	1.719
	KN·m	2.331
Ductility factor, μ	5.17	

Observations and failure modes:

- Mode of failure was sheathing nail tear through under the end stud in tension. This led to significant amounts of uplift displacement between end stud in tension and bottom plate.
- Sheathing nails removed from bottom plate displayed significant bending deformation. Sheathing nails removed from any other location experienced virtually no bending deformation.
- No failure around 4 x 1 ft panel segments

Table A.18. EEEP Parameters of 9-8-P-2

EEEP Parameters	units	negative	positive
F_{yield}	Kips	-2.007	1.429
	KN	-8.927	6.357
Δ_{yield}	in.	-1.210	0.212
	mm	-30.72	5.38
$\Delta_{failure}$	in.	-2.752	1.711
	mm	-69.90	43.46

Table A.19. Displacement components of 9-8-P-2

	inches	mm	% of Total
Total Displacement	2.4	61.0	
Shear Deformation	0.5	12.7	20.8
Rigid Body Motion	1.9	49.3	79.2
Bending and Slip	0.0	0.0	0.0

Table A.20. Data of each Primary cycle of 9-8-P-2

Primary	average displacement		average load		work per cycle		cyclic stiffness		Damping
cycle #	in.	mm	Kips	KN	Kip·ft.	KN·m	Kip/in.	KN/mm	ratio
1	0.082	2.078	0.426	1.894	0.003	0.004	5.316	0.931	0.179
2	0.119	3.033	0.509	2.264	0.005	0.007	4.301	0.753	0.167
3	0.160	4.064	0.587	2.613	0.009	0.012	3.714	0.650	0.182
4	0.322	8.179	0.840	3.736	0.028	0.038	2.628	0.460	0.199
5	0.481	12.216	1.035	4.602	0.048	0.065	2.159	0.378	0.185
6	0.638	16.194	1.198	5.328	0.070	0.094	1.883	0.330	0.174
7	1.116	28.349	1.665	7.405	0.183	0.248	1.492	0.261	0.188
8	1.587	40.300	1.840	8.185	0.302	0.410	1.158	0.203	0.197
9	2.111	53.608	1.649	7.333	0.452	0.612	0.759	0.133	0.237
10	2.882	73.199	1.225	5.450	0.479	0.650	0.447	0.078	0.271
11	3.143	79.835	0.643	2.861	0.401	0.544	0.197	0.035	0.366

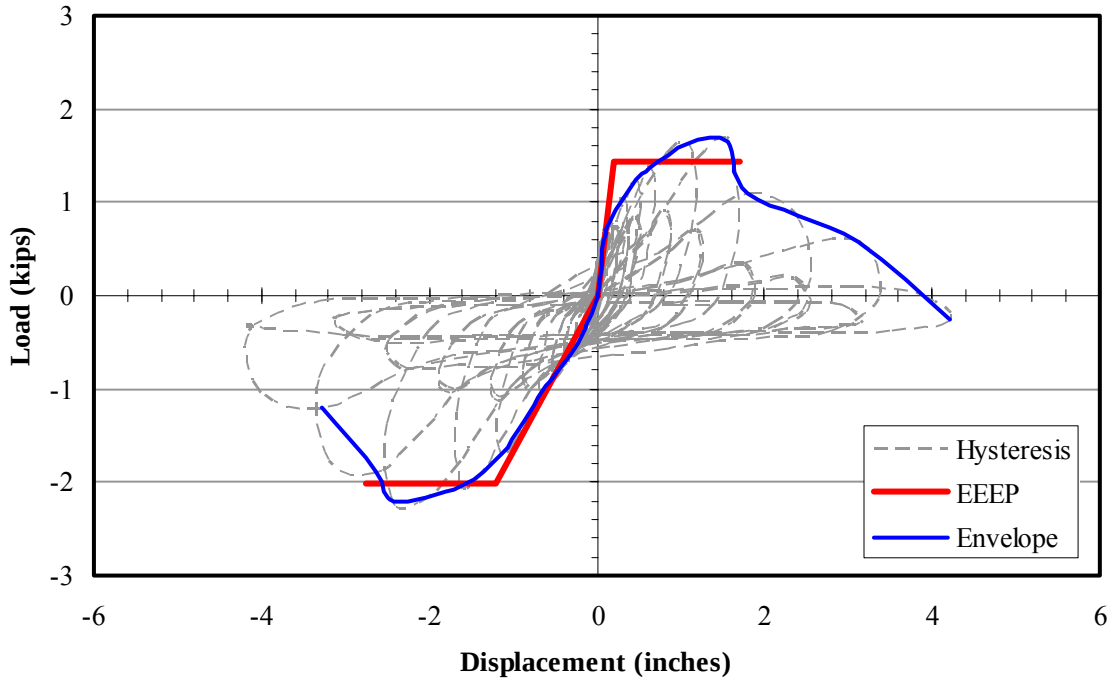

Figure A.21. Load vs. displacement, envelope and EEEP curves of 9-8-P-2

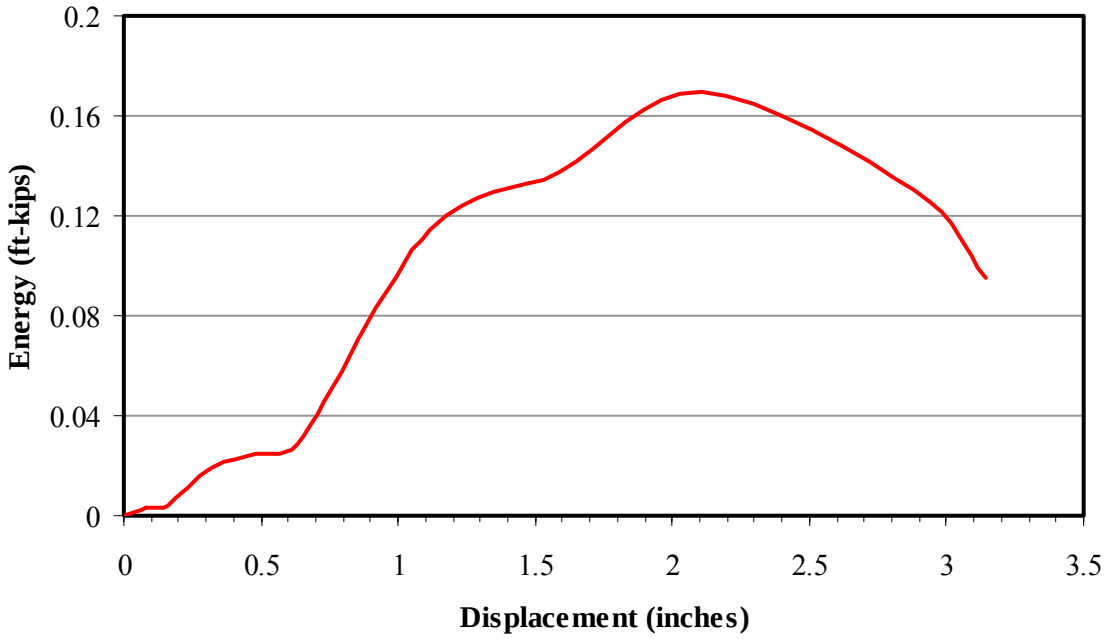

Figure A.22. Hysteretic energy dissipated per cycle vs. displacement of 9-8-P-2

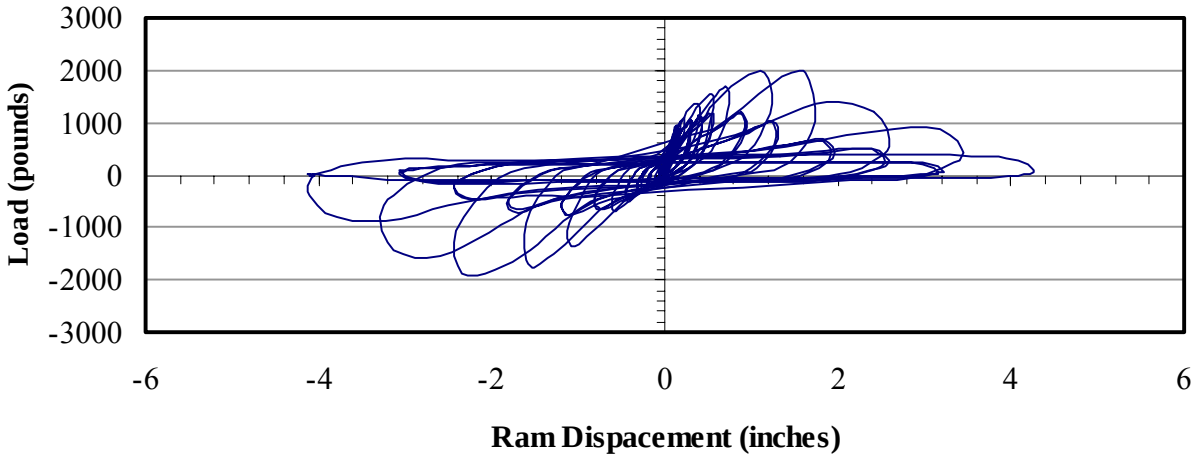

Figure A.23. Load vs. displacement of 9-8-P-2

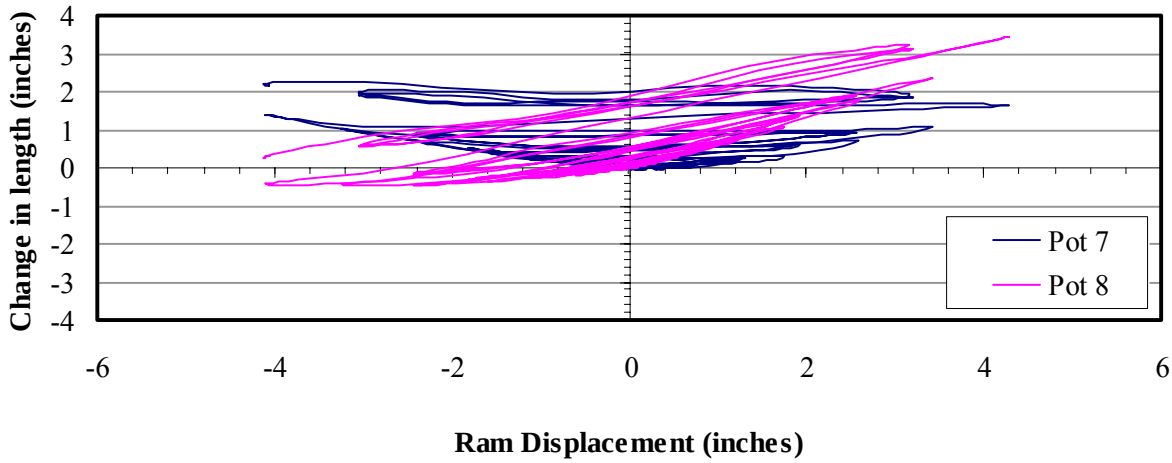

Figure A.24. Change in length of diagonal measuring Pots 7 and 8 vs. ram displacement of 9-8-P-2

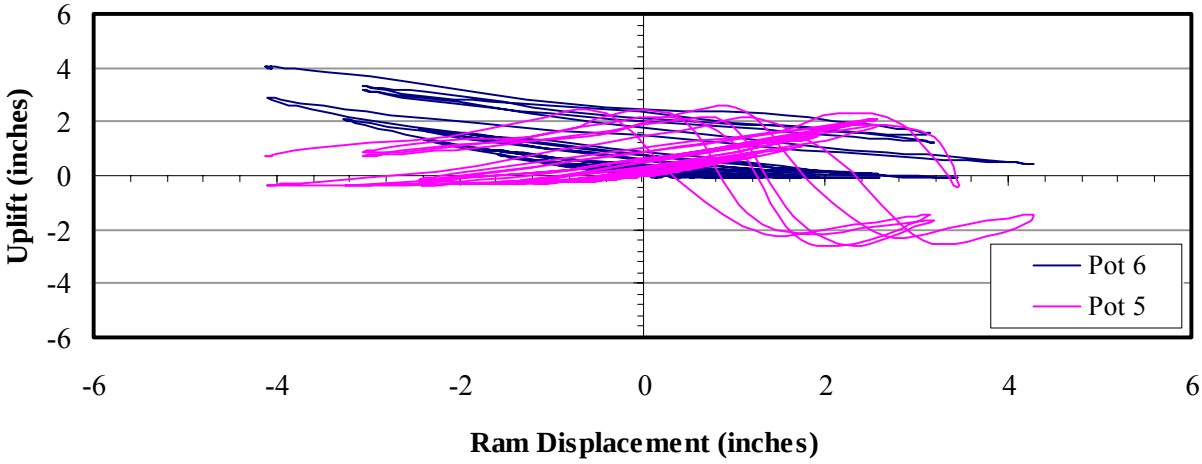

Figure A.25. Uplift displacement vs. ram displacement of 9-8-P-2

Table A.21. Performance Parameters of 9-8-P-3

Specimen	9-8-P-3	
Peak load, F_{peak}	Kips	2.211
	KN	9.835
Drift at peak load, Δ_{peak}	in.	1.527
	mm	38.79
Yield load, F_{yield}	Kips	1.830
	KN	8.140
Drift at yield load, Δ_{yield}	in.	0.551
	mm	13.99
Proportional limit, $0.4F_{peak}$	Kips	0.884
	KN	3.934
Drift at prop. limit, $\Delta@0.4F_{peak}$	in.	0.269
	mm	6.83
Failure load or $0.8F_{peak}$	Kips	1.769
	KN	7.868
Drift at failure, $\Delta_{failure}$	in.	1.668
	mm	42.37
Elastic stiffness, K_e $@0.4F_{peak}$	Kip/in.	3.445
	KN/mm	0.603
Work until failure	Kip·ft.	3.236
	KN·m	4.387
Ductility factor, μ	3.10	

Observations and failure modes:

- Mode of failure was sheathing nail tear through under the end stud in tension. This led to significant amounts of uplift displacement between end stud in tension and bottom plate.
- Sheathing nails removed from bottom plate displayed significant bending deformation. Sheathing nails removed from any other location experienced virtually no bending deformation.
- No failure around 4 x 1 ft panel segments
- Cross grain crack formed in bottom plate at anchor bolt closest to hydraulic actuator

Table A.22. EEEP Parameters of 9-8-P-3

EEEP Parameters	units	negative	positive
F_{yield}	Kips	-2.008	1.653
	KN	-8.929	7.351
Δ_{yield}	in.	-0.470	0.632
	mm	-11.93	16.05
$\Delta_{failure}$	in.	-1.688	1.648
	mm	-42.88	41.86

Table A.23. Displacement components of 9-8-P-3

	inches	mm	% of Total
Total Displacement	1.5	38.1	
Shear Deformation	0.5	12.7	33.3
Rigid Body Motion	1.0	25.4	66.7
Bending and Slip	0.0	0.0	0.0

Table A.24. Data of each Primary cycle of 9-8-P-3

Primary	average displacement		average load		work per cycle		cyclic stiffness		Damping
cycle #	in.	mm	Kips	KN	Kip·ft.	KN·m	Kip/in.	KN/mm	ratio
1	0.080	2.037	0.439	1.951	0.003	0.004	5.425	0.950	0.175
2	0.120	3.051	0.557	2.477	0.005	0.007	4.668	0.818	0.153
3	0.160	4.051	0.685	3.047	0.009	0.012	4.285	0.750	0.152
4	0.327	8.315	1.026	4.564	0.029	0.040	3.132	0.548	0.166
5	0.483	12.275	1.302	5.789	0.060	0.081	2.685	0.470	0.180
6	0.635	16.138	1.486	6.611	0.092	0.125	2.334	0.409	0.186
7	1.133	28.785	1.978	8.799	0.240	0.325	1.746	0.306	0.205
8	1.527	38.792	2.211	9.835	0.380	0.515	1.450	0.254	0.215
9	1.680	42.662	1.688	7.510	0.694	0.940	1.009	0.177	0.467
10	2.695	68.462	0.755	3.356	0.386	0.523	0.274	0.048	0.351
11	3.138	79.718	0.360	1.602	0.318	0.431	0.098	0.017	0.459

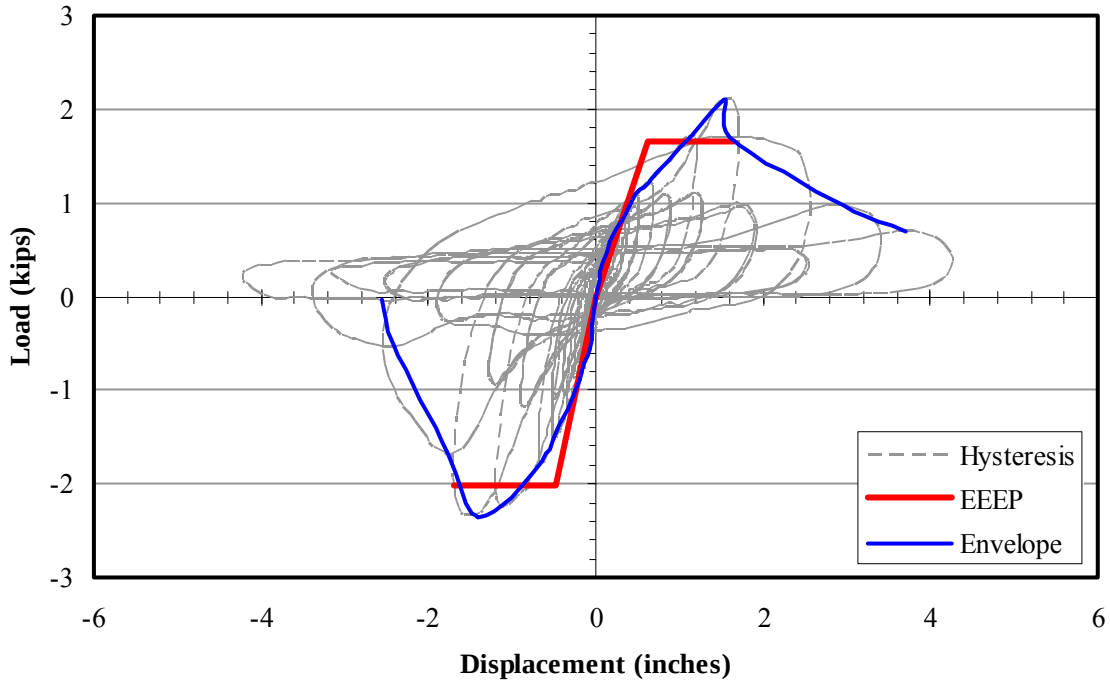

Figure A.26. Load vs. displacement, envelope and EEEP curves of 9-8-P-3

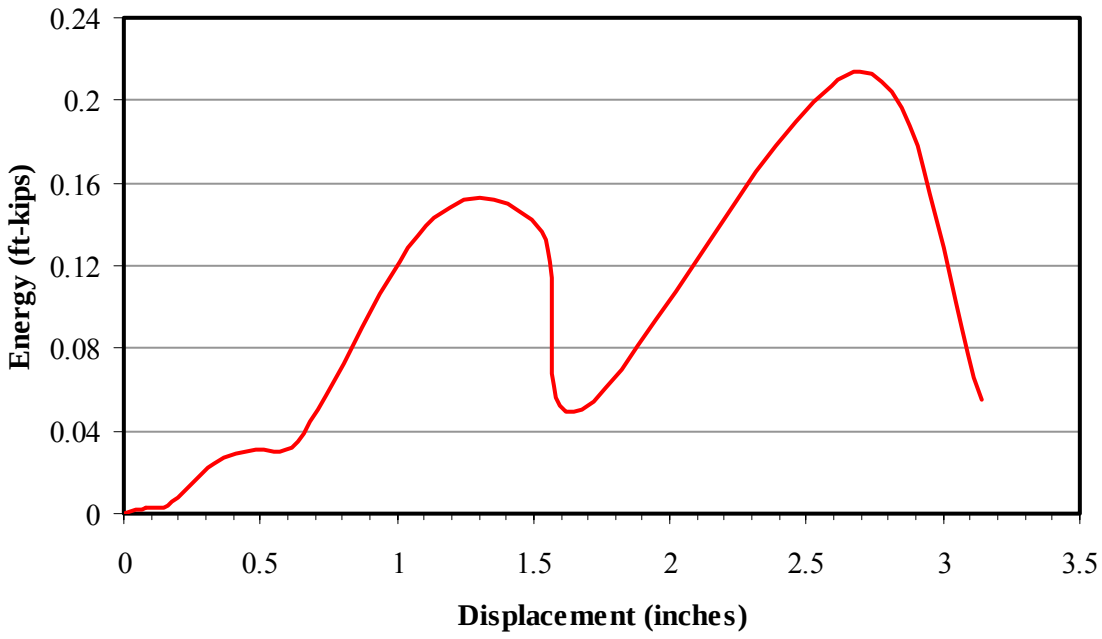

Figure A.27. Hysteretic energy dissipated per cycle vs. displacement of 9-8-P-3

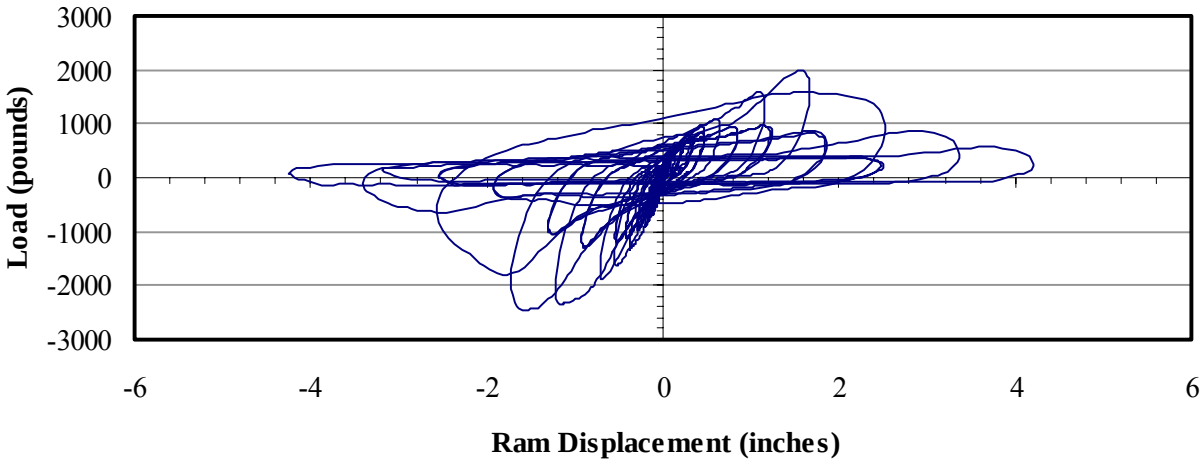

Figure A.28. Load vs. displacement of 9-8-P-3

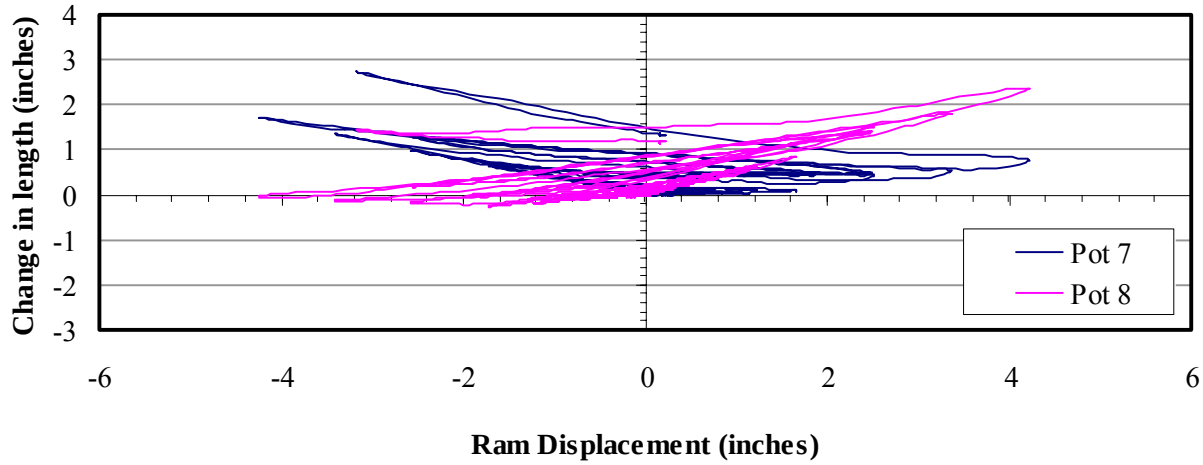

Figure A.29. Change in length of diagonal measuring Pots 7 and 8 vs. ram displacement of 9-8-P-3

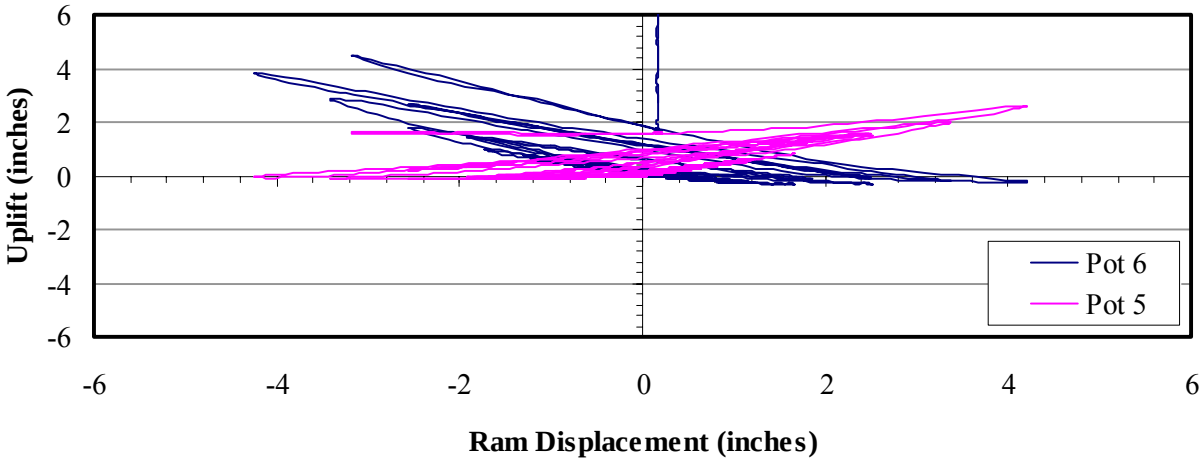

Figure A.30. Uplift displacement vs. ram displacement of 9-8-P-3

Table A.25. Performance Parameters of 9-9-P-1

Specimen	9-9-P-1	
Peak load, F_{peak}	Kips	2.216
	KN	9.858
Drift at peak load, Δ_{peak}	in.	1.542
	mm	39.16
Yield load, F_{yield}	Kips	2.038
	KN	9.064
Drift at yield load, Δ_{yield}	in.	0.683
	mm	17.36
Proportional limit, $0.4F_{peak}$	Kips	0.887
	KN	3.943
Drift at prop. limit, $\Delta@0.4F_{peak}$	in.	0.297
	mm	7.55
Failure load or $0.8F_{peak}$	Kips	1.773
	KN	7.887
Drift at failure, $\Delta_{failure}$	in.	2.232
	mm	56.69
Elastic stiffness, K_e $@0.4F_{peak}$	Kip/in.	2.985
	KN/mm	0.523
Work until failure	Kip·ft.	2.902
	KN·m	3.934
Ductility factor, μ	3.28	

Observations and failure modes:

- Mode of failure was sheathing nail tear through under the end stud in tension. This led to significant amounts of uplift displacement between end stud in tension and bottom plate
- Sheathing nails removed from bottom plate within 2 ft of either end stud displayed significant bending deformation
- Sheathing nails along center portion of bottom plate experienced withdrawal; thus, bending deformation was not as significant
- Sheathing nails removed from any other location experienced virtually no bending deformation.

Table A.26. EEEP Parameters of 9-9-P-1

EEEP Parameters	units	negative	positive
F_{yield}	Kips	-2.244	1.831
	KN	-9.982	8.146
Δ_{yield}	in.	-0.759	0.607
	mm	-19.28	15.43
$\Delta_{failure}$	in.	-2.368	2.096
	mm	-60.14	53.23

Table A.27. Displacement components of 9-9-P-1

	inches	mm	% of Total
Total Displacement	1.5	38.1	
Shear Deformation	0.5	12.7	33.3
Rigid Body Motion	1.0	25.4	66.7
Bending and Slip	0.0	0.0	0.0

Table A.28. Data of each Primary cycle of 9-9-P-1

Primary	average displacement		average load		work per cycle		cyclic stiffness		Damping
cycle #	in.	mm	Kips	KN	Kip·ft.	KN·m	Kip/in.	KN/mm	ratio
1	0.082	2.094	0.364	1.619	0.002	0.003	4.395	0.770	0.144
2	0.125	3.186	0.500	2.223	0.005	0.006	3.983	0.697	0.141
3	0.165	4.202	0.600	2.671	0.008	0.011	3.630	0.636	0.149
4	0.335	8.505	0.962	4.279	0.026	0.035	2.873	0.503	0.155
5	0.499	12.672	1.289	5.735	0.051	0.069	2.584	0.452	0.151
6	0.666	16.913	1.604	7.133	0.079	0.107	2.408	0.422	0.141
7	0.974	24.729	2.085	9.275	0.229	0.310	2.137	0.374	0.214
8	1.542	39.160	2.216	9.858	0.346	0.469	1.455	0.255	0.195
9	2.068	52.527	2.049	9.115	0.583	0.790	0.987	0.173	0.261
10	2.740	69.599	0.961	4.276	0.492	0.667	0.350	0.061	0.355
11	3.409	86.594	0.387	1.721	0.302	0.409	0.113	0.020	0.436

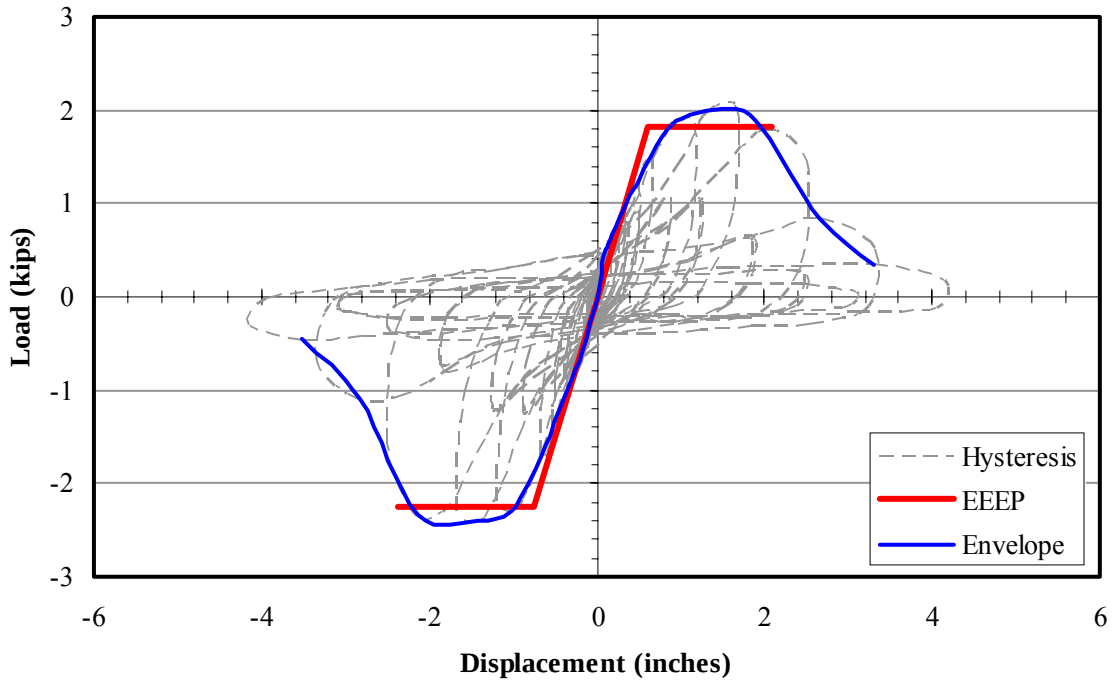

Figure A.31. Load vs. displacement, envelope and EEEP curves of 9-9-P-1

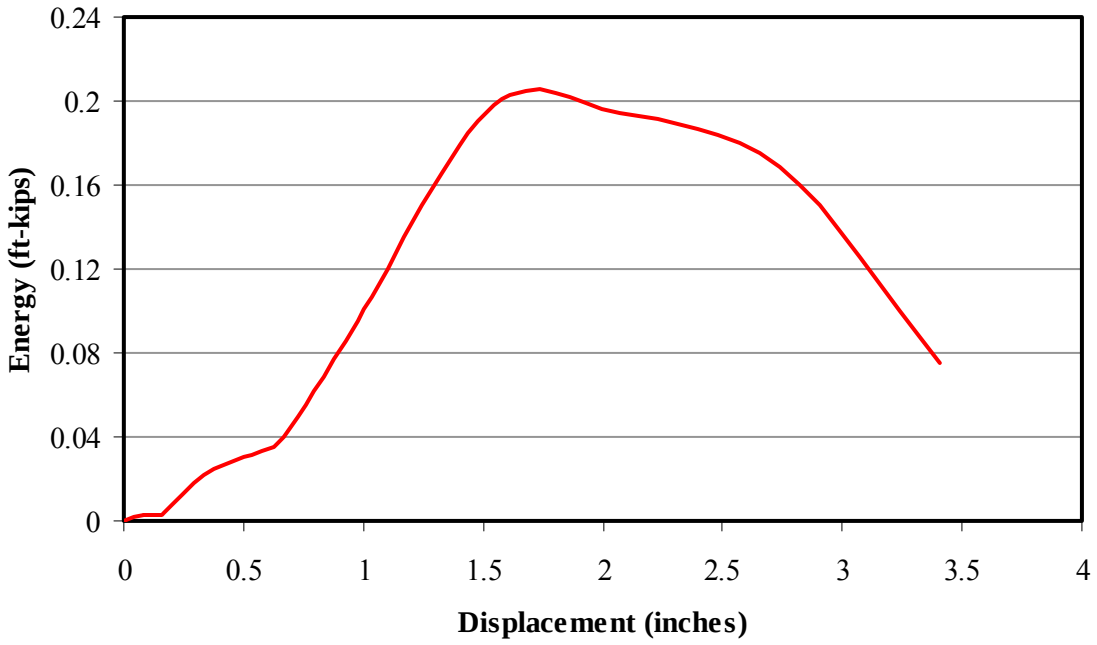

Figure A.32. Hysteretic energy dissipated per cycle vs. displacement of 9-9-P-1

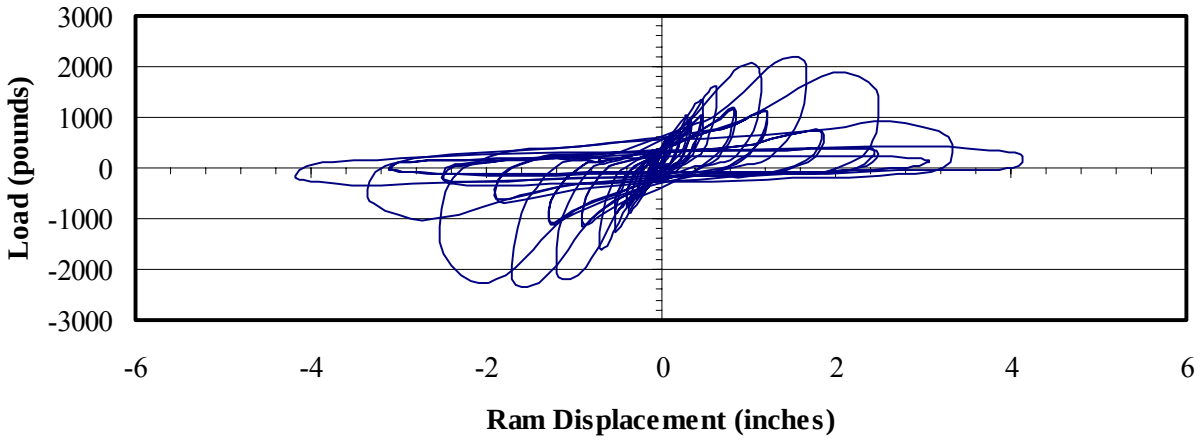

Figure A.33. Load vs. displacement of 9-9-P-1

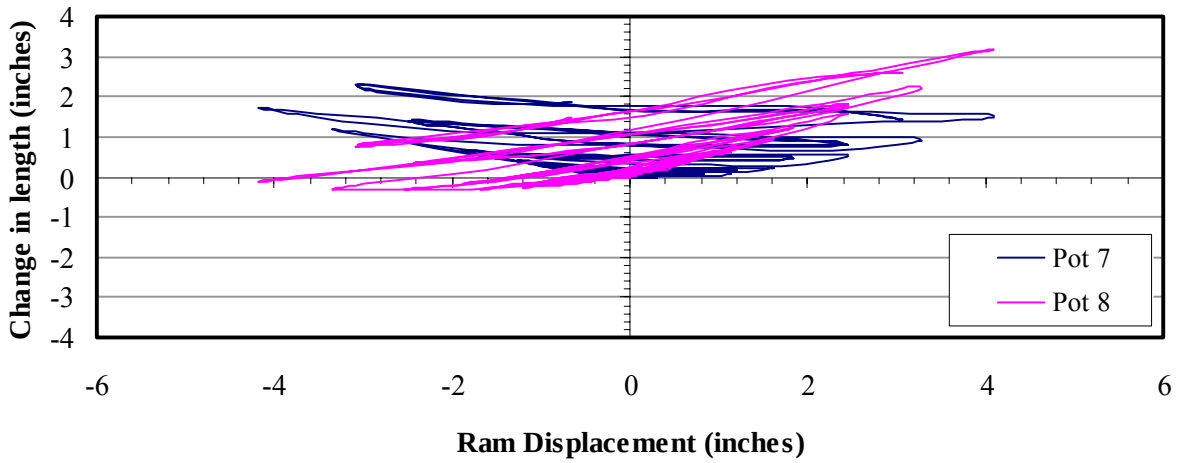

Figure A.34. Change in length of diagonal measuring Pots 7 and 8 vs. ram displacement of 9-9-P-1

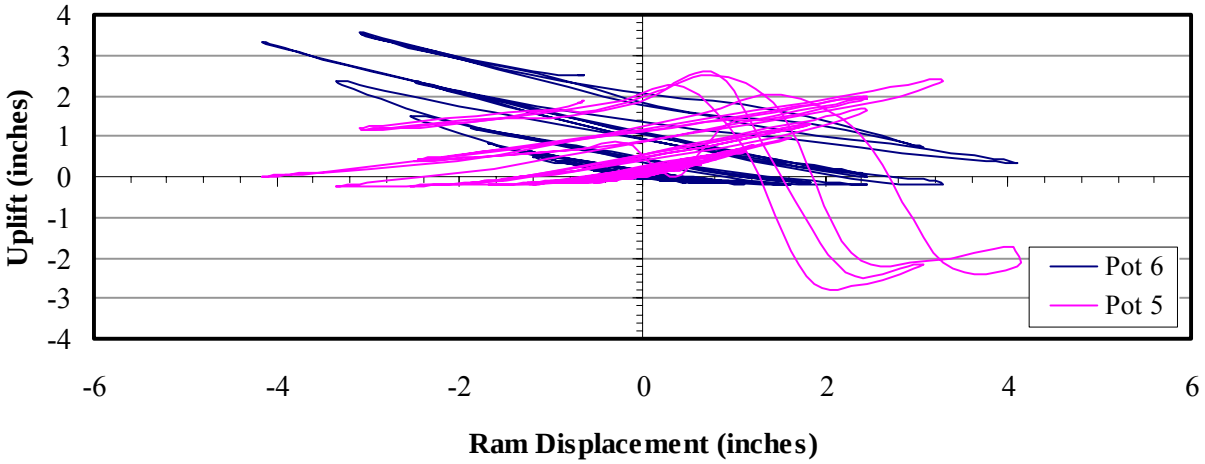

Figure A.35. Uplift displacement vs. ram displacement of 9-9-P-1

Table A.29. Performance Parameters of 9-9-P-2

Specimen	9-9-P-2	
Peak load, F_{peak}	Kips	2.200
	KN	9.787
Drift at peak load, Δ_{peak}	in.	1.006
	mm	25.56
Yield load, F_{yield}	Kips	1.939
	KN	8.623
Drift at yield load, Δ_{yield}	in.	0.430
	mm	10.91
Proportional limit, $0.4F_{peak}$	Kips	0.880
	KN	3.915
Drift at prop. limit, $\Delta@0.4F_{peak}$	in.	0.194
	mm	4.94
Failure load or $0.8F_{peak}$	Kips	1.760
	KN	7.830
Drift at failure, $\Delta_{failure}$	in.	1.650
	mm	41.90
Elastic stiffness, K_e $@0.4F_{peak}$	Kip/in.	5.242
	KN/mm	0.918
Work until failure	Kip·ft.	2.187
	KN·m	2.965
Ductility factor, μ	4.56	

Observations and failure modes:

- Mode of failure was sheathing nail tear through under the end stud in tension. This led to significant amounts of uplift displacement between end stud in tension and bottom plate.
- Sheathing nails removed from bottom plate displayed significant bending deformation. Sheathing nails removed from any other location experienced virtually no bending deformation.
- All sheathing nails along bottom plate experienced tear through as wall was tested to complete failure

Table A.30. EEEP Parameters of 9-9-P-2

EEEP Parameters	units	negative	Positive
F_{yield}	Kips	-1.944	1.933
	KN	-8.647	8.600
Δ_{yield}	in.	-0.270	0.589
	mm	-6.85	14.97
$\Delta_{failure}$	in.	-1.757	1.542
	mm	-44.64	39.16

Table A.31. Displacement components of 9-9-P-2

	inches	mm	% of Total
Total Displacement	1.1	27.9	
Shear Deformation	0.4	10.2	36.4
Rigid Body Motion	0.7	17.8	63.6
Bending and Slip	0.0	0.0	0.0

Table A.32. Data of each Primary cycle of 9-9-P-2

Primary	average displacement		average load		work per cycle		cyclic stiffness		Damping
cycle #	in.	mm	Kips	KN	Kip·ft.	KN·m	Kip/in.	KN/mm	ratio
1	0.085	2.148	0.559	2.487	0.004	0.006	6.614	1.158	0.177
2	0.127	3.232	0.723	3.217	0.007	0.009	5.680	0.995	0.142
3	0.170	4.307	0.843	3.750	0.012	0.016	4.972	0.871	0.161
4	0.320	8.127	1.228	5.464	0.039	0.053	3.881	0.680	0.192
5	0.473	12.018	1.530	6.804	0.072	0.098	3.260	0.571	0.191
6	0.629	15.989	1.762	7.839	0.106	0.144	2.816	0.493	0.183
7	1.006	25.564	2.200	9.787	0.270	0.365	2.188	0.383	0.232
8	1.430	36.314	2.077	9.241	0.364	0.494	1.452	0.254	0.234
9	1.945	49.416	1.305	5.806	0.462	0.626	0.688	0.120	0.355
10	3.141	79.780	0.237	1.050	0.260	0.352	0.075	0.013	0.667

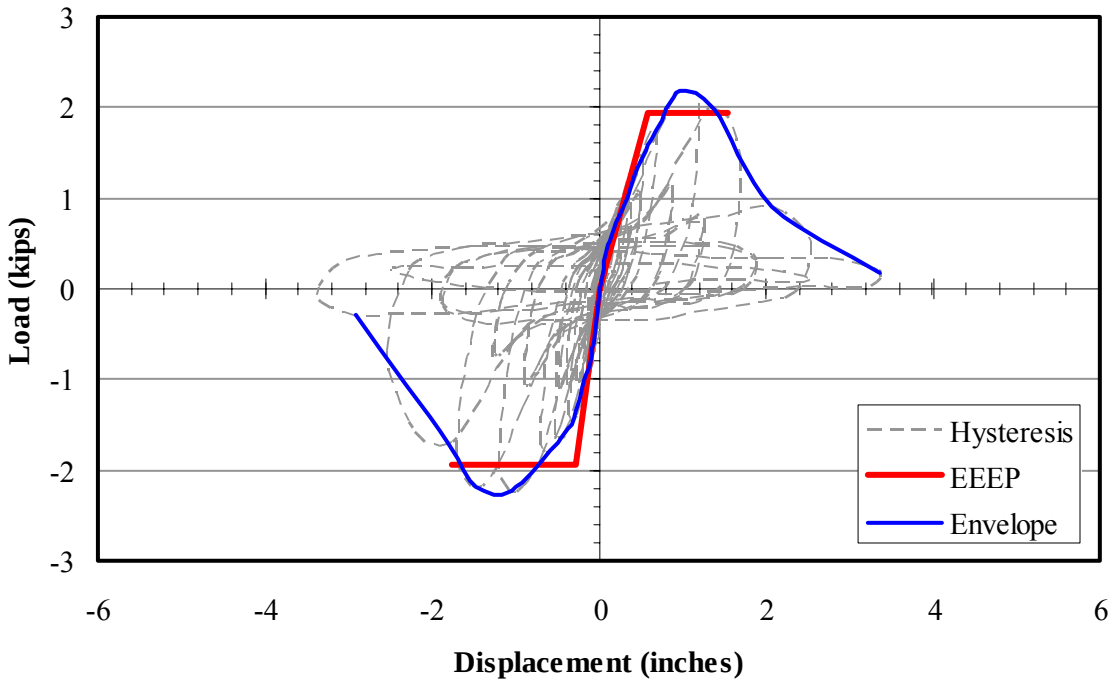

Figure A.36. Load vs. displacement, envelope and EEEP curves of 9-9-P-2

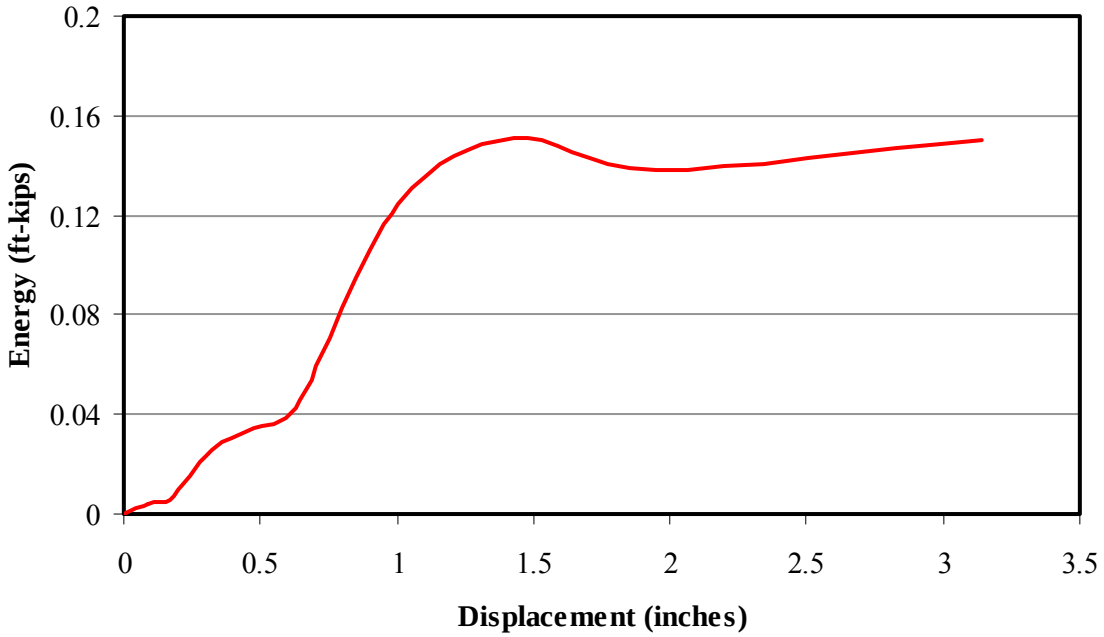

Figure A.37. Hysteretic energy dissipated per cycle vs. displacement of 9-9-P-2

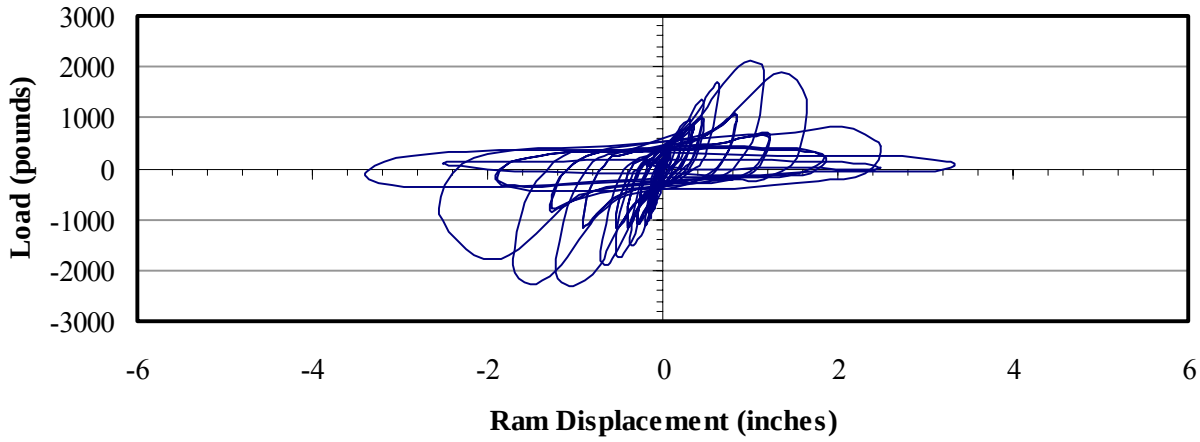

Figure A.38. Load vs. displacement of 9-9-P-2

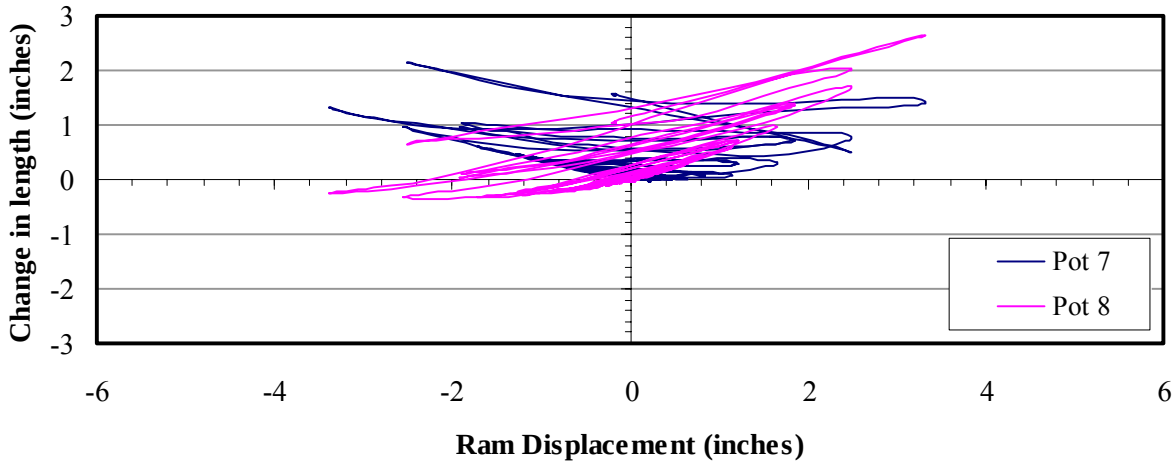

Figure A.39. Change in length of diagonal measuring Pots 7 and 8 vs. ram displacement of 9-9-P-2

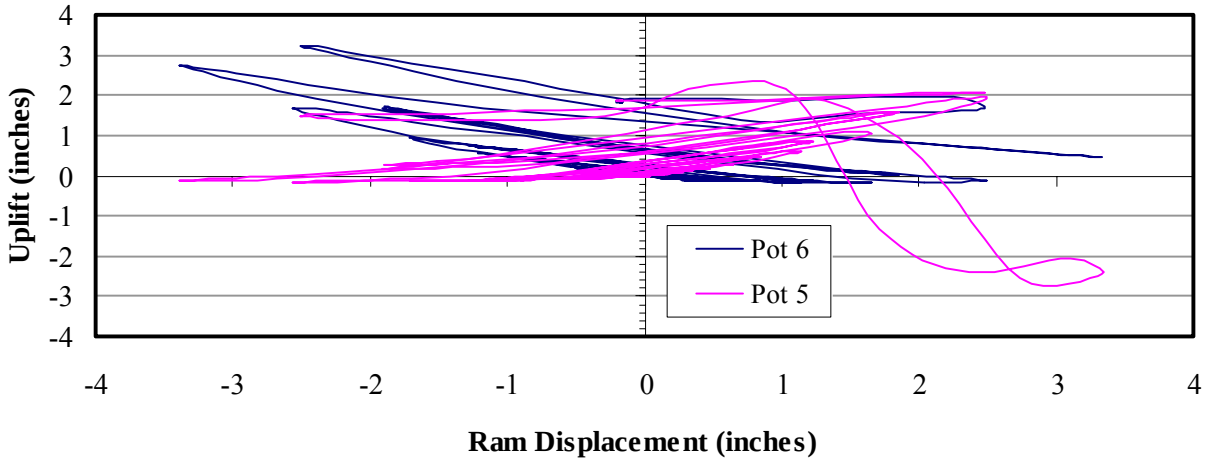

Figure A.40. Uplift displacement vs. ram displacement of 9-9-P-2

Table A.33. Performance Parameters of 9-9-P-3

Specimen	9-9-P-3	
Peak load, F_{peak}	Kips	1.900
	KN	8.453
Drift at peak load, Δ_{peak}	in.	1.545
	mm	39.24
Yield load, F_{yield}	Kips	1.707
	KN	7.591
Drift at yield load, Δ_{yield}	in.	0.679
	mm	17.24
Proportional limit, $0.4F_{peak}$	Kips	0.760
	KN	3.381
Drift at prop. limit, $\Delta@0.4F_{peak}$	in.	0.304
	mm	7.73
Failure load or $0.8F_{peak}$	Kips	1.520
	KN	6.763
Drift at failure, $\Delta_{failure}$	in.	1.854
	mm	47.10
Elastic stiffness, K_e $@0.4F_{peak}$	Kip/in.	2.546
	KN/mm	0.446
Work until failure	Kip·ft.	1.933
	KN·m	2.620
Ductility factor, μ	2.73	

Observations and failure modes:

- Mode of failure was sheathing nail tear through under the end stud in tension. This led to significant amounts of uplift displacement between end stud in tension and bottom plate.
- Sheathing nails removed from bottom plate displayed significant bending deformation. Sheathing nails removed from any other location experienced virtually no bending deformation.
- All sheathing nails along bottom plate experienced tear through as wall was tested to complete failure

Table A.34. EEEP Parameters of 9-9-P-3

EEEP Parameters	units	negative	positive
F_{yield}	Kips	-1.992	1.421
	KN	-8.860	6.322
Δ_{yield}	in.	-0.640	0.718
	mm	-16.25	18.24
$\Delta_{failure}$	in.	-1.751	1.957
	mm	-44.48	49.71

Table A.35. Displacement components of 9-9-P-3

	inches	mm	% of Total
Total Displacement	1.4	35.6	
Shear Deformation	0.4	10.2	28.6
Rigid Body Motion	1.0	25.4	71.4
Bending and Slip	0.0	0.0	0.0

Table A.36. Data of each Primary cycle of 9-9-P-3

Primary	average displacement		average load		work per cycle		cyclic stiffness		Damping
cycle #	in.	mm	Kips	KN	Kip·ft.	KN·m	Kip/in.	KN/mm	ratio
1	0.082	2.076	0.336	1.497	0.002	0.002	4.115	0.721	0.124
2	0.125	3.170	0.448	1.992	0.005	0.006	3.582	0.627	0.159
3	0.166	4.228	0.523	2.328	0.009	0.012	3.142	0.550	0.192
4	0.334	8.489	0.833	3.706	0.025	0.035	2.486	0.435	0.174
5	0.500	12.710	1.136	5.053	0.048	0.065	2.267	0.397	0.162
6	0.668	16.957	1.360	6.051	0.075	0.101	2.036	0.357	0.157
7	1.090	27.681	1.847	8.216	0.213	0.289	1.722	0.302	0.205
8	1.545	39.238	1.900	8.453	0.313	0.424	1.250	0.219	0.206
9	1.872	47.560	1.501	6.675	0.543	0.736	0.813	0.142	0.373
10	2.471	62.771	0.746	3.319	0.401	0.543	0.307	0.054	0.420

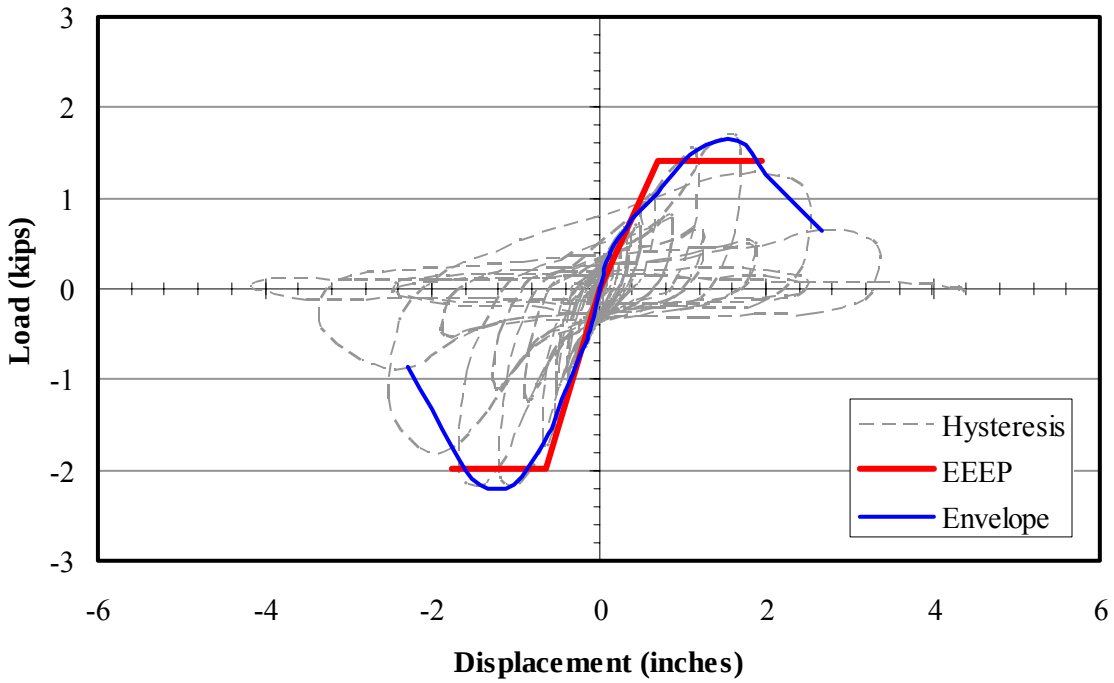

Figure A.41. Load vs. displacement, envelope and EEEP curves of 9-9-P-3

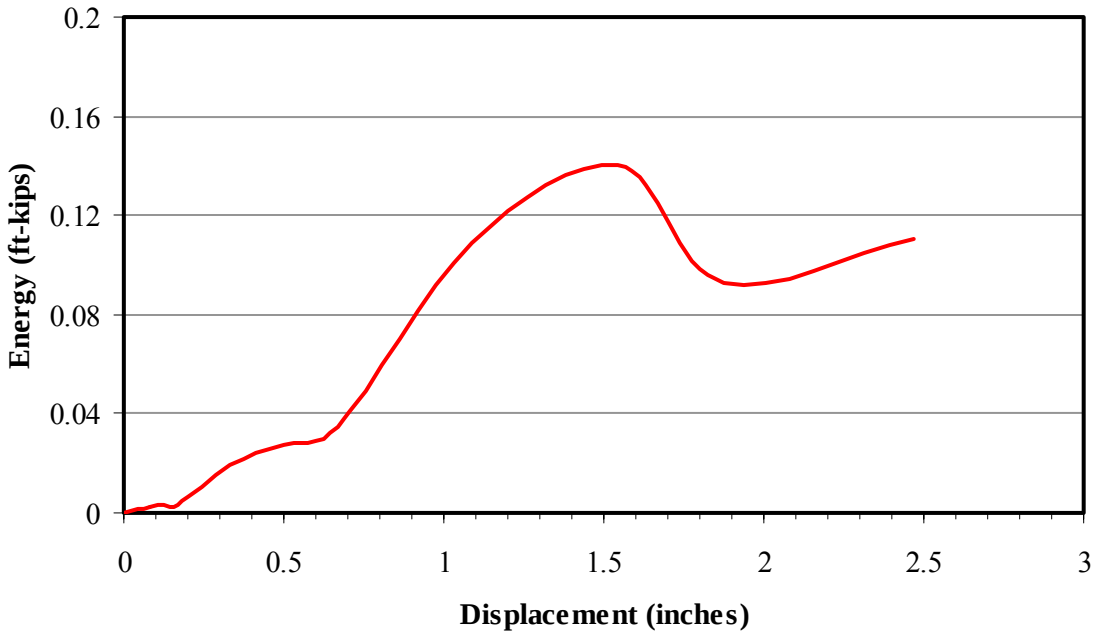

Figure A.42. Hysteretic energy dissipated per cycle vs. displacement of 9-9-P-3

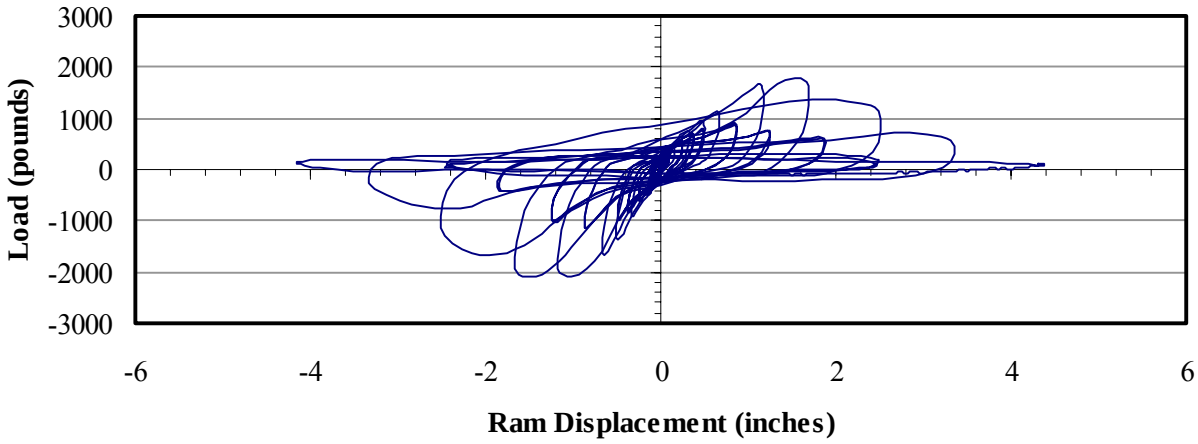

Figure A.43. Load vs. displacement of 9-9-P-3

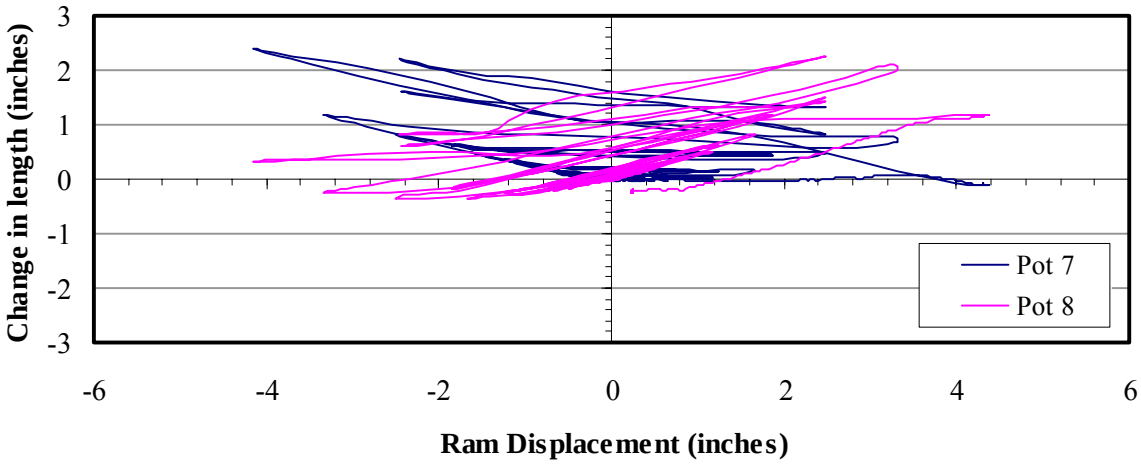

Figure A.44. Change in length of diagonal measuring Pots 7 and 8 vs. ram displacement of 9-9-P-3

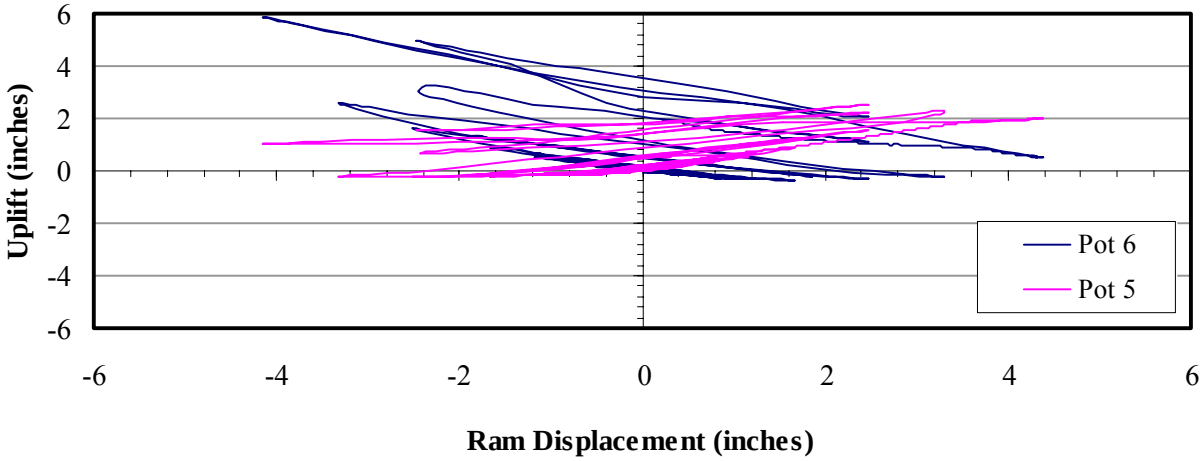

Figure A.45. Uplift displacement vs. ram displacement of 9-9-P-3

Table A.37. Performance Parameters of 10-8-P-2

Specimen	10-8-P-2	
Peak load, F_{peak}	Kips	2.049
	KN	9.115
Drift at peak load, Δ_{peak}	in.	1.687
	mm	42.86
Yield load, F_{yield}	Kips	1.848
	KN	8.222
Drift at yield load, Δ_{yield}	in.	0.821
	mm	20.84
Proportional limit, $0.4F_{peak}$	Kips	0.820
	KN	3.646
Drift at prop. limit, $\Delta@0.4F_{peak}$	in.	0.364
	mm	9.24
Failure load or $0.8F_{peak}$	Kips	1.639
	KN	7.292
Drift at failure, $\Delta_{failure}$	in.	2.261
	mm	57.44
Elastic stiffness, K_e $@0.4F_{peak}$	Kip/in.	2.255
	KN/mm	0.395
Work until failure	Kip·ft.	2.863
	KN·m	3.882
Ductility factor, μ	2.77	

Observations and failure modes:

- Mode of failure was sheathing nail tear through under the end stud in tension. This led to significant amounts of uplift displacement between end stud in tension and bottom plate.
- Sheathing nails removed from bottom plate displayed significant bending deformation. Sheathing nails removed from any other location experienced virtually no bending deformation.
- All sheathing nails along bottom plate experienced tear through as wall was tested to complete failure
- No failure occurred around 4 x 2 panel segments

Table A.38. EEEP Parameters of 10-8-P-2

EEEP Parameters	units	negative	positive
F_{yield}	Kips	-1.941	1.756
	KN	-8.633	7.811
Δ_{yield}	in.	-0.873	0.768
	mm	-22.18	19.50
$\Delta_{failure}$	in.	-2.223	2.300
	mm	-56.45	58.43

Table A.39. Displacement components of 10-8-P-2

	inches	mm	% of Total
Total Displacement	1.9	48.3	
Shear Deformation	0.4	10.2	21.1
Rigid Body Motion	1.5	38.1	78.9
Bending and Slip	0.0	0.0	0.0

Table A.40. Data of each Primary cycle of 10-8-P-2

Primary	average displacement		average load		work per cycle		cyclic stiffness		Damping
cycle #	in.	mm	Kips	KN	Kip·ft.	KN·m	Kip/in.	KN/mm	ratio
1	0.074	1.878	0.269	1.195	0.001	0.002	3.632	0.636	0.144
2	0.113	2.875	0.356	1.585	0.004	0.005	3.147	0.551	0.169
3	0.150	3.823	0.449	1.995	0.006	0.008	2.981	0.522	0.175
4	0.306	7.766	0.722	3.210	0.022	0.030	2.363	0.414	0.193
5	0.453	11.501	0.964	4.289	0.044	0.059	2.129	0.373	0.192
6	0.601	15.264	1.199	5.331	0.072	0.097	1.994	0.349	0.190
7	1.056	26.819	1.821	8.100	0.195	0.265	1.724	0.302	0.194
8	1.499	38.083	2.042	9.085	0.318	0.430	1.362	0.238	0.198
9	2.054	52.159	1.922	8.548	0.549	0.745	0.948	0.166	0.268
10	2.919	74.140	0.719	4.378	0.521	0.706	2.616	0.458	0.581

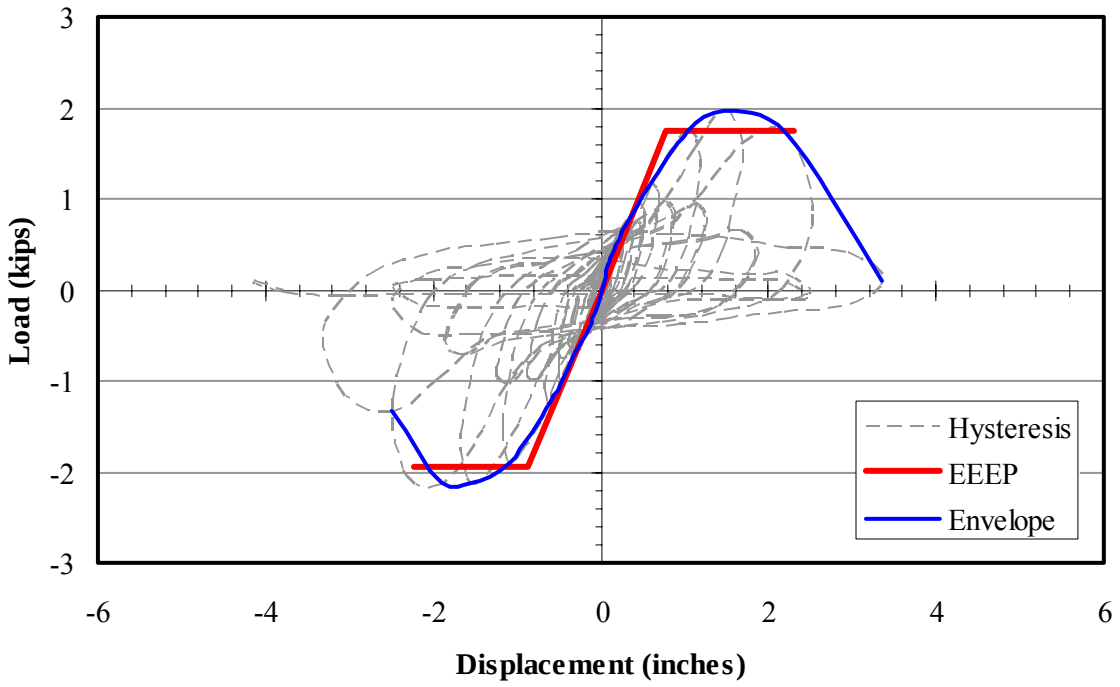

Figure A.46. Load vs. displacement, envelope and EEEP curves of 10-8-P-2

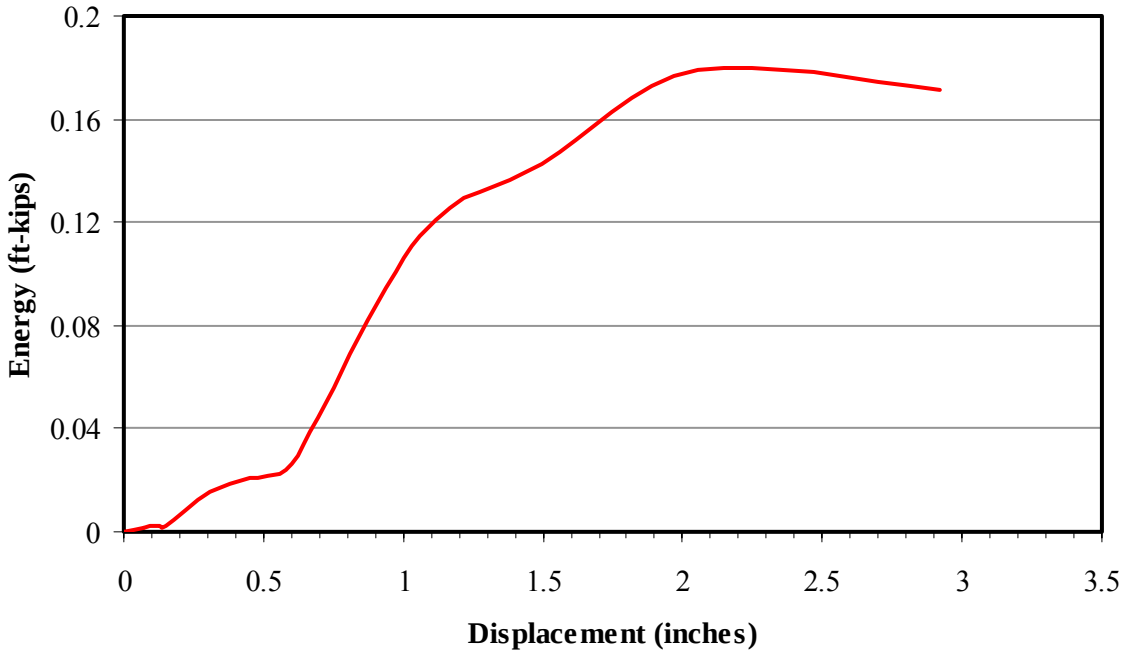

Figure A.47. Hysteretic energy dissipated per cycle vs. displacement of 10-8-P-2

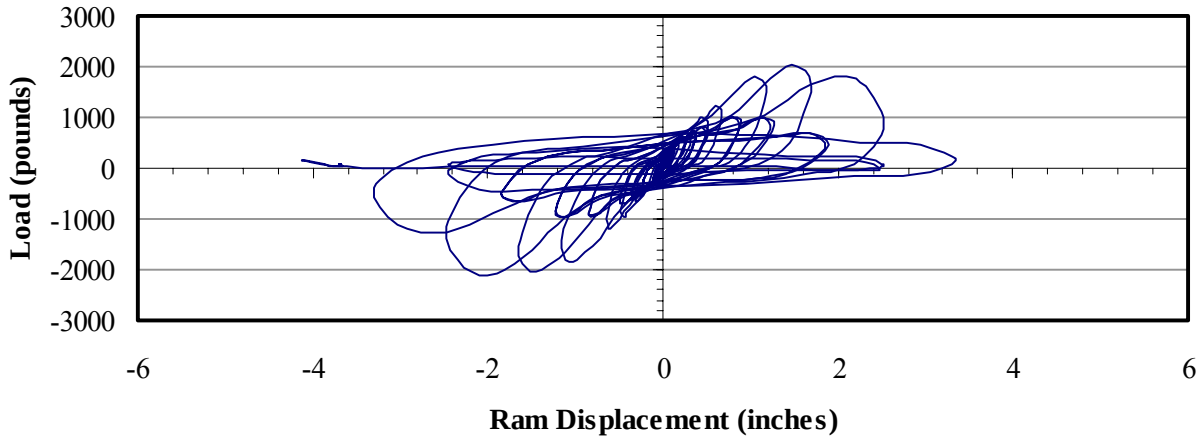

Figure A.48. Load vs. displacement of 10-8-P-2

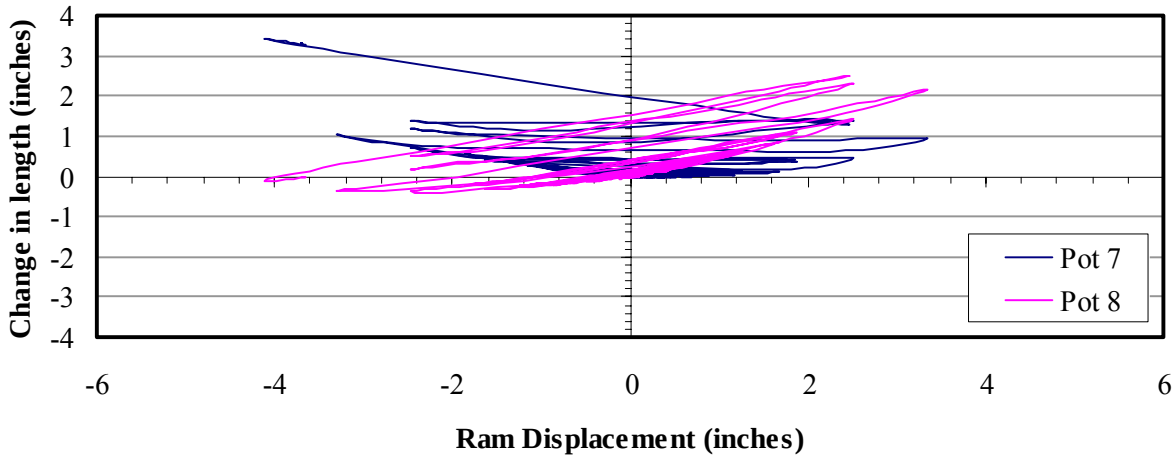

Figure A.49. Change in length of diagonal measuring Pots 7 and 8 vs. ram displacement of 10-8-P-2

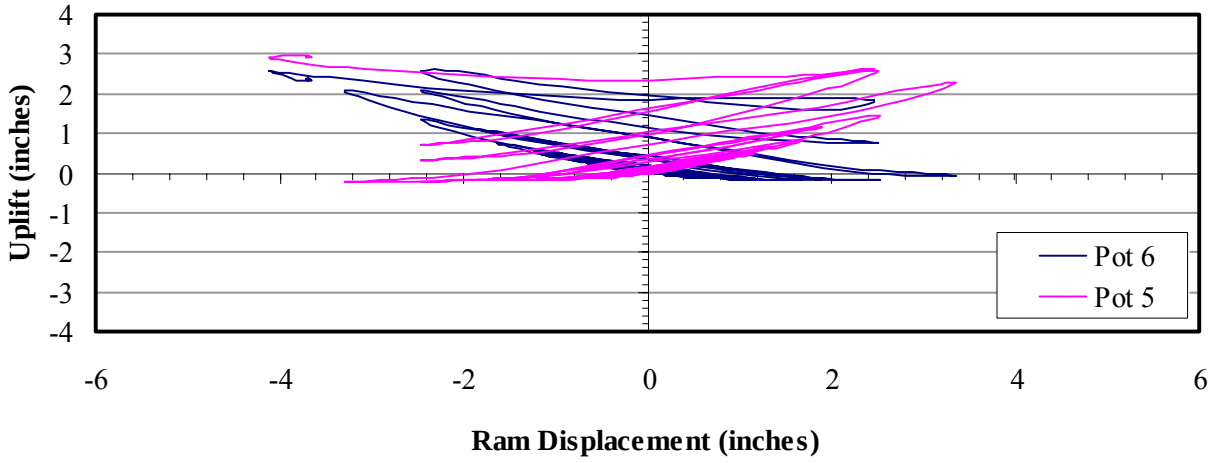

Figure A.50. Uplift displacement vs. ram displacement of 10-8-P-2

Table A.41. Performance Parameters of 10-8-P-3

Specimen	10-8-P-3	
Peak load, F_{peak}	Kips	2.052
	KN	9.125
Drift at peak load, Δ_{peak}	in.	1.514
	mm	38.45
Yield load, F_{yield}	Kips	1.800
	KN	8.006
Drift at yield load, Δ_{yield}	in.	0.584
	mm	14.84
Proportional limit, $0.4F_{peak}$	Kips	0.821
	KN	3.650
Drift at prop. limit, $\Delta@0.4F_{peak}$	in.	0.267
	mm	6.77
Failure load or $0.8F_{peak}$	Kips	1.641
	KN	7.300
Drift at failure, $\Delta_{failure}$	in.	2.101
	mm	53.38
Elastic stiffness, K_e $@0.4F_{peak}$	Kip/in.	3.291
	KN/mm	0.576
Work until failure	Kip·ft.	1.933
	KN·m	2.621
Ductility factor, μ	3.76	

Observations and failure modes:

- Mode of failure was sheathing nail tear through under the end stud in tension. This led to significant amounts of uplift displacement between end stud in tension and bottom plate.
- Sheathing nails removed from bottom plate displayed significant bending deformation. Sheathing nails removed from any other location experienced virtually no bending deformation.
- All sheathing nails along bottom plate experienced tear through as wall was tested to complete failure
- No failure occurred around 4 x 2 ft panel segments

Table A.42. EEEP Parameters of 10-8-P-3

EEEP Parameters	units	negative	positive
F_{yield}	Kips	-1.875	1.724
	KN	-8.341	7.670
Δ_{yield}	in.	-0.448	0.720
	mm	-11.37	18.30
$\Delta_{failure}$	in.	-1.984	2.219
	mm	-50.38	56.37

Table A.43. Displacement components of 10-8-P-3

	inches	mm	% of Total
Total Displacement	1.6	40.6	
Shear Deformation	0.5	12.7	31.3
Rigid Body Motion	1.1	27.9	68.7
Bending and Slip	0.0	0.0	0.0

Table A.44. Data of each Primary cycle of 10-8-P-3

Primary	average displacement		average load		work per cycle		cyclic stiffness		Damping
cycle #	in.	mm	Kips	KN	Kip·ft.	KN·m	Kip/in.	KN/mm	ratio
1	0.076	1.920	0.329	1.463	0.002	0.002	4.405	0.771	0.128
2	0.114	2.901	0.470	2.090	0.004	0.005	4.104	0.719	0.137
3	0.152	3.861	0.578	2.569	0.007	0.010	3.777	0.661	0.156
4	0.306	7.783	0.919	4.089	0.027	0.036	2.988	0.523	0.181
5	0.455	11.568	1.167	5.189	0.051	0.069	2.554	0.447	0.182
6	0.604	15.352	1.392	6.193	0.079	0.107	2.299	0.403	0.179
7	1.064	27.021	1.929	8.582	0.213	0.289	1.812	0.317	0.198
8	1.514	38.454	2.052	9.125	0.349	0.473	1.355	0.237	0.214
9	2.075	52.704	1.695	7.540	0.494	0.670	0.826	0.145	0.270
10	2.742	69.658	0.761	3.387	0.401	0.544	0.279	0.049	0.366
11	3.412	86.664	0.363	1.615	0.252	0.342	0.106	0.019	0.385

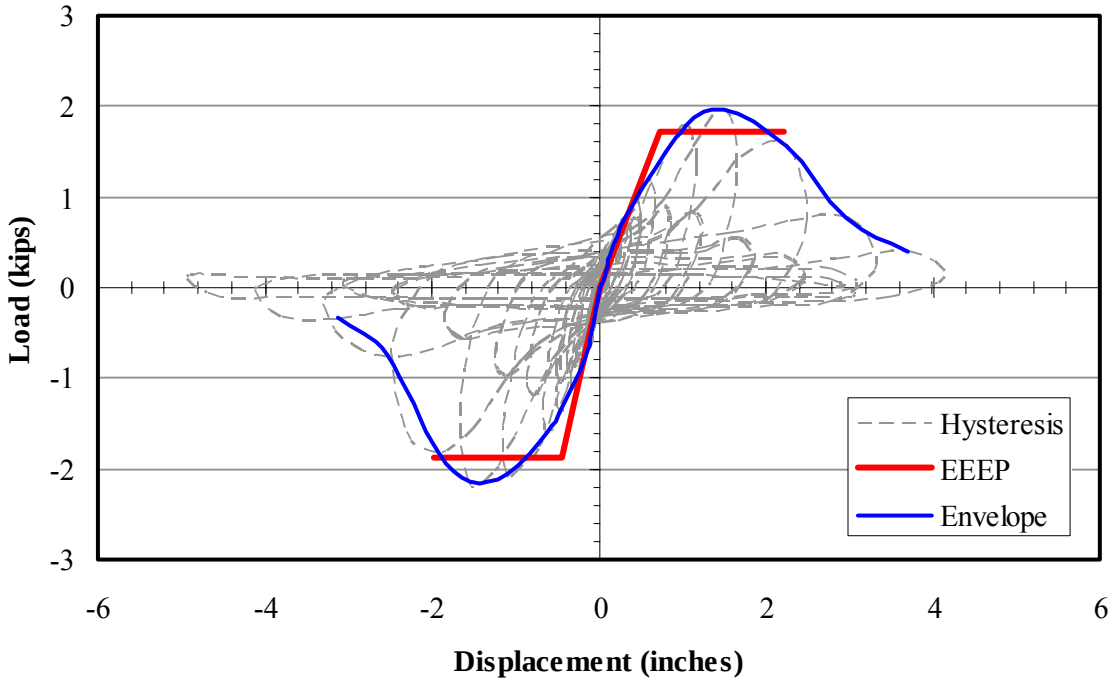

Figure A.51. Load vs. displacement, envelope and EEEP curves of 10-8-P-3

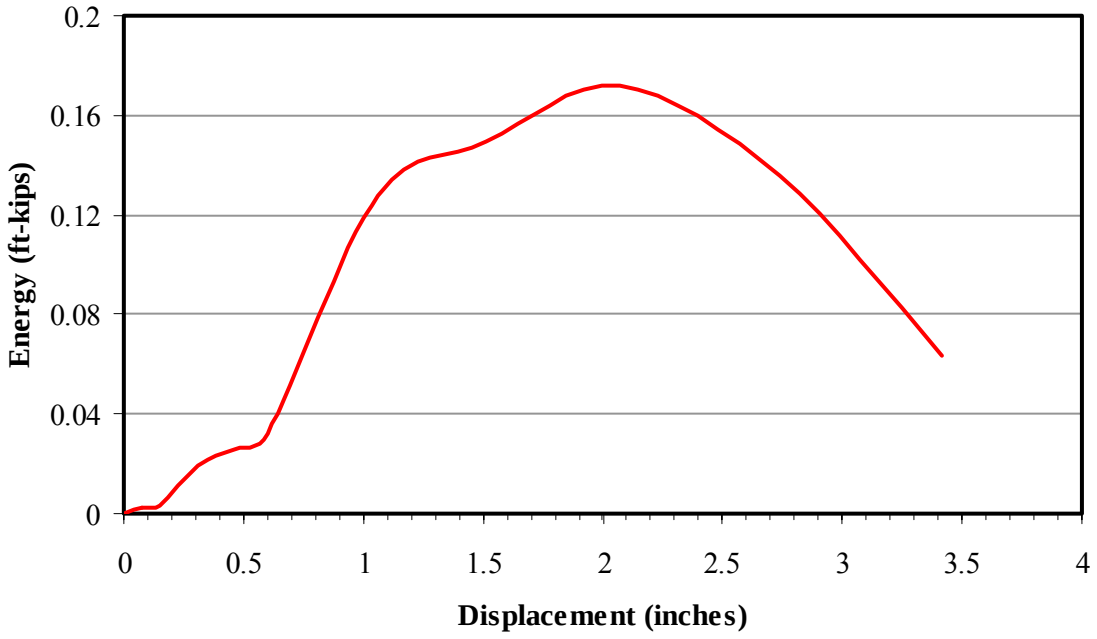

Figure A.52. Hysteretic energy dissipated per cycle vs. displacement of 10-8-P-3

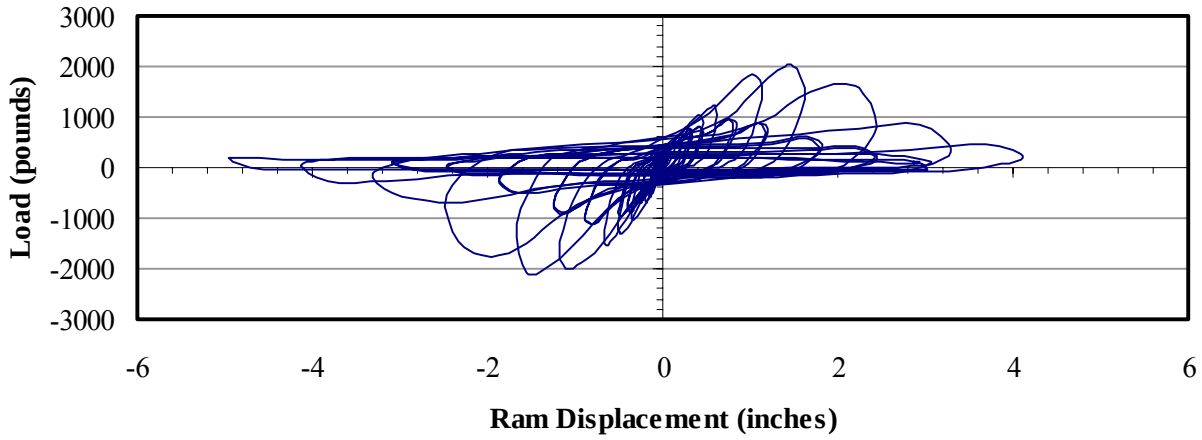

Figure A.53. Load vs. displacement of 10-8-P-3

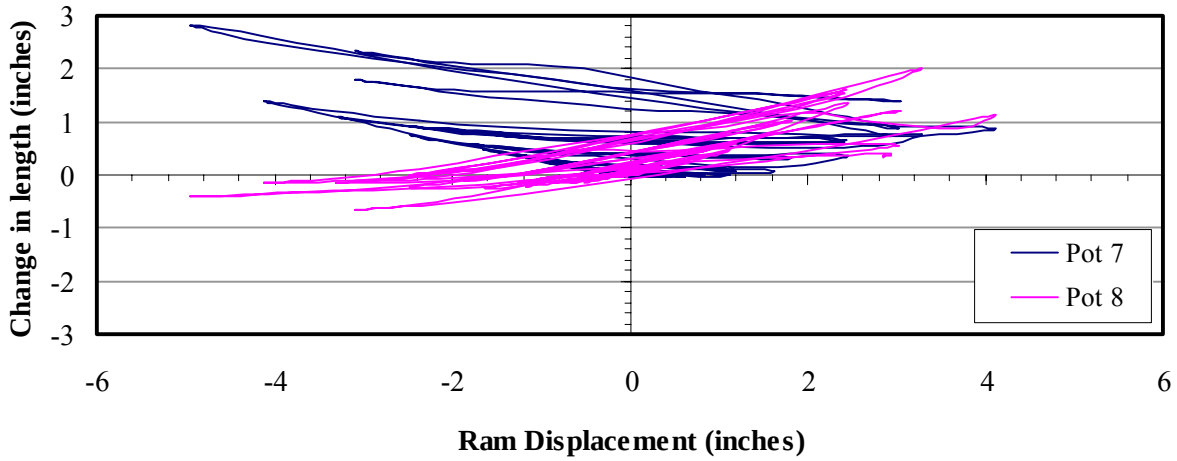

Figure A.54. Change in length of diagonal measuring Pots 7 and 8 vs. ram displacement of 10-8-P-3

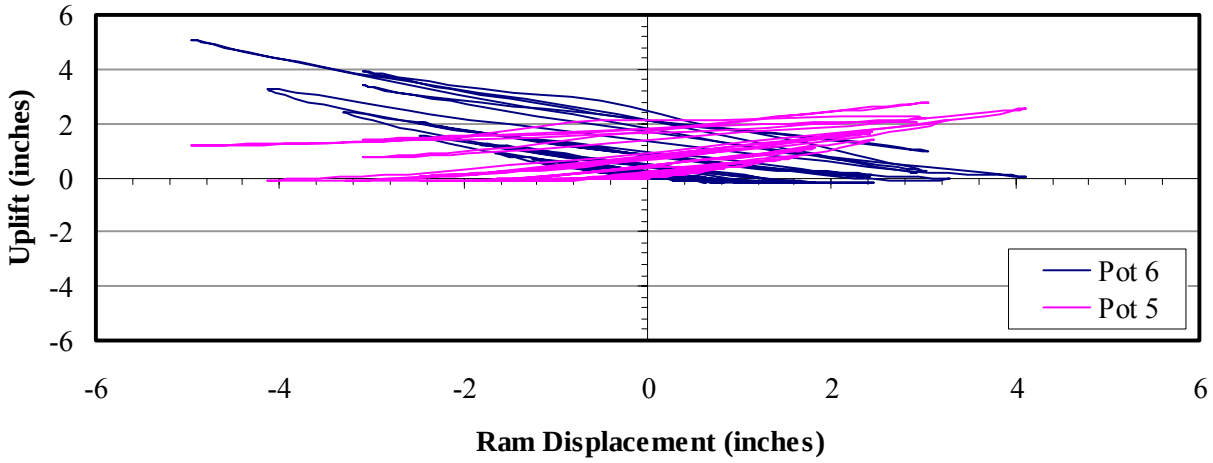

Figure A.55 Uplift displacement vs. ram displacement of 10-8-P-3

Table A.45. Performance Parameters of 10-10-P-1

Specimen	10-10-P-1	
Peak load, F_{peak}	Kips	1.989
	KN	8.847
Drift at peak load, Δ_{peak}	in.	1.521
	mm	38.63
Yield load, F_{yield}	Kips	1.791
	KN	7.967
Drift at yield load, Δ_{yield}	in.	0.722
	mm	18.34
Proportional limit, $0.4F_{peak}$	Kips	0.796
	KN	3.539
Drift at prop. limit, $\Delta@0.4F_{peak}$	in.	0.321
	mm	8.15
Failure load or $0.8F_{peak}$	Kips	1.591
	KN	7.078
Drift at failure, $\Delta_{failure}$	in.	2.155
	mm	54.75
Elastic stiffness, K_e $@0.4F_{peak}$	Kip/in.	2.482
	KN/mm	0.435
Work until failure	Kip·ft.	2.633
	KN·m	3.569
Ductility factor, μ	3.03	

Observations and failure modes:

- Mode of failure was sheathing nail tear through under the end stud in tension. This led to significant amounts of uplift displacement between end stud in tension and bottom plate.
- Sheathing nails along bottom plate within 2 ft of either end stud experienced tear through and significant bending deformation.
- Sheathing nails along center portion of bottom plate experienced withdrawal; thus, bending deformation was not as significant.
- Sheathing nails removed from any other location experienced virtually no bending deformation.

Table A.46. EEEP Parameters of 10-10-P-1

EEEP Parameters	units	negative	positive
F_{yield}	Kips	-1.966	1.617
	KN	-8.744	7.191
Δ_{yield}	in.	-0.795	0.649
	mm	-20.20	16.48
$\Delta_{failure}$	in.	-2.059	2.251
	mm	-52.31	57.19

Table A.47. Displacement components of 10-10-P-1

	inches	mm	% of Total
Total Displacement	1.6	40.6	
Shear Deformation	0.4	10.2	25.0
Rigid Body Motion	1.2	30.5	75.0
Bending and Slip	0.0	0.0	0.0

Table A.48. Data of each Primary cycle of 10-10-P-1

Primary	average displacement		average load		work per cycle		cyclic stiffness		Damping
cycle #	in.	mm	Kips	KN	Kip·ft.	KN·m	Kip/in.	KN/mm	ratio
1	0.070	1.773	0.250	1.113	0.002	0.003	3.641	0.638	0.241
2	0.114	2.898	0.381	1.693	0.004	0.006	3.311	0.580	0.183
3	0.152	3.863	0.455	2.023	0.007	0.010	2.977	0.521	0.197
4	0.309	7.844	0.767	3.411	0.025	0.034	2.483	0.435	0.201
5	0.459	11.665	1.064	4.734	0.046	0.062	2.315	0.405	0.179
6	0.608	15.447	1.299	5.776	0.070	0.095	2.132	0.373	0.169
7	1.072	27.219	1.791	7.965	0.188	0.255	1.668	0.292	0.187
8	1.521	38.627	1.989	8.847	0.289	0.392	1.306	0.229	0.182
9	2.084	52.927	1.823	8.107	0.477	0.647	0.884	0.155	0.241
10	2.406	61.106	0.946	4.208	0.510	0.691	0.393	0.069	0.426
11	3.335	84.703	0.297	1.320	0.276	0.374	0.089	0.016	0.520

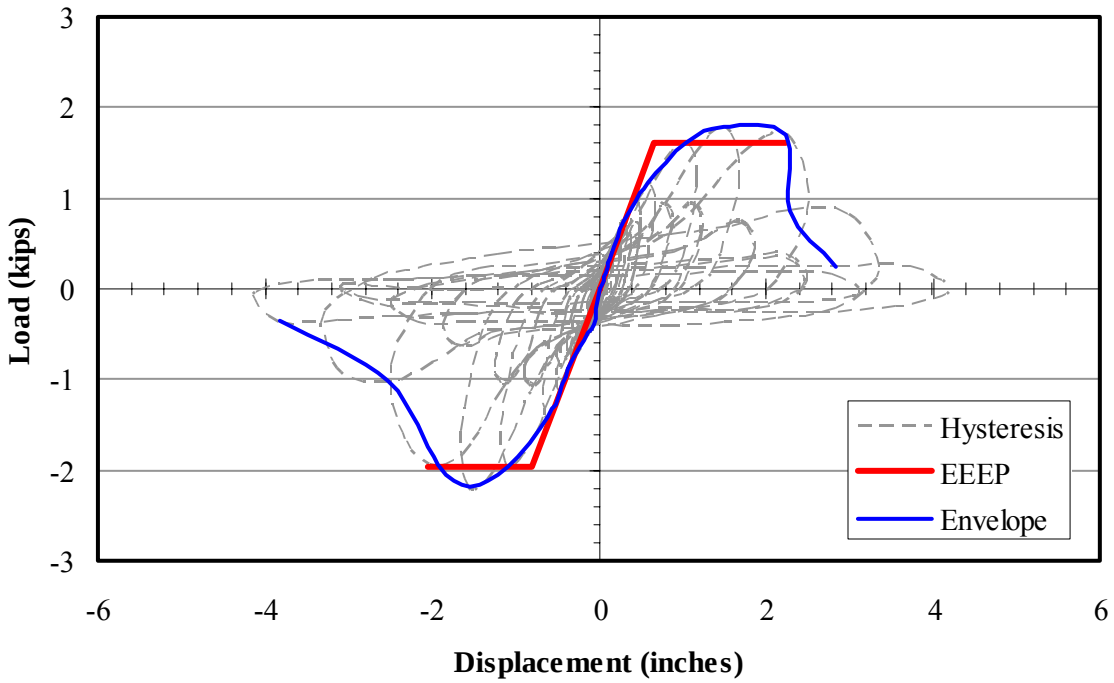

Figure A.56. Load vs. displacement, envelope and EEEP curves of 10-10-P-1

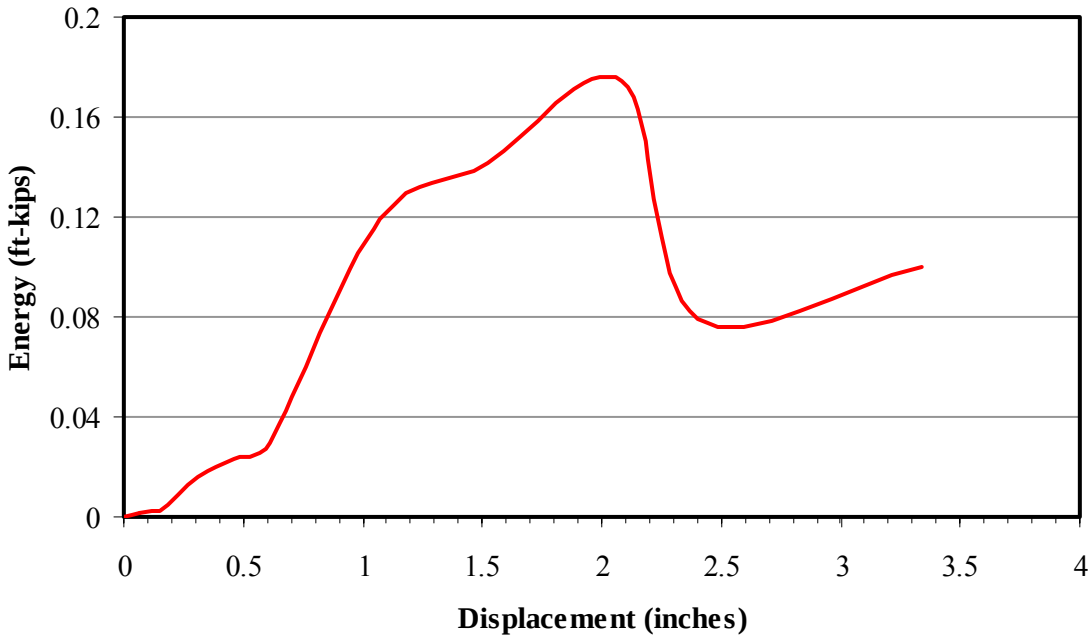

Figure A.57. Hysteretic energy dissipated per cycle vs. displacement of 10-10-P-1

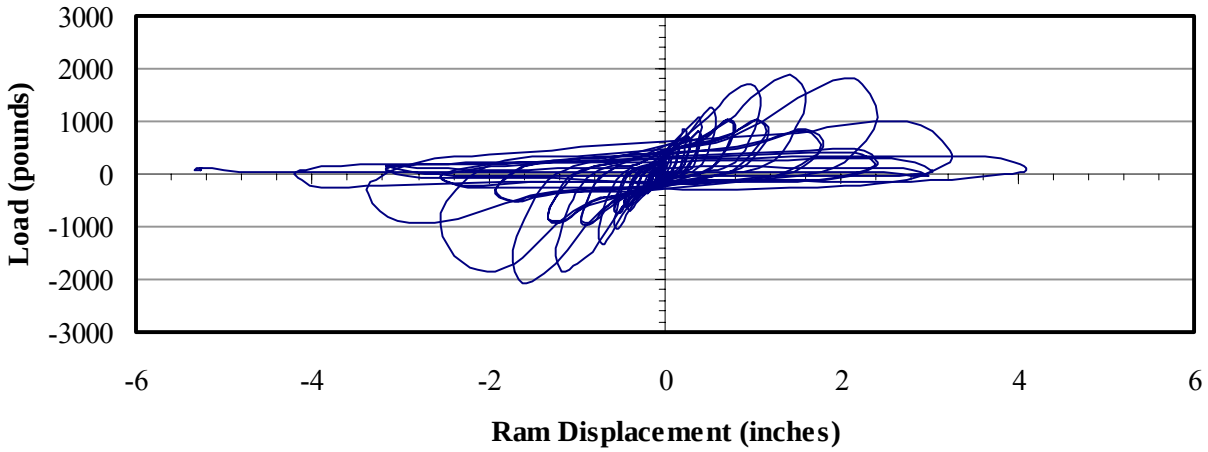

Figure A.58. Load vs. displacement of 10-10-P-1

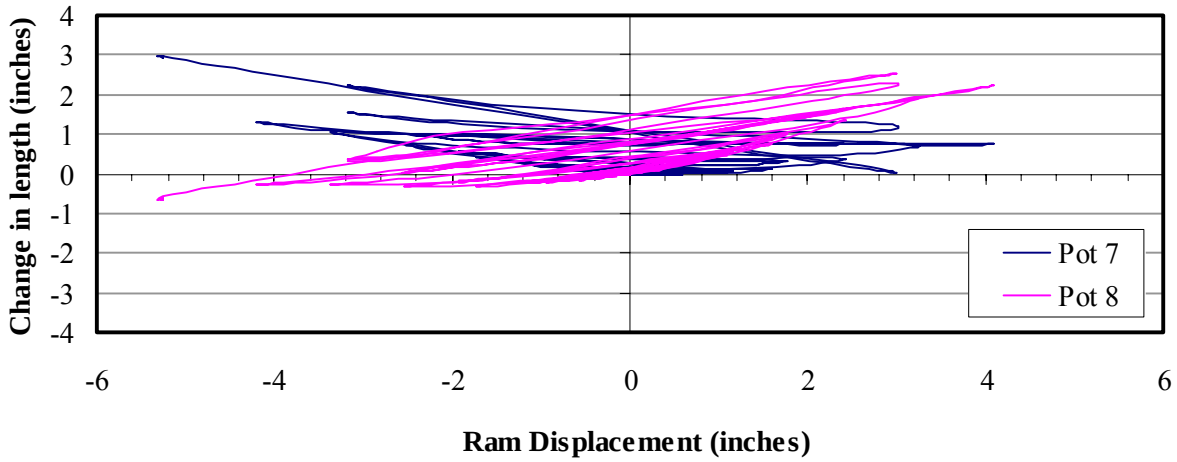

Figure A.59. Change in length of diagonal measuring Pots 7 and 8 vs. ram displacement of 10-10-P-1

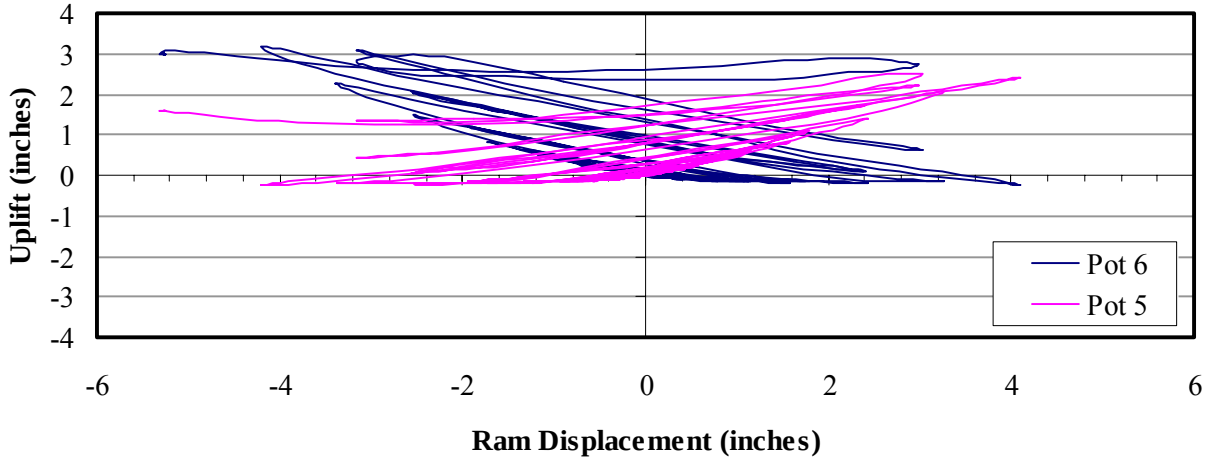

Figure A.60. Uplift displacement vs. ram displacement of 10-10-P-1

Table A.49. Performance Parameters of 10-10-P-2

Specimen	10-10-P-2	
Peak load, F_{peak}	Kips	1.878
	KN	8.352
Drift at peak load, Δ_{peak}	in.	1.227
	mm	31.16
Yield load, F_{yield}	Kips	1.650
	KN	7.338
Drift at yield load, Δ_{yield}	in.	0.457
	mm	11.61
Proportional limit, $0.4F_{peak}$	Kips	0.751
	KN	3.341
Drift at prop. limit, $\Delta@0.4F_{peak}$	in.	0.208
	mm	5.29
Failure load or $0.8F_{peak}$	Kips	1.502
	KN	6.681
Drift at failure, $\Delta_{failure}$	in.	1.761
	mm	44.72
Elastic stiffness, K_e $@0.4F_{peak}$	Kip/in.	3.670
	KN/mm	0.643
Work until failure	Kip·ft.	1.718
	KN·m	2.330
Ductility factor, μ	4.06	

Observations and failure modes:

- Mode of failure was sheathing nail tear through under the end stud in tension. This led to significant amounts of uplift displacement between end stud in tension and bottom plate.
- Sheathing nails along bottom plate within 2 ft of either end stud experienced tear through and significant bending deformation.
- Sheathing nails along center portion of bottom plate experienced withdrawal; thus, bending deformation was not as significant.
- Sheathing nails removed from any other location experienced virtually no bending deformation

Table A.50. EEEP Parameters of 10-10-P-2

EEEP Parameters	units	negative	positive
F_{yield}	Kips	-1.718	1.582
	KN	-7.641	7.035
Δ_{yield}	In.	-0.526	0.388
	mm	-13.36	9.86
$\Delta_{failure}$	In.	-1.423	2.099
	mm	-36.14	53.30

Table A.51. Displacement components of 10-10-P-2

	inches	mm	% of Total
Total Displacement	1.1	27.9	
Shear Deformation	0.4	10.2	36.4
Rigid Body Motion	0.7	17.8	63.6
Bending and Slip	0.0	0.0	0.0

Table A.52. Data of each Primary cycle of 10-10-P-2

Primary	average displacement		average load		work per cycle		cyclic stiffness		Damping
cycle #	in.	mm	Kips	KN	Kip·ft.	KN·m	Kip/in.	KN/mm	ratio
1	0.082	2.087	0.381	1.693	0.002	0.003	4.634	0.812	0.115
2	0.125	3.171	0.504	2.243	0.004	0.006	4.035	0.707	0.123
3	0.165	4.202	0.611	2.718	0.007	0.009	3.693	0.647	0.127
4	0.293	7.435	0.998	4.439	0.025	0.034	3.414	0.598	0.164
5	0.432	10.979	1.276	5.674	0.050	0.068	2.950	0.517	0.172
6	0.577	14.648	1.456	6.475	0.077	0.104	2.523	0.442	0.175
7	1.015	25.787	1.849	8.226	0.204	0.277	1.820	0.319	0.207
8	1.311	33.311	1.788	7.951	0.308	0.417	1.371	0.240	0.251
9	1.969	50.018	1.291	5.742	0.392	0.531	0.654	0.115	0.292
10	2.599	66.020	0.647	2.878	0.433	0.587	0.248	0.043	0.486
11	3.808	96.710	0.296	1.317	0.226	0.307	0.184	0.032	0.591

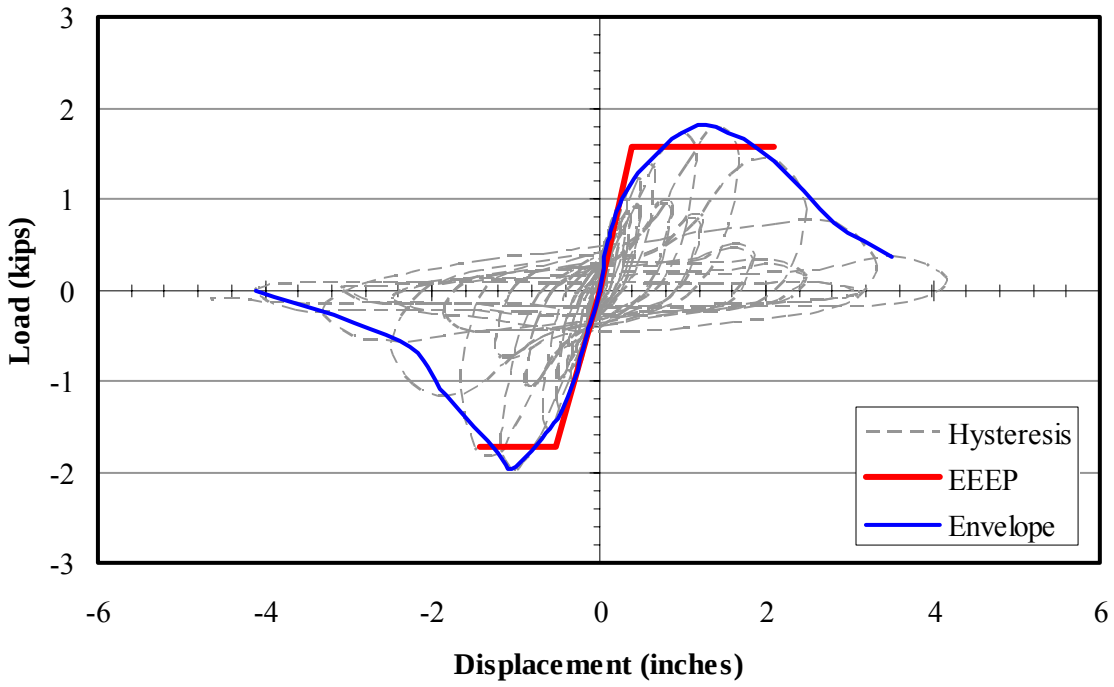

Figure A.61. Load vs. displacement, envelope and EEEP curves of 10-10-P-2

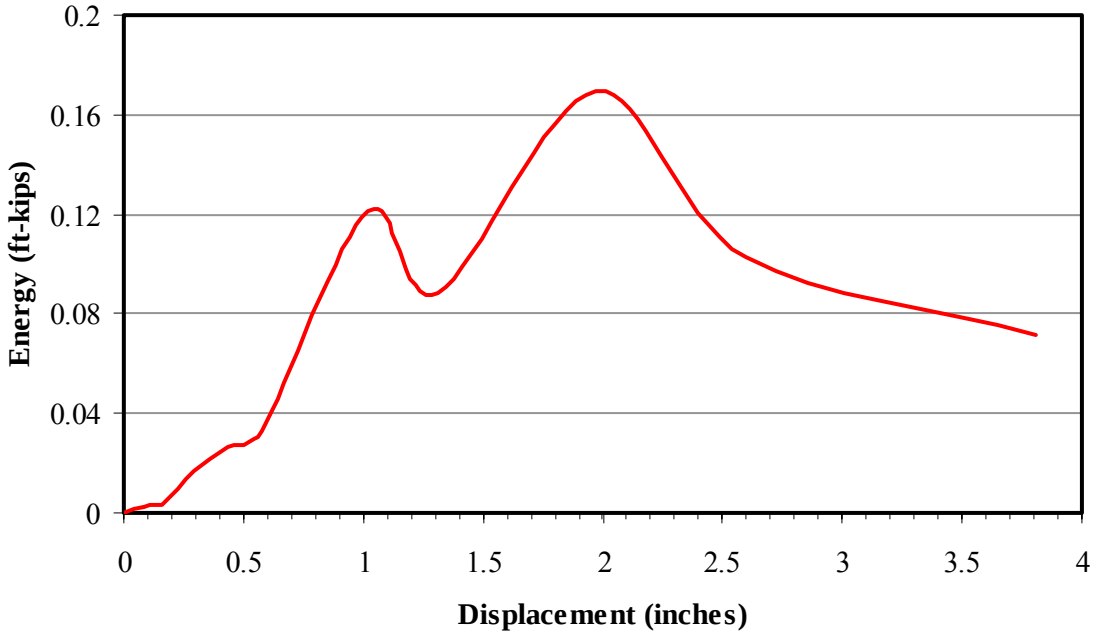

Figure A.62. Hysteretic energy dissipated per cycle vs. displacement of 10-10-P-2

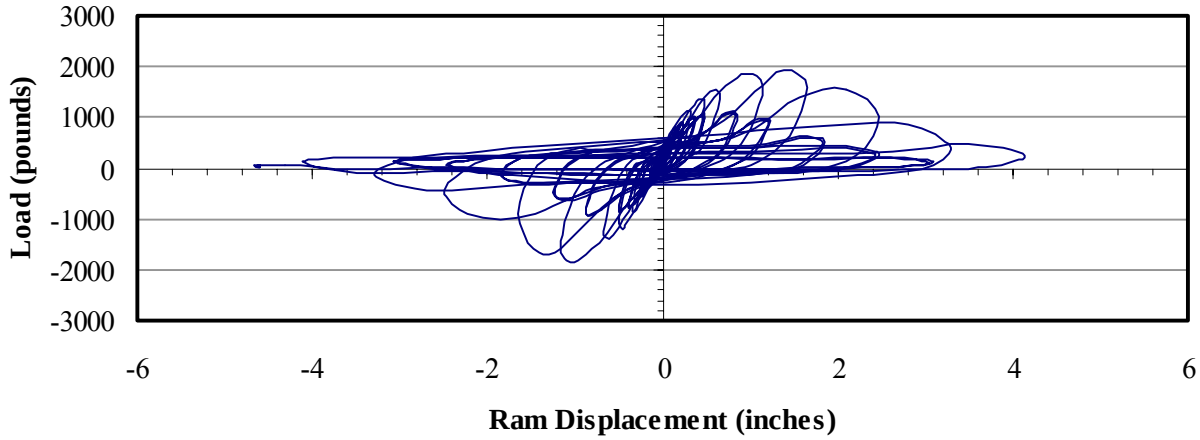

Figure A.63. Load vs. displacement of 10-10-P-2

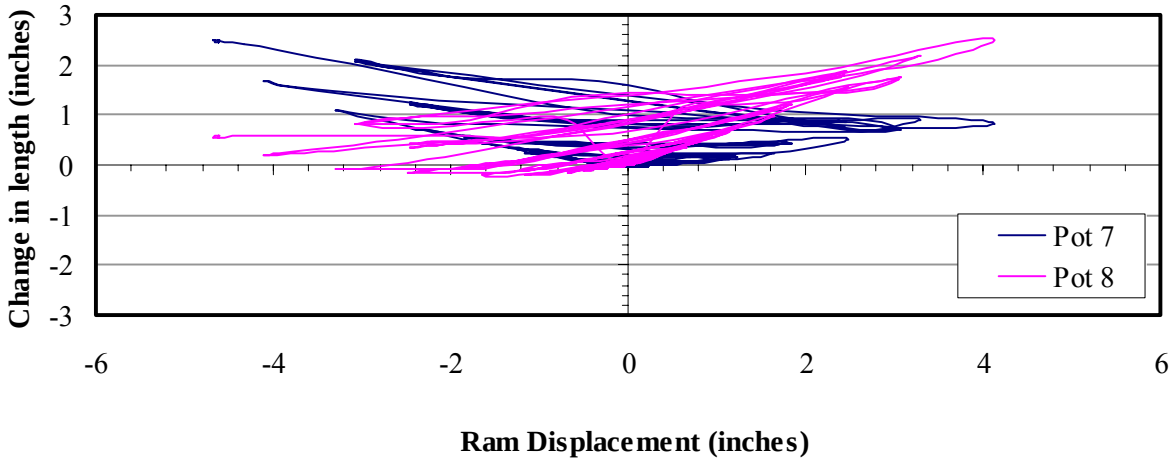

Figure A.64. Change in length of diagonal measuring Pots 7 and 8 vs. ram displacement of 10-10-P-2

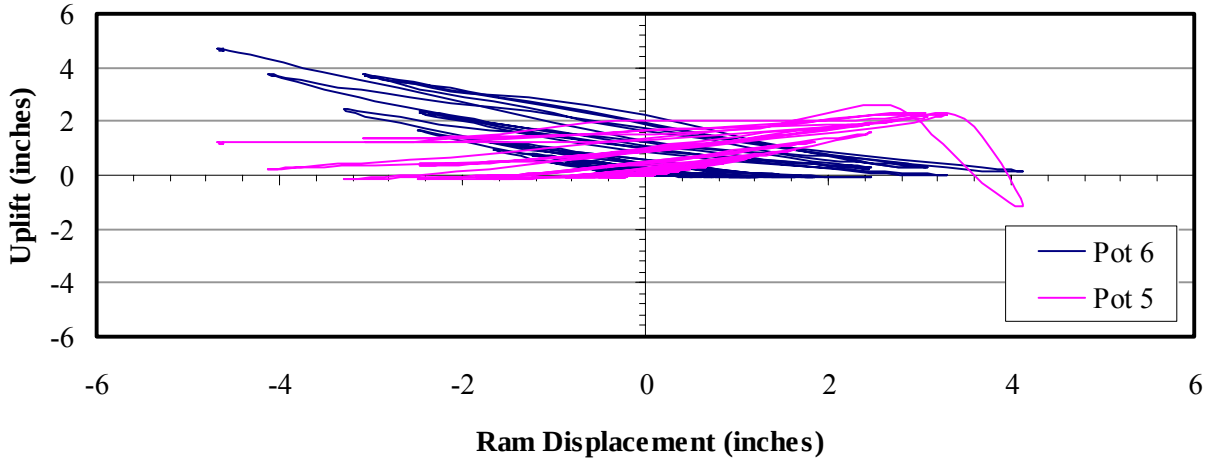

Figure A.65 Uplift displacement vs. ram displacement of 10-10-P-2

Table A.53. Performance Parameters of 10-10-P-3

Specimen	10-10-P-3	
Peak load, F_{peak}	Kips	1.749
	KN	7.778
Drift at peak load, Δ_{peak}	in.	1.258
	mm	31.96
Yield load, F_{yield}	Kips	1.498
	KN	6.662
Drift at yield load, Δ_{yield}	in.	0.531
	mm	13.48
Proportional limit, $0.4F_{peak}$	Kips	0.699
	KN	3.111
Drift at prop. limit, $\Delta@0.4F_{peak}$	in.	0.247
	mm	6.29
Failure load or $0.8F_{peak}$	Kips	1.399
	KN	6.222
Drift at failure, $\Delta_{failure}$	in.	1.874
	mm	47.60
Elastic stiffness, K_e $@0.4F_{peak}$	Kip/in.	2.878
	KN/mm	0.504
Work until failure	Kip·ft.	2.434
	KN·m	3.300
Ductility factor, μ	3.49	

Observations and failure modes:

- Mode of failure was sheathing nail tear through under the end stud in tension. This led to significant amounts of uplift displacement between end stud in tension and bottom plate.
- Sheathing nails along bottom plate within 2 ft of either end stud experienced tear through and significant bending deformation.
- Sheathing nails along center portion of bottom plate experienced withdrawal; thus, bending deformation was not as significant.
- Sheathing nails removed from any other location experienced virtually no bending deformation

Table A.54. EEEP Parameters of 10-10-P-3

EEEP Parameters	units	negative	positive
F_{yield}	Kips	-1.519	1.477
	KN	-6.756	6.568
Δ_{yield}	in.	-0.461	0.601
	mm	-11.70	15.26
$\Delta_{failure}$	in.	-1.452	2.296
	mm	-36.87	58.32

Table A.55. Displacement components of 10-10-P-3

	inches	mm	% of Total
Total Displacement	1.1	27.9	
Shear Deformation	0.3	7.6	27.3
Rigid Body Motion	0.8	20.3	72.7
Bending and Slip	0.0	0.0	0.0

Table A.56. Data of each Primary cycle of 10-10-P-3

Primary	average displacement		average load		work per cycle		cyclic stiffness		Damping
cycle #	in.	mm	Kips	KN	Kip·ft.	KN·m	Kip/in.	KN/mm	ratio
1	0.077	1.952	0.313	1.391	0.002	0.002	0.002	0.002	4.021
2	0.112	2.840	0.425	1.890	0.004	0.006	0.014	0.019	3.785
3	0.147	3.745	0.505	2.247	0.008	0.010	0.035	0.047	3.417
4	0.301	7.639	0.817	3.634	0.030	0.040	0.084	0.114	2.708
5	0.445	11.297	1.019	4.534	0.053	0.071	0.187	0.254	2.284
6	0.592	15.024	1.221	5.433	0.080	0.108	0.357	0.484	2.060
7	1.040	26.427	1.659	7.378	0.208	0.282	0.655	0.888	1.592
8	1.348	34.243	1.631	7.255	0.280	0.380	1.105	1.498	1.212
9	2.027	51.487	1.306	5.810	0.387	0.524	1.725	2.339	0.643
10	2.948	74.868	0.851	3.784	0.412	0.558	2.434	3.300	0.290
11	3.590	91.300	0.348	1.547	0.322	0.437	3.101	4.204	0.162

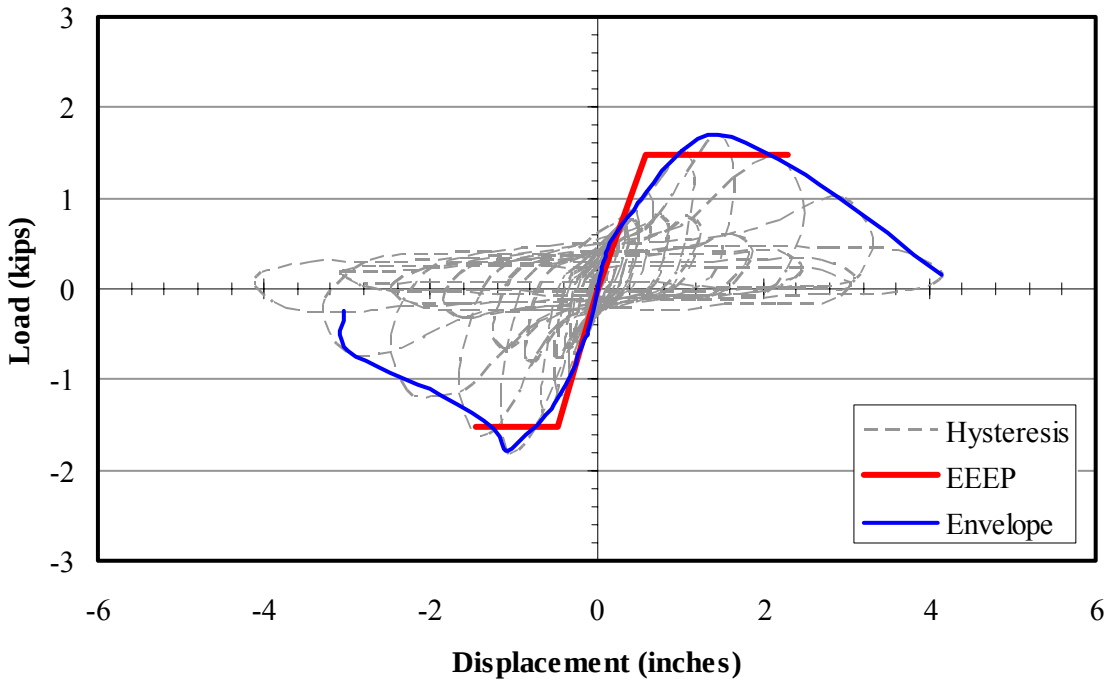

Figure A.66. Load vs. displacement, envelope and EEEP curves of 10-10-P-3

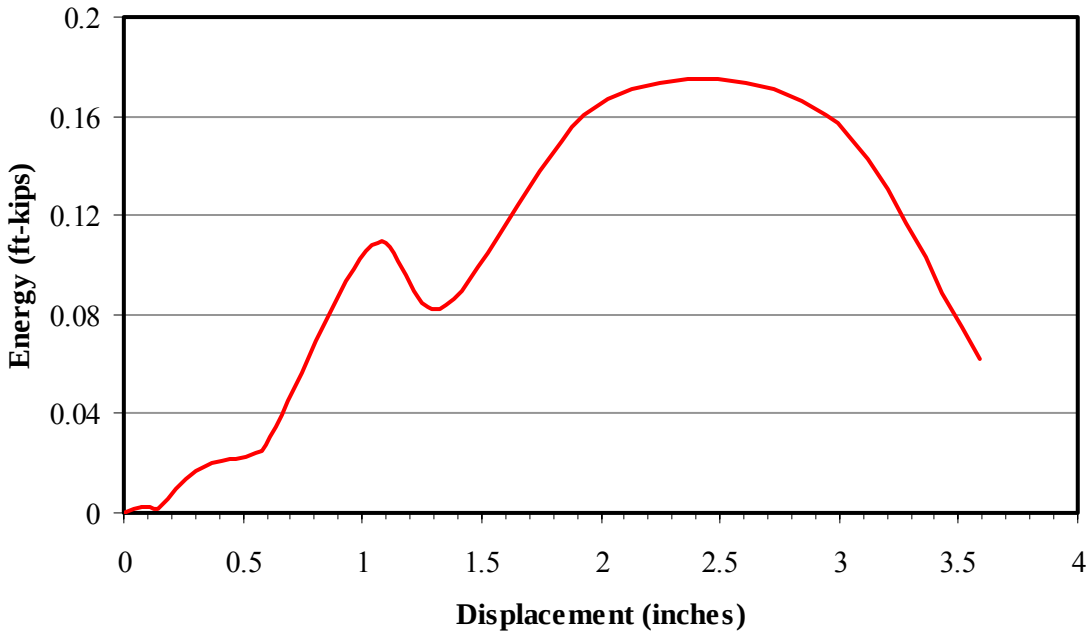

Figure A.67. Hysteretic energy dissipated per cycle vs. displacement of 10-10-P-3

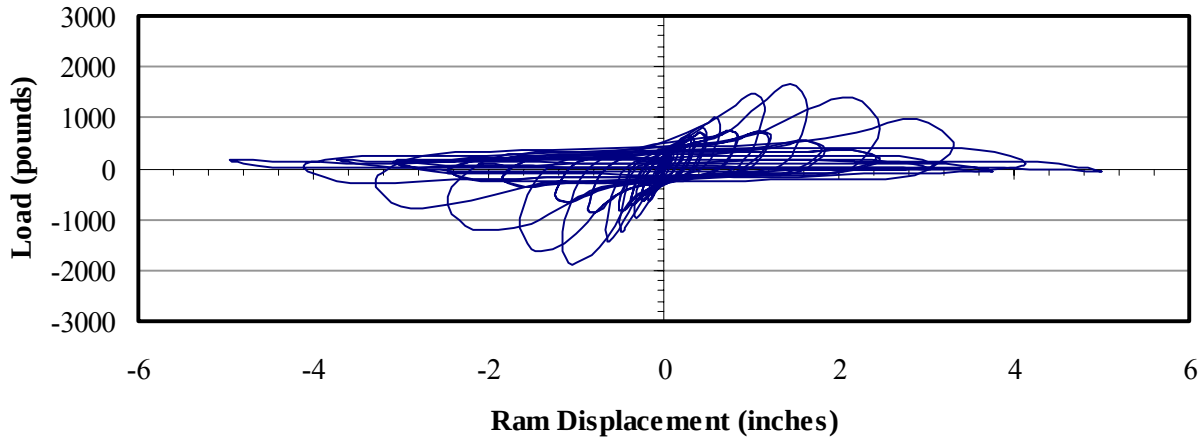

Figure A.68. Load vs. displacement of 10-10-P-3

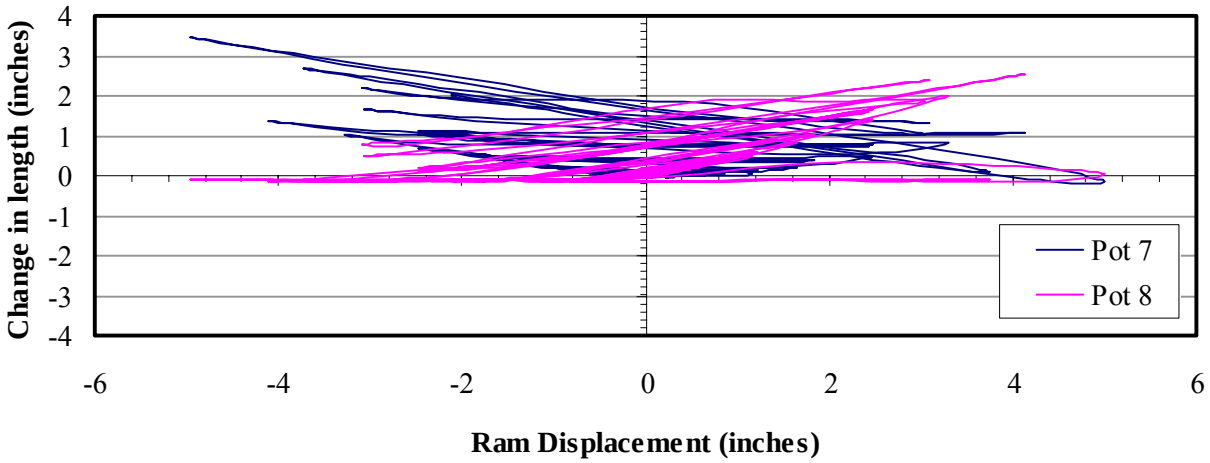

Figure A.69. Change in length of diagonal measuring Pots 7 and 8 vs. ram displacement of 10-10-P-3

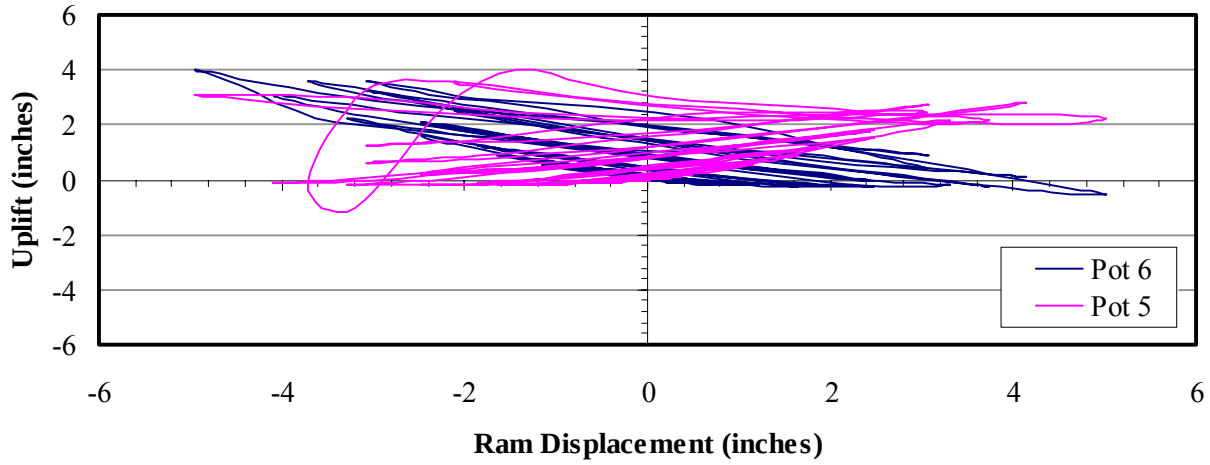

Figure A.70. Uplift displacement vs. ram displacement of 10-10-P-3

Table A.57. Performance Parameters of 9-ALT9-P-1

Specimen	9-ALT9-P-1	
Peak load, F_{peak}	Kips	1.978
	KN	8.799
Drift at peak load, Δ_{peak}	in.	1.325
	mm	33.65
Yield load, F_{yield}	Kips	1.779
	KN	7.913
Drift at yield load, Δ_{yield}	in.	0.433
	mm	10.99
Proportional limit, $0.4F_{peak}$	Kips	0.791
	KN	3.520
Drift at prop. limit, $\Delta@0.4F_{peak}$	in.	0.192
	mm	4.89
Failure load or $0.8F_{peak}$	Kips	1.583
	KN	7.040
Drift at failure, $\Delta_{failure}$	in.	1.672
	mm	42.48
Elastic stiffness, K_e $@0.4F_{peak}$	Kip/in.	4.105
	KN/mm	0.719
Work until failure	Kip·ft.	2.387
	KN·m	3.236
Ductility factor, μ	3.88	

Observations and failure modes:

- Mode of failure was sheathing nail tear through under the end stud in tension. This led to significant amounts of uplift displacement between end stud in tension and bottom plate.
- Sheathing nails removed from bottom plate displayed significant bending deformation. Sheathing nails removed from any other location experienced virtually no bending deformation.
- All sheathing nails along bottom plate experienced tear through as wall was tested to complete failure
- Tear through was more sudden and brittle than walls sheathed with normal strand OSB
- Cross grain crack formed at anchor bolts nearest end studs

Table A.58. EEEP Parameters of 9-ALT9-P-1

EEEP Parameters	units	negative	positive
F_{yield}	Kips	-1.621	1.937
	KN	-7.210	8.617
Δ_{yield}	in.	-0.414	0.451
	mm	-10.52	11.46
$\Delta_{failure}$	in.	-1.709	1.636
	mm	-43.40	41.56

Table A.59. Displacement component of 9-ALT9-P-1

	inches	Mm	% of Total
Total Displacement	1.6	40.6	
Shear Deformation	0.3	7.6	18.8
Rigid Body Motion	1.3	33.0	81.2
Bending and Slip	0.0	0.0	0.0

Table A.60. Data of each Primary cycle of 9-ALT9-P-1

Primary	average displacement		average load		work per cycle		cyclic stiffness		Damping
cycle #	in.	mm	Kips	KN	Kip·ft.	KN·m	Kip/in.	KN/mm	ratio
1	0.078	1.970	0.442	1.965	0.003	0.004	5.694	0.997	0.182
2	0.121	3.071	0.594	2.644	0.007	0.010	4.918	0.861	0.189
3	0.165	4.190	0.713	3.173	0.012	0.016	4.324	0.757	0.197
4	0.331	8.415	1.143	5.084	0.042	0.057	3.454	0.605	0.211
5	0.487	12.371	1.490	6.628	0.078	0.106	3.066	0.537	0.206
6	0.646	16.408	1.713	7.619	0.117	0.158	2.655	0.465	0.202
7	1.076	27.341	1.953	8.688	0.283	0.383	1.817	0.318	0.257
8	1.517	38.533	1.896	8.433	0.388	0.527	1.255	0.220	0.258
9	1.795	45.593	1.386	6.166	0.485	0.657	0.773	0.135	0.372

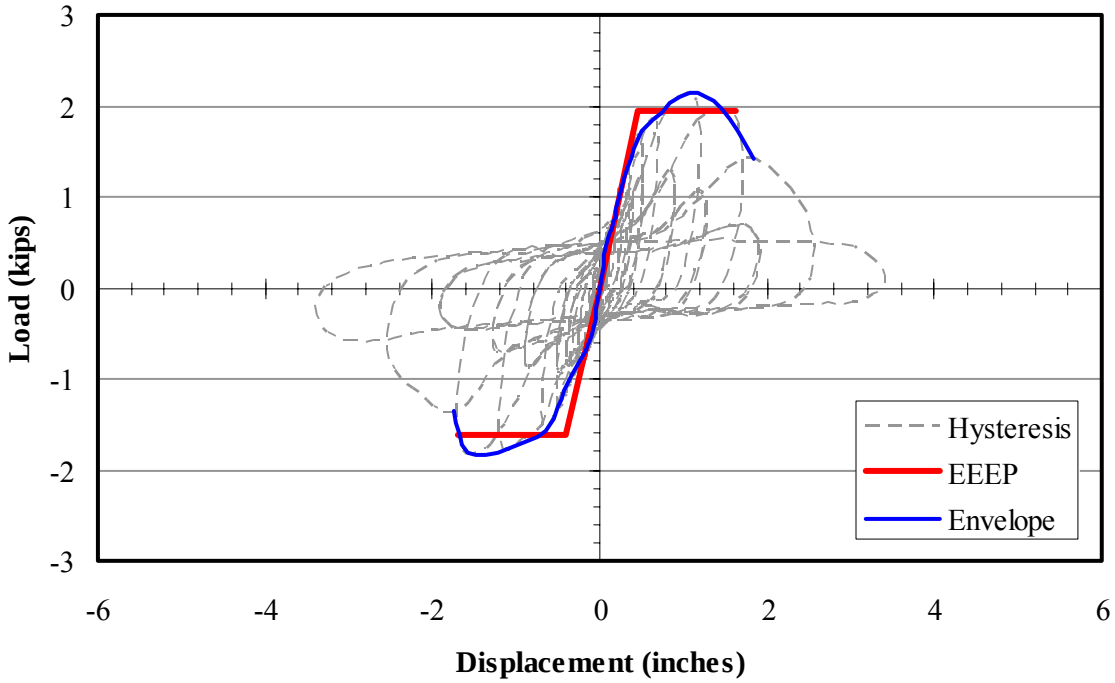

Figure A.71. Load vs. displacement, envelope and EEEP curves of 9-ALT9-P-1

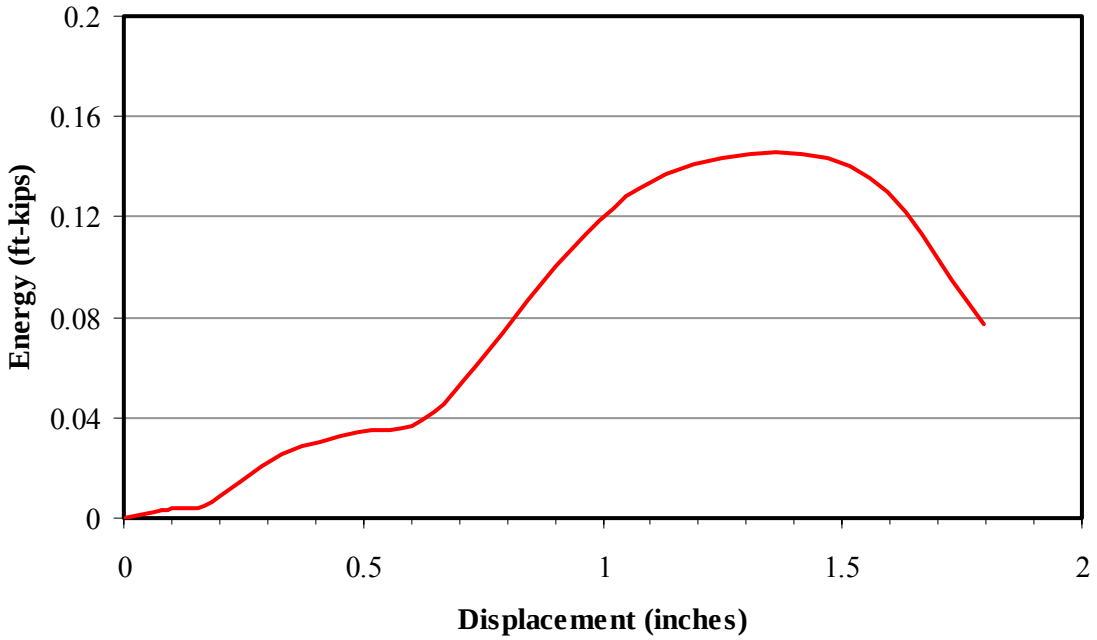

Figure A.72. Hysteretic energy dissipated per cycle vs. displacement of 9-ALT9-P-1

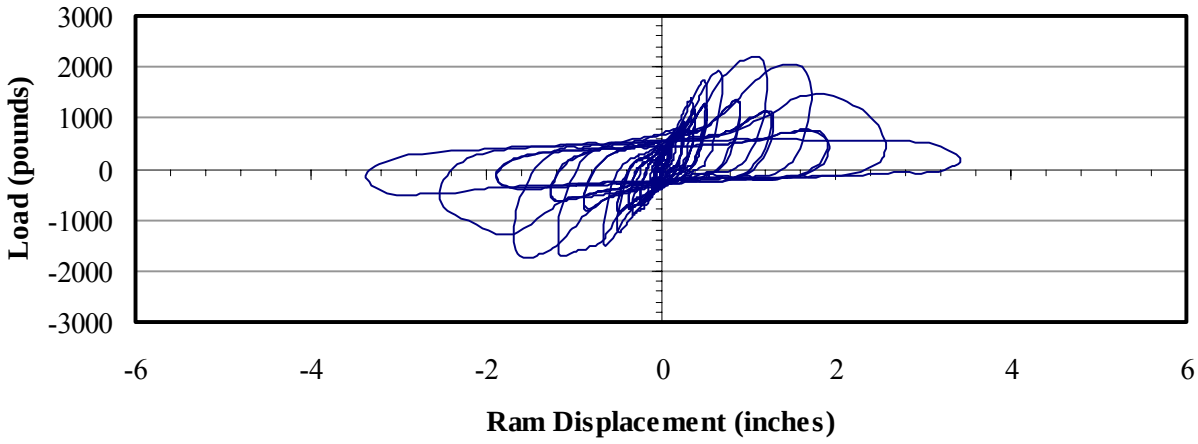

Figure A.73. Load vs. displacement of 9-ALT9-P-1

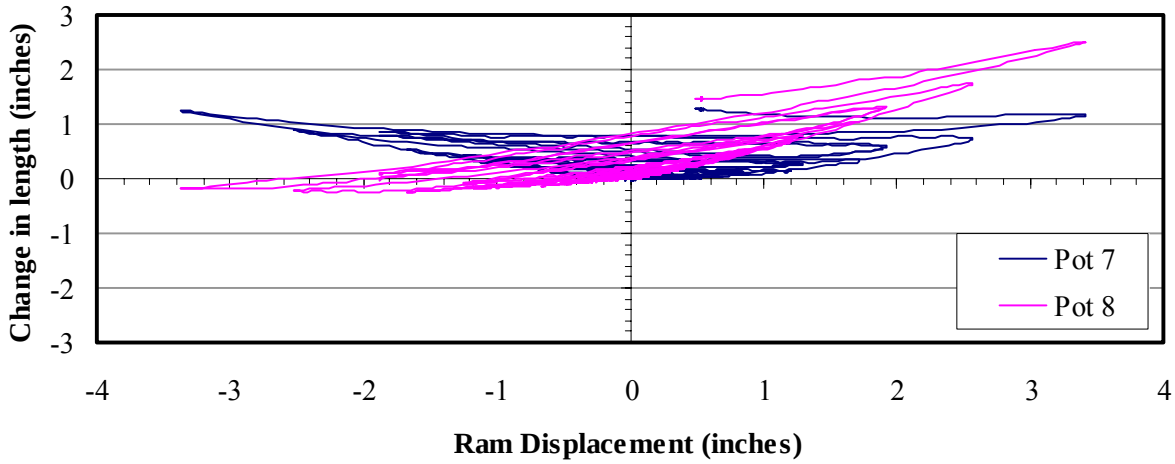

Figure A.74. Change in length of diagonal measuring Pots 7 and 8 vs. ram displacement of 9-ALT9-P-1

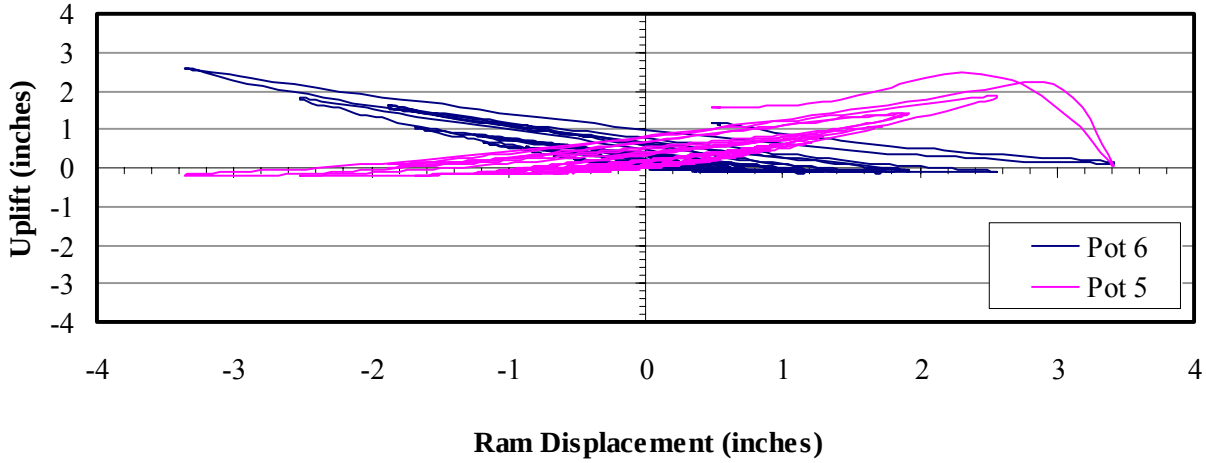

Figure A.75. Uplift displacement vs. ram displacement of 9-ALT9-P-1

Table A.61. Performance Parameters of 9-ALT9-P-2

Specimen	9-ALT9-P-2	
Peak load, F_{peak}	Kips	2.168
	KN	9.641
Drift at peak load, Δ_{peak}	in.	1.261
	mm	32.03
Yield load, F_{yield}	Kips	1.937
	KN	8.615
Drift at yield load, Δ_{yield}	in.	0.593
	mm	15.05
Proportional limit, $0.4F_{peak}$	Kips	0.867
	KN	3.856
Drift at prop. limit, $\Delta@0.4F_{peak}$	in.	0.265
	mm	6.73
Failure load or $0.8F_{peak}$	Kips	1.734
	KN	7.713
Drift at failure, $\Delta_{failure}$	in.	1.649
	mm	41.88
Elastic stiffness, K_e $@0.4F_{peak}$	Kip/in.	3.275
	KN/mm	0.574
Work until failure	Kip·ft.	2.518
	KN·m	3.413
Ductility factor, μ	2.79	

Observations and failure modes:

- Mode of failure was sheathing nail tear through under the end stud in tension. This led to significant amounts of uplift displacement between end stud in tension and bottom plate.
- Sheathing nails removed from bottom plate displayed significant bending deformation. Sheathing nails removed from any other location experienced virtually no bending deformation.
- All sheathing nails along bottom plate experienced tear through as wall was tested to complete failure
- Tear through was more sudden and brittle than walls sheathed with normal strand OSB
- Cross grain crack formed at anchor bolts nearest end studs

Table A.62. EEEP Parameters of 9-ALT9-P-2

EEEP Parameters	units	negative	positive
F_{yield}	Kips	-1.953	1.921
	KN	-8.687	8.542
Δ_{yield}	in.	-0.568	0.617
	mm	-14.43	15.67
$\Delta_{failure}$	in.	-1.670	1.627
	mm	-42.42	41.33

Table A.63. Displacement component of 9-ALT9-P-2

	inches	mm	% of Total
Total Displacement	1.4	35.6	
Shear Deformation	0.4	10.2	28.6
Rigid Body Motion	1.0	25.4	71.4
Bending and Slip	0.0	0.0	0.0

Table A.64. Data of each Primary cycle of 9-ALT9-P-2

Primary	average displacement		average load		work per cycle		cyclic stiffness		Damping
cycle #	in.	mm	Kips	KN	Kip·ft.	KN·m	Kip/in.	KN/mm	ratio
1	0.082	2.076	0.426	1.897	0.003	0.003	5.208	0.912	0.137
2	0.123	3.122	0.547	2.433	0.006	0.009	4.445	0.778	0.179
3	0.165	4.191	0.627	2.790	0.011	0.015	3.800	0.665	0.205
4	0.327	8.301	1.012	4.503	0.038	0.051	3.098	0.542	0.217
5	0.491	12.482	1.376	6.119	0.072	0.097	2.800	0.490	0.203
6	0.653	16.594	1.673	7.442	0.108	0.146	2.562	0.449	0.188
7	1.089	27.673	2.151	9.570	0.277	0.375	1.975	0.346	0.225
8	1.461	37.098	2.087	9.281	0.434	0.588	1.431	0.251	0.272
9	1.832	46.525	1.391	6.186	0.571	0.774	0.765	0.134	0.431
10	3.175	80.640	0.425	1.890	0.327	0.443	0.525	0.092	0.953

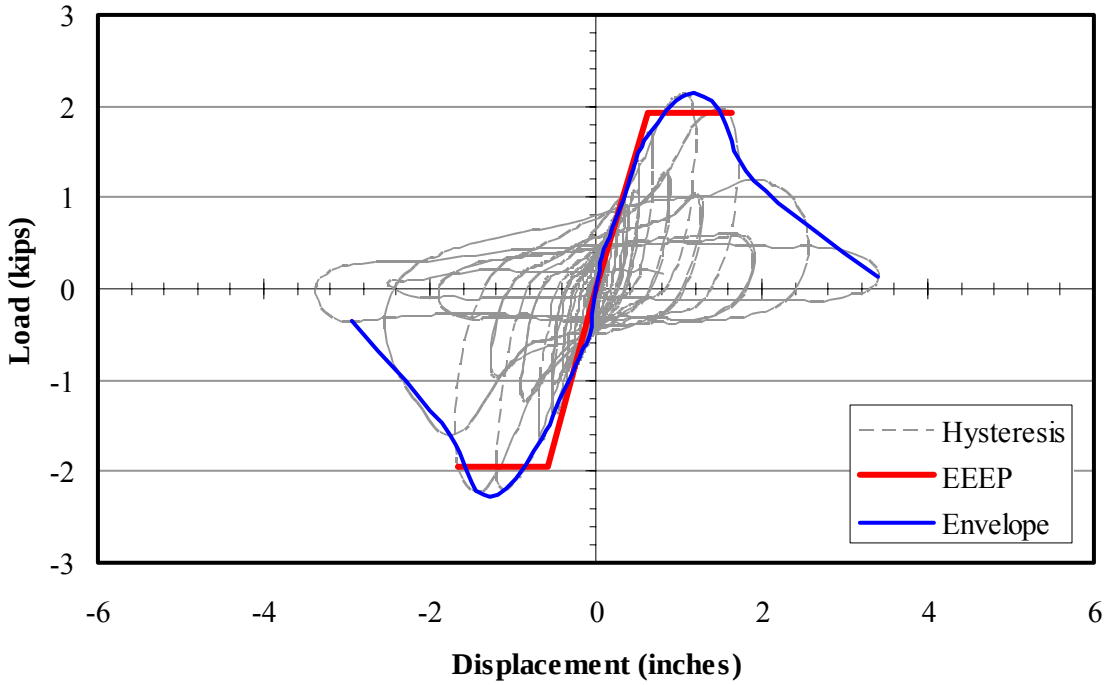

Figure A.76. Load vs. displacement, envelope and EEEP curves of 9-ALT9-P-2

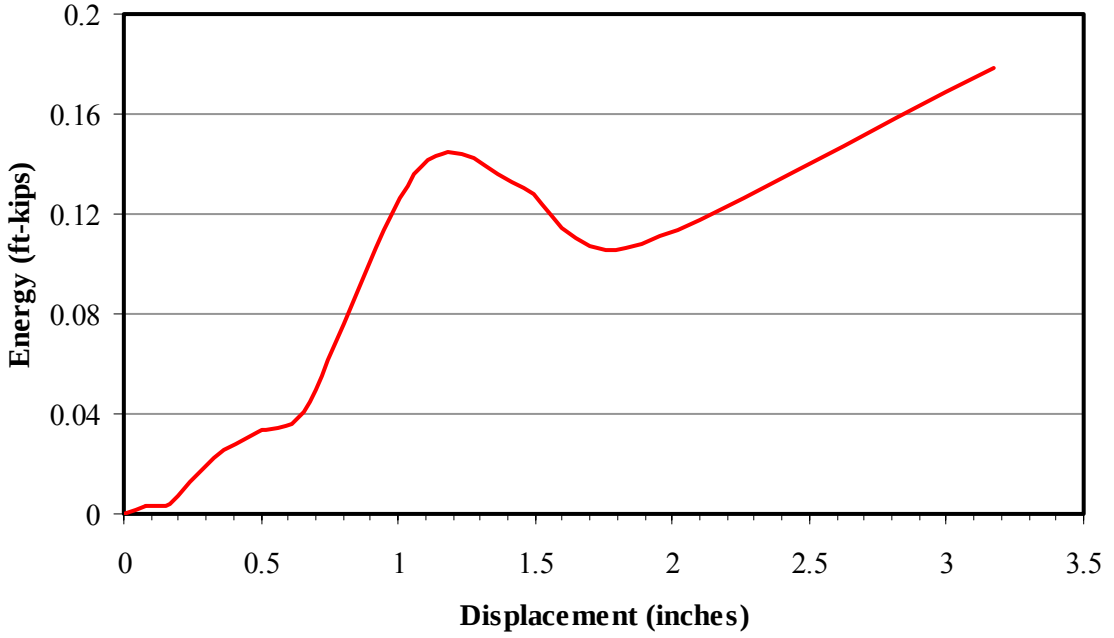

Figure A.77. Hysteretic energy dissipated per cycle vs. displacement of 9-ALT9-P-2

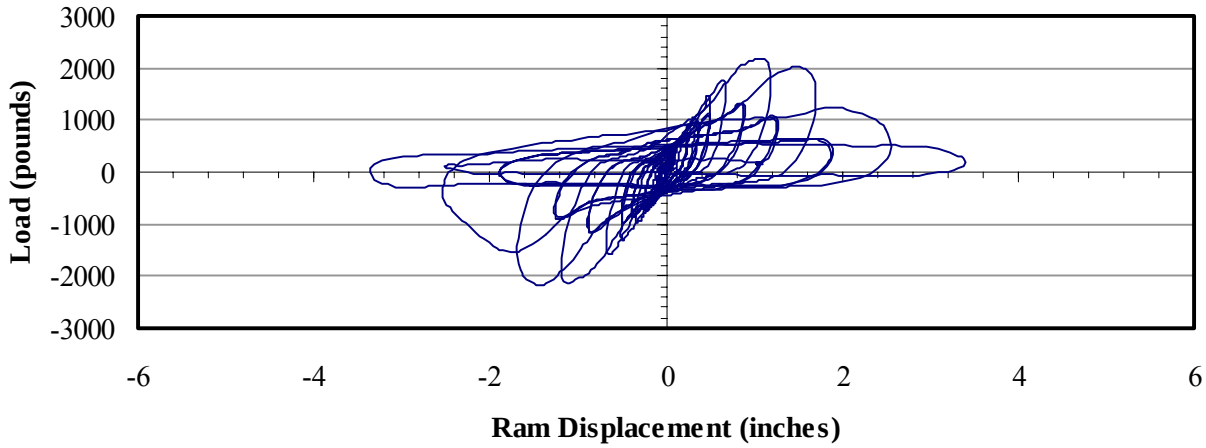

Figure A.78. Load vs. displacement of 9-ALT9-P-2

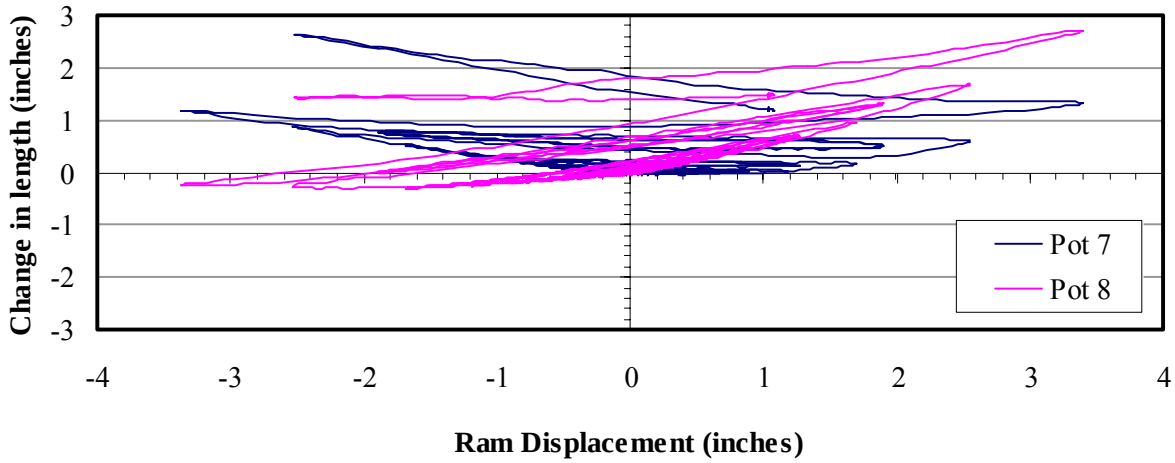

Figure A.79. Change in length of diagonal measuring Pots 7 and 8 vs. ram displacement of 9-ALT9-P-2

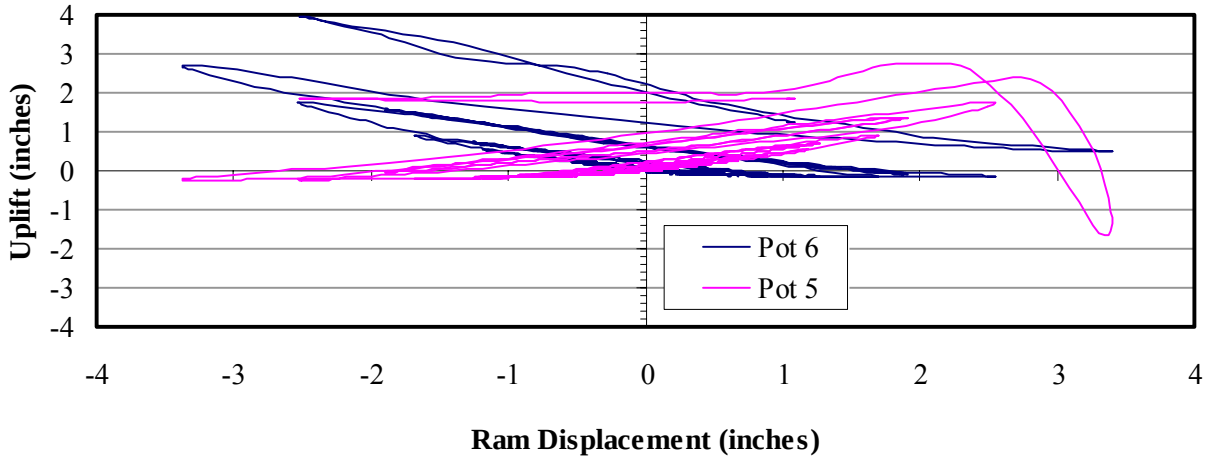

Figure A.80. Uplift displacement vs. ram displacement of 9-ALT9-P-2

Table A.65. Performance Parameters of 9-ALT9-P-3

Specimen	9-ALT9-P-3	
Peak load, F_{peak}	Kips	2.086
	KN	9.278
Drift at peak load, Δ_{peak}	in.	1.246
	mm	31.65
Yield load, F_{yield}	Kips	1.913
	KN	8.511
Drift at yield load, Δ_{yield}	in.	0.507
	mm	12.87
Proportional limit, $0.4F_{peak}$	Kips	0.834
	KN	3.711
Drift at prop. limit, $\Delta@0.4F_{peak}$	in.	0.217
	mm	5.51
Failure load or $0.8F_{peak}$	Kips	1.669
	KN	7.422
Drift at failure, $\Delta_{failure}$	in.	1.556
	mm	39.51
Elastic stiffness, K_e $@0.4F_{peak}$	Kip/in.	5.662
	KN/mm	0.992
Work until failure	Kip·ft.	2.392
	KN·m	3.243
Ductility factor, μ	4.77	

Observations and failure modes:

- Mode of failure was sheathing nail tear through under the end stud in tension. This led to significant amounts of uplift displacement between end stud in tension and bottom plate.
- Sheathing nails removed from bottom plate displayed significant bending deformation. Sheathing nails removed from any other location experienced virtually no bending deformation.
- All sheathing nails along bottom plate experienced tear through as wall was tested to complete failure
- Tear through was more sudden and brittle than walls sheathed with normal strand OSB

Table A.66. EEEP Parameters of 9-ALT9-P-3

EEEP Parameters	units	negative	positive
F_{yield}	Kips	-2.098	1.729
	KN	-9.332	7.690
Δ_{yield}	in.	-0.816	0.198
	mm	-20.72	5.02
$\Delta_{failure}$	in.	-1.620	1.491
	mm	-41.15	37.87

Table A.67. Displacement component of 9-ALT9-P-3

	inches	mm	% of Total
Total Displacement	1.4	35.6	
Shear Deformation	0.3	7.6	21.4
Rigid Body Motion	1.1	27.9	78.6
Bending and Slip	0.0	0.0	0.0

Table A.68. Data of each Primary cycle of 9-ALT9-P-3

Primary	average displacement		average load		work per cycle		cyclic stiffness		Damping
cycle #	in.	mm	Kips	KN	Kip·ft.	KN·m	Kip/in.	KN/mm	ratio
1	0.085	2.156	0.546	2.426	0.003	0.004	6.430	1.126	0.110
2	0.123	3.124	0.742	3.302	0.007	0.009	6.053	1.060	0.141
3	0.165	4.181	0.869	3.865	0.012	0.016	5.302	0.928	0.157
4	0.331	8.395	1.169	5.199	0.041	0.056	3.560	0.623	0.206
5	0.486	12.356	1.500	6.672	0.077	0.104	3.100	0.543	0.202
6	0.646	16.401	1.727	7.683	0.117	0.158	2.680	0.469	0.200
7	1.091	27.706	2.079	9.247	0.284	0.385	1.905	0.334	0.239
8	1.436	36.469	1.957	8.704	0.394	0.534	1.362	0.238	0.268
9	1.751	44.484	1.255	5.582	0.474	0.642	0.723	0.127	0.415
10	2.750	69.760	0.635	2.823	0.359	0.487	0.164	0.029	0.753

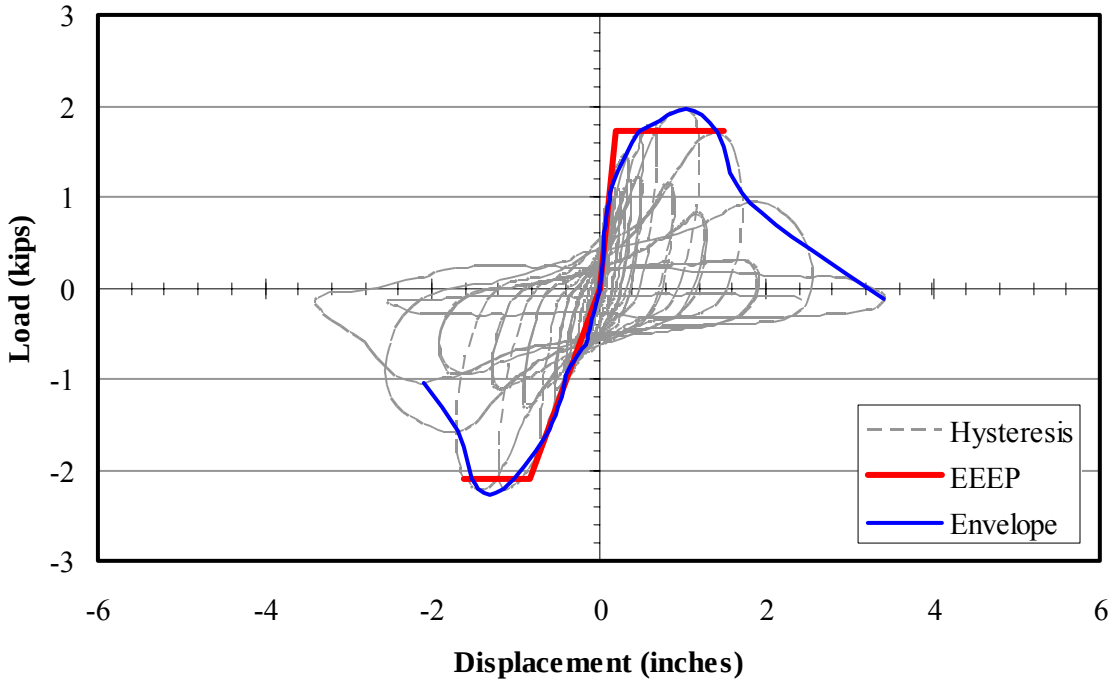

Figure A.81. Load vs. displacement, envelope and EEEP curves of 9-ALT9-P-3

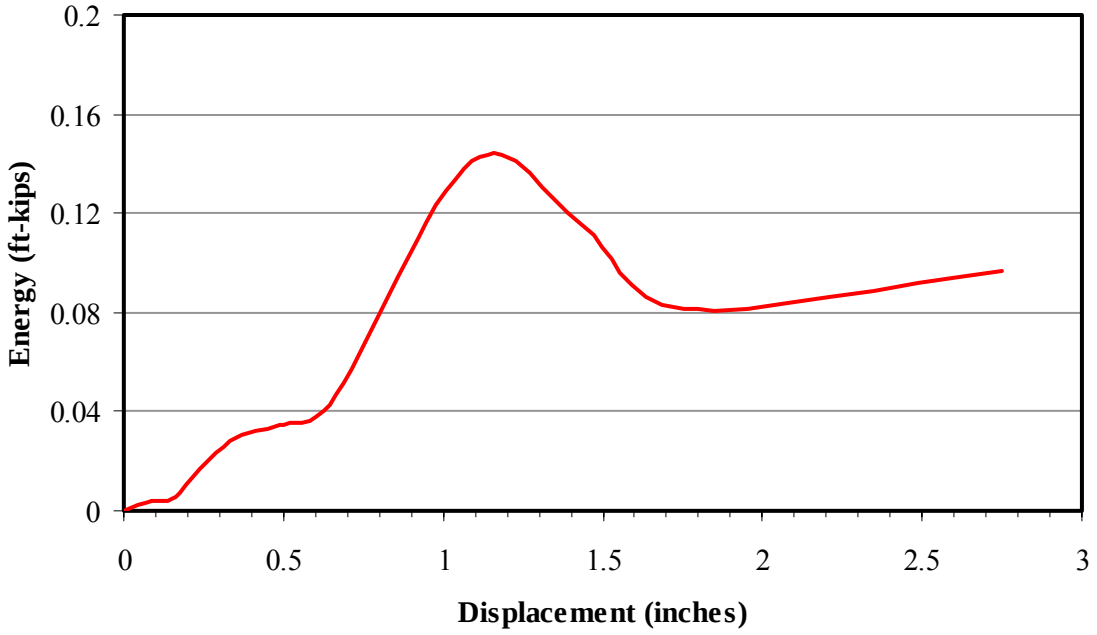

Figure A.82. Hysteretic energy dissipated per cycle vs. displacement of 9-ALT9-P-3

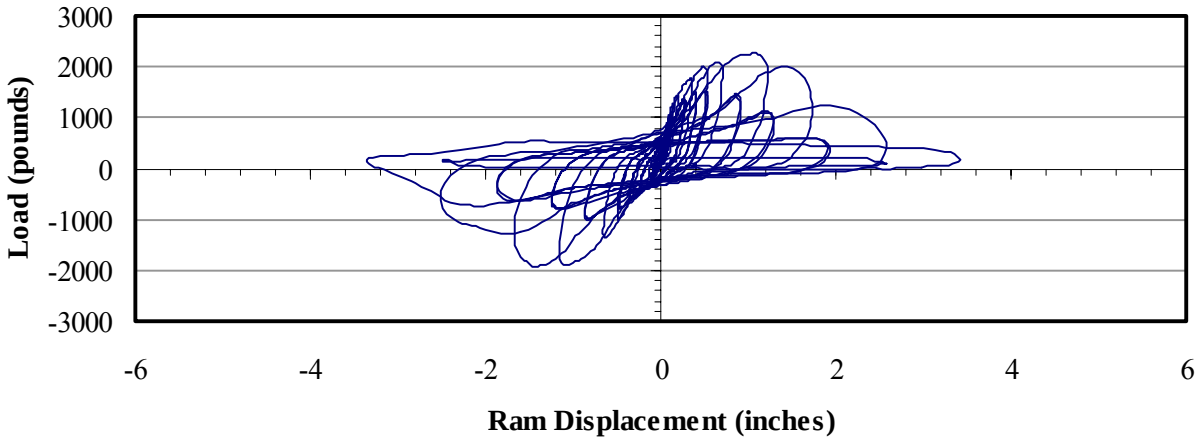

Figure A.83. Load vs. displacement of 9-ALT9-P-3

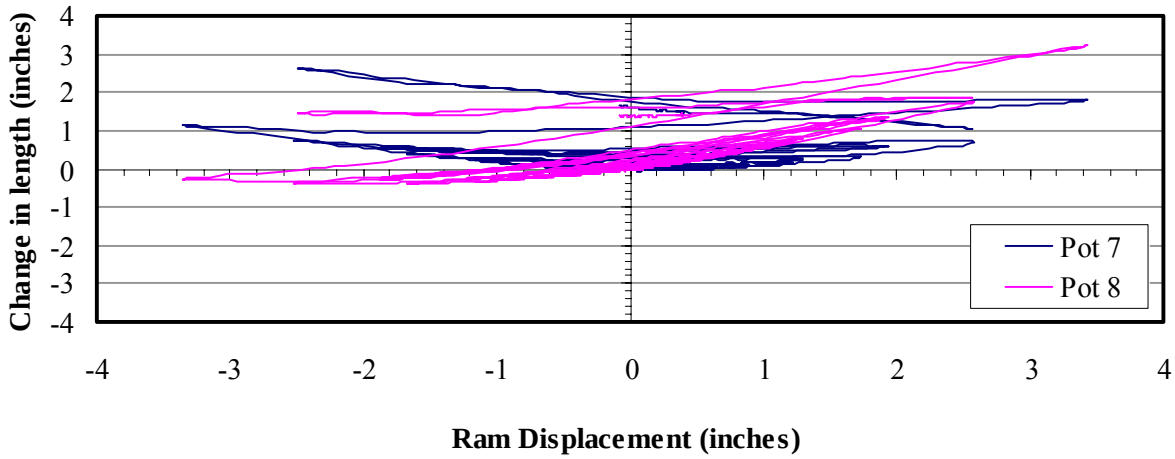

Figure A.84. Change in length of diagonal measuring Pots 7 and 8 vs. ram displacement of 9-ALT9-P-3

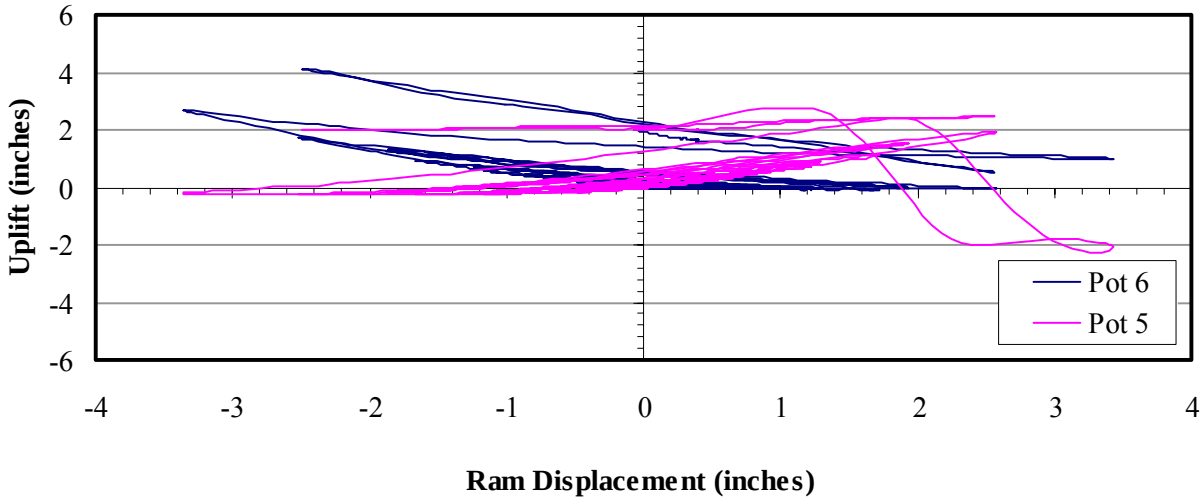

Figure A.85. Uplift displacement vs. ram displacement of 9-ALT9-P-3

Table A.69. Performance Parameters of 8-8.5-P-1

Specimen	8-8.5-P-1	
Peak load, F_{peak}	Kips	2.999
	KN	13.340
Drift at peak load, Δ_{peak}	in.	1.958
	mm	49.74
Yield load, F_{yield}	Kips	2.647
	KN	11.772
Drift at yield load, Δ_{yield}	in.	0.509
	mm	12.92
Proportional limit, $0.4F_{peak}$	Kips	1.200
	KN	5.336
Drift at prop. limit, $\Delta@0.4F_{peak}$	in.	0.231
	mm	5.87
Failure load or $0.8F_{peak}$	Kips	2.399
	KN	10.672
Drift at failure, $\Delta_{failure}$	in.	2.587
	mm	65.71
Elastic stiffness, K_e $@0.4F_{peak}$	Kip/in.	5.444
	KN/mm	0.953
Work until failure	Kip·ft.	4.730
	KN·m	6.412
Ductility factor, μ	5.24	

Observations and failure modes:

- Mode of failure was sheathing nail tear through under the end stud in tension along the edge of the panel in the 2 x 12. Sheathing nails in bottom plate pulled heads through the panel. This led to significant amounts of uplift displacement between end stud in tension and bottom plate.
- Sheathing nails removed from bottom plate and 2 x 12 displayed significant bending deformation.
- Sheathing nails removed from any other location experienced virtually no bending deformation.
- Bottom plate remained attached to 2 x 12 and the rest of wall separated from bottom plate as wall was tested to complete failure.

Table A.70. EEEP Parameters of 8-8.5-P-1

EEEP Parameters	units	negative	positive
F_{yield}	Kips	-2.541	2.752
	KN	-11.302	12.241
Δ_{yield}	in.	-0.607	0.411
	mm	-15.41	10.44
$\Delta_{failure}$	in.	-2.688	2.486
	mm	-68.28	63.14

Table A.71. Displacement components of 8-8.5-P-1

	inches	mm	% of Total
Total Displacement	2.3	58.4	
Shear Deformation	1.0	25.4	43.5
Rigid Body Motion	1.3	33.0	56.5
Bending and Slip	0.0	0.0	0.0

Table A.72. Data of each Primary cycle of 8-8.5-P-1

Primary	average displacement		average load		work per cycle		cyclic stiffness		Damping
cycle #	in.	mm	Kips	KN	Kip·ft.	KN·m	Kip/in.	KN/mm	Ratio
1	0.085	2.154	0.558	2.484	0.003	0.003	6.346	1.111	0.097
2	0.127	3.214	0.793	3.525	0.007	0.009	6.170	1.080	0.122
3	0.169	4.280	0.974	4.332	0.012	0.016	5.730	1.003	0.133
4	0.328	8.343	1.521	6.768	0.040	0.054	4.623	0.810	0.153
5	0.480	12.181	1.881	8.367	0.079	0.108	3.926	0.687	0.168
6	0.661	16.786	2.145	9.541	0.121	0.165	3.246	0.568	0.164
7	1.104	28.044	2.664	11.849	0.310	0.421	2.413	0.423	0.201
8	1.571	39.898	2.901	12.904	0.471	0.639	1.846	0.323	0.197
9	2.295	58.294	2.951	13.128	0.778	1.055	1.287	0.225	0.219
10	2.739	69.571	2.083	9.267	0.875	1.187	0.760	0.133	0.293

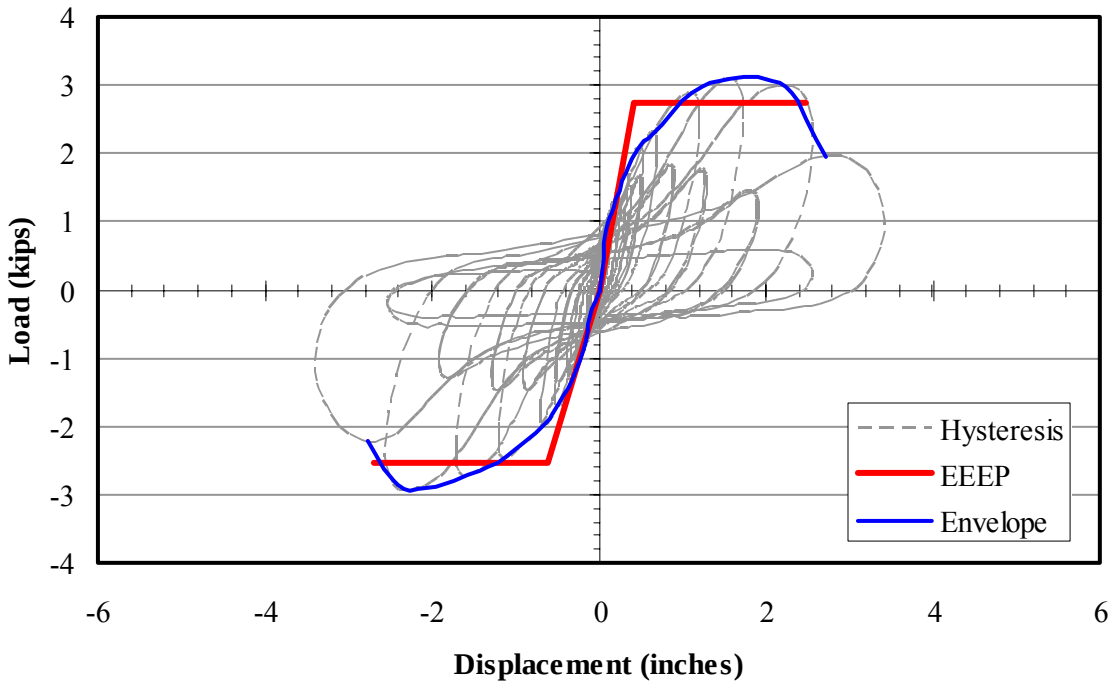

Figure A.86. Load vs. displacement, envelope and EEEP curves of 8-8.5-P-1

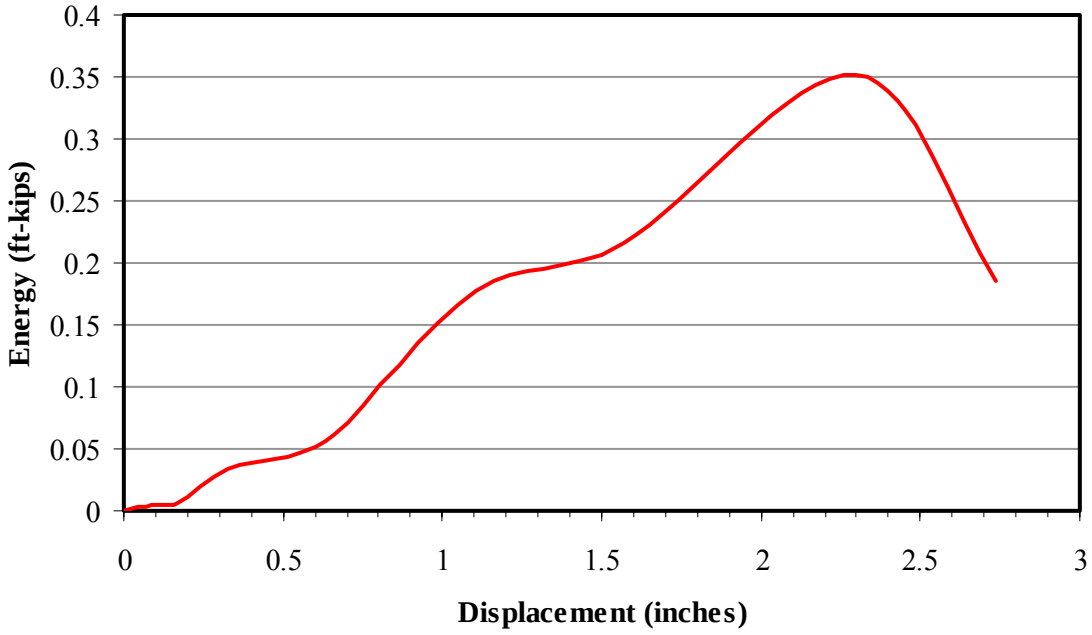

Figure A.87. Hysteretic energy dissipated per cycle vs. displacement of 8-8.5-P-1

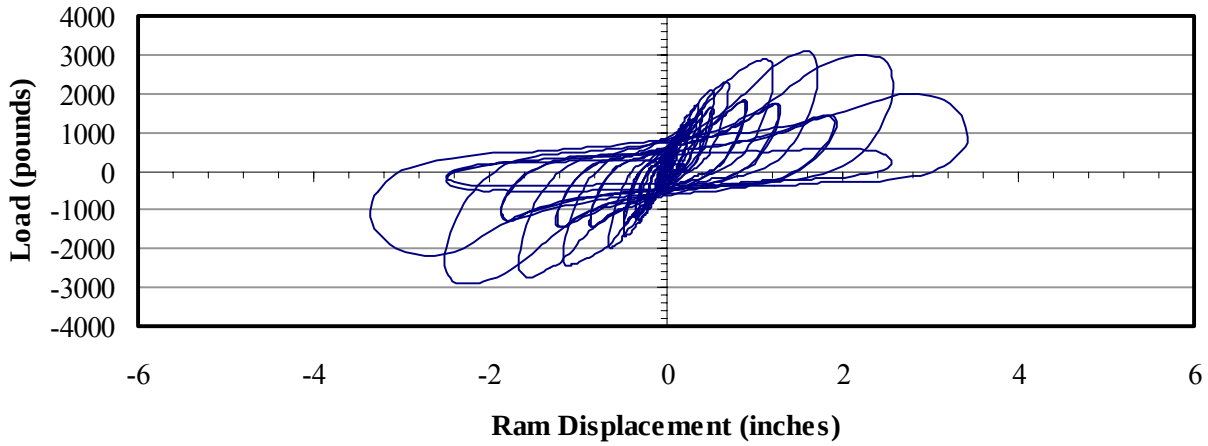

Figure A.88. Load vs. displacement of 8-8.5-P-1

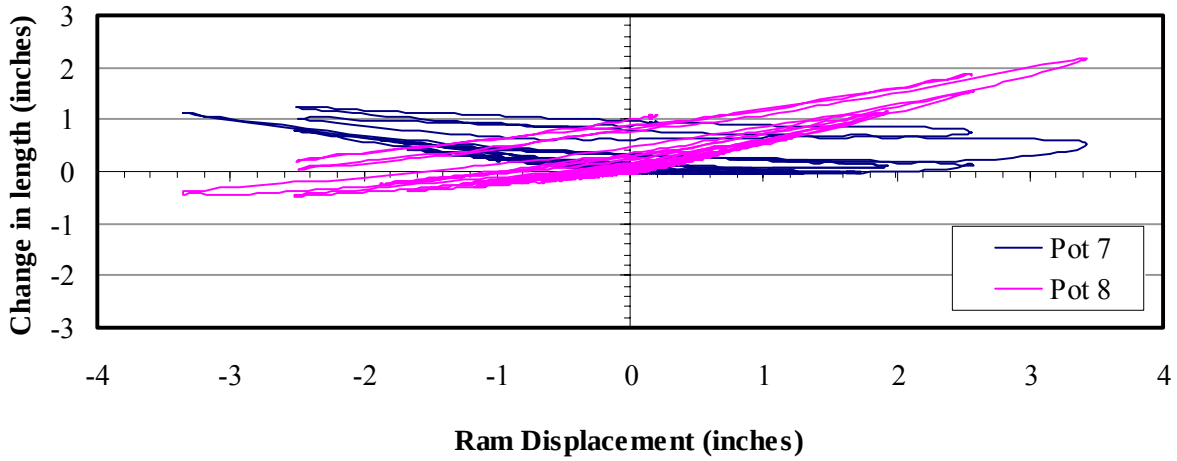

Figure A.89. Change in length of diagonal measuring Pots 7 and 8 vs. ram displacement of 8-8.5-P-1

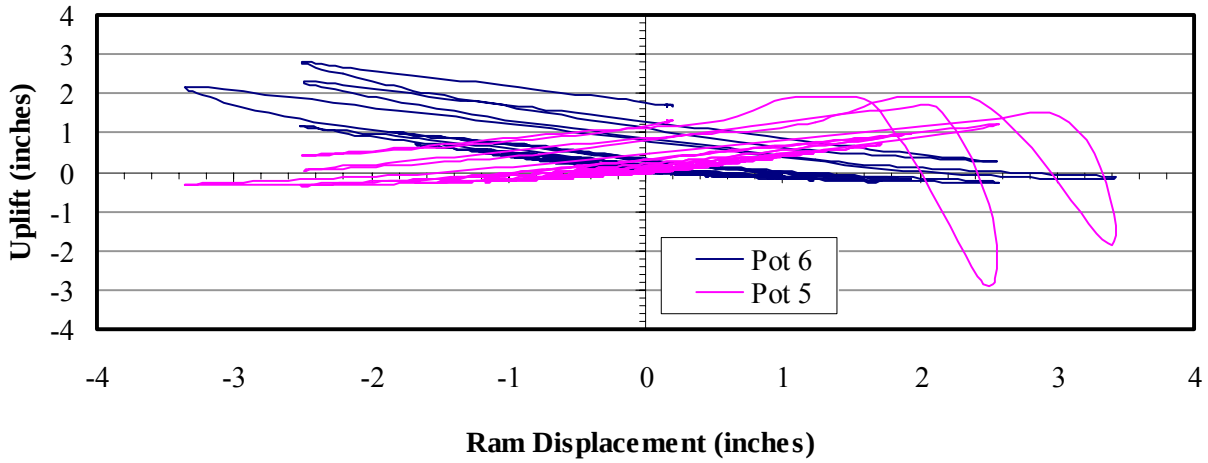

Figure A.90. Uplift displacement vs. ram displacement of 8-8.5-P-1

Table A.73. Performance Parameters of 8-8.5-P-2

Specimen	8-8.5-P-2	
Peak load, F_{peak}	Kips	3.032
	KN	13.486
Drift at peak load, Δ_{peak}	in.	1.874
	mm	47.59
Yield load, F_{yield}	Kips	2.554
	KN	11.361
Drift at yield load, Δ_{yield}	in.	0.559
	mm	14.19
Proportional limit, $0.4F_{peak}$	Kips	1.213
	KN	5.394
Drift at prop. limit, $\Delta@0.4F_{peak}$	in.	0.265
	mm	6.74
Failure load or $0.8F_{peak}$	Kips	2.426
	KN	10.789
Drift at failure, $\Delta_{failure}$	in.	2.147
	mm	54.53
Elastic stiffness, K_e $@0.4F_{peak}$	Kip/in.	4.666
	KN/mm	0.817
Work until failure	Kip·ft.	2.957
	KN·m	4.009
Ductility factor, μ	3.90	

Observations and failure modes:

- Mode of failure was sheathing nail tear through under the end stud in tension along the edge of the panel in the 2 x 12. Sheathing nails in bottom plate pulled heads through the panel. This led to significant amounts of uplift displacement between end stud in tension and bottom plate.
- Sheathing nails removed from bottom plate and 2 x 12 displayed significant bending deformation.
- Sheathing nails removed from any other location experienced virtually no bending deformation.
- Bottom plate remained attached to 2 x 12 and the rest of wall separated from bottom plate as wall was tested to complete failure.

Table A.74. EEEP Parameters of 8-8.5-P-2

EEEP Parameters	units	negative	positive
F_{yield}	Kips	-2.725	2.383
	KN	-12.120	10.601
Δ_{yield}	in.	-0.659	0.458
	mm	-16.75	11.64
$\Delta_{failure}$	in.	-2.359	1.935
	mm	-59.91	49.16

Table A.75. Displacement components of 8-8.5-P-2

	inches	mm	% of Total
Total Displacement	2.2	55.9	
Shear Deformation	0.8	20.3	36.4
Rigid Body Motion	1.4	35.6	63.6
Bending and Slip	0.0	0.0	0.0

Table A.76. Data of each Primary cycle of 8-8.5-P-2

Primary	average displacement		average load		work per cycle		cyclic stiffness		Damping
cycle #	in.	mm	Kips	KN	Kip·ft.	KN·m	Kip/in.	KN/mm	Ratio
1	0.082	2.088	0.532	2.365	0.002	0.003	6.478	1.134	0.108
2	0.126	3.209	0.764	3.397	0.006	0.008	6.051	1.060	0.120
3	0.164	4.168	0.938	4.171	0.011	0.015	5.714	1.001	0.142
4	0.324	8.227	1.383	6.153	0.043	0.059	4.273	0.748	0.185
5	0.487	12.380	1.676	7.456	0.084	0.114	3.441	0.603	0.197
6	0.648	16.472	1.912	8.504	0.126	0.171	2.950	0.517	0.195
7	1.122	28.490	2.605	11.589	0.312	0.423	2.323	0.407	0.204
8	1.559	39.591	2.936	13.058	0.494	0.669	1.883	0.330	0.206
9	2.093	53.152	2.723	12.112	0.772	1.046	1.292	0.226	0.256
10	2.941	74.700	1.347	5.993	0.597	0.810	0.612	0.107	0.373

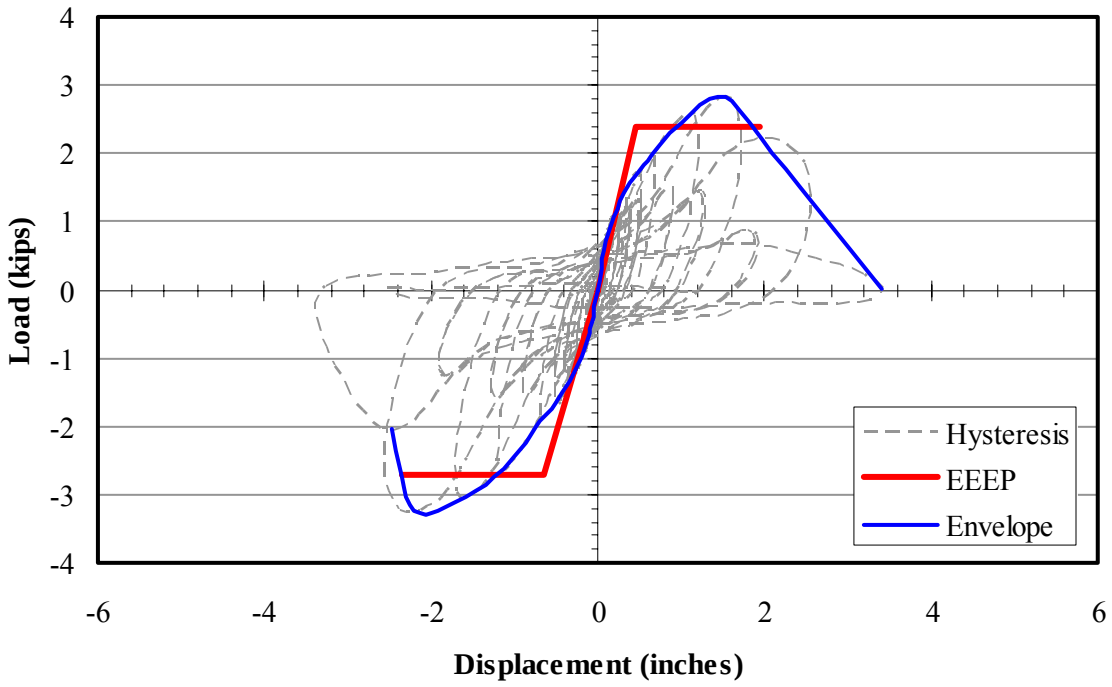

Figure A.91. Load vs. displacement, envelope and EEEP curves of 8-8.5-P-2

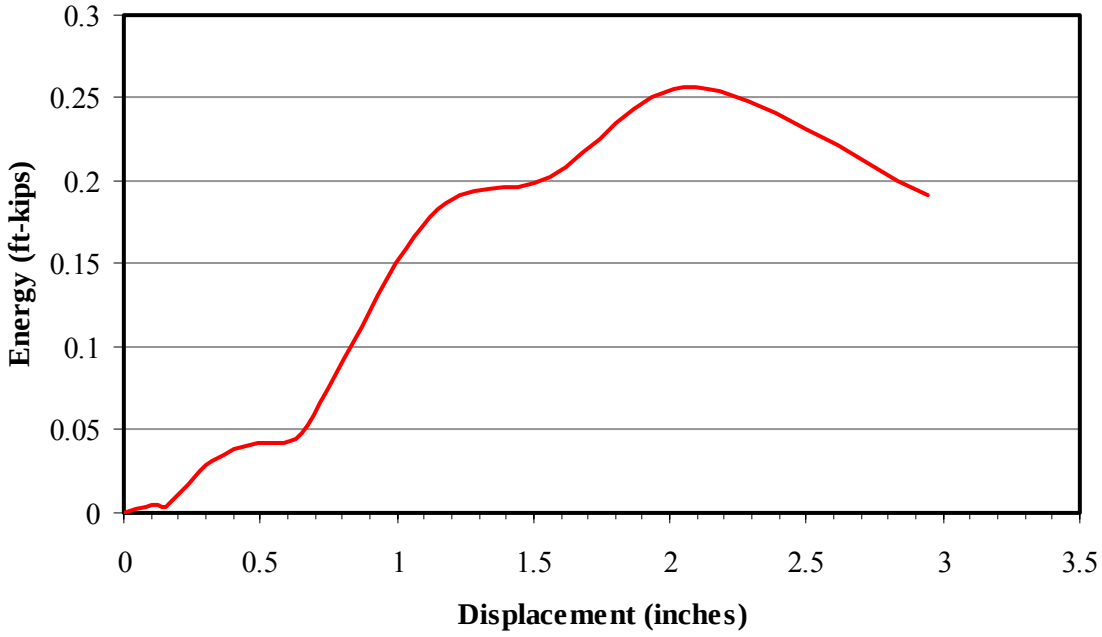

Figure A.92. Hysteretic energy dissipated per cycle vs. displacement of 8-8.5-P-2

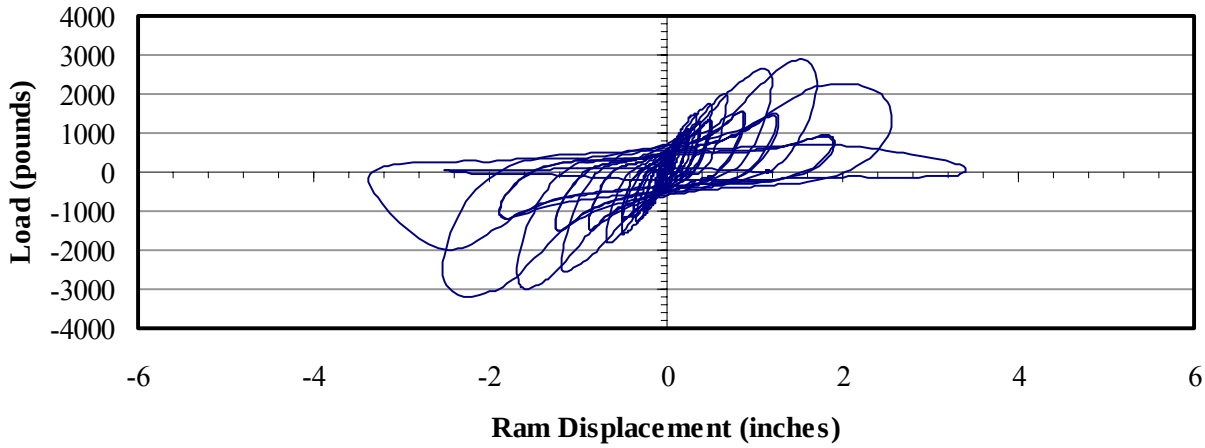

Figure A.93. Load vs. displacement of 8-8.5-P-2

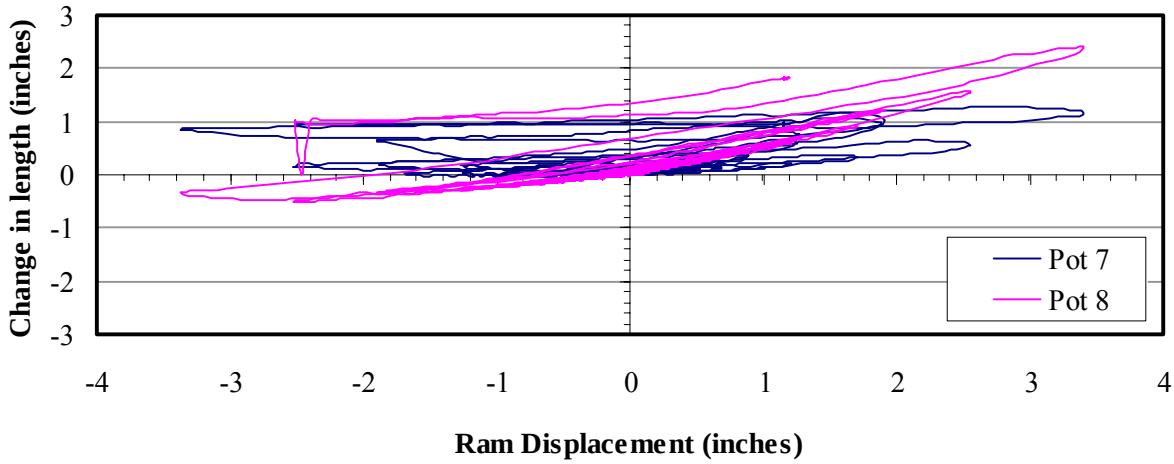

Figure A.94. Change in length of diagonal measuring Pots 7 and 8 vs. ram displacement of 8-8.5-P-2

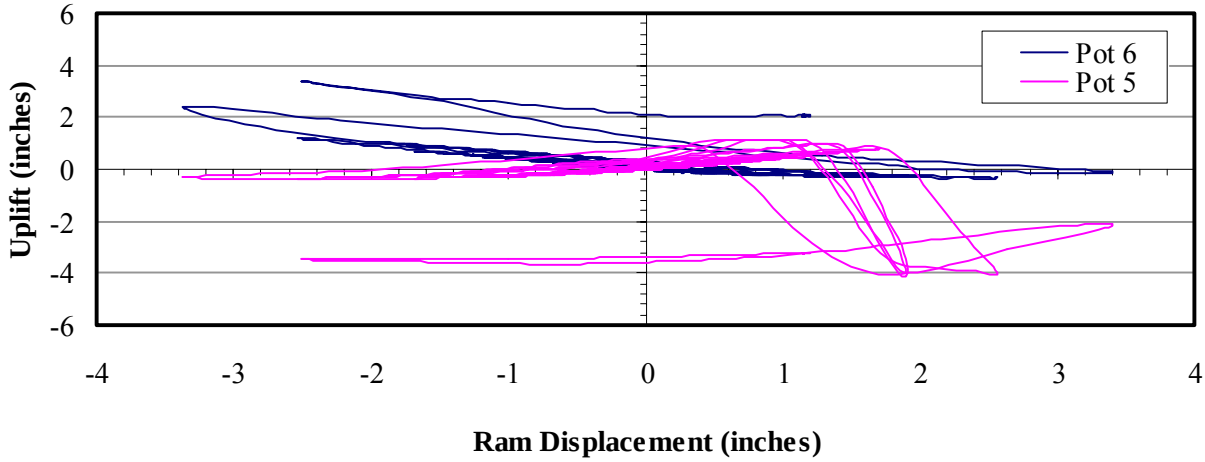

Figure A.95. Uplift displacement vs. ram displacement of 8-8.5-P-2

Table A.77. Performance Parameters of 8-8.5-P-3

Specimen	8-8.5-P-3	
Peak load, F_{peak}	Kips	2.862
	KN	12.729
Drift at peak load, Δ_{peak}	in.	1.579
	mm	40.11
Yield load, F_{yield}	Kips	2.546
	KN	11.326
Drift at yield load, Δ_{yield}	in.	0.514
	mm	13.06
Proportional limit, $0.4F_{peak}$	Kips	1.145
	KN	5.092
Drift at prop. limit, $\Delta@0.4F_{peak}$	in.	0.231
	mm	5.87
Failure load or $0.8F_{peak}$	Kips	2.289
	KN	10.183
Drift at failure, $\Delta_{failure}$	in.	2.107
	mm	53.53
Elastic stiffness, K_e $@0.4F_{peak}$	Kip/in.	5.021
	KN/mm	0.879
Work until failure	Kip·ft.	4.118
	KN·m	5.583
Ductility factor, μ	4.12	

Observations and failure modes:

- Mode of failure was sheathing nail tear through under the end stud in tension along the edge of the panel in the 2 x 12. Sheathing nails in bottom plate pulled heads through the panel. This led to significant amounts of uplift displacement between end stud in tension and bottom plate.
- Sheathing nails removed from bottom plate and 2 x 12 displayed significant bending deformation.
- Sheathing nails removed from any other location experienced virtually no bending deformation.
- Bottom plate remained attached to 2 x 12 and the rest of wall separated from bottom plate as wall was tested to complete failure.

Table A.78. EEEP Parameters of 8-8.5-P-3

EEEP Parameters	units	negative	positive
F_{yield}	Kips	-2.493	2.600
	KN	-11.089	11.563
Δ_{yield}	In.	-0.448	0.580
	mm	-11.38	14.74
$\Delta_{failure}$	In.	-1.934	2.281
	mm	-49.12	57.94

Table A.79. Displacement components of 8-8.5-P-3

	inches	mm	% of Total
Total Displacement	1.6	40.6	
Shear Deformation	0.6	15.2	37.5
Rigid Body Motion	1.0	25.4	62.5
Bending and Slip	0.0	0.0	0.0

Table A.80. Data of each Primary cycle of 8-8.5-P-3

Primary	average displacement		average load		work per cycle		cyclic stiffness		Damping
cycle #	in.	mm	Kips	KN	Kip·ft.	KN·m	Kip/in.	KN/mm	Ratio
1	0.085	2.156	0.513	2.280	0.002	0.003	6.019	1.054	0.091
2	0.126	3.205	0.741	3.295	0.005	0.006	5.860	1.026	0.096
3	0.167	4.241	0.936	4.164	0.009	0.012	5.610	0.982	0.105
4	0.331	8.410	1.465	6.516	0.037	0.051	4.423	0.775	0.148
5	0.493	12.520	1.853	8.243	0.078	0.105	3.760	0.658	0.163
6	0.658	16.713	2.140	9.519	0.121	0.165	3.253	0.570	0.165
7	1.112	28.242	2.687	11.952	0.322	0.437	2.417	0.423	0.206
8	1.579	40.110	2.862	12.729	0.494	0.670	1.812	0.317	0.209
9	2.079	52.802	2.628	11.691	0.780	1.058	1.273	0.223	0.272
10	2.221	56.421	1.096	4.877	0.640	0.868	0.492	0.086	0.500

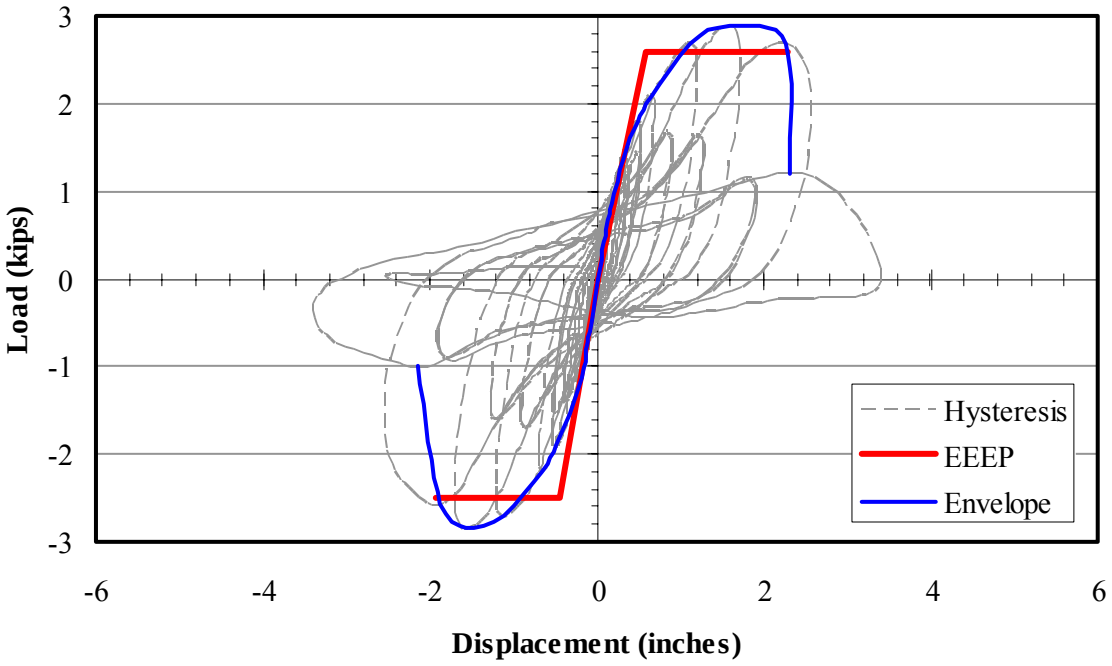

Figure A.96. Load vs. displacement, envelope and EEEP curves of 8-8.5-P-3

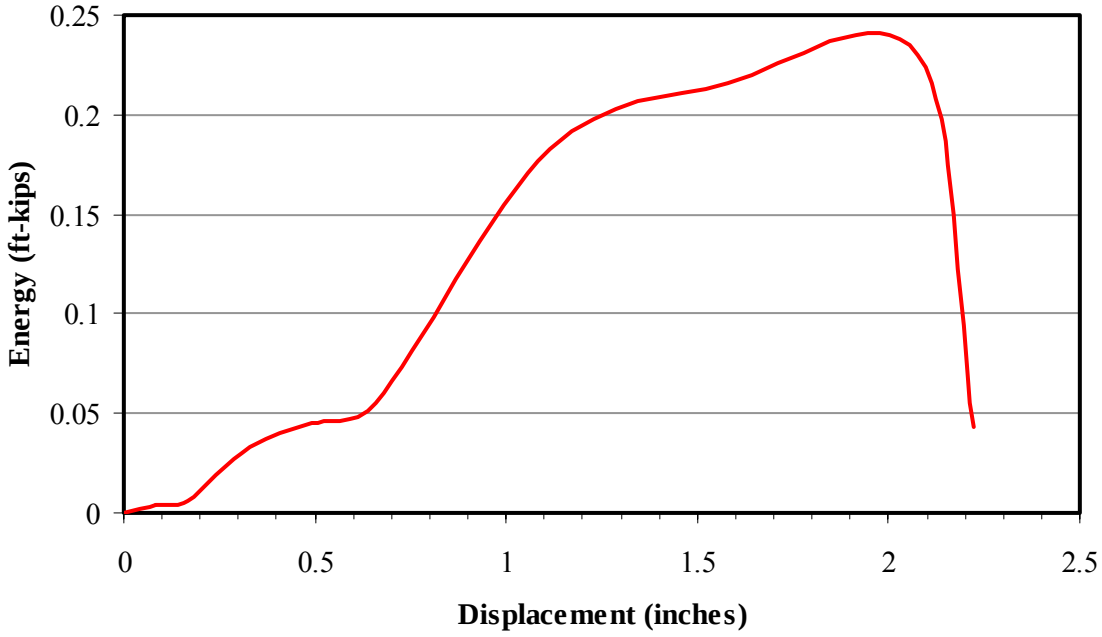

Figure A.97. Hysteretic energy dissipated per cycle vs. displacement of 8-8.5-P-3

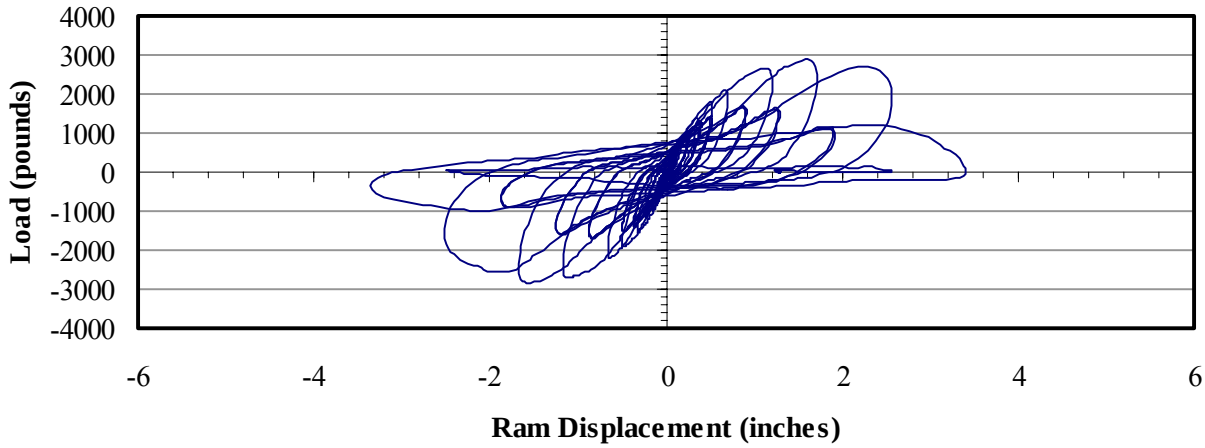

Figure A.98. Load vs. displacement of 8-8.5-P-3

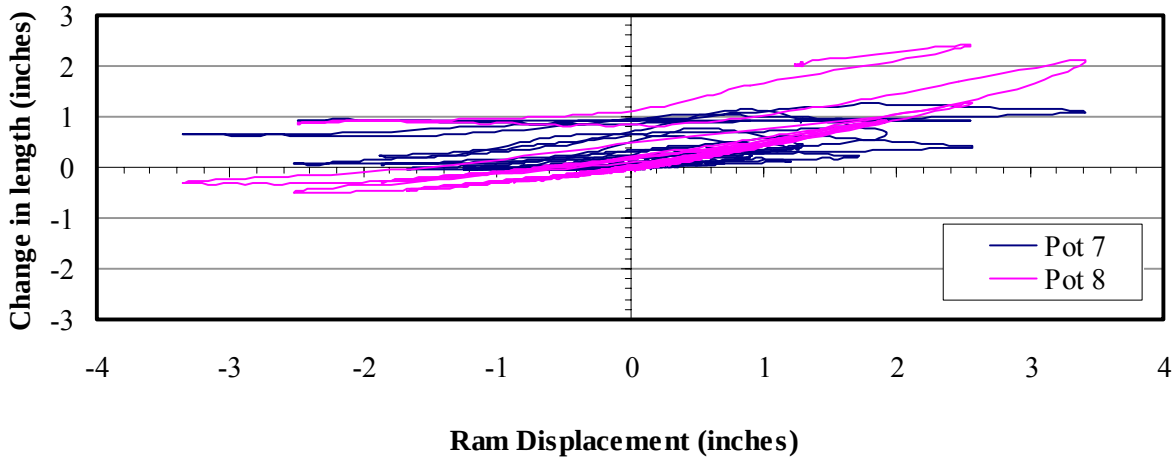

Figure A.99. Change in length of diagonal measuring Pots 7 and 8 vs. ram displacement of 8-8.5-P-3

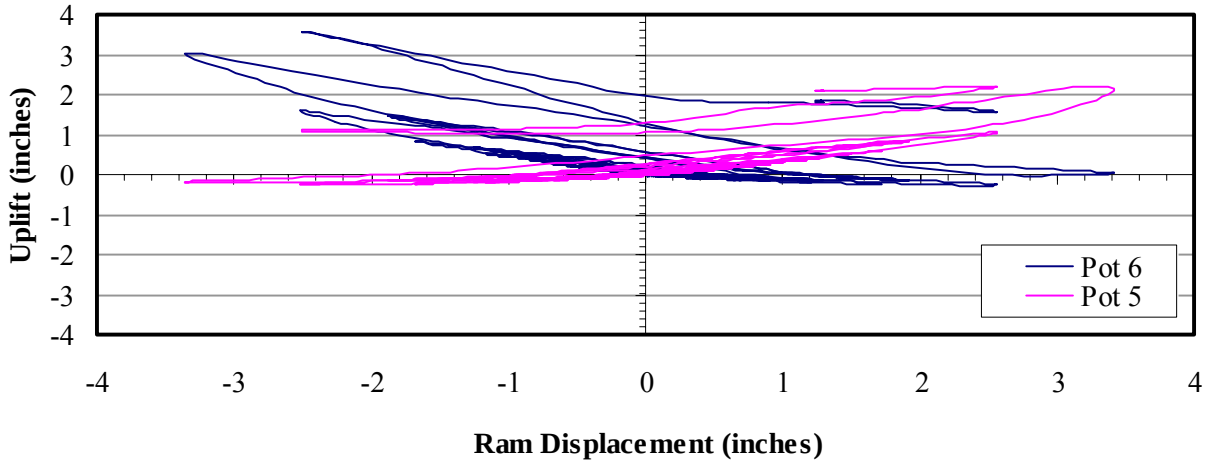

Figure A.100. Uplift displacement vs. ram displacement of 8-8.5-P-3

Table A.81. Performance Parameters of 9-8-E-1

Specimen	9-8-E-1	
Peak load, F_{peak}	Kips	4.413
	KN	19.628
Drift at peak load, Δ_{peak}	in.	3.355
	mm	85.22
Yield load, F_{yield}	Kips	3.997
	KN	17.780
Drift at yield load, Δ_{yield}	in.	0.707
	mm	17.95
Proportional limit, $0.4F_{peak}$	Kips	1.765
	KN	7.851
Drift at prop. limit, $\Delta@0.4F_{peak}$	in.	0.313
	mm	7.94
Failure load or $0.8F_{peak}$	Kips	4.369
	KN	19.431
Drift at failure, $\Delta_{failure}$	in.	3.996
	mm	101.49
Elastic stiffness, K_e $@0.4F_{peak}$	Kip/in.	5.669
	KN/mm	0.993
Work until failure	Kip·ft.	7.167
	KN·m	9.716
Ductility factor, μ	5.66	

Observations and failure modes:

- Significant sheathing nail tear through along blocking and common center stud in 4 x 8 ft panels. Sheathing nails in end stud and bottom plates experienced a combination of pulled heads through panel and withdrawal in 4 x 8 ft panels.
- Sheathing nails along blocking of 4 x 1 ft panels experienced minor tear through and pulled heads. Sheathing nails in top plate of 4 x 1 ft panels did not experience any significant damage.
- All sheathing nails removed from perimeter of 4 x 8 ft panels displayed significant bending deformation. Sheathing nails removed from perimeter of 4 x 1 ft panels experienced minor bending deformation.
- Minor separation of top plate and studs

Table A.82. EEEP Parameters of 9-8-E-1

EEEP Parameters	units	negative	positive
F_{yield}	Kips	-3.993	4.002
	KN	-17.759	17.801
Δ_{yield}	in.	-0.742	0.672
	mm	-18.84	17.07
$\Delta_{failure}$	in.	-4.105	3.887
	mm	-104.26	98.73

Table A.83. Displacement components of 9-8-E-1

	inches	mm	% of Total
Total Displacement	4.1	104.1	
Shear Deformation	3.6	91.4	87.8
Rigid Body Motion	0.5	12.7	12.2
Bending and Slip	0.0	0.0	0.0

Table A.84. Data of each Primary cycle of 9-8-E-1

Primary	average displacement		average load		work per cycle		cyclic stiffness		Damping
cycle #	in.	mm	Kips	KN	Kip·ft.	KN·m	Kip/in.	KN/mm	Ratio
1	0.155	3.950	1.120	4.982	0.012	0.016	7.205	1.262	0.131
2	0.234	5.932	1.479	6.577	0.021	0.028	6.330	1.109	0.115
3	0.310	7.879	1.765	7.853	0.035	0.048	5.691	0.997	0.123
4	0.543	13.800	2.610	11.609	0.132	0.178	4.815	0.843	0.177
5	0.805	20.455	3.111	13.836	0.233	0.316	3.867	0.677	0.178
6	1.069	27.142	3.370	14.989	0.337	0.457	3.156	0.553	0.179
7	1.880	47.761	4.127	18.356	0.890	1.207	2.198	0.385	0.219
8	2.667	67.739	4.317	19.204	1.214	1.646	1.620	0.284	0.201
9	3.996	101.493	4.369	19.431	1.920	2.604	1.093	0.191	0.210

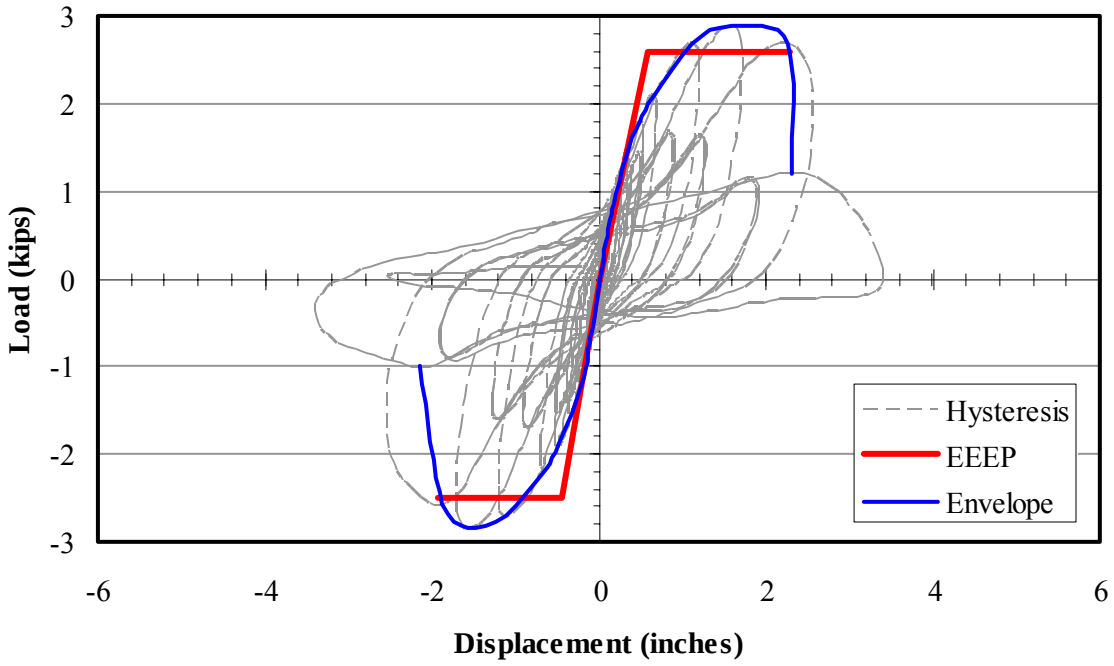

Figure A.101. Load vs. displacement, envelope and EEEP curves of 9-8-E-1

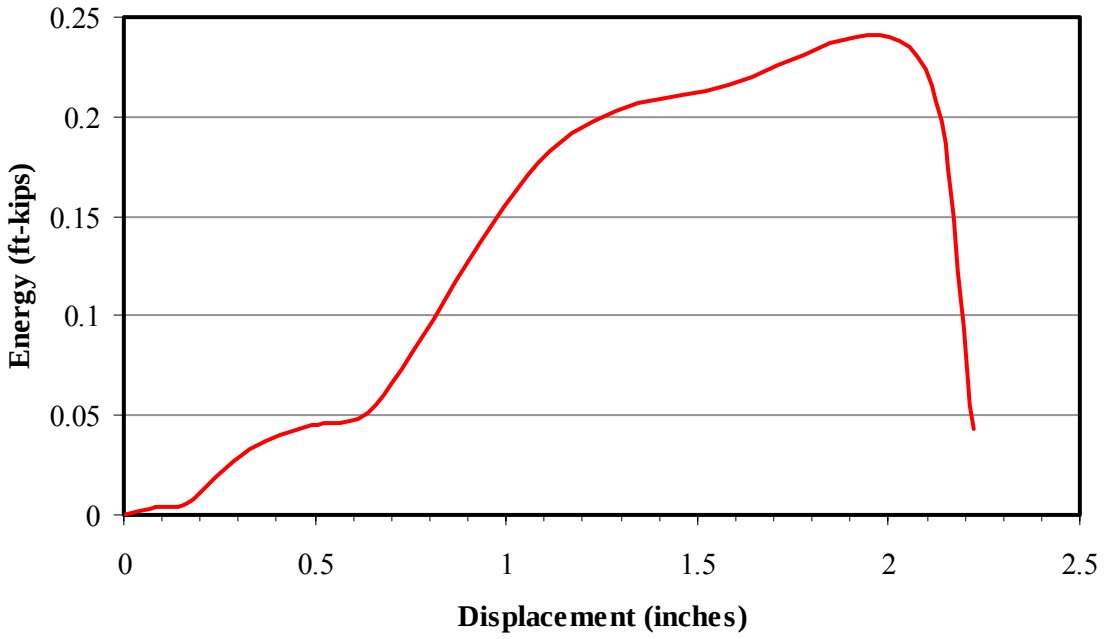

Figure A.102. Hysteretic energy dissipated per cycle vs. displacement of 9-8-E-1

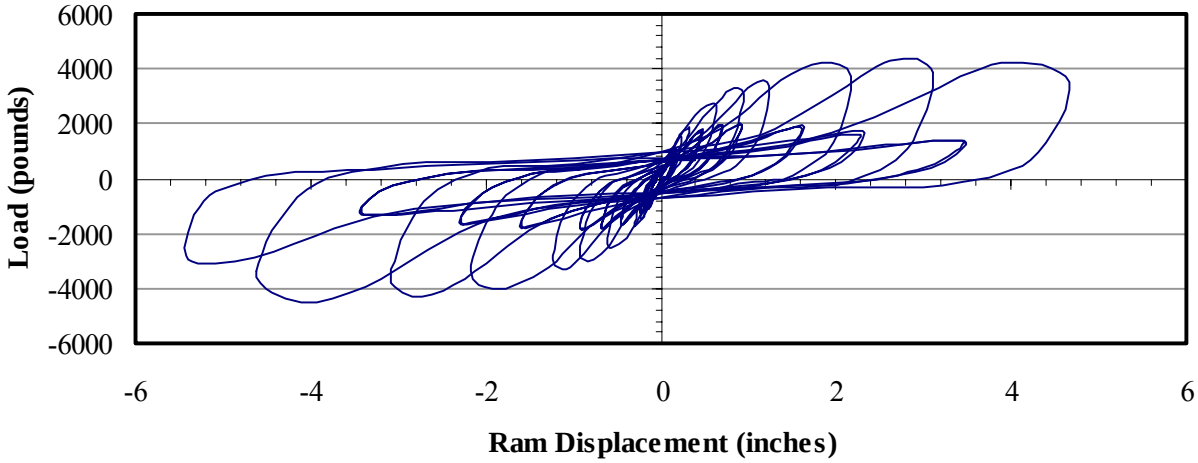

Figure A.103. Load vs. displacement of 9-8-E-1

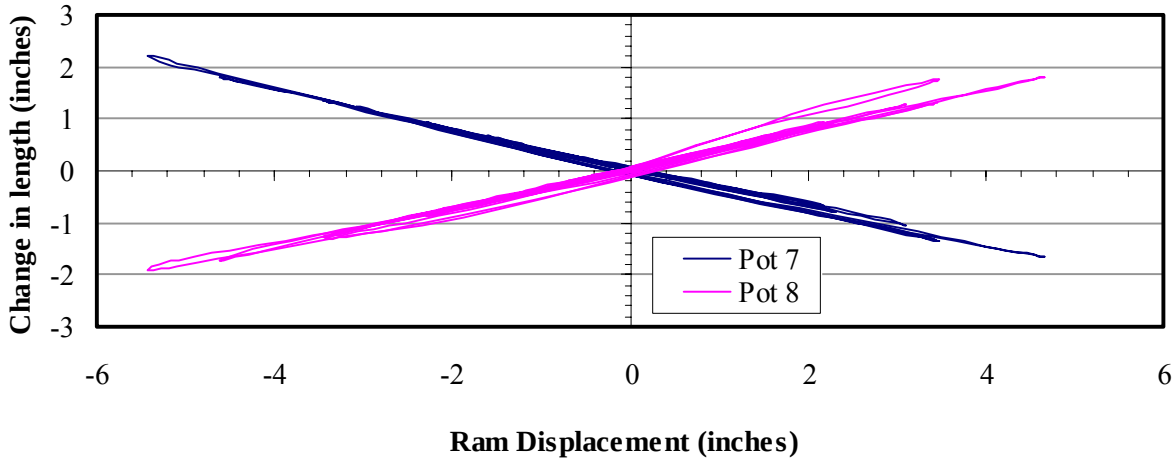

Figure A.104. Change in length of diagonal measuring Pots 7 and 8 vs. ram displacement of 9-8-E-1

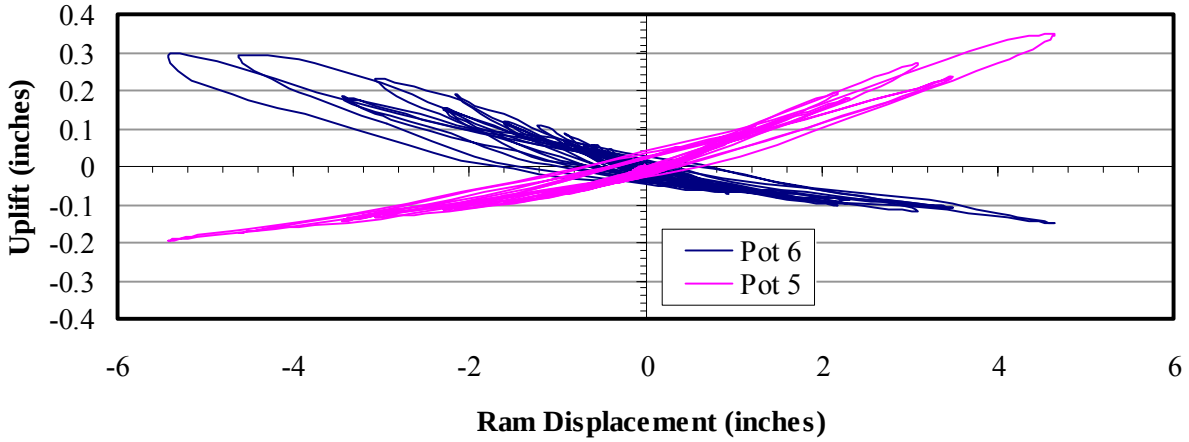

Figure A.105. Uplift displacement vs. ram displacement of 9-8-E-1

Table A.85. Performance Parameters of 9-8-E-2

Specimen	9-8-E-2	
Peak load, F_{peak}	Kips	4.020
	KN	17.881
Drift at peak load, Δ_{peak}	in.	2.743
	mm	69.67
Yield load, F_{yield}	Kips	3.601
	KN	16.017
Drift at yield load, Δ_{yield}	in.	0.593
	mm	15.05
Proportional limit, $0.4F_{peak}$	Kips	1.608
	KN	7.152
Drift at prop. limit, $\Delta@0.4F_{peak}$	in.	0.265
	mm	6.72
Failure load or $0.8F_{peak}$	Kips	3.393
	KN	15.091
Drift at failure, $\Delta_{failure}$	in.	4.692
	mm	119.17
Elastic stiffness, K_e $@0.4F_{peak}$	Kip/in.	6.163
	KN/mm	1.079
Work until failure	Kip·ft.	9.904
	KN·m	13.427
Ductility factor, μ	8.02	

Observations and failure modes:

- Significant sheathing nail tear through along blocking, common center stud and corners of 4 x 8 ft panels.
- Sheathing nails along blocking of 4 x 1 ft panels experienced minor tear through and pulled heads. Sheathing nails in top plate of 4 x 1 ft panels did not experience any significant damage.
- All sheathing nails removed from perimeter of 4 x 8 ft panels displayed significant bending deformation. Sheathing nails removed from perimeter of 4 x 1 ft panels experienced minor bending deformation.
- Minor separation of top plate and studs

Table A.86. EEEP Parameters of 9-8-E-2

EEEP Parameters	units	negative	positive
F_{yield}	Kips	-3.706	3.496
	KN	-16.485	15.549
Δ_{yield}	in.	-0.672	0.513
	mm	-17.07	13.04
$\Delta_{failure}$	in.	-4.866	4.518
	mm	-123.59	114.75

Table A.87. Displacement components of 9-8-E-2

	inches	mm	% of Total
Total Displacement	3.2	81.3	
Shear Deformation	2.7	68.6	84.4
Rigid Body Motion	0.5	12.7	15.6
Bending and Slip	0.0	0.0	0.0

Table A.88. Data of each Primary cycle of 9-8-E-2

Primary	average displacement		average load		work per cycle		cyclic stiffness		Damping
cycle #	in.	mm	Kips	KN	Kip·ft.	KN·m	Kip/in.	KN/mm	Ratio
1	0.083	2.115	0.724	3.220	0.004	0.006	8.644	1.514	0.134
2	0.124	3.155	1.020	4.537	0.009	0.012	8.195	1.435	0.134
3	0.165	4.183	1.244	5.535	0.015	0.020	7.547	1.322	0.137
4	0.329	8.348	1.855	8.250	0.052	0.070	5.647	0.989	0.163
5	0.486	12.338	2.273	10.109	0.093	0.126	4.678	0.819	0.161
6	0.653	16.591	2.549	11.338	0.135	0.183	3.903	0.683	0.155
7	1.106	28.085	3.162	14.063	0.359	0.487	2.860	0.501	0.196
8	1.570	39.886	3.514	15.631	0.535	0.726	2.238	0.392	0.185
9	2.312	58.724	3.942	17.534	0.964	1.307	1.705	0.299	0.202
10	3.126	79.412	3.993	17.762	1.220	1.655	1.277	0.224	0.187
11	3.973	100.914	3.783	16.829	1.400	1.898	0.953	0.167	0.178
12	4.811	122.207	3.294	14.653	1.438	1.949	0.684	0.120	0.173

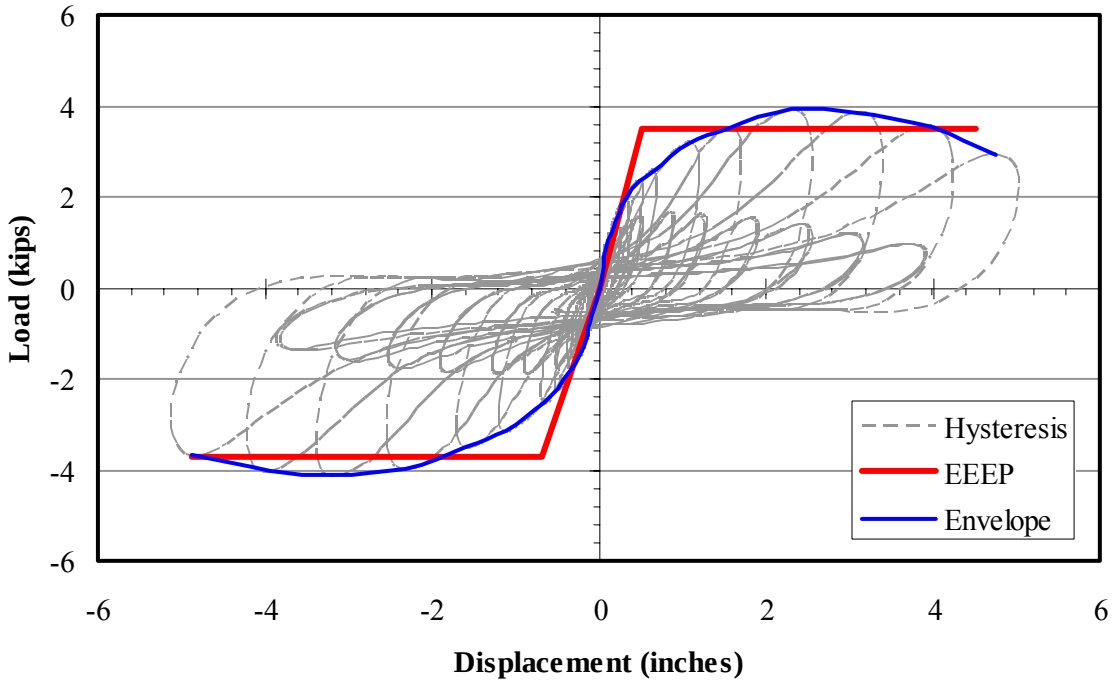

Figure A.106. Load vs. displacement, envelope and EEEP curves of 9-8-E-2

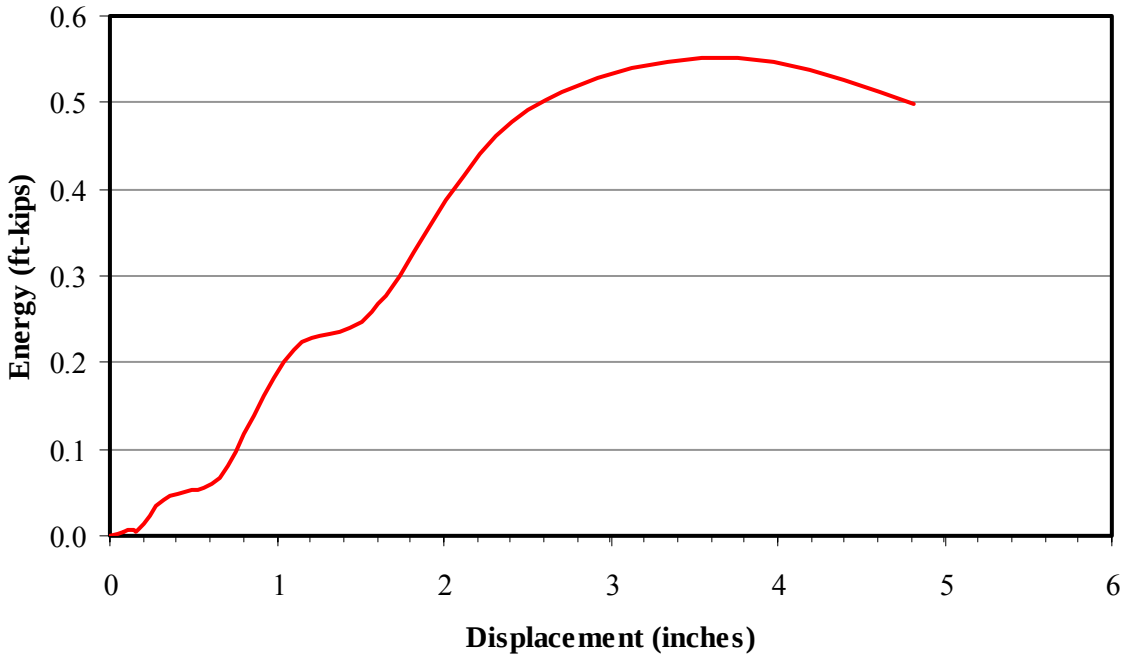

Figure A.107. Hysteretic energy dissipated per cycle vs. displacement of 9-8-E-2

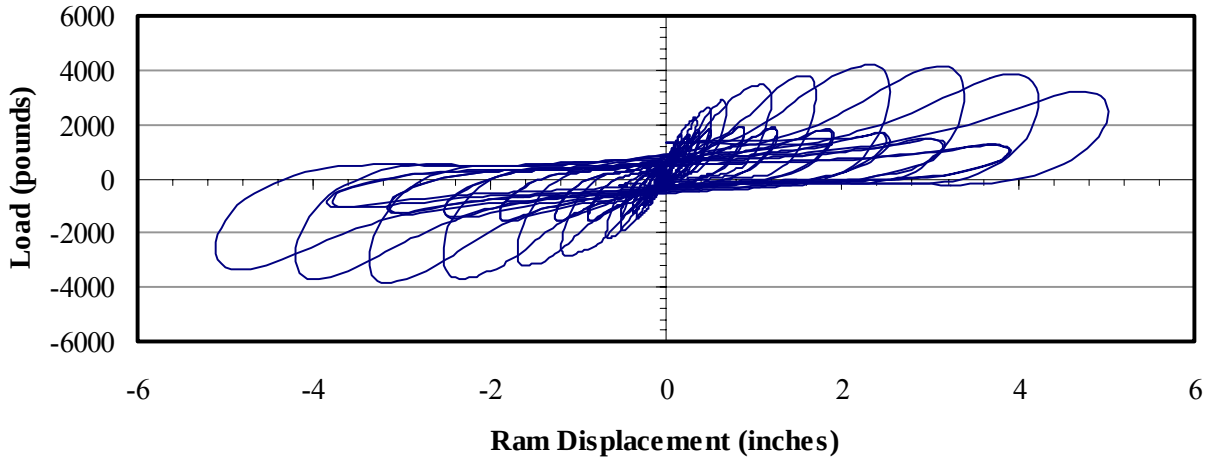

Figure A.108. Load vs. displacement of 9-8-E-2

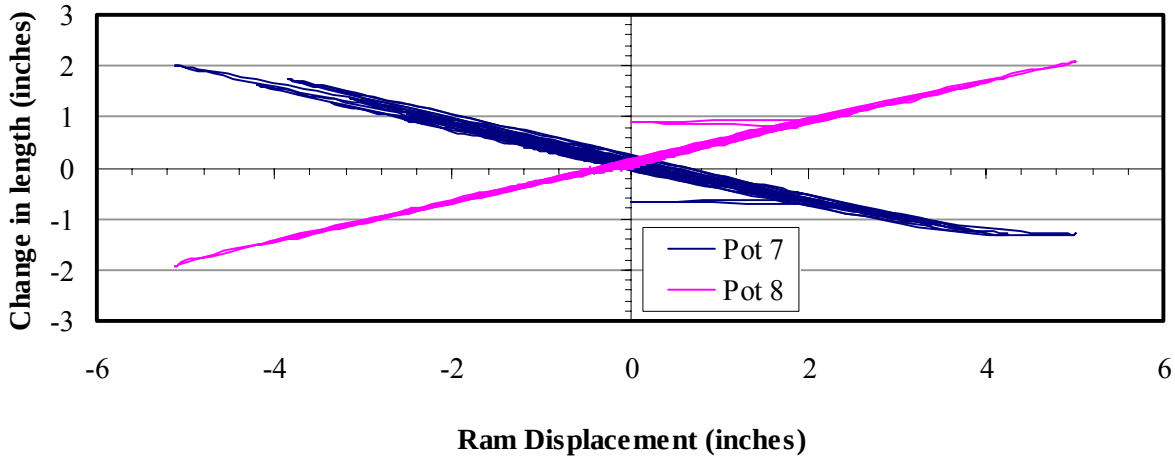

Figure A.109. Change in length of diagonal measuring Pots 7 and 8 vs. ram displacement of 9-8-E-2

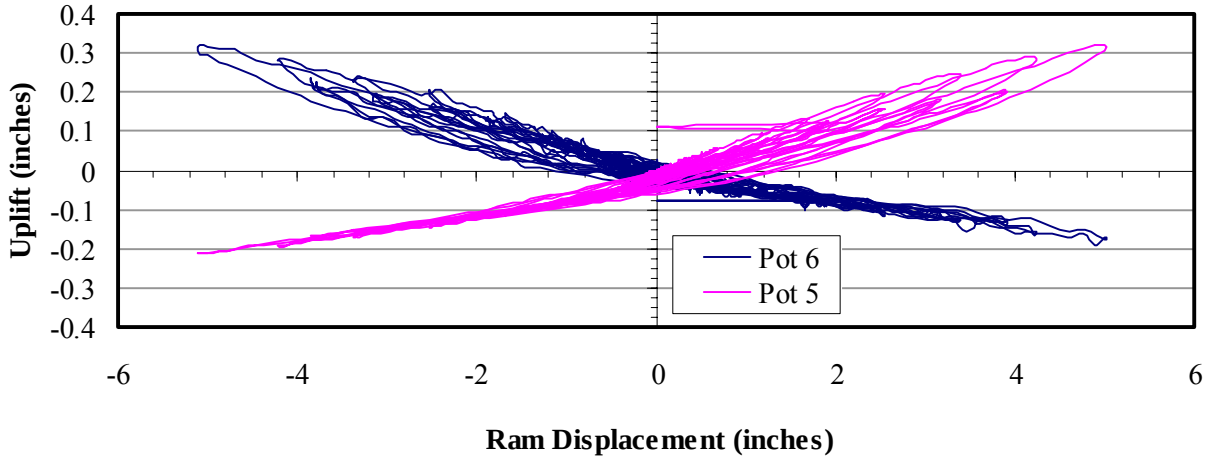

Figure A.110. Uplift displacement vs. ram displacement of 9-8-E-2

Table A.89. Performance Parameters of 9-8-E-3

Specimen	9-8-E-3	
Peak load, F_{peak}	Kips	4.563
	KN	20.297
Drift at peak load, Δ_{peak}	in.	3.164
	mm	80.36
Yield load, F_{yield}	Kips	3.982
	KN	17.710
Drift at yield load, Δ_{yield}	in.	0.650
	mm	16.50
Proportional limit, $0.4F_{peak}$	Kips	1.825
	KN	8.119
Drift at prop. limit, $\Delta@0.4F_{peak}$	in.	0.298
	mm	7.56
Failure load or $0.8F_{peak}$	Kips	3.825
	KN	17.012
Drift at failure, $\Delta_{failure}$	in.	4.759
	mm	120.89
Elastic stiffness, K_e $@0.4F_{peak}$	Kip/in.	6.149
	KN/mm	1.077
Work until failure	Kip·ft.	10.866
	KN·m	14.731
Ductility factor, μ	7.34	

Observations and failure modes:

- Significant sheathing nail tear through along blocking, common center stud and corners of 4 x 8 ft panels.
- Sheathing nails along blocking of 4 x 1 ft panels experienced minor tear through and pulled heads. Sheathing nails in top plate of 4 x 1 ft panels did not experience any significant damage.
- All sheathing nails removed from perimeter of 4 x 8 ft panels displayed significant bending deformation. Sheathing nails removed from perimeter of 4 x 1 ft panels experienced minor bending deformation.
- Minor separation of top plate and studs

Table A.90. EEEP Parameters of 9-8-E-3

EEEP Parameters	units	negative	positive
F_{yield}	Kips	-4.082	3.882
	KN	-18.155	17.265
Δ_{yield}	in.	-0.620	0.679
	mm	-15.75	17.25
$\Delta_{failure}$	in.	-4.761	4.758
	mm	-120.92	120.86

Table A.91. Displacement components of 9-8-E-3

	inches	mm	% of Total
Total Displacement	4.1	104.1	
Shear Deformation	3.5	88.9	85.4
Rigid Body Motion	0.6	15.2	14.6
Bending and Slip	0.0	0.0	0.0

Table A.92. Data of each Primary cycle of 9-8-E-3

Primary	average displacement		average load		Work per cycle		cyclic stiffness		Damping
cycle #	in.	mm	Kips	KN	Kip·ft.	KN·m	Kip/in.	KN/mm	Ratio
1	0.084	2.142	0.713	3.173	0.003	0.005	8.524	1.493	0.110
2	0.123	3.124	1.040	4.625	0.008	0.011	8.449	1.480	0.121
3	0.162	4.125	1.273	5.660	0.014	0.019	7.832	1.371	0.133
4	0.324	8.235	1.828	8.131	0.052	0.071	5.638	0.987	0.168
5	0.485	12.311	2.191	9.746	0.094	0.128	4.518	0.791	0.169
6	0.643	16.333	2.518	11.199	0.138	0.187	3.913	0.685	0.163
7	1.116	28.340	3.313	14.735	0.375	0.508	2.969	0.520	0.194
8	1.585	40.264	3.809	16.944	0.579	0.785	2.404	0.421	0.183
9	2.380	60.444	4.379	19.476	1.037	1.406	1.840	0.322	0.190
10	3.164	80.363	4.563	20.297	1.353	1.834	1.443	0.253	0.179
11	3.943	100.153	4.330	19.258	1.543	2.092	1.098	0.192	0.173
12	4.759	120.889	3.825	17.012	1.617	2.192	0.804	0.141	0.170

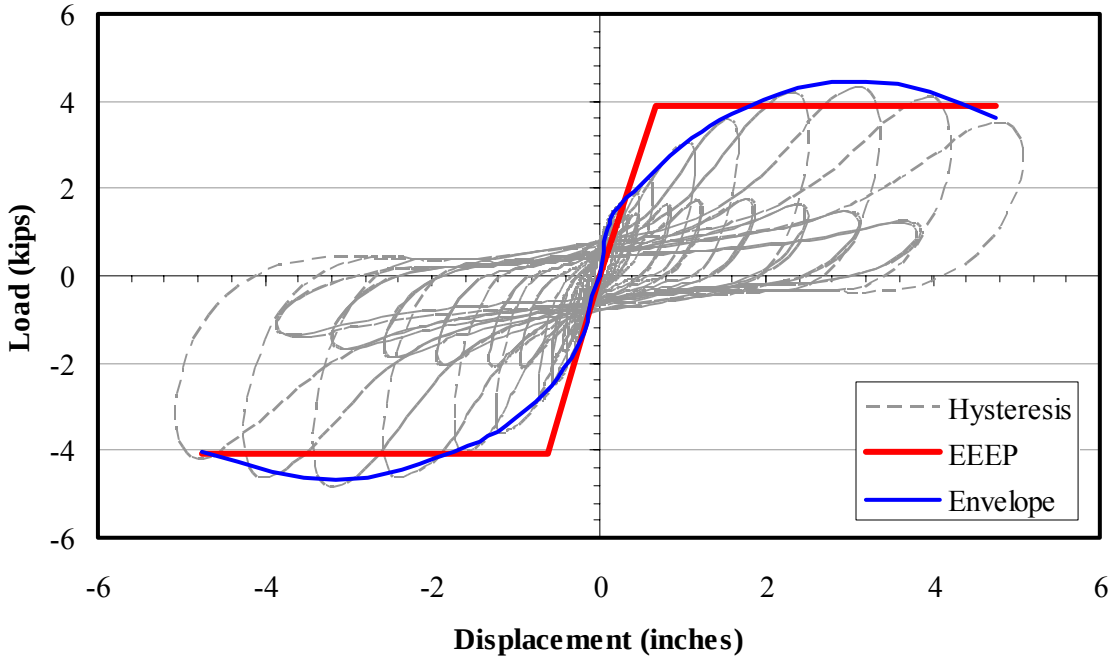

Figure A.111. Load vs. displacement, envelope and EEEP curves of 9-8-E-3

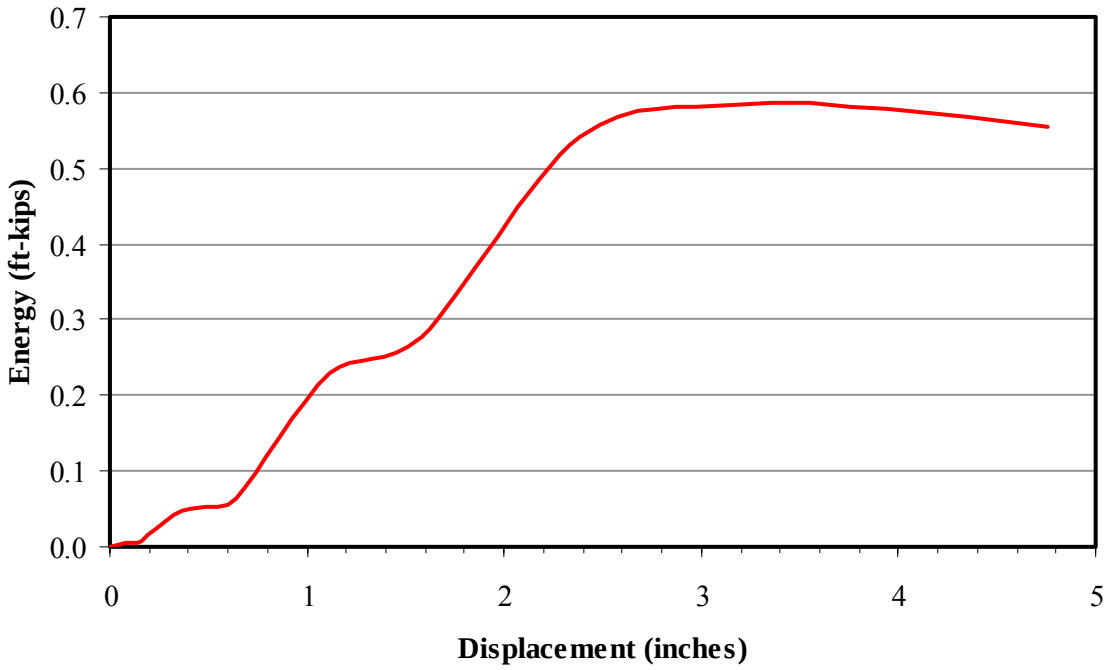

Figure A.112. Hysteretic energy dissipated per cycle vs. displacement of 9-8-E-3

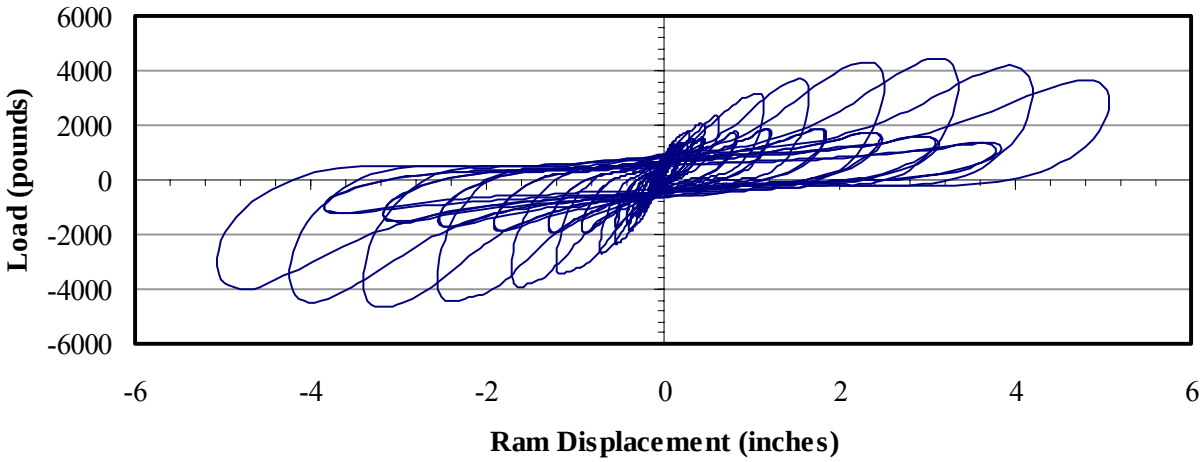

Figure A.113. Load vs. displacement of Wall 9-8-E-3

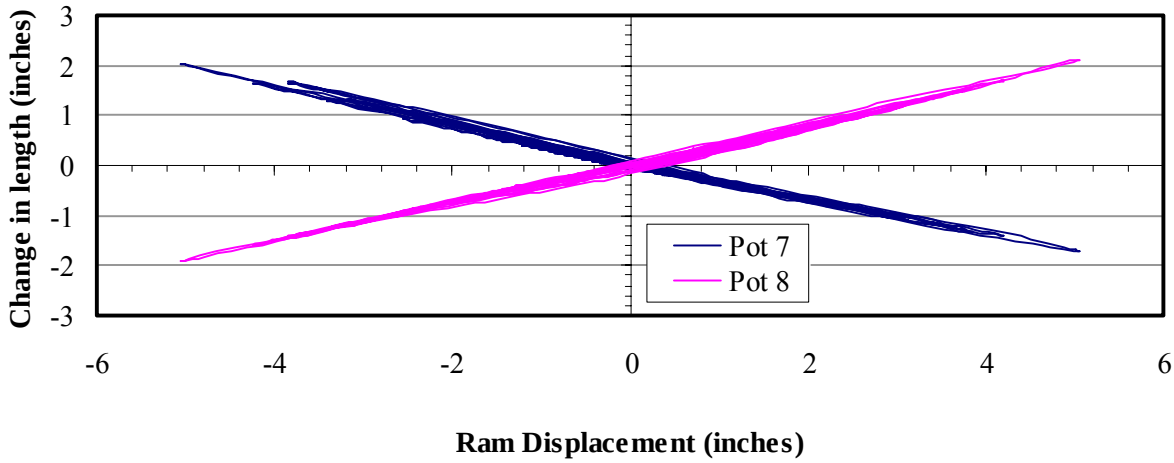

Figure A.114. Change in length of diagonal measuring Pots 7 and 8 vs. ram displacement of 9-8-E-3

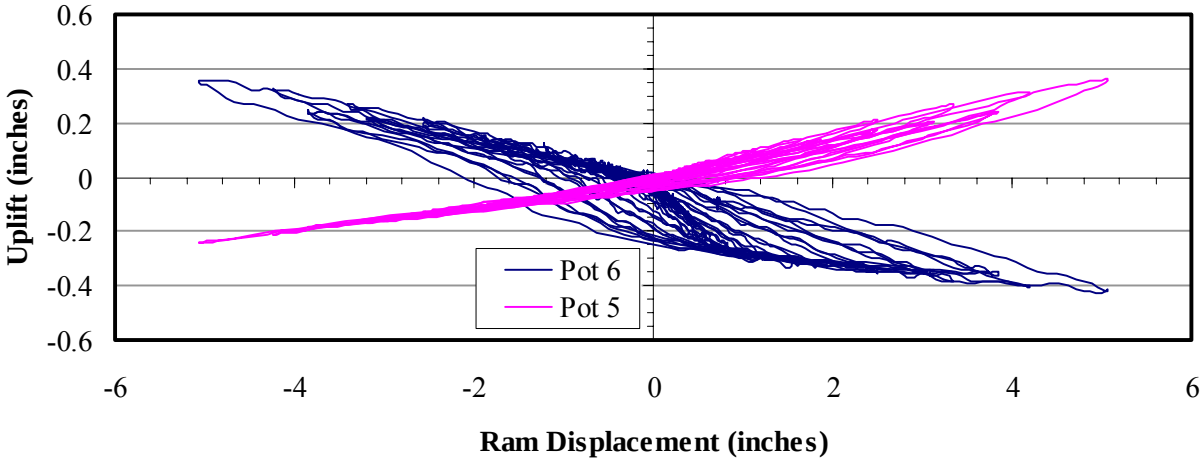

Figure A.115. Uplift displacement vs. ram displacement of 9-8-E-3

Table A.93. Performance Parameters of 9-9-E-1

Specimen	9-9-E-1	
Peak load, F_{peak}	Kips	4.521
	KN	20.110
Drift at peak load, Δ_{peak}	in.	2.333
	mm	59.27
Yield load, F_{yield}	Kips	4.032
	KN	17.933
Drift at yield load, Δ_{yield}	in.	0.420
	mm	10.67
Proportional limit, $0.4F_{peak}$	Kips	1.808
	KN	8.044
Drift at prop. limit, $\Delta@0.4F_{peak}$	in.	0.188
	mm	4.79
Failure load or $0.8F_{peak}$	Kips	3.617
	KN	16.088
Drift at failure, $\Delta_{failure}$	in.	3.755
	mm	95.38
Elastic stiffness, K_e $@0.4F_{peak}$	Kip/in.	9.664
	KN/mm	1.692
Work until failure	Kip·ft.	8.810
	KN·m	11.944
Ductility factor, μ	8.97	

Observations and failure modes:

- Significant sheathing nail tear through and pulled heads near the corners of the panels and along common center stud
- Minor withdrawal (0..5 in.) was experienced by all sheathing nails except those in common center stud
- All sheathing nails removed from perimeter of panels experienced significant bending deformation
- Minor separation between top plate and studs

Table A.94. EEEP Parameters of 9-9-E-1

EEEP Parameters	units	negative	positive
F_{yield}	Kips	-4.088	3.975
	KN	-18.185	17.681
Δ_{yield}	in.	-0.459	0.382
	mm	-11.65	9.70
$\Delta_{failure}$	in.	-3.937	3.574
	mm	-99.99	90.77

Table A.95. Displacement components of 9-9-E-1

	inches	mm	% of Total
Total Displacement	2.4	61.0	
Shear Deformation	2.0	50.8	83.3
Rigid Body Motion	0.4	10.2	16.7
Bending and Slip	0.0	0.0	0.0

Table A.96. Data of each Primary cycle of 9-9-E-1

Primary	average displacement		average load		work per cycle		cyclic stiffness		Damping
cycle #	in.	mm	Kips	KN	Kip·ft.	KN·m	Kip/in.	KN/mm	Ratio
1	0.083	2.099	0.985	4.381	0.005	0.007	11.916	2.087	0.120
2	0.124	3.161	1.377	6.125	0.011	0.015	11.068	1.938	0.126
3	0.166	4.205	1.698	7.554	0.020	0.027	10.265	1.798	0.135
4	0.324	8.232	2.483	11.046	0.071	0.097	7.671	1.343	0.169
5	0.485	12.320	2.971	13.215	0.128	0.173	6.129	1.073	0.169
6	0.645	16.382	3.271	14.548	0.185	0.250	5.073	0.888	0.167
7	1.115	28.317	3.905	17.368	0.469	0.636	3.502	0.613	0.206
8	1.588	40.324	4.223	18.783	0.685	0.929	2.660	0.466	0.195
9	2.333	59.271	4.521	20.110	1.155	1.566	1.938	0.339	0.209
10	3.161	80.288	4.278	19.028	1.396	1.892	1.354	0.237	0.197
11	3.939	100.057	3.399	15.118	1.370	1.857	0.864	0.151	0.196
12	4.616	117.243	2.186	9.723	1.150	1.560	0.473	0.083	0.218

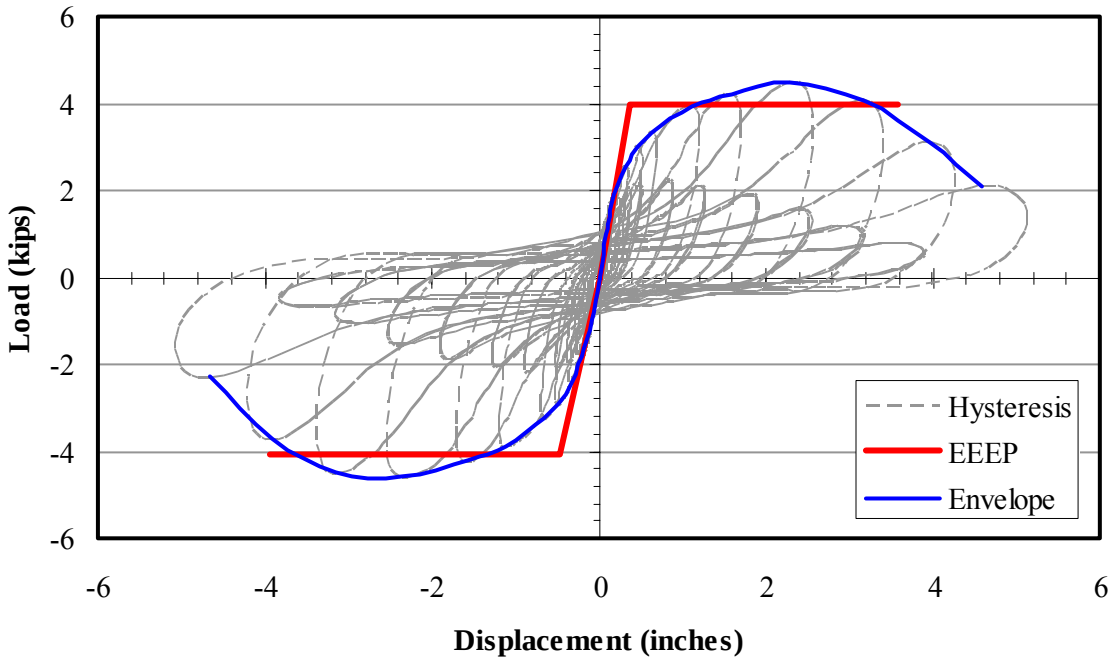

Figure A.116. Load vs. displacement, envelope and EEEP curves of 9-9-E-1

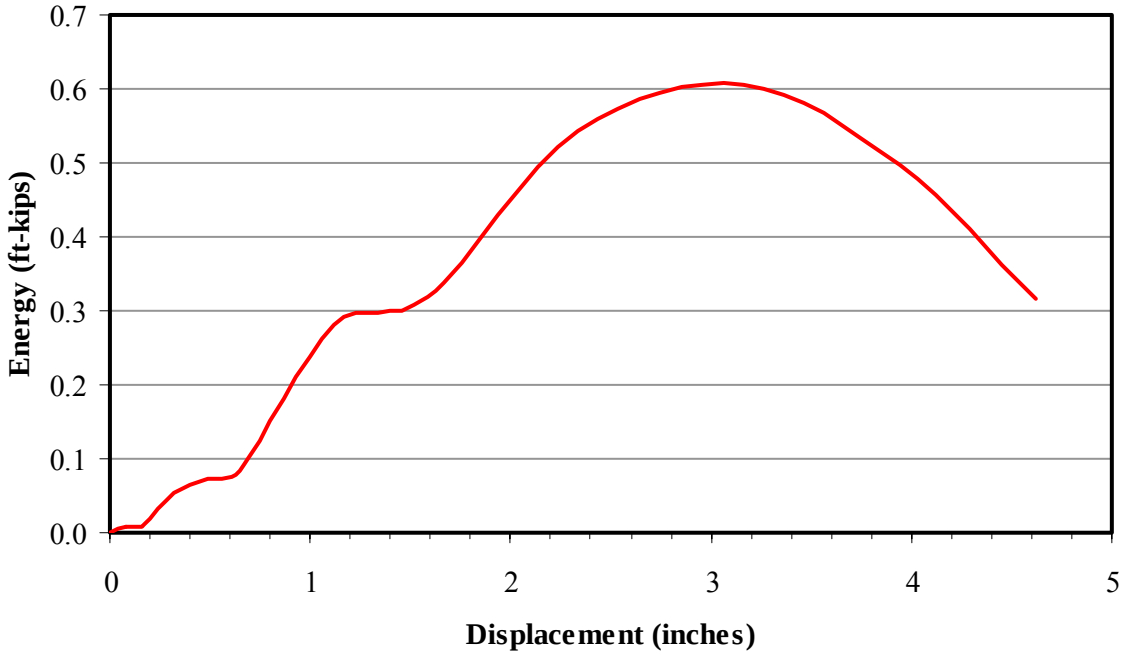

Figure A.117. Hysteretic energy dissipated per cycle vs. displacement of 9-9-E-1

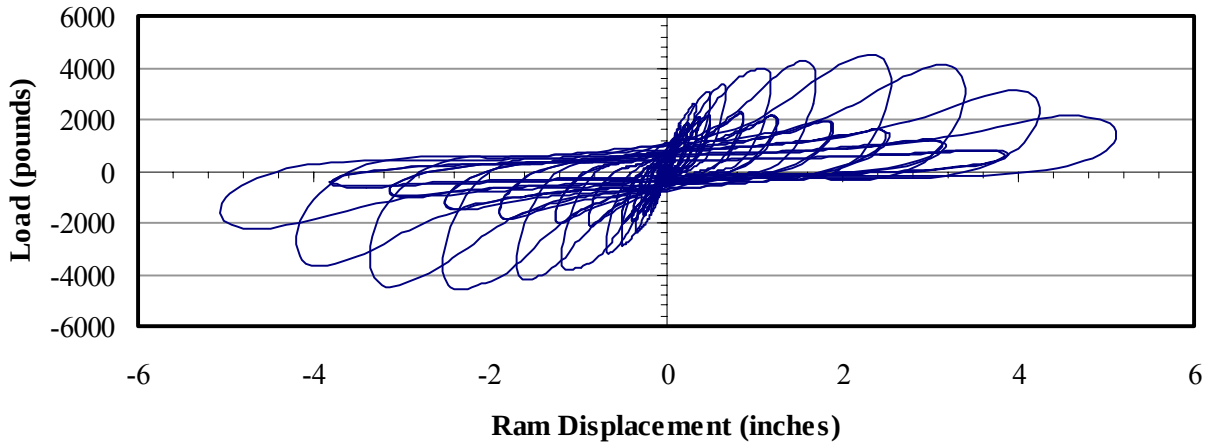

Figure A.118. Load vs. displacement of 9-9-E-1

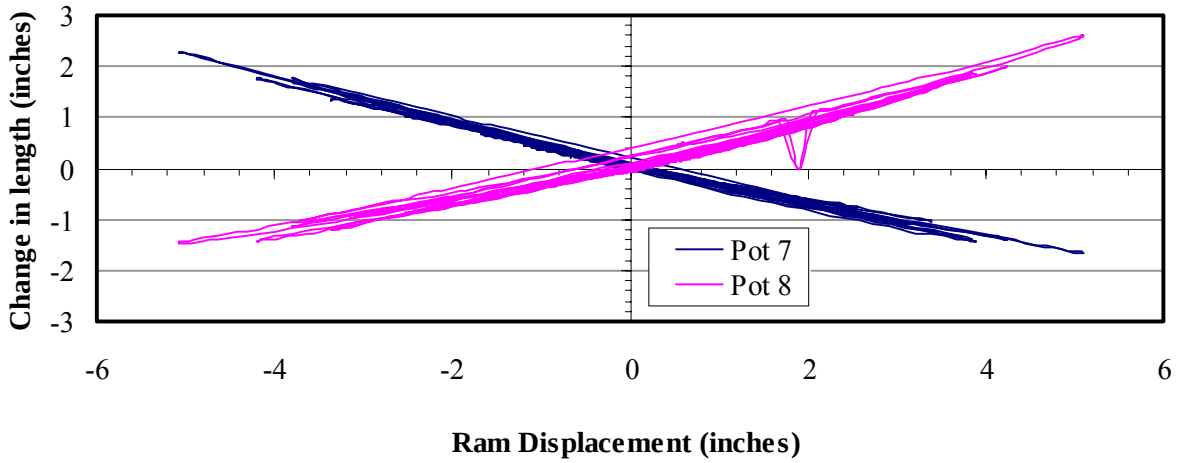

Figure A.119. Change in length of diagonal measuring Pots 7 and 8 vs. ram displacement of 9-9-E-1

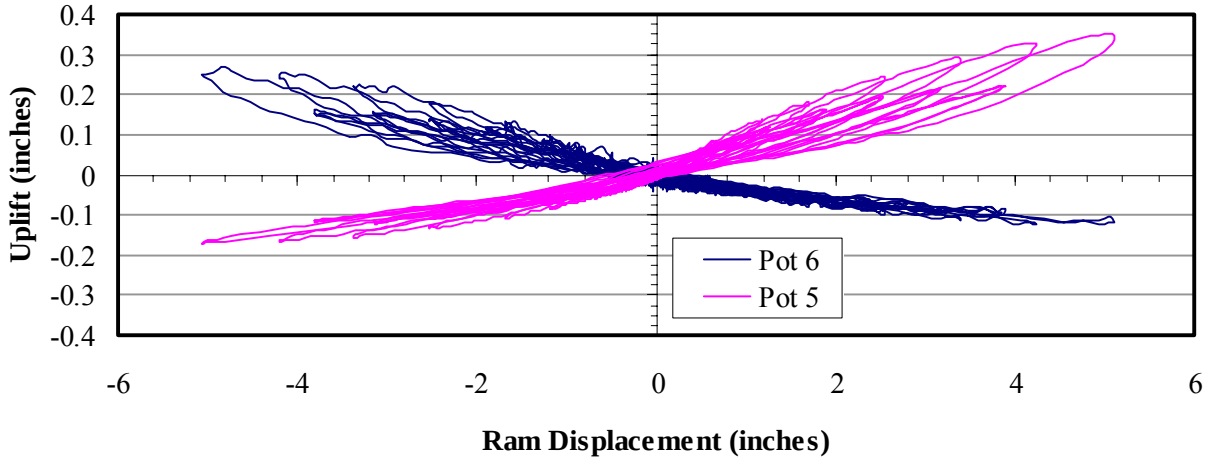

Figure A.120. Uplift displacement vs. ram displacement of 9-9-E-1

Table A.97. Performance Parameters of 9-9-E-2

Specimen	9-9-E-2	
Peak load, F_{peak}	Kips	4.425
	KN	19.683
Drift at peak load, Δ_{peak}	in.	2.372
	mm	60.25
Yield load, F_{yield}	Kips	3.949
	KN	17.565
Drift at yield load, Δ_{yield}	in.	0.441
	mm	11.21
Proportional limit, $0.4F_{peak}$	Kips	1.770
	KN	7.873
Drift at prop. limit, $\Delta@0.4F_{peak}$	in.	0.198
	mm	5.03
Failure load or $0.8F_{peak}$	Kips	3.540
	KN	15.746
Drift at failure, $\Delta_{failure}$	in.	3.833
	mm	97.36
Elastic stiffness, K_e $@0.4F_{peak}$	Kip/in.	9.920
	KN/mm	1.737
Work until failure	Kip·ft.	8.686
	KN·m	11.776
Ductility factor, μ	9.56	

Observations and failure modes:

- Significant sheathing nail tear through and pulled heads near the corners of the panels and along common center stud
- Minor withdrawal (0..5 in.) was experienced by all sheathing nails except those in common center stud
- All sheathing nails removed from perimeter of panels experienced significant bending deformation
- Minor separation between top plate and studs

Table A.98. EEEP Parameters of 9-9-E-2

EEEP Parameters	units	negative	positive
F_{yield}	Kips	-4.166	3.732
	KN	-18.530	16.601
Δ_{yield}	in.	-0.314	0.569
	mm	-7.97	14.46
$\Delta_{failure}$	in.	-3.949	3.717
	mm	-100.32	94.40

Table A.99. Displacement components of 9-9-E-2

	inches	mm	% of Total
Total Displacement	2.4	61.0	
Shear Deformation	1.9	48.3	79.2
Rigid Body Motion	0.4	10.2	16.7
Bending and Slip	0.1	2.5	4.1

Table A.100. Data of each Primary cycle of 9-9-E-2

Primary	average displacement		average load		work per cycle		cyclic stiffness		Damping
cycle #	in.	mm	Kips	KN	Kip·ft.	KN·m	Kip/in.	KN/mm	Ratio
1	0.082	2.076	0.965	4.293	0.004	0.006	11.809	2.068	0.102
2	0.122	3.103	1.335	5.939	0.010	0.014	10.921	1.912	0.119
3	0.164	4.168	1.613	7.174	0.018	0.025	9.836	1.722	0.132
4	0.324	8.235	2.353	10.466	0.067	0.090	7.237	1.267	0.166
5	0.476	12.083	2.814	12.515	0.120	0.162	5.916	1.036	0.171
6	0.642	16.312	3.105	13.812	0.177	0.239	4.830	0.846	0.169
7	1.111	28.224	3.766	16.751	0.458	0.620	3.389	0.593	0.209
8	1.584	40.232	4.101	18.240	0.673	0.913	2.589	0.453	0.198
9	2.372	60.246	4.425	19.683	1.121	1.519	1.866	0.327	0.204
10	3.154	80.101	4.292	19.089	1.382	1.873	1.362	0.238	0.195
11	3.932	99.880	3.487	15.509	1.379	1.869	0.888	0.155	0.192
12	4.531	115.081	2.329	10.361	1.123	1.522	0.514	0.090	0.203

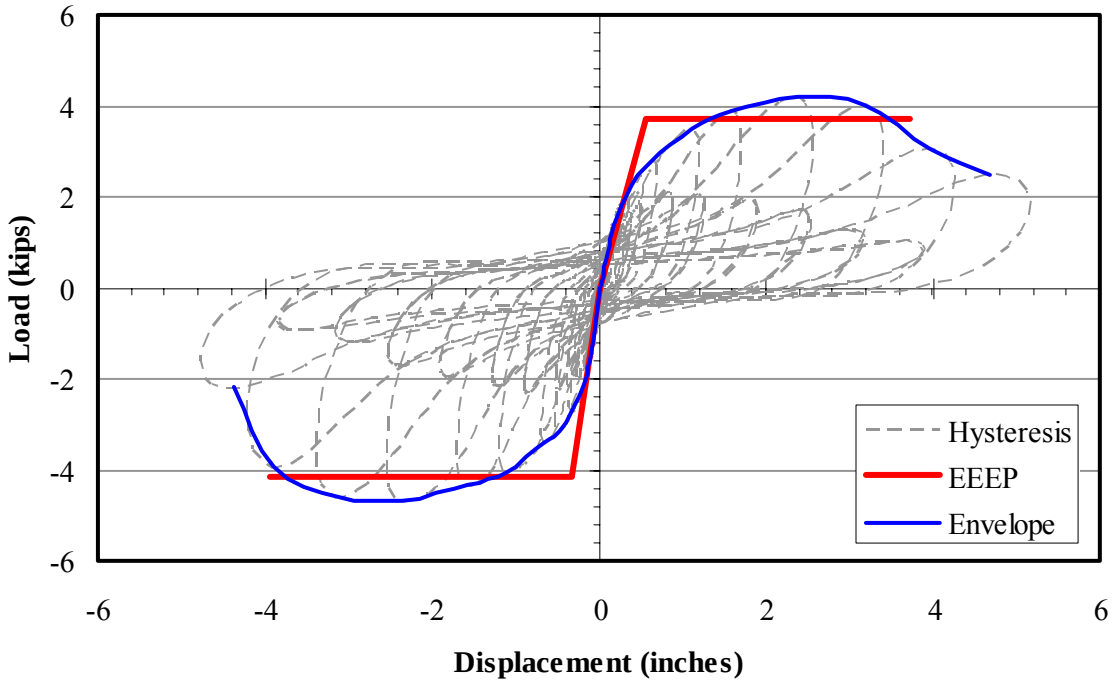

Figure A.121. Load vs. displacement, envelope and EEEP curves of 9-9-E-2

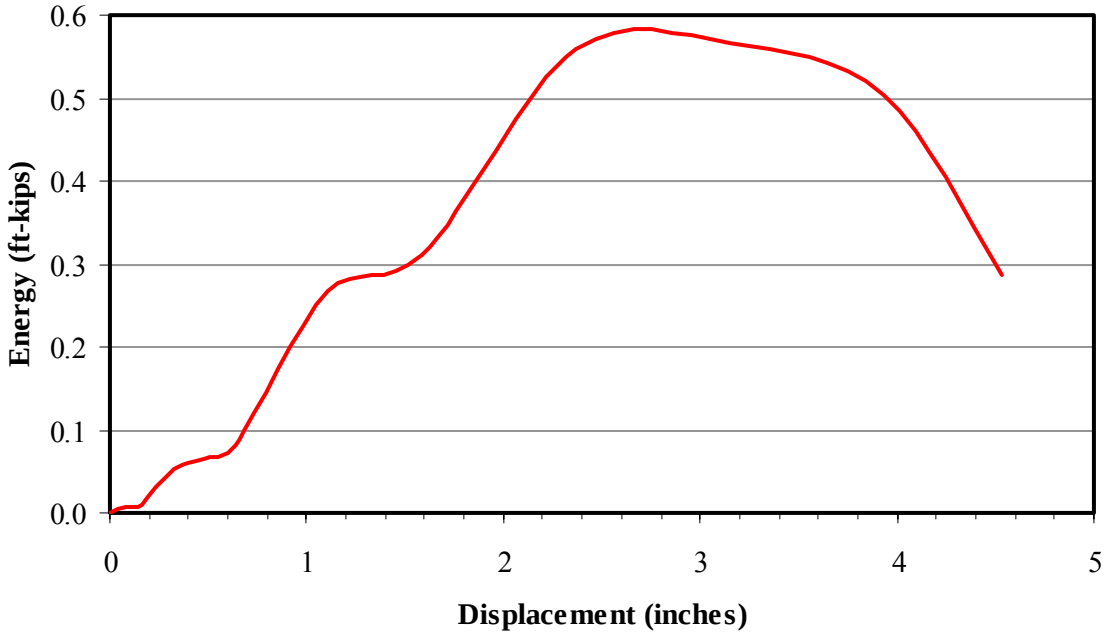

Figure A.122. Hysteretic energy dissipated per cycle vs. displacement of 9-9-E-2

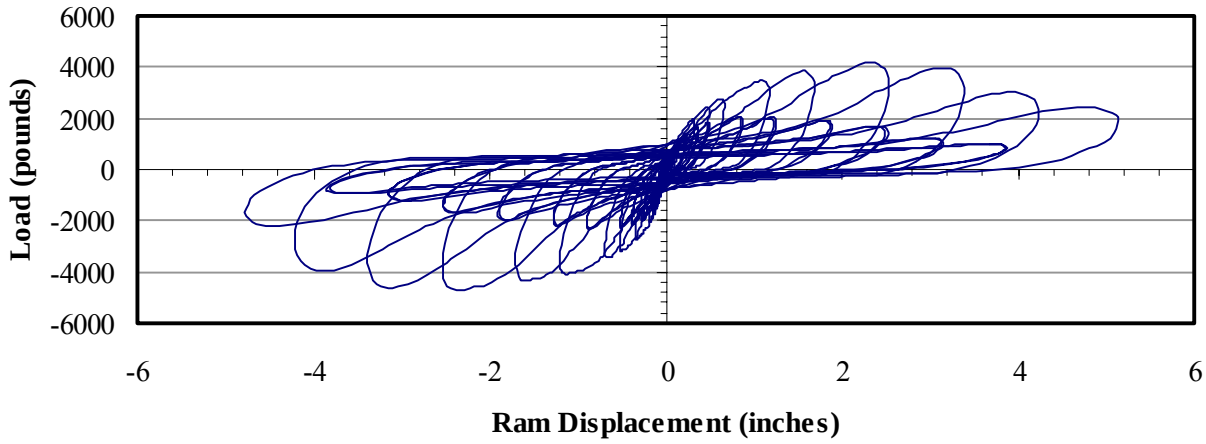

Figure A.123. Load vs. displacement of 9-9-E-2

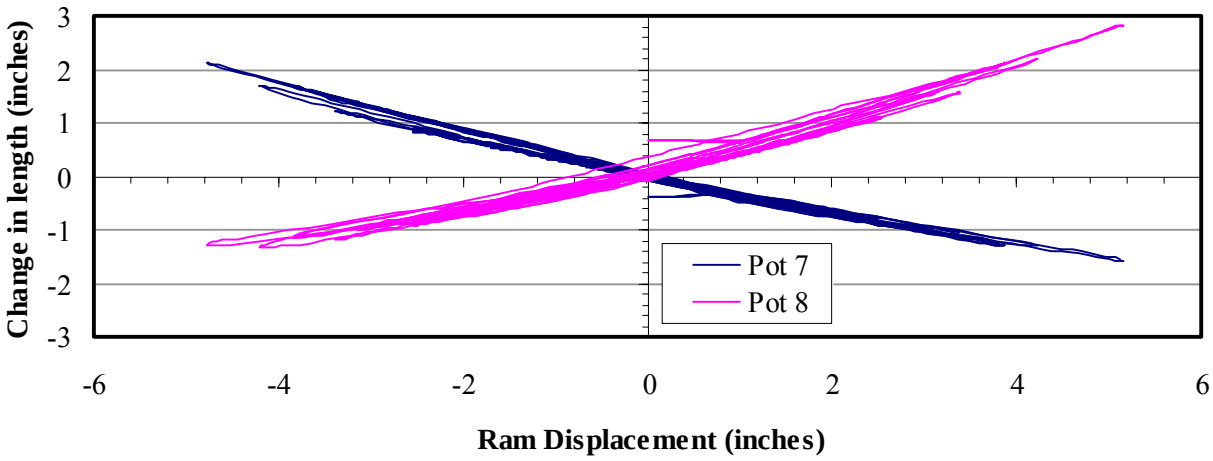

Figure A.124. Change in length of diagonal measuring Pots 7 and 8 vs. ram displacement of 9-9-E-2

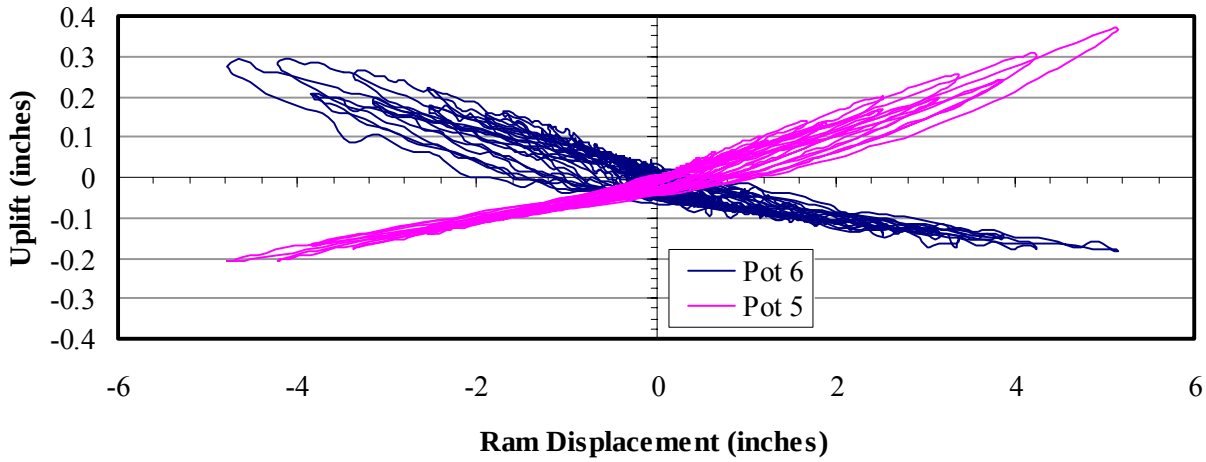

Figure A.125. Uplift displacement vs. ram displacement of 9-9-E-2

Table A.101. Performance Parameters of 9-9-E-3

Specimen	9-9-E-3	
Peak load, F_{peak}	Kips	4.842
	KN	21.539
Drift at peak load, Δ_{peak}	in.	2.743
	mm	69.68
Yield load, F_{yield}	Kips	4.283
	KN	19.049
Drift at yield load, Δ_{yield}	in.	0.684
	mm	17.38
Proportional limit, $0.4F_{peak}$	Kips	1.937
	KN	8.616
Drift at prop. limit, $\Delta@0.4F_{peak}$	in.	0.309
	mm	7.85
Failure load or $0.8F_{peak}$	Kips	3.874
	KN	17.231
Drift at failure, $\Delta_{failure}$	in.	4.062
	mm	103.17
Elastic stiffness, K_e $@0.4F_{peak}$	Kip/in.	6.369
	KN/mm	1.115
Work until failure	Kip·ft.	9.066
	KN·m	12.292
Ductility factor, μ	6.05	

Observations and failure modes:

- Significant sheathing nail tear through and pulled heads near the corners of the panels and along common center stud
- Minor withdrawal (0..5 in.) was experienced by all sheathing nails except those in common center stud
- All sheathing nails removed from perimeter of panels experienced significant bending deformation
- Minor separation between top plate and studs

Table A.102. EEEP Parameters of 9-9-E-3

EEEP Parameters	units	negative	positive
F_{yield}	Kips	-4.346	4.219
	KN	-19.333	18.766
Δ_{yield}	in.	-0.599	0.770
	mm	-15.21	19.56
$\Delta_{failure}$	in.	-4.180	3.944
	mm	-106.16	100.19

Table A.103. Displacement components of 9-9-E-3

	inches	mm	% of Total
Total Displacement	2.4	61.0	
Shear Deformation	1.9	48.3	79.2
Rigid Body Motion	0.5	12.7	20.8
Bending and Slip	0.0	0.0	0.0

Table A.104. Data of each Primary cycle of 9-9-E-3

Primary	average displacement		average load		work per cycle		cyclic stiffness		Damping
cycle #	in.	mm	Kips	KN	Kip·ft.	KN·m	Kip/in.	KN/mm	Ratio
1	0.083	2.109	0.796	3.539	0.004	0.005	9.558	1.674	0.115
2	0.123	3.117	1.102	4.900	0.009	0.012	8.958	1.569	0.129
3	0.162	4.122	1.357	6.037	0.016	0.021	8.361	1.464	0.137
4	0.328	8.340	2.028	9.020	0.057	0.077	6.177	1.082	0.163
5	0.491	12.460	2.521	11.212	0.105	0.143	5.140	0.900	0.162
6	0.652	16.572	2.926	13.014	0.164	0.222	4.486	0.786	0.164
7	1.128	28.656	3.746	16.662	0.444	0.602	3.321	0.582	0.201
8	1.599	40.620	4.219	18.766	0.678	0.919	2.639	0.462	0.192
9	2.363	60.025	4.774	21.233	1.181	1.601	2.020	0.354	0.200
10	3.139	79.727	4.791	21.312	1.491	2.021	1.527	0.267	0.189
11	3.979	101.065	4.154	18.478	1.629	2.209	1.043	0.183	0.188
12	4.409	111.985	2.116	9.410	1.194	1.618	0.477	0.084	0.242

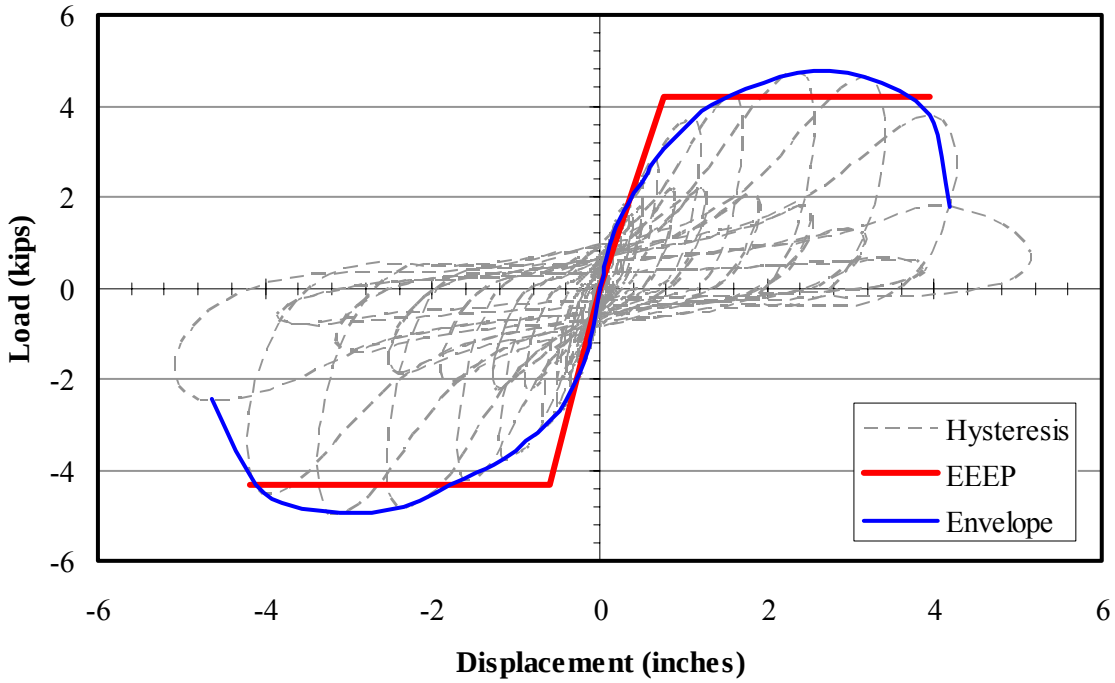

Figure A.126. Load vs. displacement, envelope and EEEP curves of 9-9-E-3

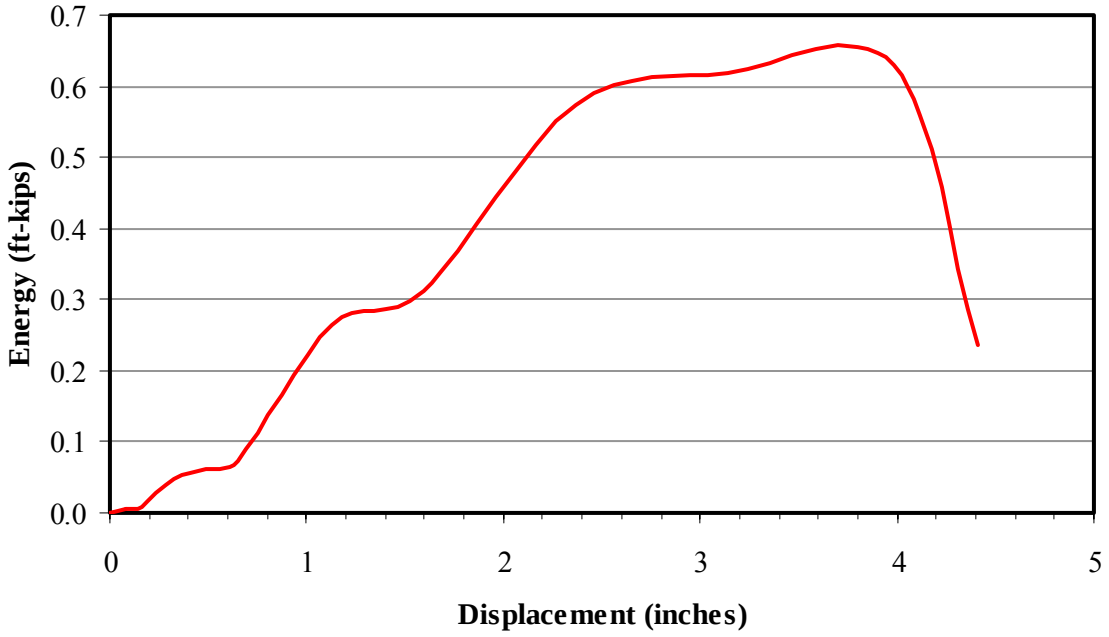

Figure A.127. Hysteretic energy dissipated per cycle vs. displacement of 9-9-E-3

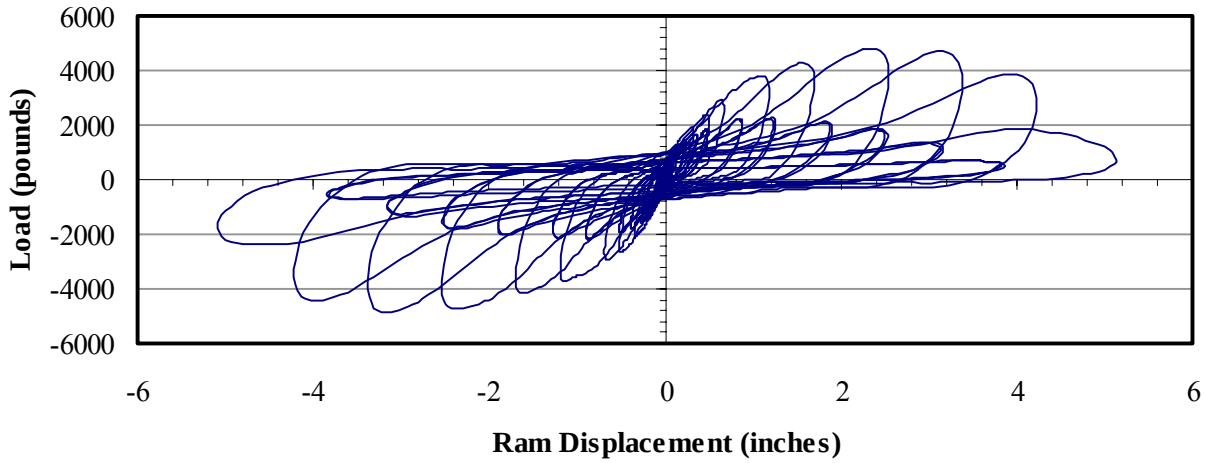

Figure A.128. Load vs. displacement of 9-9-E-3

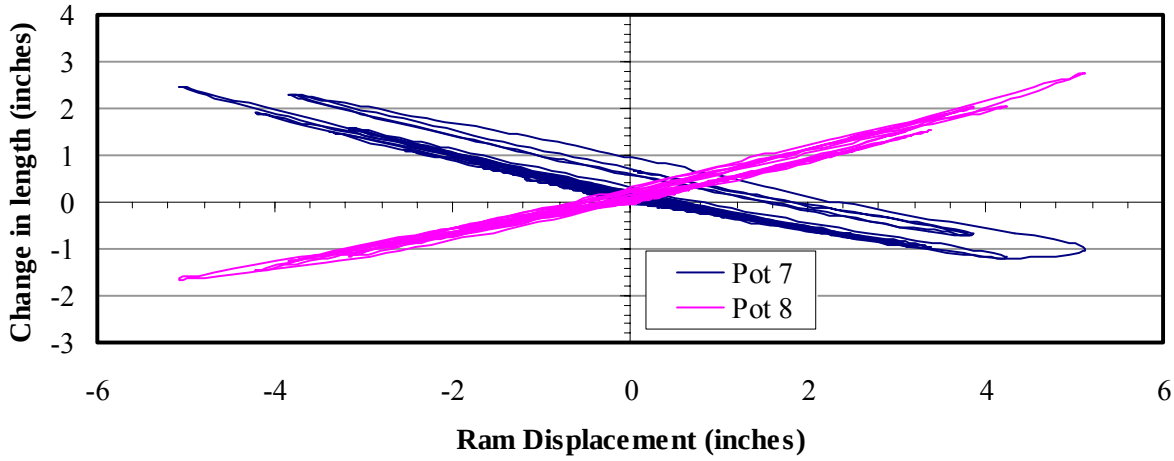

Figure A.129. Change in length of diagonal measuring Pots 7 and 8 vs. ram displacement of 9-9-E-3

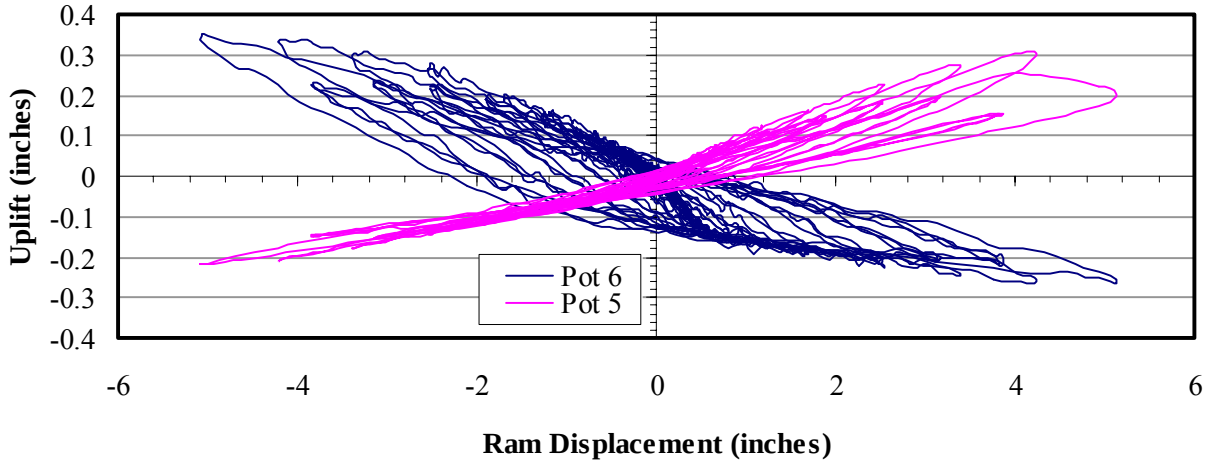

Figure A.130. Uplift displacement vs. ram displacement of 9-9-E-3

Table A.105. Performance Parameters of 10-10-E-1

Specimen	10-10-E-1	
Peak load, F_{peak}	Kips	4.610
	KN	20.507
Drift at peak load, Δ_{peak}	in.	3.833
	mm	97.35
Yield load, F_{yield}	Kips	4.099
	KN	18.234
Drift at yield load, Δ_{yield}	in.	0.892
	mm	22.66
Proportional limit, $0.4F_{peak}$	Kips	1.844
	KN	8.203
Drift at prop. limit, $\Delta@0.4F_{peak}$	in.	0.401
	mm	10.19
Failure load or $0.8F_{peak}$	Kips	4.239
	KN	18.855
Drift at failure, $\Delta_{failure}$	in.	4.589
	mm	116.56
Elastic stiffness, K_e $@0.4F_{peak}$	Kip/in.	4.601
	KN/mm	0.806
Work until failure	Kip·ft.	8.084
	KN·m	10.959
Ductility factor, μ	5.15	

Observations and failure modes:

- Sheathing nails along common center stud and within 4 ft of corner along 10 ft edge and near corner of 4 ft edge experienced minor tear through; however, not as severe as corresponding 10 ft configurations due to limitations of test apparatus.
- All sheathing nails removed from perimeter of panels experienced significant bending deformation

Table A.106. EEEP Parameters of 10-10-E-1

EEEP Parameters	units	negative	Positive
F_{yield}	Kips	-4.298	3.901
	KN	-19.116	17.352
Δ_{yield}	in.	-0.873	0.912
	mm	-22.16	23.17
$\Delta_{failure}$	in.	-4.608	4.570
	mm	-117.05	116.08

Table A.107. Displacement components of 10-10-E-1

	inches	mm	% of Total
Total Displacement	3.2	81.3	
Shear Deformation	2.7	68.6	84.4
Rigid Body Motion	0.5	12.7	15.6
Bending and Slip	0.0	0.0	0.0

Table A.108. Data of each Primary cycle of 10-10-E-1

Primary	average displacement		average load		work per cycle		cyclic stiffness		Damping
cycle #	in.	mm	Kips	KN	Kip·ft.	KN·m	Kip/in.	KN/mm	Ratio
1	0.153	3.884	0.973	4.327	0.011	0.015	6.359	1.114	0.146
2	0.234	5.932	1.328	5.908	0.024	0.032	5.683	0.995	0.145
3	0.311	7.910	1.595	7.096	0.038	0.052	5.117	0.896	0.146
4	0.629	15.970	2.464	10.961	0.143	0.194	3.917	0.686	0.176
5	0.937	23.799	3.073	13.669	0.258	0.350	3.280	0.574	0.171
6	1.245	31.618	3.448	15.339	0.382	0.518	2.771	0.485	0.170
7	2.189	55.590	4.230	18.814	1.008	1.366	1.932	0.338	0.208
8	3.108	78.938	4.589	20.412	1.433	1.943	1.476	0.258	0.192
9	4.589	116.564	4.239	18.855	2.046	2.774	0.923	0.162	0.201

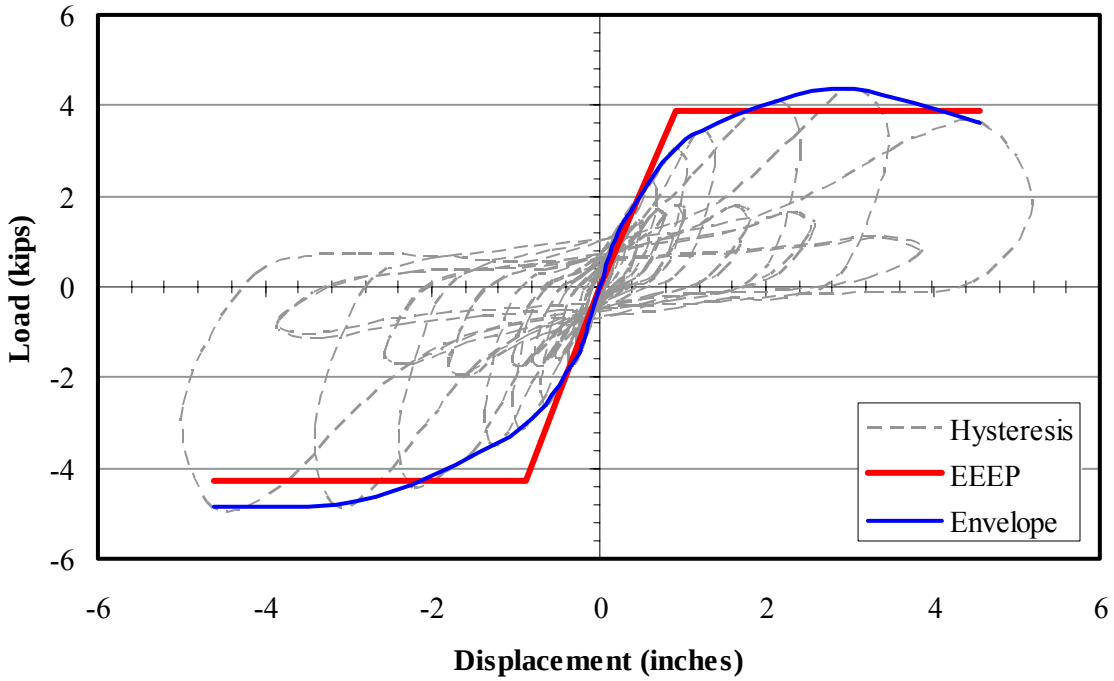

Figure A.131. Load vs. displacement, envelope and EEEP curves of 10-10-E-1

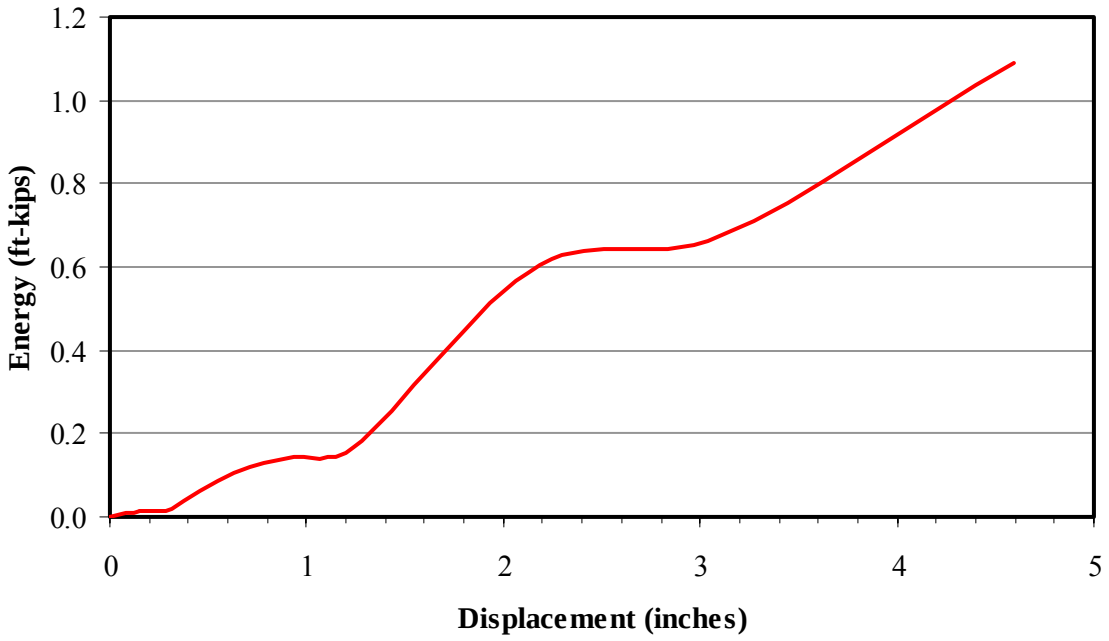

Figure A.132. Hysteretic energy dissipated per cycle vs. displacement of 10-10-E-1

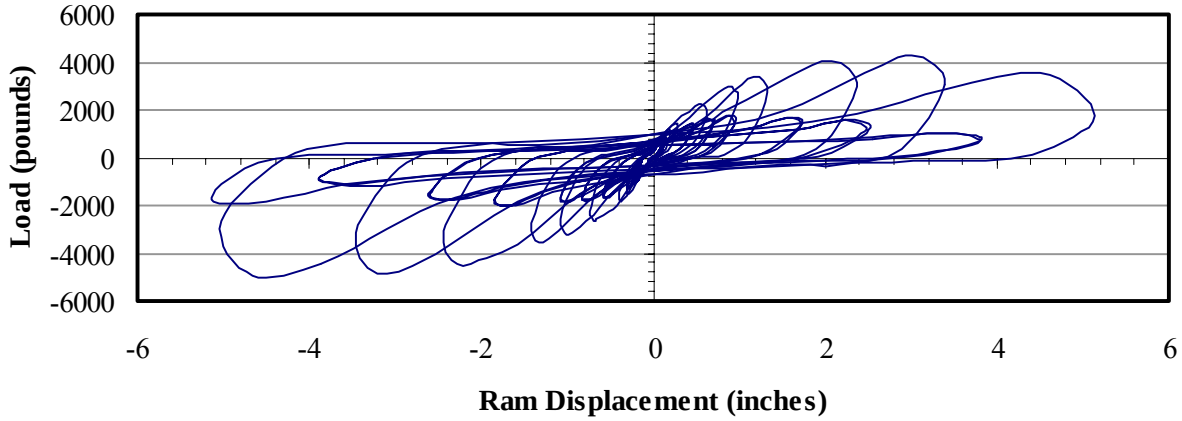

Figure A.133. Load vs. displacement of 10-10-E-1

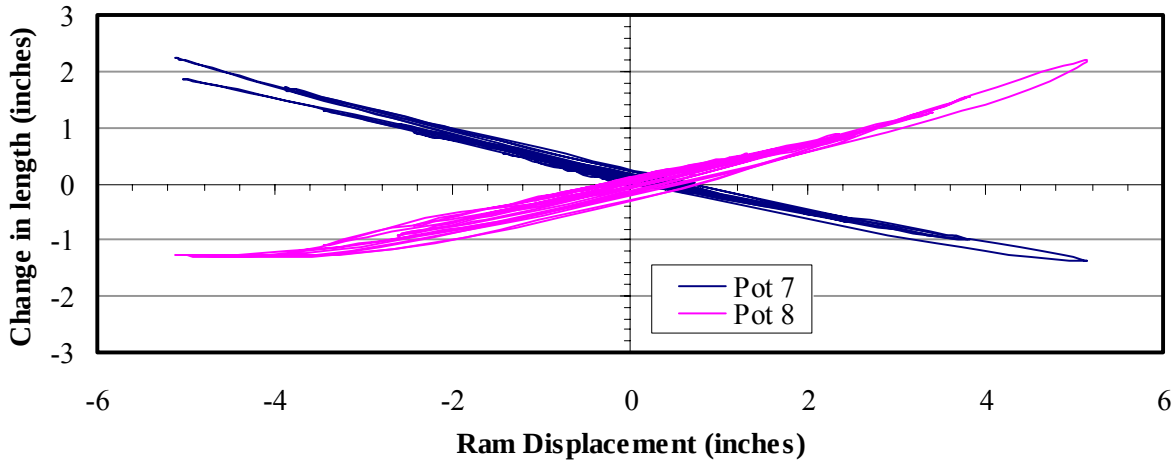

Figure A.134. Change in length of diagonal measuring Pots 7 and 8 vs. ram displacement of 10-10-E-1

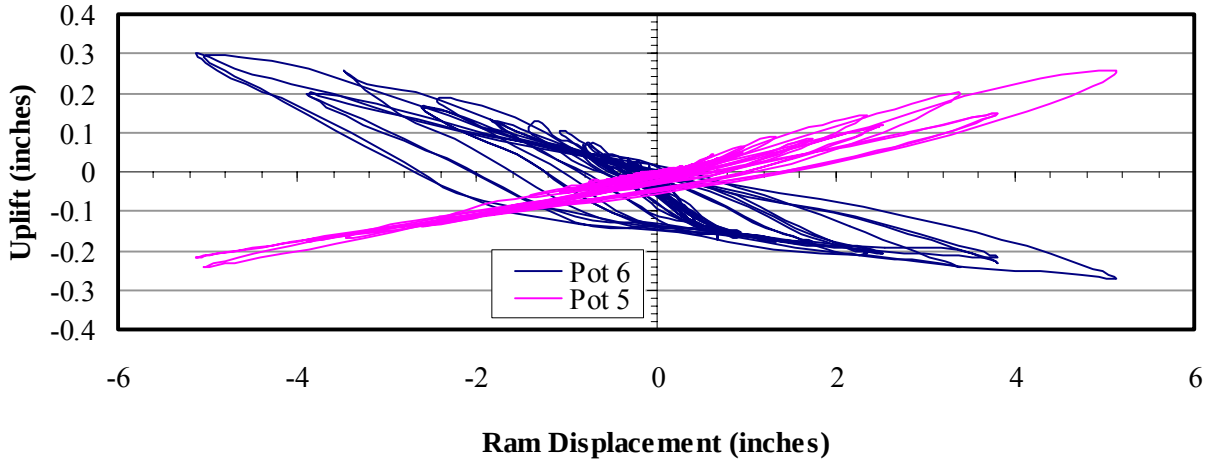

Figure A.135. Uplift displacement vs. ram displacement of 10-10-E-1

Table A.109. Performance Parameters of 10-10-E-2

Specimen	10-10-E-2	
Peak load, F_{peak}	Kips	3.990
	KN	17.748
Drift at peak load, Δ_{peak}	in.	3.238
	mm	82.24
Yield load, F_{yield}	Kips	3.568
	KN	15.872
Drift at yield load, Δ_{yield}	in.	0.898
	mm	22.80
Proportional limit, $0.4F_{peak}$	Kips	1.596
	KN	7.099
Drift at prop. limit, $\Delta@0.4F_{peak}$	in.	0.401
	mm	10.18
Failure load or $0.8F_{peak}$	Kips	3.746
	KN	16.662
Drift at failure, $\Delta_{failure}$	in.	4.346
	mm	110.40
Elastic stiffness, K_e $@0.4F_{peak}$	Kip/in.	4.038
	KN/mm	0.707
Work until failure	Kip·ft.	7.211
	KN·m	9.776
Ductility factor, μ	4.88	

Observations and failure modes:

- Sheathing nails along common center stud and within 4 ft of corner along 10 ft edge and near corner of 4 ft edge experienced minor tear through; however, not as severe as corresponding 10 ft configurations due to limitations of test apparatus.
- All sheathing nails removed from perimeter of panels experienced significant bending deformation
- Minor separation between end studs and top and bottom plates

Table A.110. EEEP Parameters of 10-10-E-2

EEEP Parameters	units	negative	positive
F_{yield}	Kips	-4.071	3.066
	KN	-18.107	13.637
Δ_{yield}	in.	-0.832	0.963
	mm	-21.13	24.47
$\Delta_{failure}$	in.	-4.496	4.197
	mm	-114.21	106.59

Table A.111. Displacement components of 10-10-E-2

	inches	mm	% of Total
Total Displacement	3.0	76.2	
Shear Deformation	2.5	63.5	83.3
Rigid Body Motion	0.5	12.7	16.7
Bending and Slip	0.0	0.0	0.0

Table A.112. Data of each Primary cycle of 10-10-E-2

Primary	average displacement		average load		work per cycle		cyclic stiffness		Damping
cycle #	in.	mm	Kips	KN	Kip·ft.	KN·m	Kip/in.	KN/mm	Ratio
1	0.171	4.348	0.937	4.167	0.012	0.017	5.472	0.958	0.147
2	0.259	6.575	1.255	5.582	0.022	0.029	4.845	0.848	0.127
3	0.344	8.744	1.476	6.563	0.036	0.049	4.285	0.750	0.137
4	0.656	16.651	2.199	9.780	0.129	0.176	3.392	0.594	0.173
5	0.969	24.604	2.689	11.962	0.229	0.310	2.809	0.492	0.169
6	1.285	32.640	3.008	13.377	0.332	0.450	2.367	0.415	0.165
7	2.053	52.139	3.764	16.740	0.882	1.195	1.829	0.320	0.217
8	2.911	73.933	3.916	17.419	1.241	1.682	1.341	0.235	0.207
9	4.346	110.401	3.746	16.662	1.883	2.553	0.856	0.150	0.219

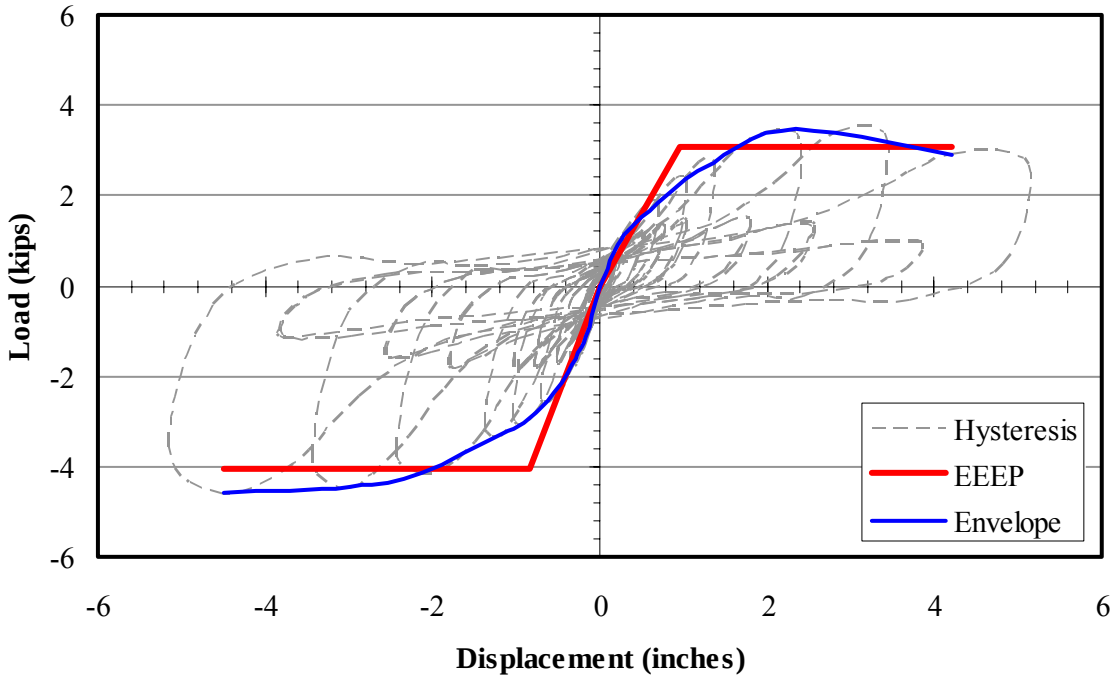

Figure A.136. Load vs. displacement, envelope and EEEP curves of 10-10-E-2

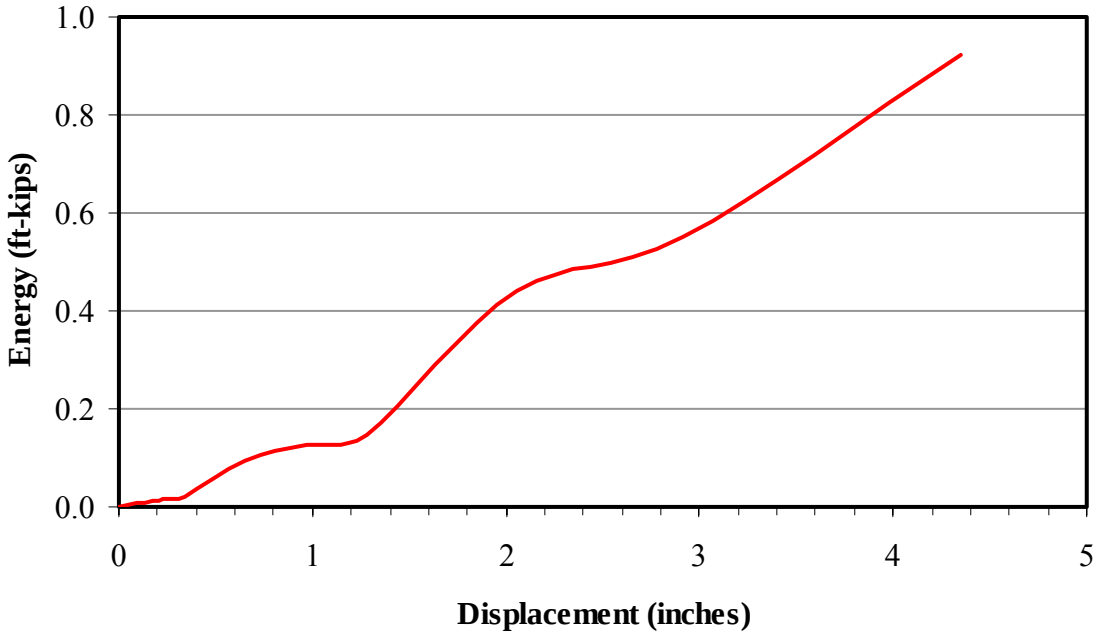

Figure A.137. Hysteretic energy dissipated per cycle vs. displacement of 10-10-E-2

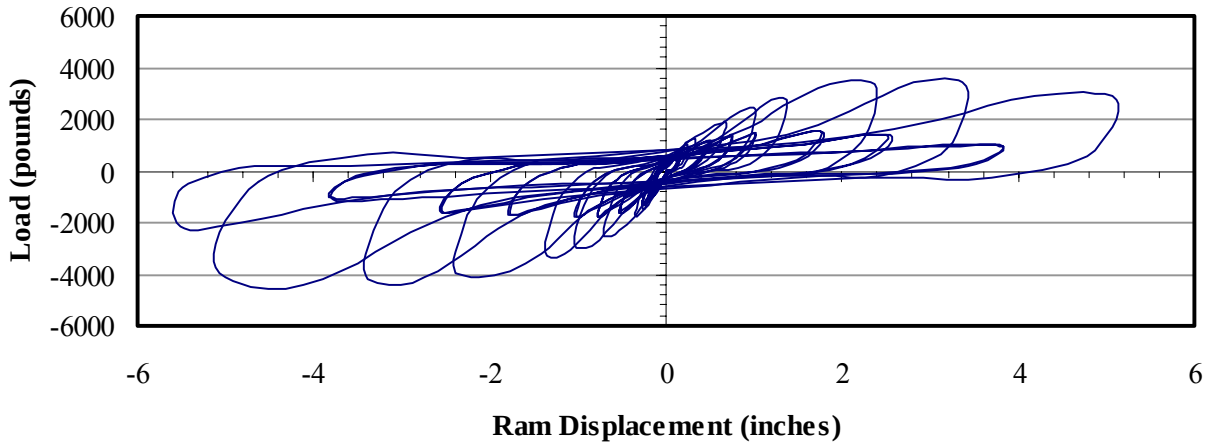

Figure A.138. Load vs. displacement of 10-10-E-2

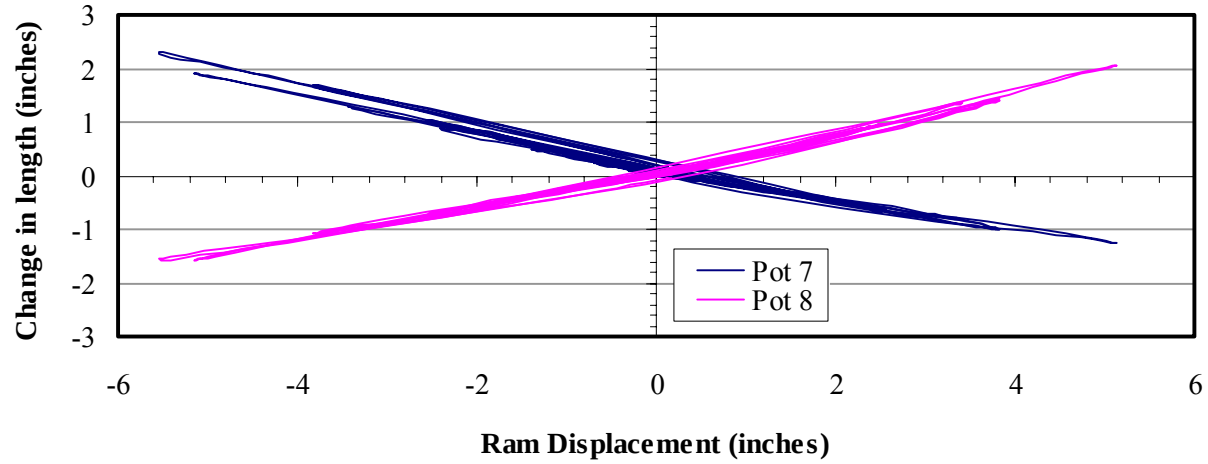

Figure A.139. Change in length of diagonal measuring Pots 7 and 8 vs. ram displacement of 10-10-E-2

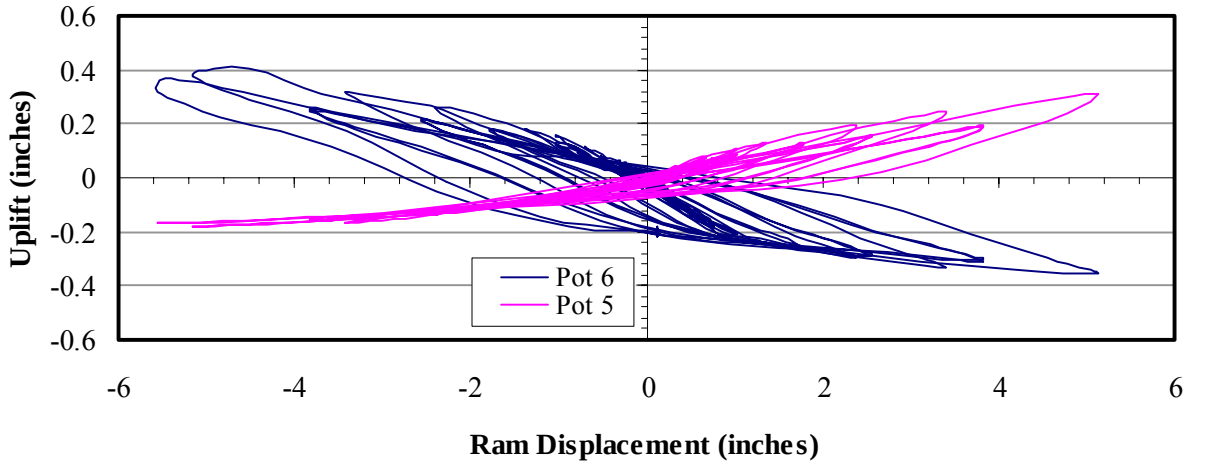

Figure A.140. Uplift displacement vs. ram displacement of 10-10-E-2

Table A.113. Performance Parameters of 10-10-E-3

Specimen	10-10-E-3	
Peak load, F_{peak}	Kips	4.243
	KN	18.872
Drift at peak load, Δ_{peak}	in.	3.418
	mm	86.82
Yield load, F_{yield}	Kips	3.836
	KN	17.063
Drift at yield load, Δ_{yield}	in.	0.538
	mm	13.66
Proportional limit, $0.4F_{peak}$	Kips	1.697
	KN	7.549
Drift at prop. limit, $\Delta@0.4F_{peak}$	in.	0.236
	mm	6.00
Failure load or $0.8F_{peak}$	Kips	3.857
	KN	17.158
Drift at failure, $\Delta_{failure}$	in.	4.606
	mm	116.99
Elastic stiffness, K_e $@0.4F_{peak}$	Kip/in.	9.529
	KN/mm	1.669
Work until failure	Kip·ft.	8.299
	KN·m	11.251
Ductility factor, μ	11.47	

Observations and failure modes:

- Sheathing nails along common center stud and within 4 ft of corner along 10 ft edge and near corner of 4 ft edge experienced minor tear through; however, not as severe as corresponding 10 ft configurations due to limitations of test apparatus.
- All sheathing nails removed from perimeter of panels experienced significant bending deformation
- Sheathing nails along end studs experienced minor (0.5 in.) withdrawal
- Minor separation between end studs and top and bottom plates

Table A.114. EEEP Parameters of 10-10-E-3

EEEP Parameters	units	negative	positive
F_{yield}	Kips	-3.952	3.720
	KN	-17.581	16.546
Δ_{yield}	in.	-0.814	0.262
	mm	-20.66	6.65
$\Delta_{failure}$	in.	-4.719	4.492
	mm	-119.87	114.11

Table A.115. Displacement components of 10-10-E-3

	inches	mm	% of Total
Total Displacement	3.2	81.3	
Shear Deformation	2.9	73.7	90.6
Rigid Body Motion	0.3	7.6	9.4
Bending and Slip	0.0	0.0	0.0

Table A.116. Data of each Primary cycle of 10-10-E-3

Primary	average displacement		average load		work per cycle		cyclic stiffness		Damping
cycle #	in.	mm	Kips	KN	Kip·ft.	KN·m	Kip/in.	KN/mm	Ratio
1	0.161	4.092	1.241	5.518	0.018	0.024	8.087	1.416	0.179
2	0.232	5.886	1.749	7.778	0.032	0.043	7.597	1.330	0.151
3	0.311	7.892	2.058	9.152	0.051	0.069	6.648	1.164	0.152
4	0.630	15.997	2.901	12.902	0.181	0.246	4.622	0.809	0.190
5	0.933	23.696	3.310	14.725	0.302	0.409	3.554	0.622	0.187
6	1.238	31.458	3.532	15.709	0.417	0.565	2.854	0.500	0.182
7	2.173	55.199	4.134	18.390	1.042	1.413	1.904	0.333	0.222
8	3.083	78.303	4.189	18.631	1.358	1.841	1.359	0.238	0.201
9	4.606	116.989	3.857	17.158	1.960	2.657	0.836	0.146	0.210

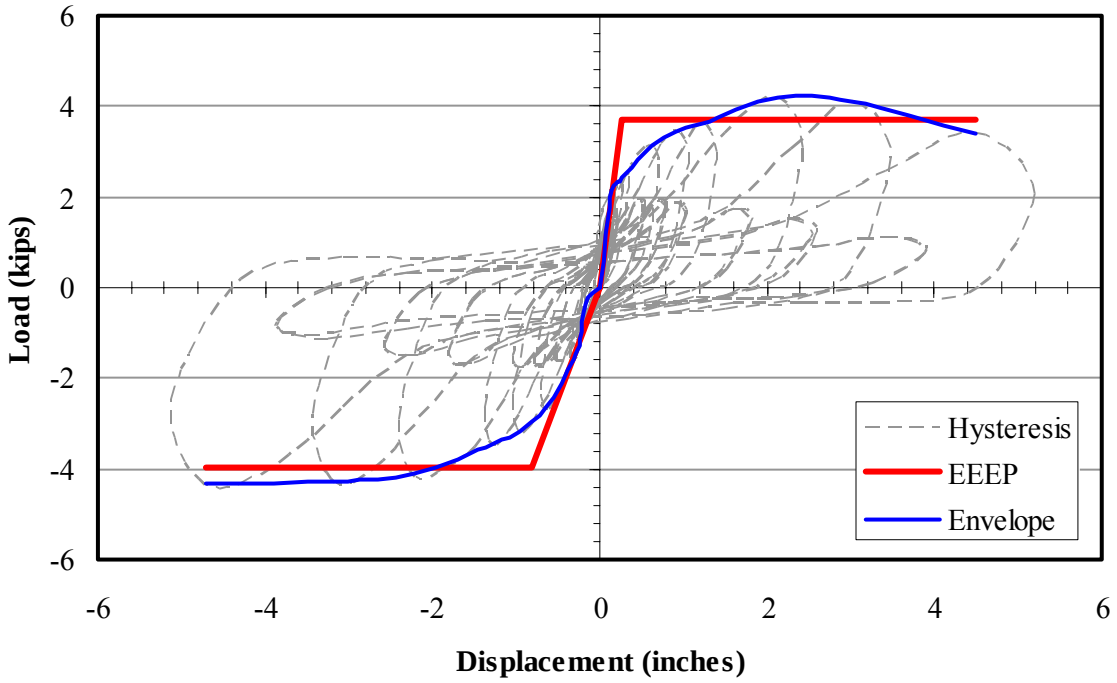

Figure A.141. Load vs. displacement, envelope and EEEP curves of 10-10-E-3

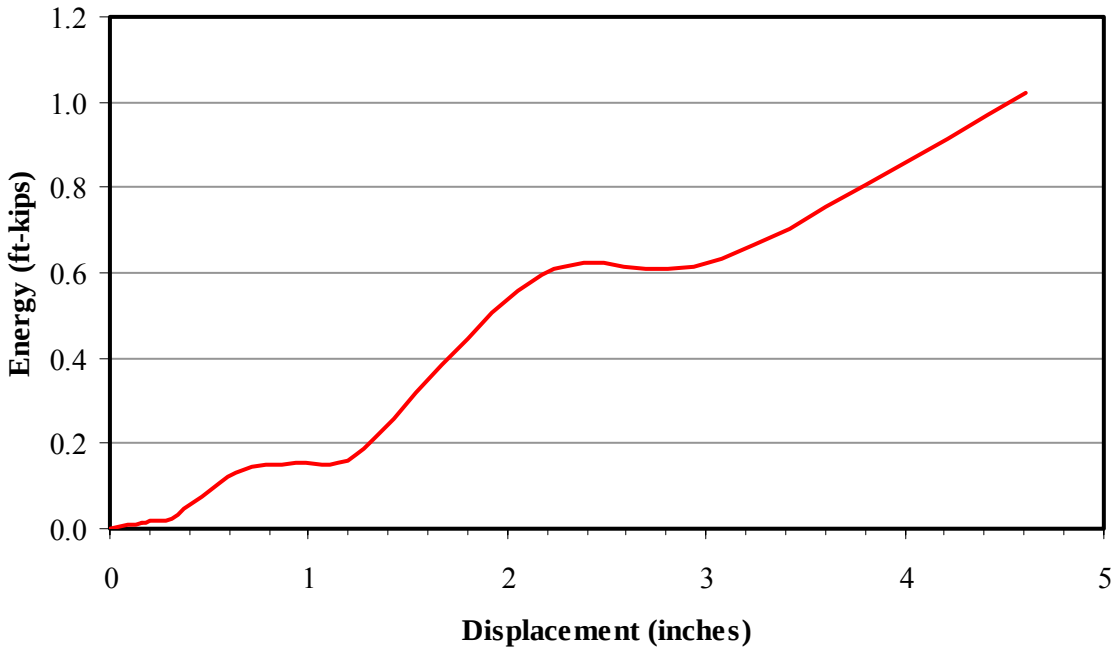

Figure A.142. Hysteretic energy dissipated per cycle vs. displacement of 10-10-E-3

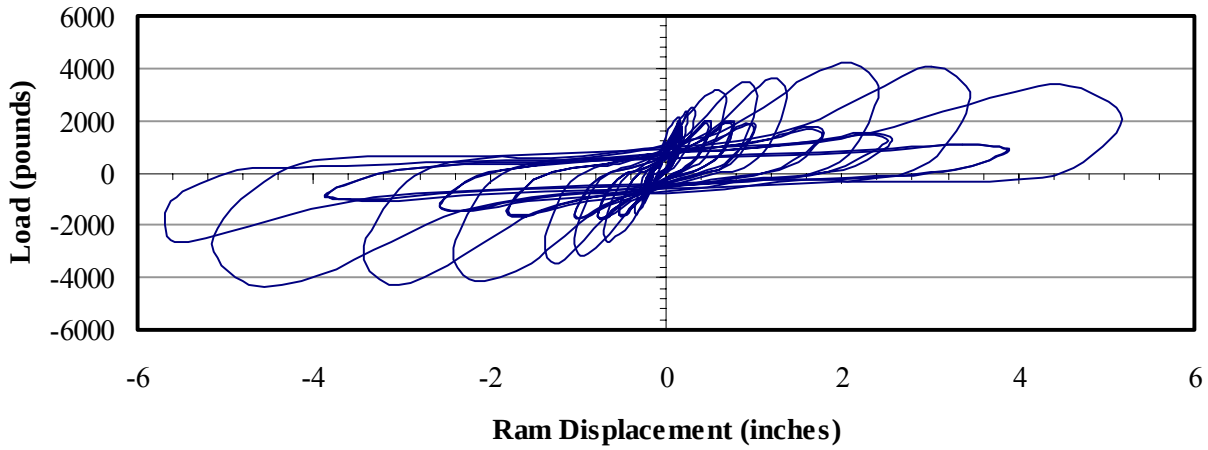

Figure A.143. Load vs. displacement of 10-10-E-3

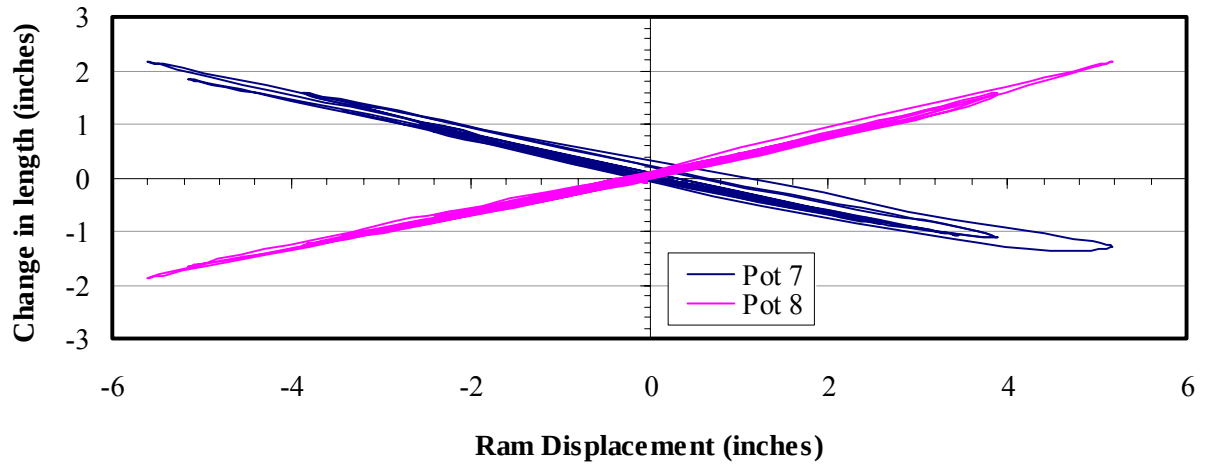

Figure A.144. Change in length of diagonal measuring Pots 7 and 8 vs. ram displacement of 10-10-E-3

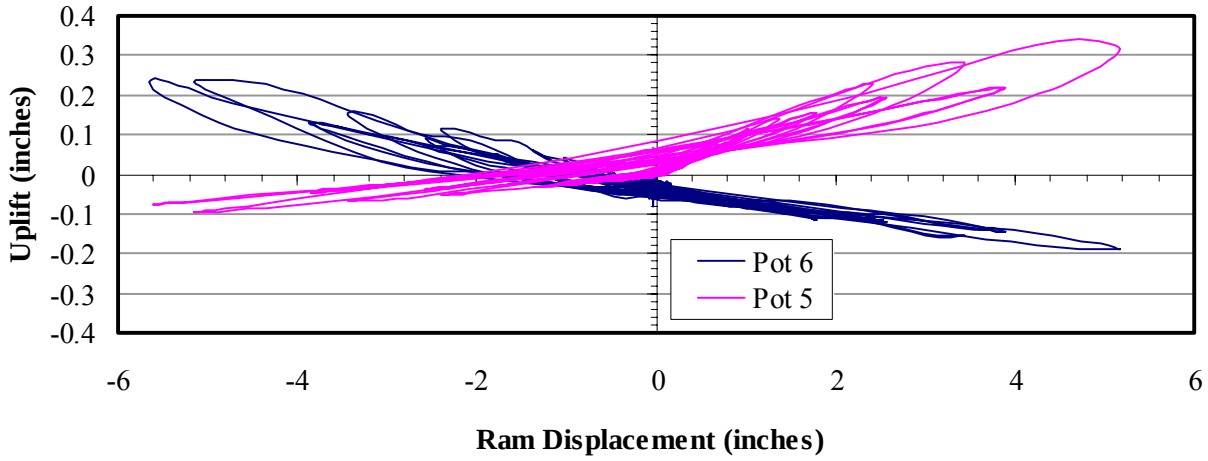

Figure A.145. Uplift displacement vs. ram displacement of 10-10-E-3

Table A.117. Performance Parameters of 10-8-E-1

Specimen	10-8-E-1	
Peak load, F_{peak}	Kips	4.218
	KN	18.763
Drift at peak load, Δ_{peak}	in.	4.520
	mm	114.81
Yield load, F_{yield}	Kips	3.733
	KN	16.602
Drift at yield load, Δ_{yield}	in.	0.836
	mm	21.23
Proportional limit, $0.4F_{peak}$	Kips	1.687
	KN	7.505
Drift at prop. limit, $\Delta@0.4F_{peak}$	in.	0.377
	mm	9.59
Failure load or $0.8F_{peak}$	Kips	4.218
	KN	18.763
Drift at failure, $\Delta_{failure}$	in.	4.520
	mm	114.81
Elastic stiffness, K_e $@0.4F_{peak}$	Kip/in.	4.471
	KN/mm	0.783
Work until failure	Kip·ft.	7.370
	KN·m	9.991
Ductility factor, μ	5.40	

Observations and failure modes:

- Tear through and pulled heads of sheathing nails near the corners and along the blocking of the 4 x 8 ft panels; however, not as severe as corresponding 9 ft configuration due to limitations of testing apparatus
- Sheathing nails along blocking in 4 x 2 ft panels pulled heads more severely than compared to corresponding 9 ft configuration. Sheathing nails in top plate were virtually undamaged.
- All sheathing nails removed from perimeter of 4 x 8 ft panels experienced significant bending deformation

Table A.118. EEEP Parameters of 10-8-E-1

EEEP Parameters	units	negative	positive
F_{yield}	Kips	-3.818	3.647
	KN	-16.984	16.221
Δ_{yield}	in.	-0.817	0.855
	mm	-20.75	21.71
$\Delta_{failure}$	in.	-4.111	4.929
	mm	-104.43	125.19

Table A.119. Displacement components of 10-8-E-1

	inches	mm	% of Total
Total Displacement	4.9	124.5	
Shear Deformation	4.0	101.6	81.6
Rigid Body Motion	0.5	12.7	10.2
Bending and Slip	0.4	10.2	8.2

Table A.120. Data of each Primary cycle of 10-8-E-1

Primary	average displacement		average load		work per cycle		cyclic stiffness		Damping
cycle #	in.	mm	Kips	KN	Kip·ft.	KN·m	Kip/in.	KN/mm	Ratio
1	0.166	4.204	0.939	4.177	0.010	0.014	5.680	0.995	0.128
2	0.248	6.311	1.282	5.701	0.021	0.029	5.160	0.904	0.127
3	0.333	8.461	1.580	7.028	0.034	0.046	4.743	0.831	0.124
4	0.669	17.004	2.394	10.649	0.134	0.182	3.575	0.626	0.160
5	1.001	25.427	2.890	12.855	0.240	0.325	2.886	0.505	0.158
6	1.329	33.765	3.215	14.300	0.352	0.478	2.418	0.423	0.157
7	2.161	54.882	3.831	17.042	0.918	1.245	1.785	0.313	0.212
8	3.318	84.266	4.085	18.169	1.298	1.760	1.231	0.216	0.183
9	4.520	114.812	4.218	18.763	2.034	2.758	0.945	0.165	0.205

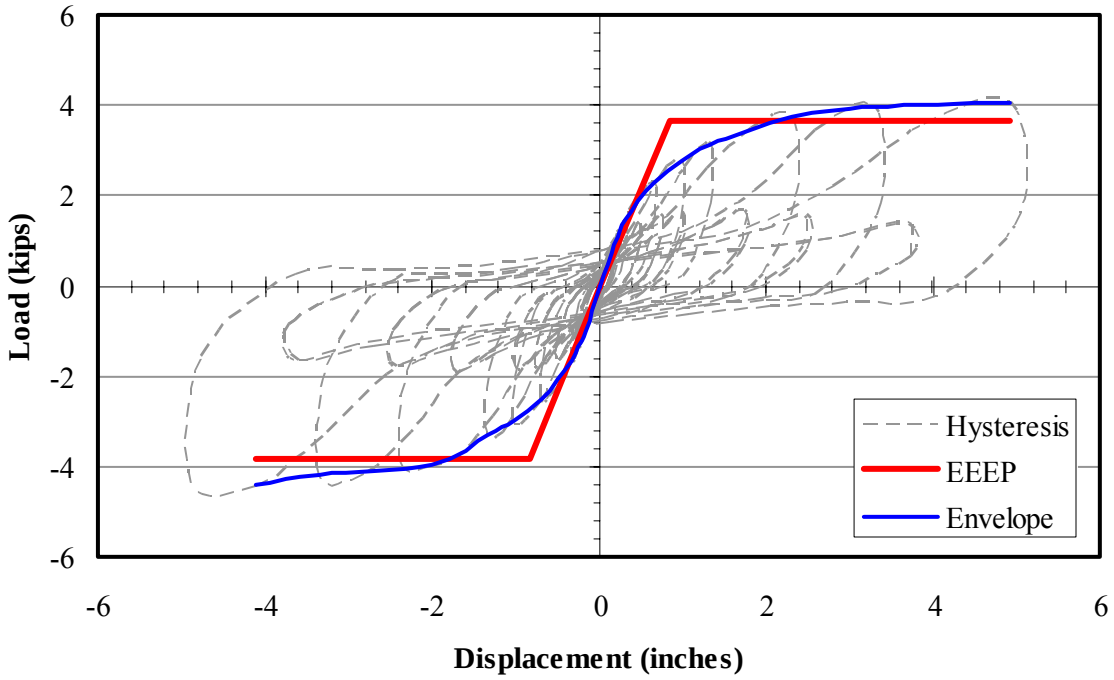

Figure A.146. Load vs. displacement, envelope and EEEP curves of 10-8-E-1

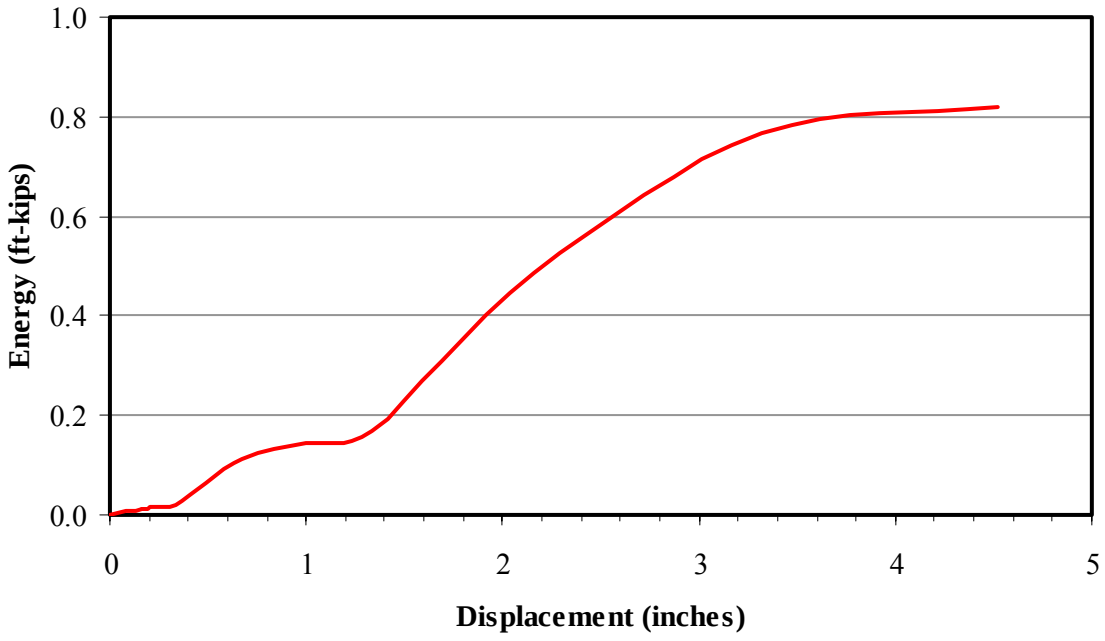

Figure A.147. Hysteretic energy dissipated per cycle vs. displacement of 10-8-E-1

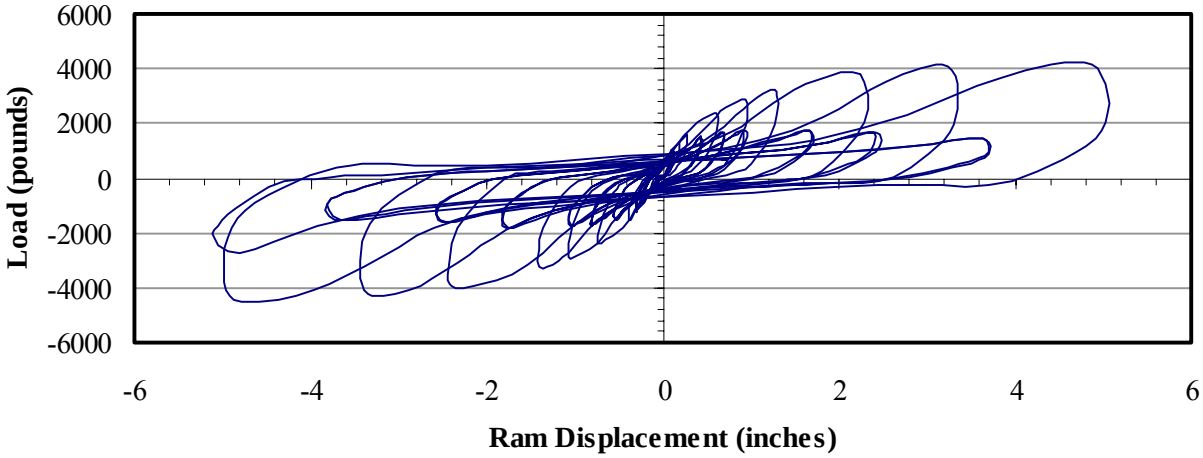

Figure A.148. Load vs. displacement of 10-8-E-1

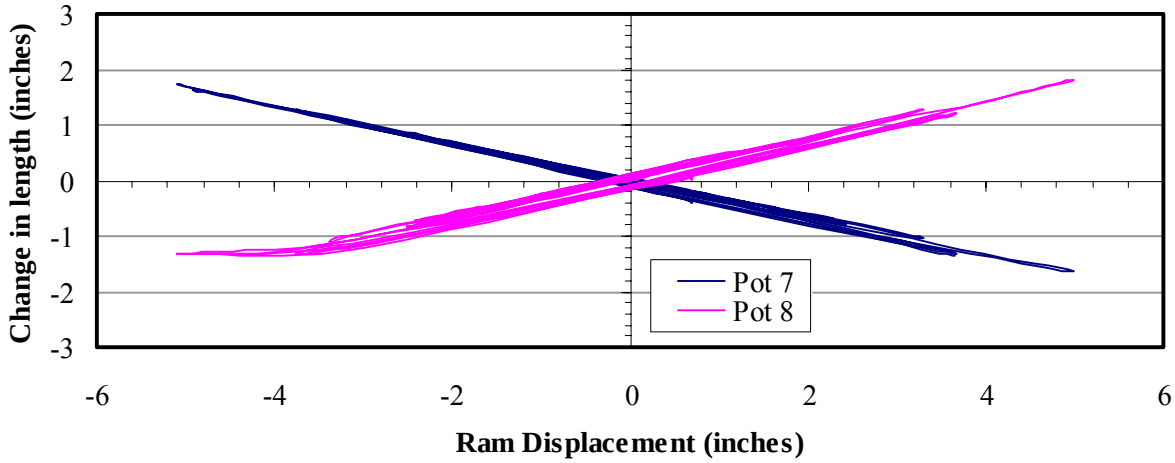

Figure A.149. Change in length of diagonal measuring Pots 7 and 8 vs. ram displacement of 10-8-E-1

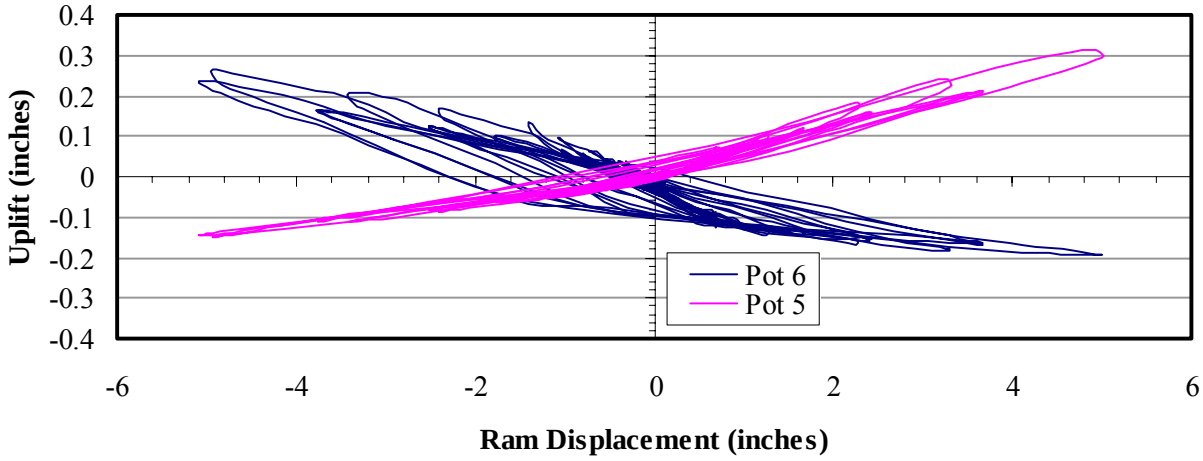

Figure A.150. Uplift displacement vs. ram displacement of 10-8-E-1

Table A.121. Performance Parameters of 10-8-E-2

Specimen	10-8-E-2	
Peak load, F_{peak}	Kips	4.262
	KN	18.956
Drift at peak load, Δ_{peak}	in.	4.556
	mm	115.71
Yield load, F_{yield}	Kips	3.747
	KN	16.669
Drift at yield load, Δ_{yield}	in.	0.988
	mm	25.09
Proportional limit, $0.4F_{peak}$	Kips	1.705
	KN	7.583
Drift at prop. limit, $\Delta@0.4F_{peak}$	in.	0.453
	mm	11.52
Failure load or $0.8F_{peak}$	Kips	4.262
	KN	18.956
Drift at failure, $\Delta_{failure}$	in.	4.556
	mm	115.71
Elastic stiffness, K_e $@0.4F_{peak}$	Kip/in.	4.286
	KN/mm	0.751
Work until failure	Kip·ft.	6.942
	KN·m	9.411
Ductility factor, μ	5.31	

Observations and failure modes:

- Tear through and pulled heads of sheathing nails near the corners and along the blocking of the 4 x 8 ft panels; however, not as severe as corresponding 9 ft configuration due to limitations of testing apparatus
- Sheathing nails along blocking in 4 x 2 ft panels pulled heads more severely than compared to corresponding 9 ft configuration. Sheathing nails in top plate were virtually undamaged.
- All sheathing nails removed from perimeter of 4 x 8 ft panels experienced significant bending deformation
- Minor separation of end studs and top and bottom plates

Table A.122. EEEP Parameters of 10-8-E-2

EEEP Parameters	units	negative	positive
F_{yield}	Kips	-3.694	3.801
	KN	-16.430	16.907
Δ_{yield}	in.	-1.317	0.659
	mm	-33.45	16.74
$\Delta_{failure}$	in.	-4.232	4.879
	mm	-107.49	123.93

Table A.123. Displacement components of 10-8-E-2

	inches	mm	% of Total
Total Displacement	5.0	127.0	
Shear Deformation	4.4	111.8	88.0
Rigid Body Motion	0.6	15.2	12.0
Bending and Slip	0.0	0.0	0.0

Table A.124. Data of each Primary cycle of 10-8-E-2

Primary	average displacement		average load		work per cycle		cyclic stiffness		Damping
cycle #	in.	mm	Kips	KN	Kip·ft.	KN·m	Kip/in.	KN/mm	Ratio
1	0.166	4.211	0.694	3.088	0.010	0.014	4.272	0.748	0.175
2	0.251	6.375	1.060	4.717	0.017	0.023	4.275	0.749	0.124
3	0.333	8.468	1.365	6.071	0.028	0.038	4.118	0.721	0.118
4	0.668	16.974	2.226	9.902	0.112	0.152	3.342	0.585	0.145
5	0.998	25.342	2.790	12.410	0.211	0.285	2.801	0.490	0.145
6	1.328	33.735	3.168	14.090	0.315	0.427	2.387	0.418	0.143
7	2.327	59.115	3.840	17.080	0.876	1.188	1.651	0.289	0.187
8	3.311	84.094	4.102	18.247	1.247	1.690	1.239	0.217	0.175
9	4.556	115.712	4.262	18.956	2.043	2.769	0.941	0.165	0.201

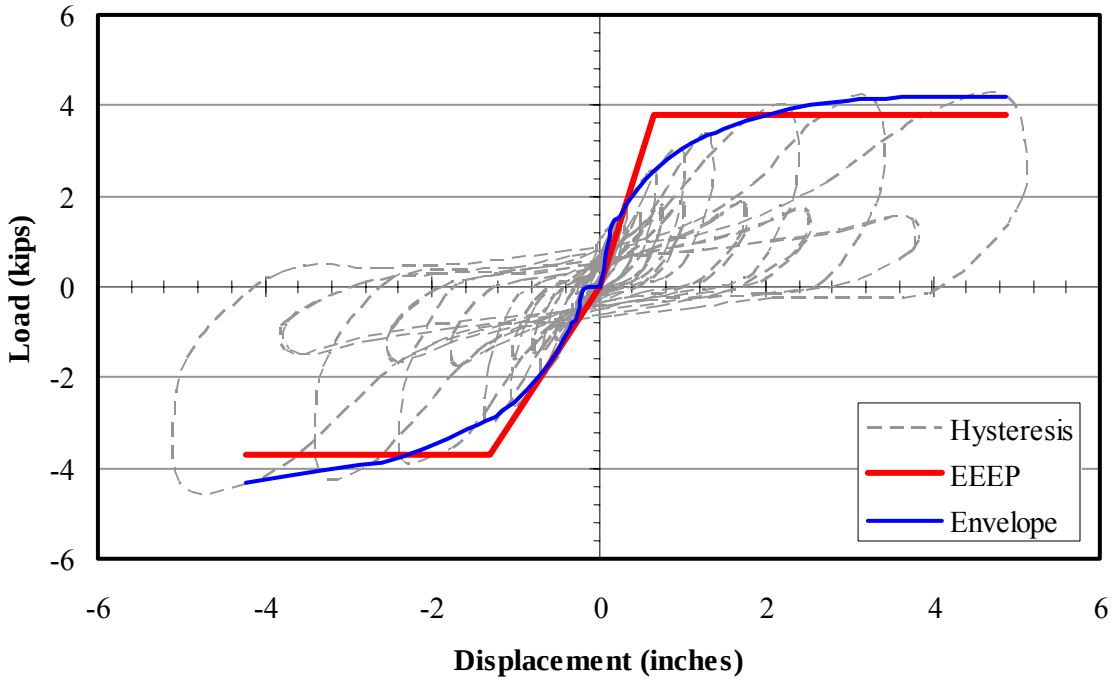

Figure A.151. Load vs. displacement, envelope and EEEP curves of 10-8-E-2

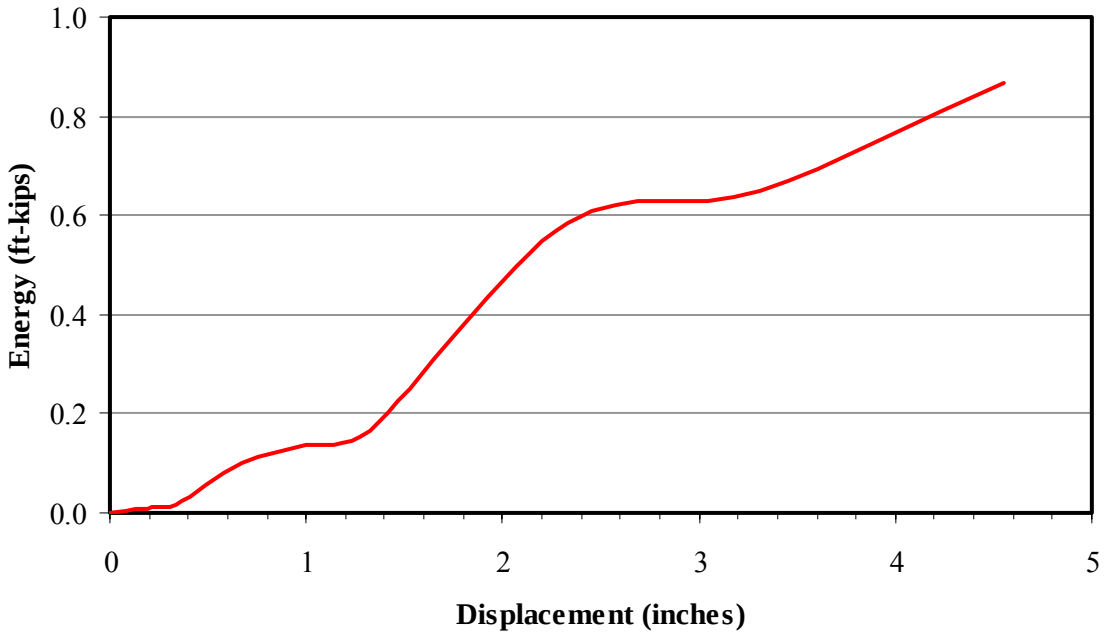

Figure A.152. Hysteretic energy dissipated per cycle vs. displacement of 10-8-E-2

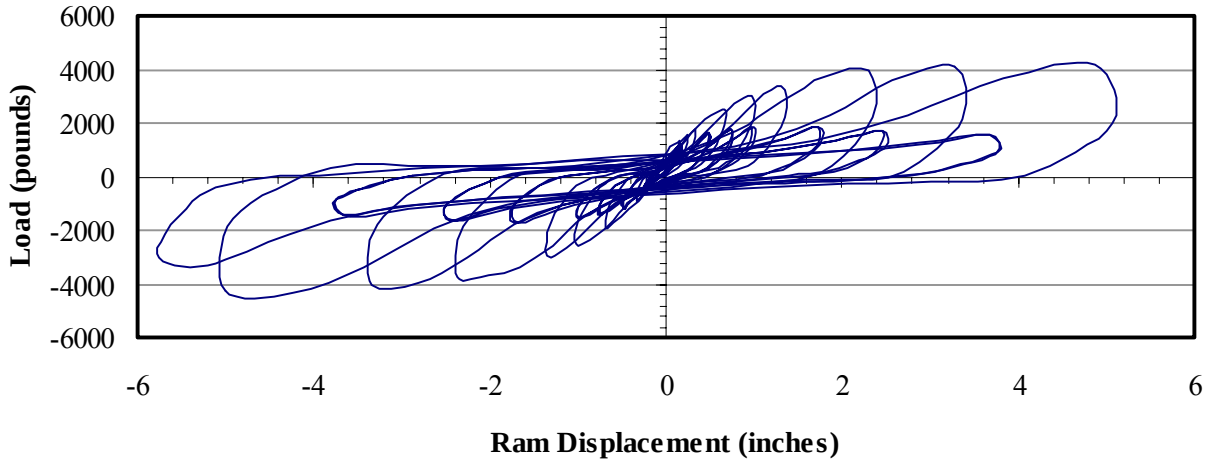

Figure A.153. Load vs. displacement of 10-8-E-2

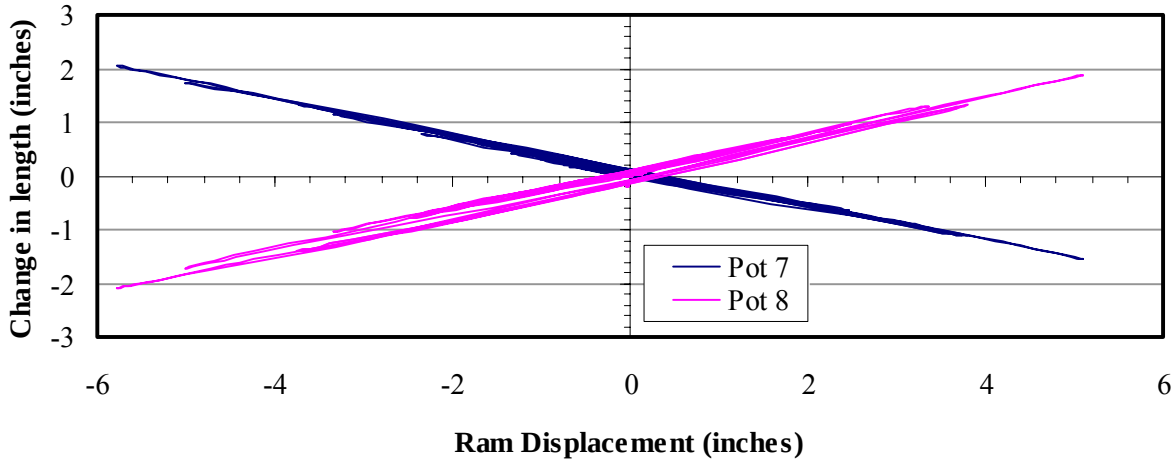

Figure A.154. Change in length of diagonal measuring Pots 7 and 8 vs. ram displacement of 10-8-E-2

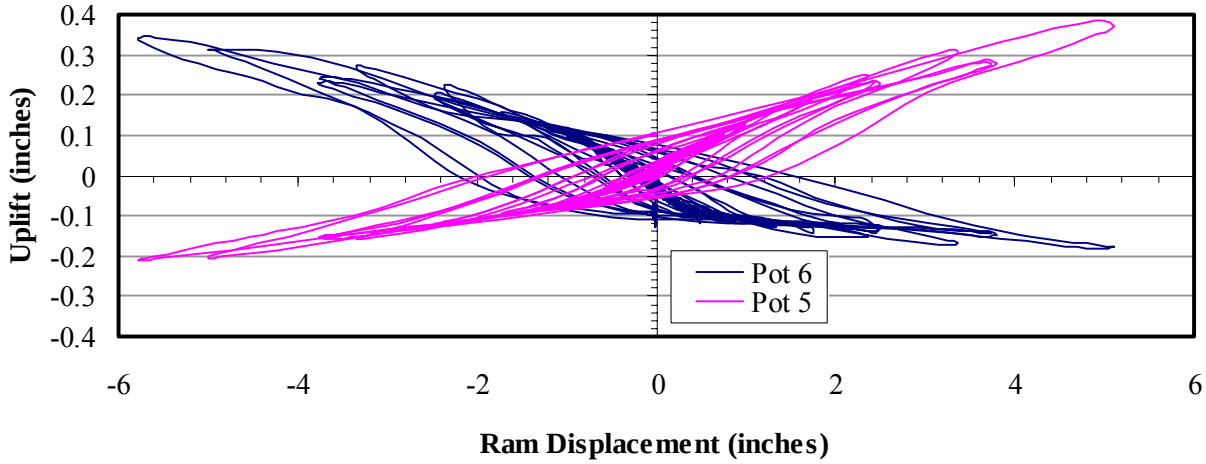

Figure A.155. Uplift displacement vs. ram displacement of 10-8-E-2

Table A.125. Performance Parameters of 10-8-E-3

Specimen	10-8-E-3	
Peak load, F_{peak}	Kips	4.391
	KN	19.533
Drift at peak load, Δ_{peak}	in.	3.901
	mm	99.08
Yield load, F_{yield}	Kips	3.917
	KN	17.422
Drift at yield load, Δ_{yield}	in.	1.076
	mm	27.34
Proportional limit, $0.4F_{peak}$	Kips	1.757
	KN	7.813
Drift at prop. limit, $\Delta@0.4F_{peak}$	in.	0.484
	mm	12.28
Failure load or $0.8F_{peak}$	Kips	4.374
	KN	19.455
Drift at failure, $\Delta_{failure}$	in.	4.642
	mm	117.92
Elastic stiffness, K_e $@0.4F_{peak}$	Kip/in.	3.654
	KN/mm	0.640
Work until failure	Kip·ft.	7.322
	KN·m	9.926
Ductility factor, μ	4.34	

Observations and failure modes:

- Tear through and pulled heads of sheathing nails near the corners and along the blocking of the 4 x 8 ft panels; however, not as severe as corresponding 9 ft configuration due to limitations of testing apparatus
- Sheathing nails along blocking in 4 x 2 ft panels pulled heads more severely than compared to corresponding 9 ft configuration. Sheathing nails in top plate were virtually undamaged.
- All sheathing nails removed from perimeter of 4 x 8 ft panels experienced significant bending deformation
- Minor separation of end studs and top and bottom plates

Table A.126. EEEP Parameters of 10-8-E-3

EEEP Parameters	units	negative	positive
F_{yield}	Kips	-4.072	3.761
	KN	-18.114	16.730
Δ_{yield}	in.	-1.172	0.981
	mm	-29.76	24.93
$\Delta_{failure}$	in.	-4.754	4.531
	mm	-120.75	115.08

Table A.127. Displacement components of 10-8-E-3

	inches	mm	% of Total
Total Displacement	4.7	119.4	
Shear Deformation	4.0	101.6	85.1
Rigid Body Motion	0.7	17.8	14.9
Bending and Slip	0.0	0.0	0.0

Table A.128. Data of each Primary cycle of 10-8-E-3

Primary	average displacement		average load		work per cycle		cyclic stiffness		Damping
cycle #	in.	mm	Kips	KN	Kip·ft.	KN·m	Kip/in.	KN/mm	Ratio
1	0.154	3.918	0.810	3.604	0.009	0.013	5.254	0.920	0.143
2	0.236	5.987	1.112	4.944	0.020	0.027	4.715	0.826	0.148
3	0.313	7.948	1.345	5.983	0.033	0.044	4.298	0.753	0.148
4	0.634	16.102	2.141	9.522	0.121	0.165	3.380	0.592	0.171
5	0.940	23.879	2.723	12.112	0.217	0.294	2.898	0.508	0.162
6	1.248	31.700	3.091	13.751	0.326	0.442	2.478	0.434	0.161
7	2.191	55.656	3.925	17.460	0.897	1.216	1.792	0.314	0.199
8	3.108	78.933	4.220	18.770	1.262	1.712	1.358	0.238	0.184
9	4.642	117.918	4.374	19.455	2.064	2.798	0.941	0.165	0.194

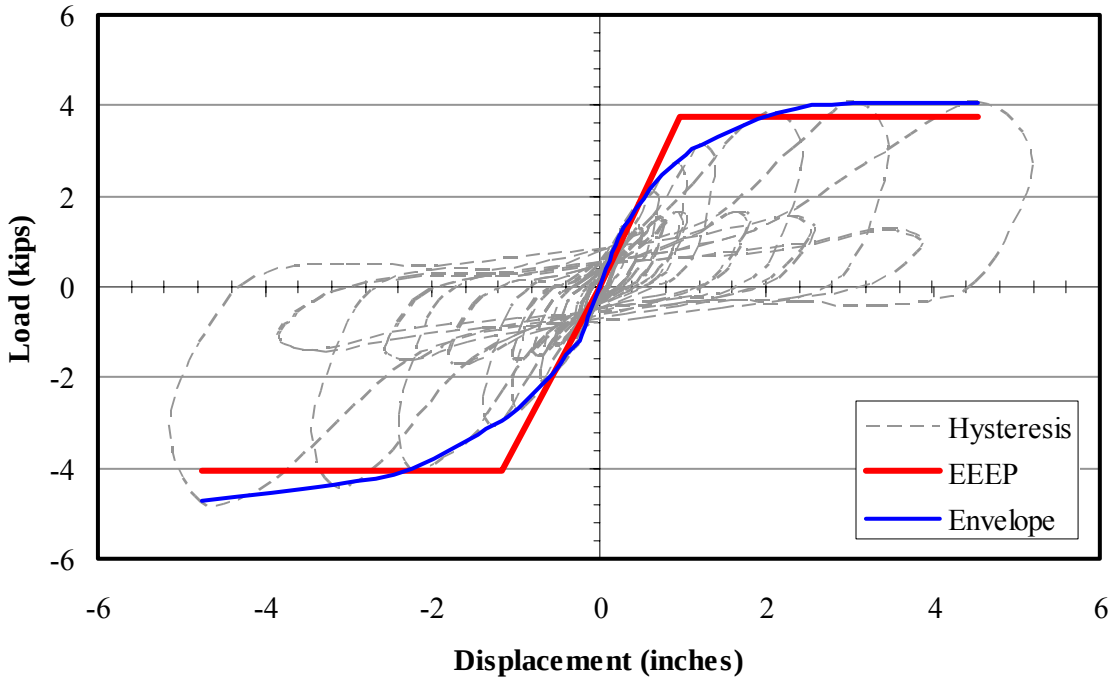

Figure A.156. Load vs. displacement, envelope and EEEP curves of 10-8-E-3

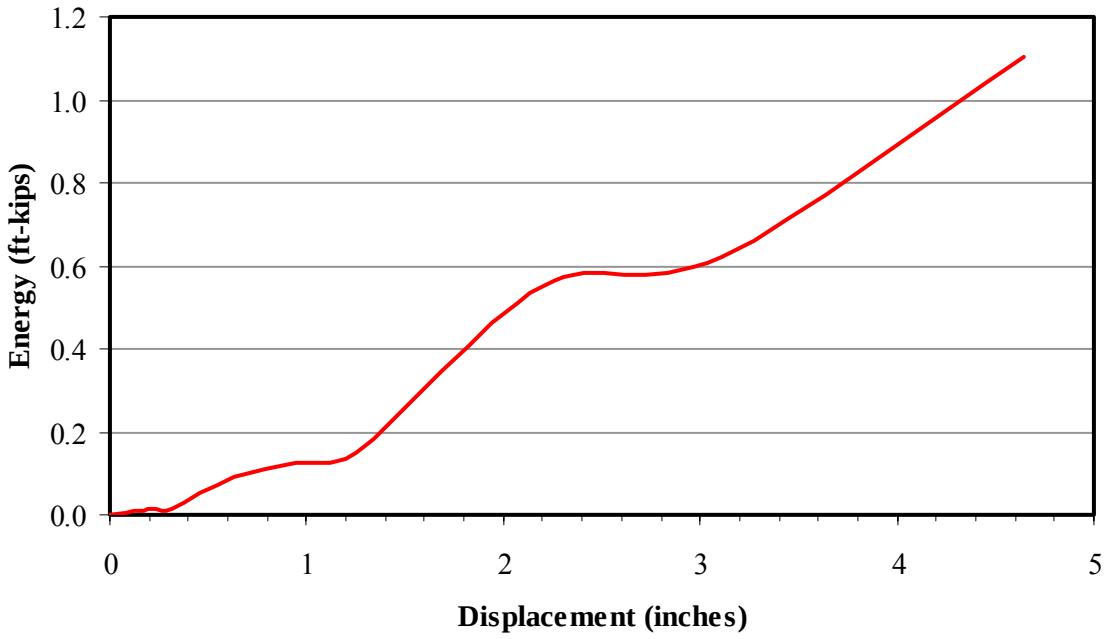

Figure A.157. Hysteretic energy dissipated per cycle vs. displacement of 10-8-E-3

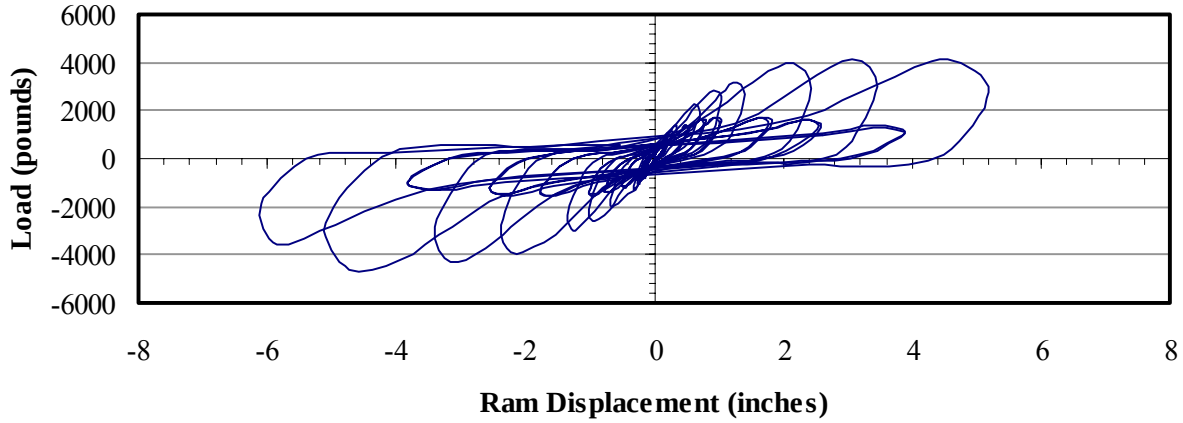

Figure A.158. Load vs. displacement of 10-8-E-3

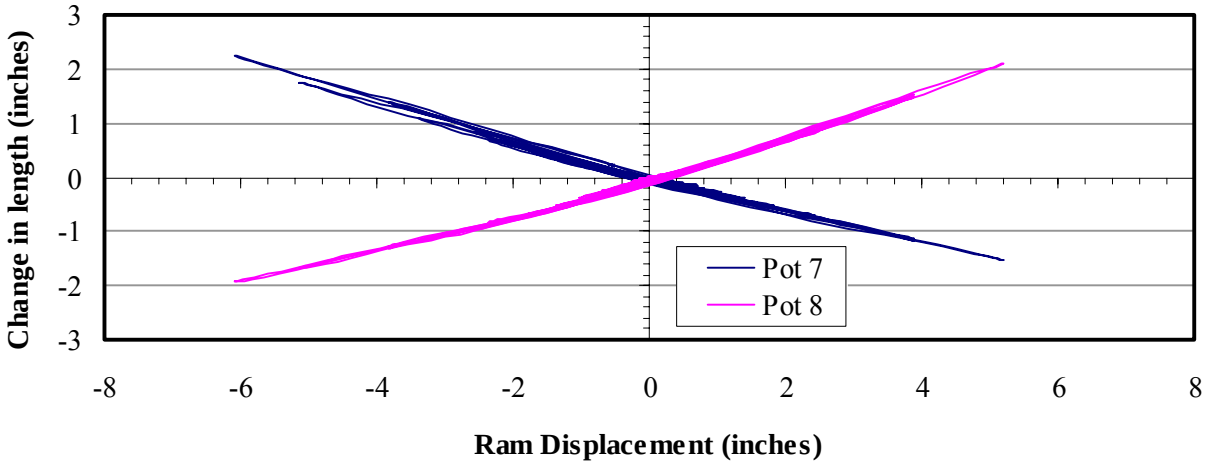

Figure A.159. Change in length of diagonal measuring Pots 7 and 8 vs. ram displacement of 10-8-E-3

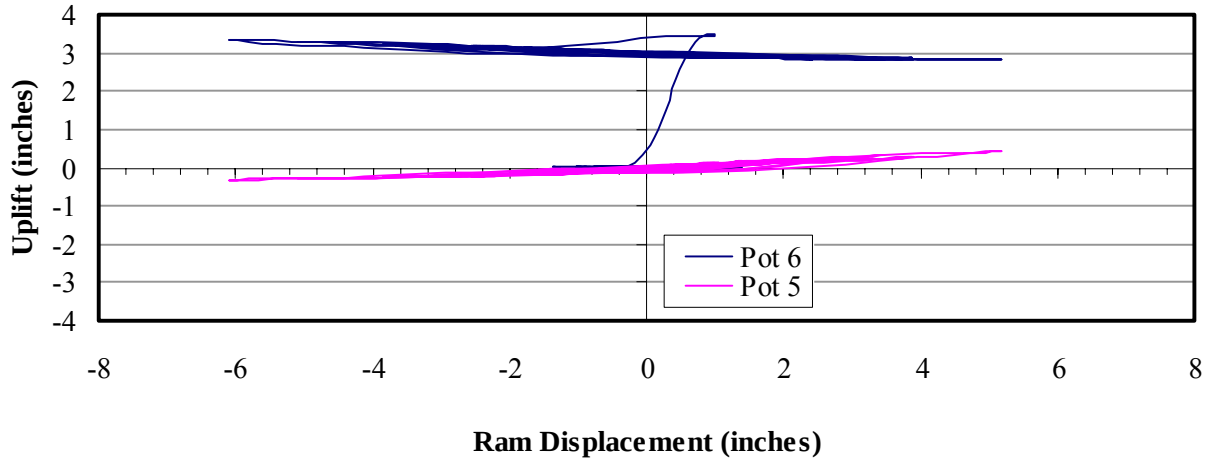

Figure A.160. Uplift displacement vs. ram displacement of 10-8-E-3

Table A.129. Performance Parameters of 9-9.5-P-1

Specimen	9-9.5-P-1	
Peak load, F_{peak}	Kips	2.777
	KN	12.353
Drift at peak load, Δ_{peak}	in.	1.858
	mm	47.20
Yield load, F_{yield}	Kips	2.422
	KN	10.773
Drift at yield load, Δ_{yield}	in.	0.589
	mm	14.97
Proportional limit, $0.4F_{peak}$	Kips	1.111
	KN	4.941
Drift at prop. limit, $\Delta@0.4F_{peak}$	in.	0.270
	mm	6.86
Failure load or $0.8F_{peak}$	Kips	2.222
	KN	9.882
Drift at failure, $\Delta_{failure}$	in.	2.426
	mm	61.61
Elastic stiffness, K_e $@0.4F_{peak}$	Kip/in.	4.110
	KN/mm	0.720
Work until failure	Kip·ft.	4.236
	KN·m	5.743
Ductility factor, μ	4.11	

Observations and failure modes:

- Mode of failure was sheathing nail withdrawal under the end stud in tension along the edge of the panel in the 2 x 12. A combination of sheathing nail withdrawal and pulling heads was experienced in those along the bottom plate. This led to significant amounts of uplift displacement between end stud in tension and bottom plate
- Sheathing nails removed from bottom plate experienced more bending deformation than those removed from 2 x 12
- Sheathing nails removed from any other location experienced virtually no bending deformation.
- Separation between bottom plate and studs was not as severe as the corresponding 8 ft configuration due to limitations of testing apparatus

Table A.130. EEEP Parameters of 9-9.5-P-1

EEEP Parameters	units	negative	positive
F_{yield}	Kips	-2.458	2.386
	KN	-10.935	10.611
Δ_{yield}	in.	-0.594	0.585
	mm	-15.09	14.85
$\Delta_{failure}$	in.	-2.578	2.273
	mm	-65.49	57.73

Table A.131. Displacement components of 9-9.5-P-1

	inches	mm	% of Total
Total Displacement	2.2	55.9	
Shear Deformation	0.7	17.8	31.8
Rigid Body Motion	1.5	38.1	68.2
Bending and Slip	0.0	0.0	0.0

Table A.132. Data of each Primary cycle of 9-9.5-P-1

Primary	average displacement		average load		work per cycle		cyclic stiffness		Damping
cycle #	in.	mm	Kips	KN	Kip·ft.	KN·m	Kip/in.	KN/mm	Ratio
1	0.083	2.098	0.482	2.145	0.002	0.003	5.853	1.025	0.108
2	0.124	3.152	0.678	3.017	0.005	0.007	5.468	0.958	0.115
3	0.161	4.084	0.833	3.706	0.009	0.013	5.179	0.907	0.135
4	0.323	8.200	1.245	5.538	0.037	0.051	3.857	0.675	0.178
5	0.479	12.169	1.566	6.967	0.075	0.102	3.270	0.573	0.191
6	0.638	16.204	1.826	8.121	0.117	0.158	2.863	0.501	0.191
7	1.086	27.596	2.385	10.608	0.299	0.406	2.196	0.385	0.221
8	1.543	39.190	2.687	11.952	0.464	0.629	1.742	0.305	0.214
9	2.133	54.181	2.731	12.146	0.777	1.053	1.279	0.224	0.254
10	2.707	68.748	1.682	7.479	0.778	1.055	0.618	0.108	0.325
11	4.150	105.500	0.286	1.273	0.233	0.315	-1.976	-0.346	0.973

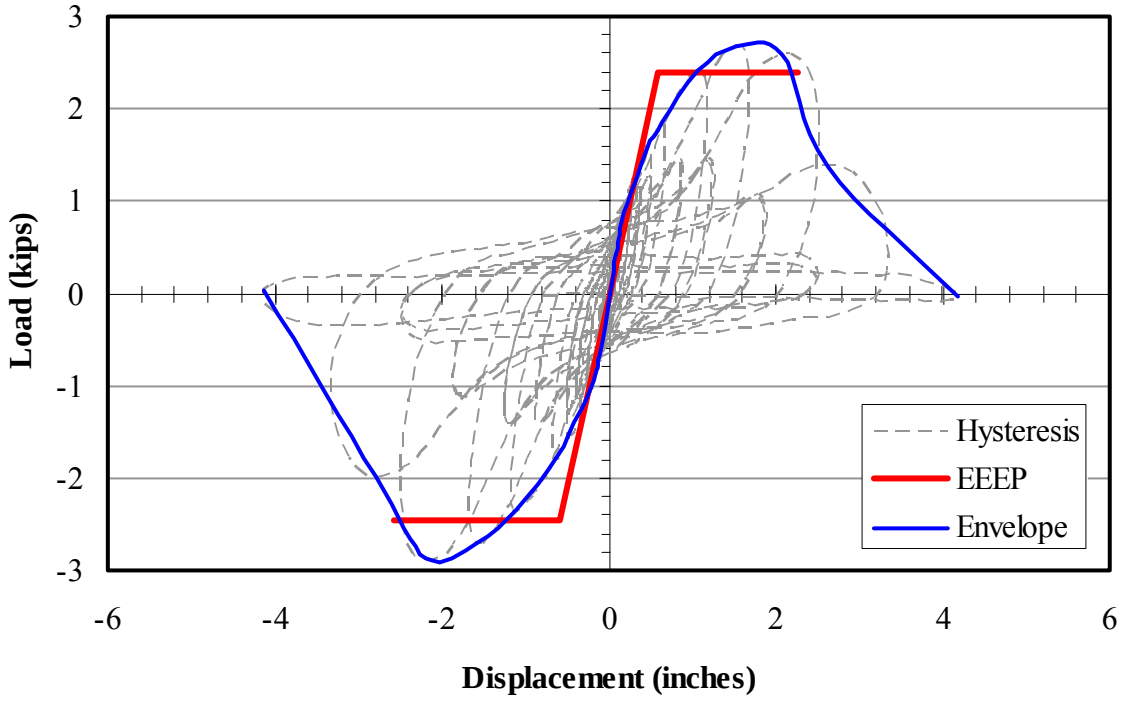

Figure A.161. Load vs. displacement, envelope and EEEP curves of 9-9.5-P-1

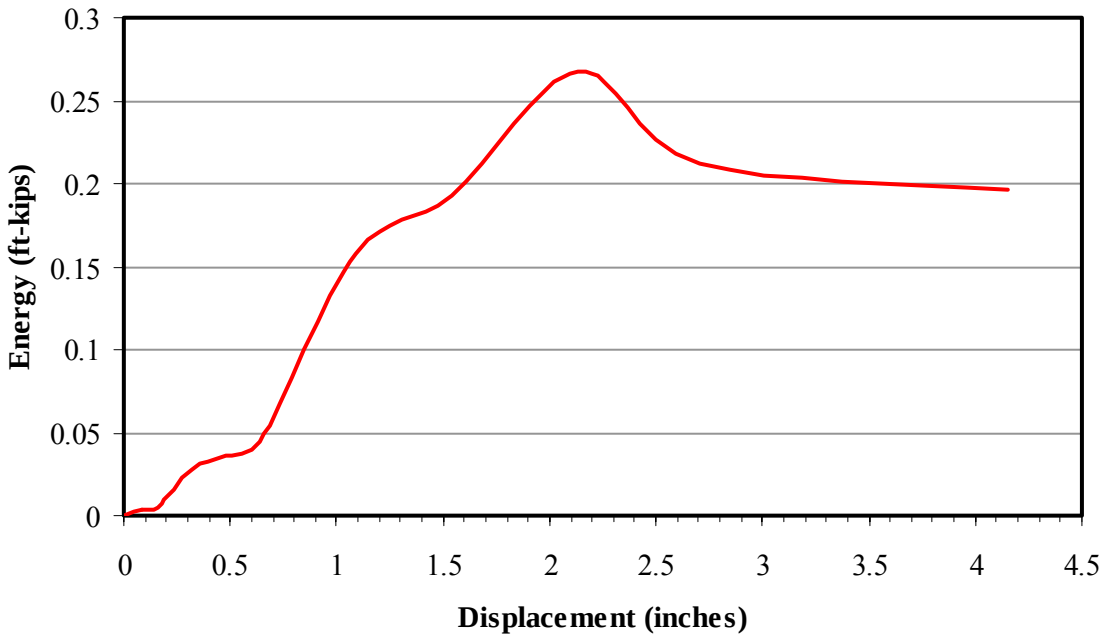

Figure A.162. Hysteretic energy dissipated per cycle vs. displacement of 9-9.5-P-1

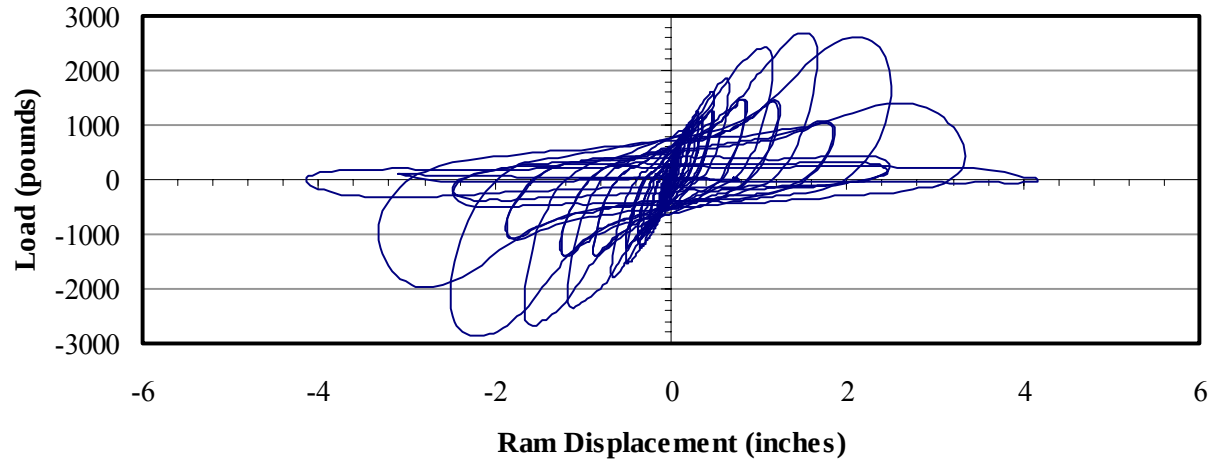

Figure A.163. Load vs. displacement of 9-9.5-P-1

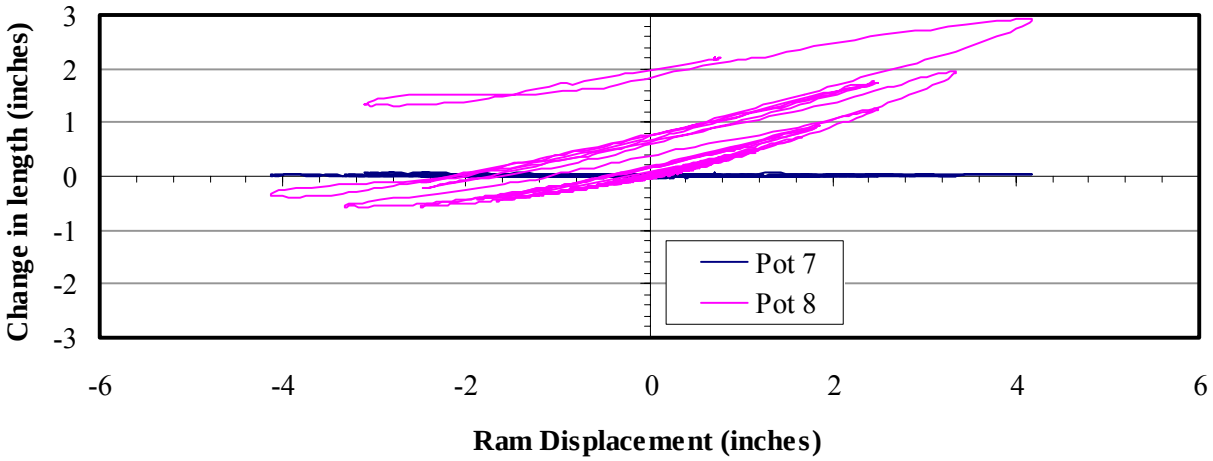

Figure A.164. Change in length of diagonal measuring Pots 7 and 8 vs. ram displacement of 9-9.5-P-1

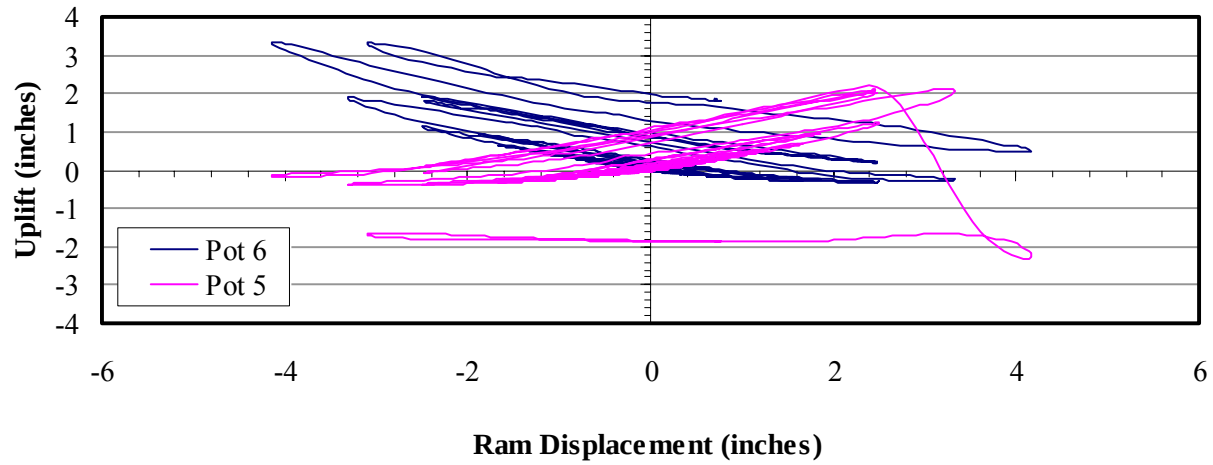

Figure A.165. Uplift displacement vs. ram displacement of 9-9.5-P-1

Table A.133. Performance Parameters of 9-9.5-P-2

Specimen	9-9.5-P-2	
Peak load, F_{peak}	Kips	2.824
	KN	12.563
Drift at peak load, Δ_{peak}	in.	1.568
	mm	39.83
Yield load, F_{yield}	Kips	2.448
	KN	10.889
Drift at yield load, Δ_{yield}	in.	0.563
	mm	14.31
Proportional limit, $0.4F_{peak}$	Kips	1.130
	KN	5.025
Drift at prop. limit, $\Delta@0.4F_{peak}$	in.	0.259
	mm	6.59
Failure load or $0.8F_{peak}$	Kips	2.260
	KN	10.050
Drift at failure, $\Delta_{failure}$	in.	2.111
	mm	53.61
Elastic stiffness, K_e $@0.4F_{peak}$	Kip/in.	4.408
	KN/mm	0.772
Work until failure	Kip·ft.	4.175
	KN·m	5.660
Ductility factor, μ	3.78	

Observations and failure modes:

- Mode of failure was sheathing nail withdrawal under the end stud in tension along the edge of the panel in the 2 x 12. A combination of sheathing nail withdrawal and pulling heads was experienced in those along the bottom plate. This led to significant amounts of uplift displacement between end stud in tension and bottom plate.
- Sheathing nails removed from bottom plate experienced more bending deformation than those removed from 2 x 12
- Separation between bottom plate and studs was not as severe as the corresponding 8 ft configuration due to limitations of testing apparatus
- Sheathing nail tear through along bottom portion of common center stud in both panels

Table A.134. EEEP Parameters of 9-9.5-P-2

EEEP Parameters	units	negative	positive
F_{yield}	Kips	-2.489	2.407
	KN	-11.069	10.708
Δ_{yield}	in.	-0.636	0.491
	Mm	-16.15	12.47
$\Delta_{failure}$	in.	-2.230	1.991
	Mm	-56.65	50.58

Table A.135. Displacement components of 9-9.5-P-2

	inches	mm	% of Total
Total Displacement	1.6	40.6	
Shear Deformation	0.6	15.2	37.5
Rigid Body Motion	1.0	25.4	62.5
Bending and Slip	0.0	0.0	0.0

Table A.136. Data of each Primary cycle of 9-9.5-P-2

Primary	average displacement		average load		work per cycle		cyclic stiffness		Damping
cycle #	in.	mm	Kips	KN	Kip·ft.	KN·m	Kip/in.	KN/mm	Ratio
1	0.082	2.088	0.480	2.135	0.002	0.003	5.843	1.023	0.112
2	0.123	3.125	0.697	3.102	0.005	0.007	5.667	0.992	0.120
3	0.163	4.134	0.849	3.777	0.010	0.014	5.218	0.914	0.141
4	0.327	8.307	1.273	5.660	0.038	0.052	3.891	0.681	0.175
5	0.480	12.187	1.607	7.147	0.076	0.103	3.350	0.587	0.189
6	0.637	16.189	1.855	8.250	0.118	0.160	2.910	0.510	0.190
7	1.103	28.023	2.517	11.195	0.302	0.409	2.281	0.400	0.208
8	1.568	39.826	2.824	12.563	0.473	0.642	1.801	0.315	0.204
9	2.094	53.181	2.664	11.850	0.768	1.041	1.273	0.223	0.263
10	2.089	53.056	1.469	6.536	0.764	1.036	0.719	0.126	0.462

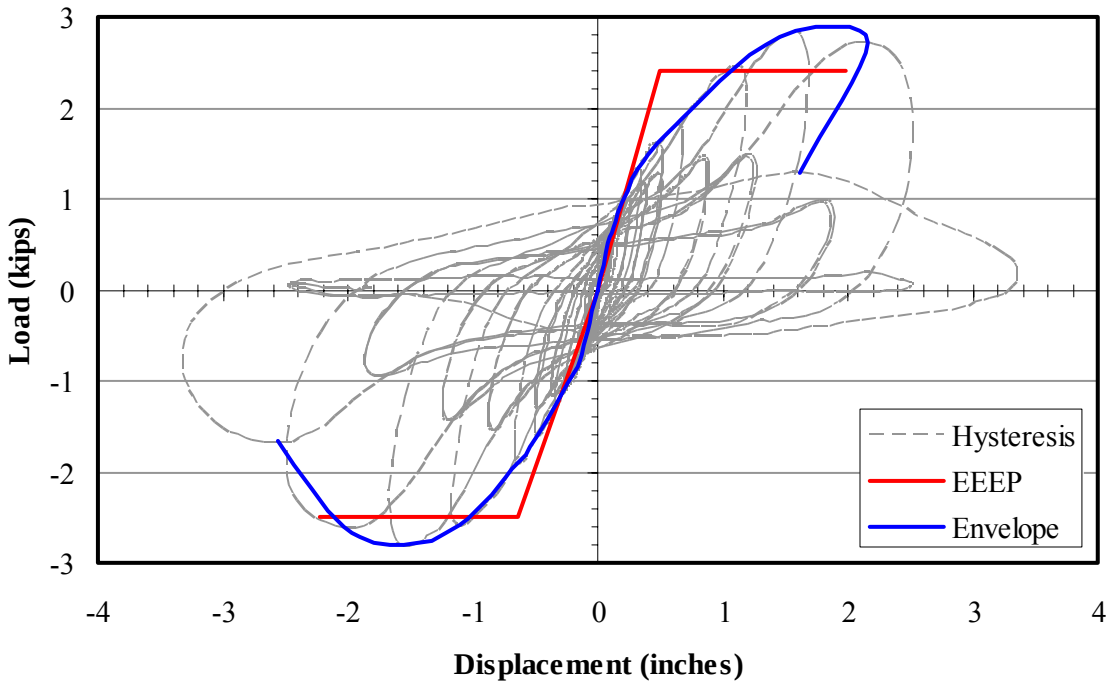

Figure A.166. Load vs. displacement, envelope and EEEP curves of 9-9.5-P-2

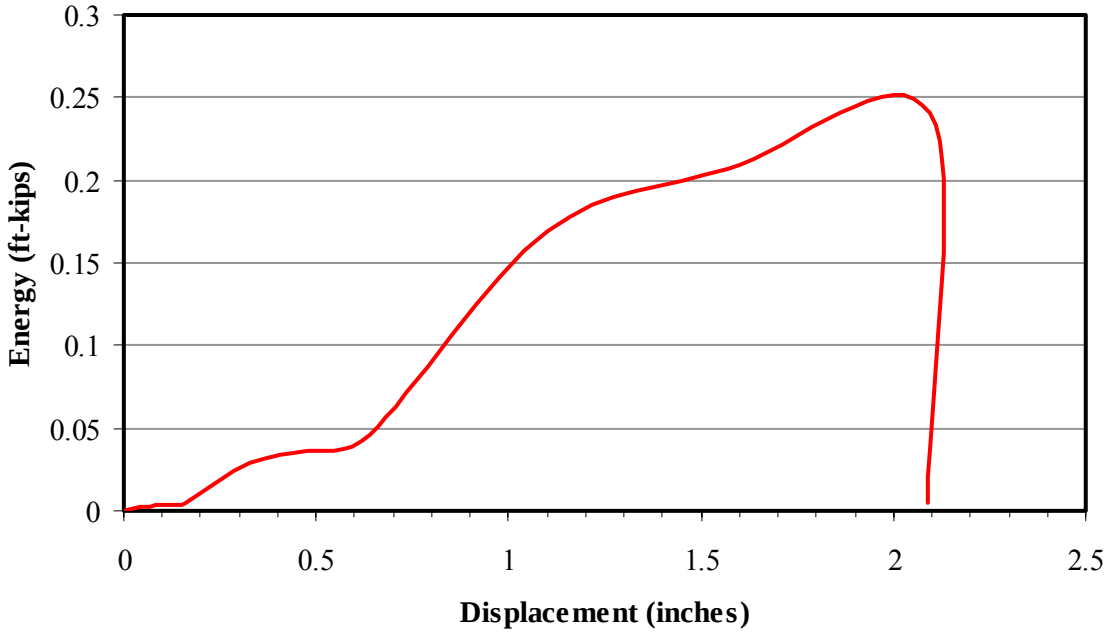

Figure A.167. Hysteretic energy dissipated per cycle vs. displacement of 9-9.5-P-2

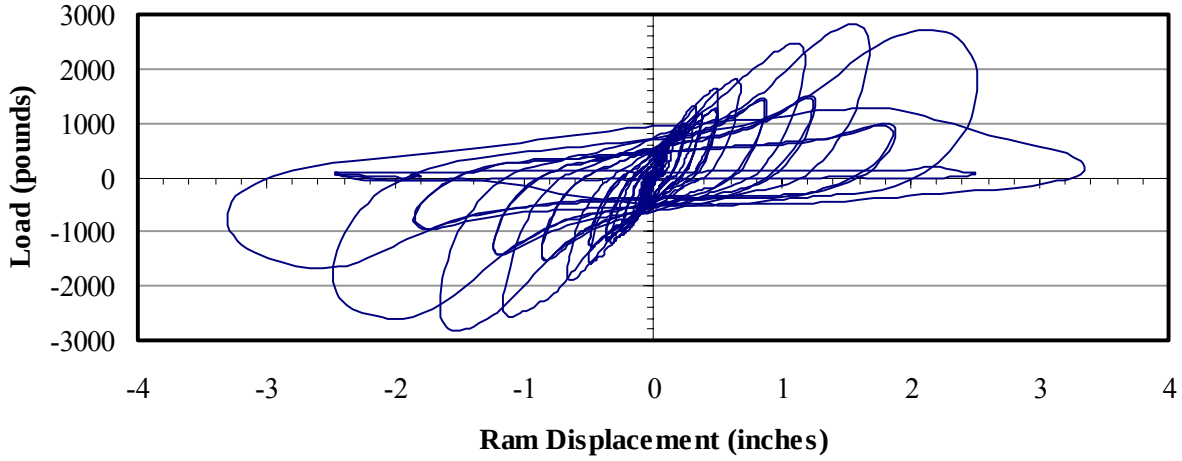

Figure A.168. Load vs. displacement of 9-9.5-P-2

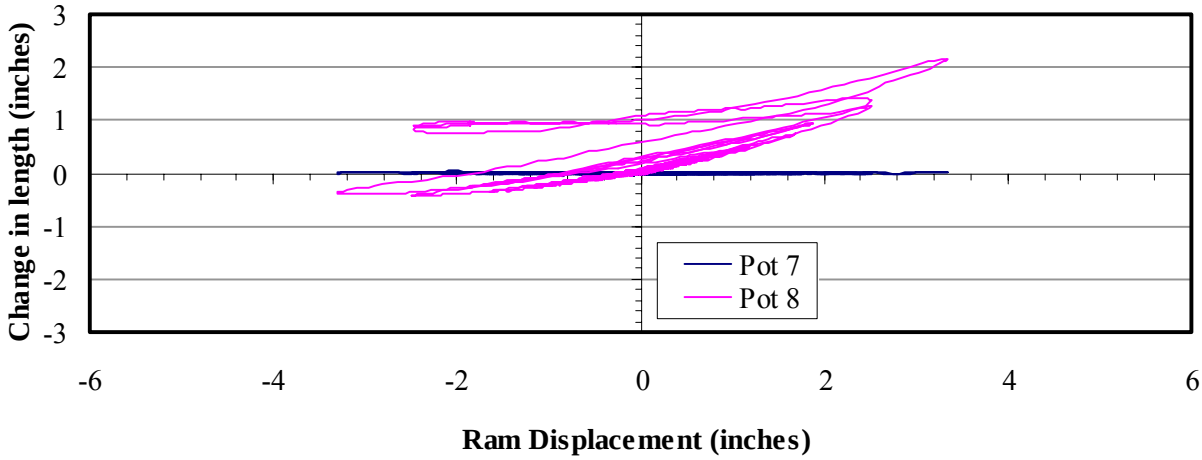

Figure A.169. Change in length of diagonal measuring Pots 7 and 8 vs. ram displacement of 9-9.5-P-2

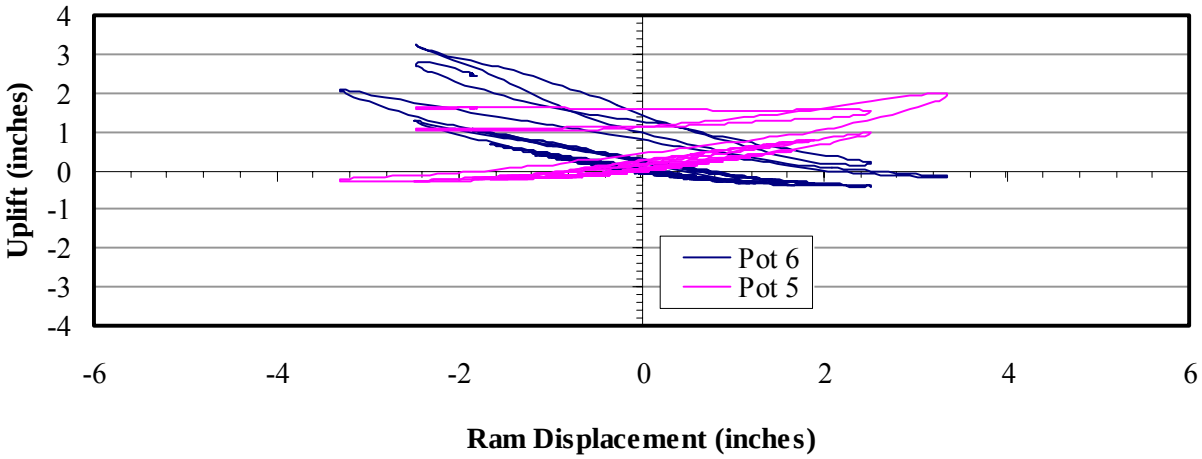

Figure A.170. Uplift displacement vs. ram displacement of 9-9.5-P-2

Table A.137 Performance Parameters of 9-9.5-P-3

Specimen	9-9.5-P-3	
Peak load, F_{peak}	Kips	3.086
	KN	13.727
Drift at peak load, Δ_{peak}	in.	1.853
	mm	47.06
Yield load, F_{yield}	Kips	2.693
	KN	11.978
Drift at yield load, Δ_{yield}	in.	0.610
	mm	15.49
Proportional limit, $0.4F_{peak}$	Kips	1.234
	KN	5.491
Drift at prop. limit, $\Delta@0.4F_{peak}$	in.	0.281
	mm	7.14
Failure load or $0.8F_{peak}$	Kips	2.469
	KN	10.982
Drift at failure, $\Delta_{failure}$	in.	2.445
	mm	62.10
Elastic stiffness, K_e $@0.4F_{peak}$	Kip/in.	4.640
	KN/mm	0.813
Work until failure	Kip·ft.	4.566
	KN·m	6.190
Ductility factor, μ	4.20	

Observations and failure modes:

- Mode of failure was sheathing nail withdrawal under the end stud in tension along the edge of the panel in the 2 x 12. A combination of sheathing nail withdrawal and pulling heads was experienced in those along the bottom plate. This led to significant amounts of uplift displacement between end stud in tension and bottom plate.
- Sheathing nails removed from bottom plate experienced more bending deformation than those removed from 2 x 12
- Separation between bottom plate and studs was not as severe as the corresponding 8 ft configuration due to limitations of testing apparatus
- Sheathing nail tear through along bottom portion of common center stud in both panels

Table A.138. EEEP Parameters of 9-9.5-P-3

EEEP Parameters	units	negative	positive
F_{yield}	Kips	-2.665	2.721
	KN	-11.854	12.102
Δ_{yield}	in.	-0.741	0.479
	mm	-18.82	12.16
$\Delta_{failure}$	in.	-2.450	2.440
	mm	-62.22	61.98

Table A.139. Displacement components of 9-9.5-P-3

	inches	mm	% of Total
Total Displacement	2.2	55.9	
Shear Deformation	0.7	17.8	31.8
Rigid Body Motion	1.5	38.1	68.2
Bending and Slip	0.0	0.0	0.0

Table A.140. Data of each Primary cycle of 9-9.5-P-3

Primary	average displacement		average load		work per cycle		cyclic stiffness		Damping
cycle #	in.	mm	Kips	KN	Kip·ft.	KN·m	Kip/in.	KN/mm	Ratio
1	0.084	2.122	0.519	2.308	0.002	0.003	6.209	1.087	0.091
2	0.121	3.080	0.752	3.346	0.005	0.007	6.201	1.086	0.110
3	0.163	4.133	0.918	4.082	0.010	0.013	5.666	0.992	0.123
4	0.323	8.193	1.377	6.125	0.033	0.045	4.280	0.749	0.143
5	0.481	12.222	1.692	7.527	0.066	0.089	3.520	0.616	0.154
6	0.641	16.276	1.974	8.779	0.104	0.141	3.083	0.540	0.157
7	1.106	28.099	2.613	11.623	0.271	0.367	2.362	0.414	0.179
8	1.538	39.060	2.970	13.211	0.441	0.598	1.932	0.338	0.185
9	2.231	56.666	3.082	13.710	0.773	1.048	1.383	0.242	0.215
10	2.591	65.805	2.014	8.959	0.882	1.196	0.778	0.136	0.323

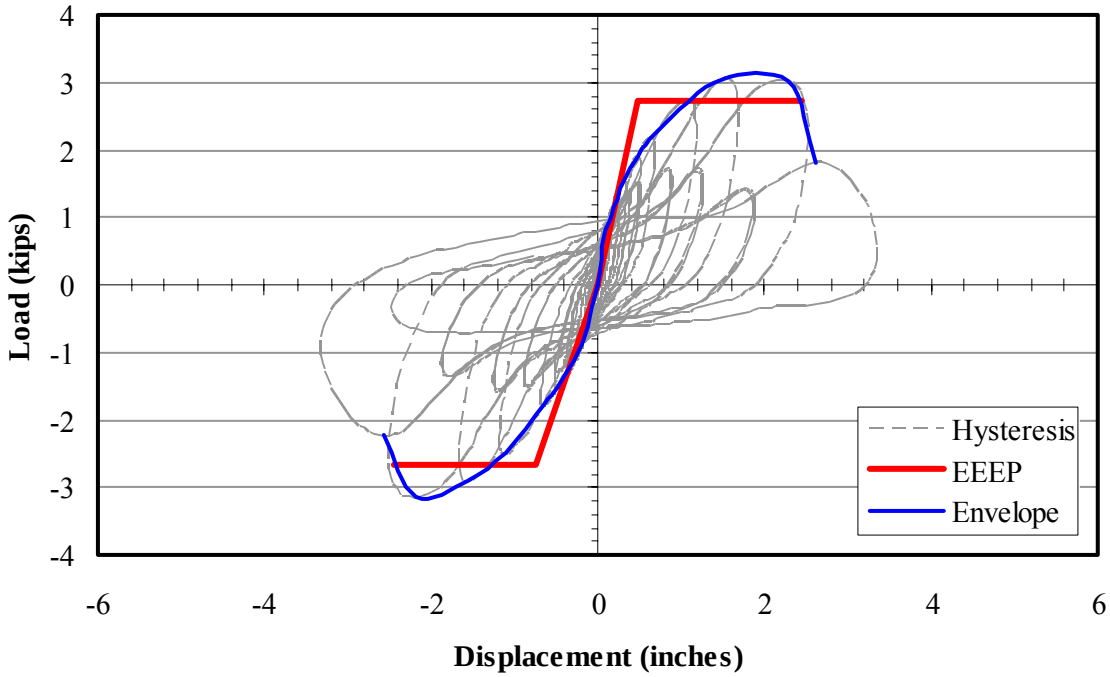

Figure A.171. Load vs. displacement, envelope and EEEP curves of 9-9.5-P-3

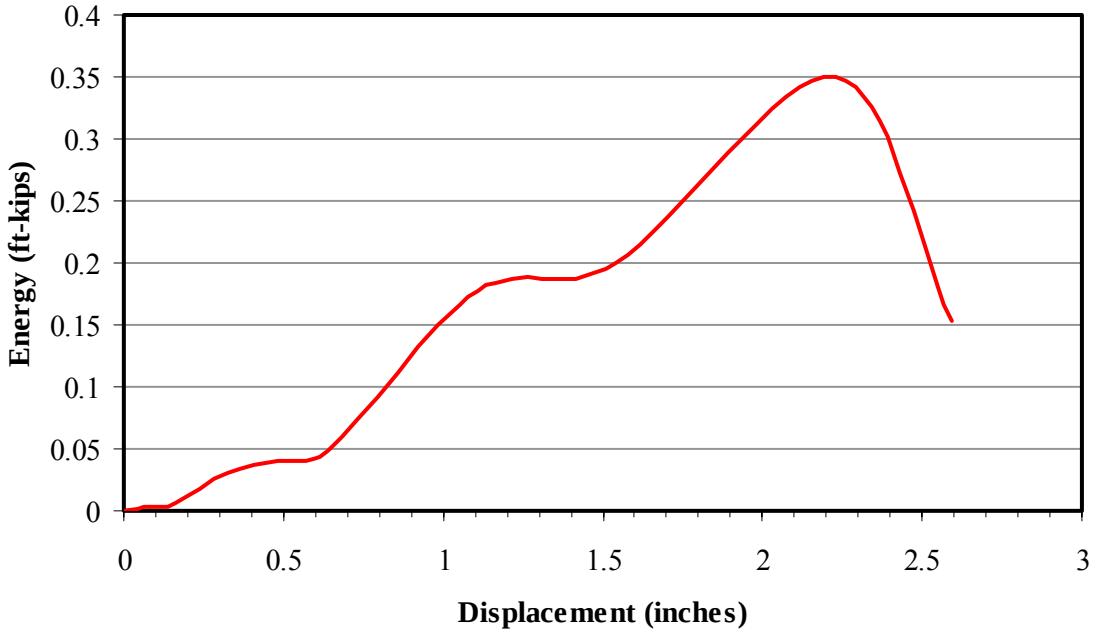

Figure A.172. Hysteretic energy dissipated per cycle vs. displacement of 9-9.5-P-3

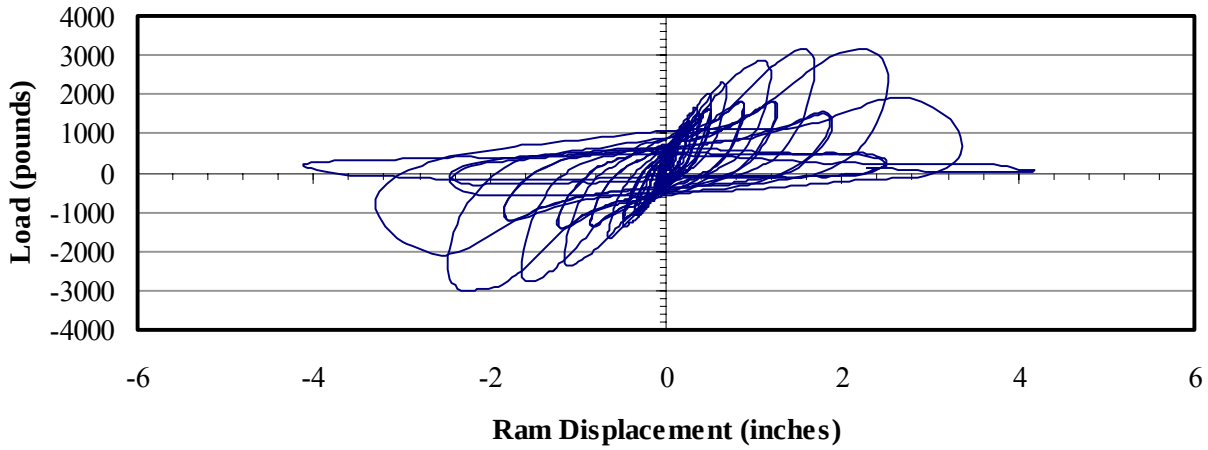

Figure A.173. Load vs. displacement of 9-9.5-P-3

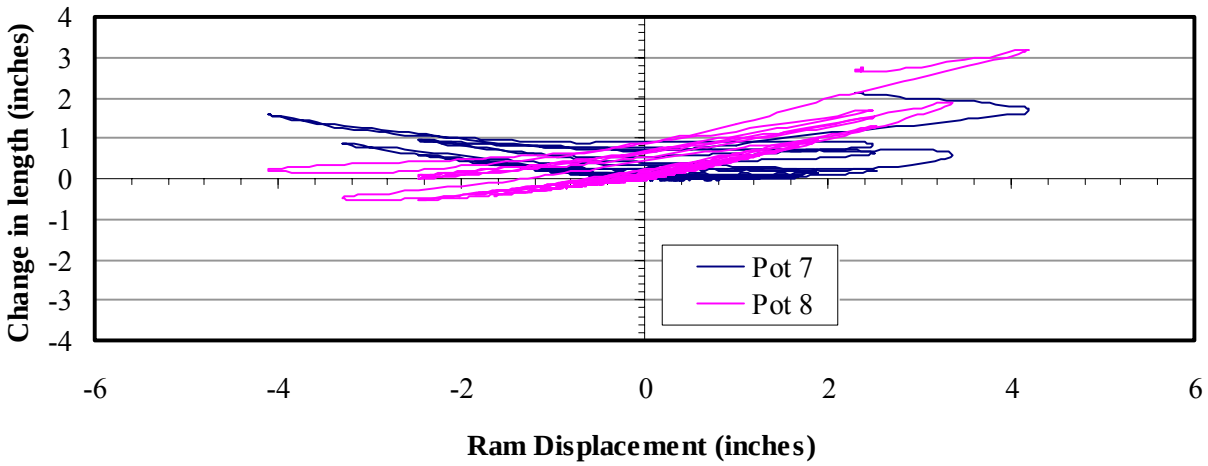

Figure A.174. Change in length of diagonal measuring Pots 7 and 8 vs. ram displacement of 9-9.5-P-3

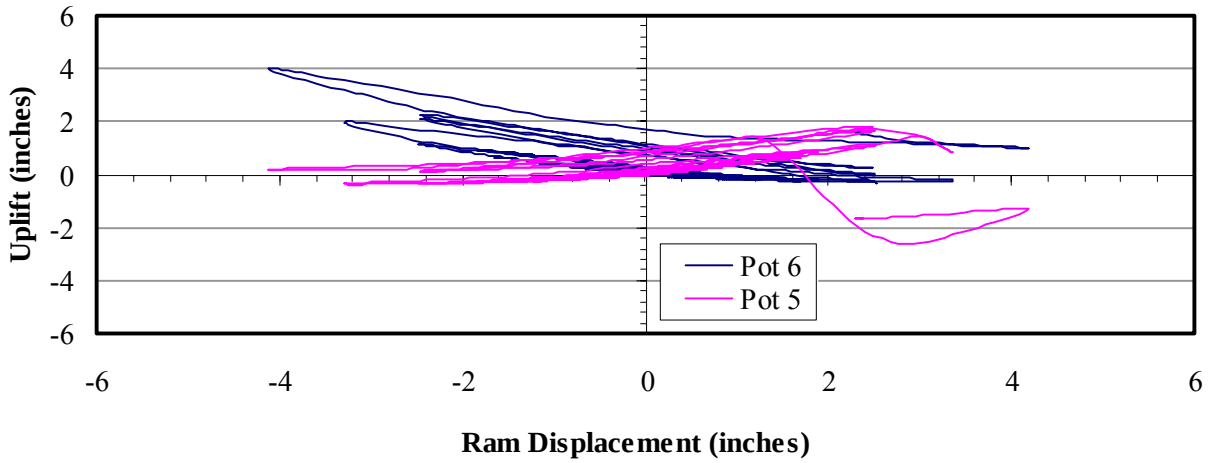

Figure A.175. Uplift displacement vs. ram displacement of 9-9.5-P-3

Vita

The author, Daniel H. Bredel, Jr., was born March 23, 1979 in Springfield, Illinois. He spent the first twelve years of his life in Carlinville, IL. The family then moved to Midlothian, VA, where he attended Clover Hill High School. Upon graduation of high school in 1997, he attended Virginia Polytechnic Institute and State University at which he earned a B.S. in civil engineering in 2001. After a short stint in the "real world," the author decided to go back to Va Tech and pursue a master's degree in civil engineering.